# IMMUNOREGULATORY EFFECTS OFVITAMIN D AND ITS MECHANISM OF ACTION IN CD4+ T CELLS

McGregor, Reuben Hendrik Cameron

*Awarding institution:*
King's College London

# IMMUNOREGULATORY EFFECTS OF VITAMIN D AND ITS MECHANISM OF ACTION IN $CD4^+$ T CELLS

A thesis submitted to the Faculty of Medicine of the University of London for the degree of Doctor of Philosophy

By

Reuben McGregor

Division of Transplantation Immunology & Mucosal Biology
MRC Centre for Transplantation
Kings College London,
5th Floor Bermondsey Wing,
Guy's Hospital,
London SE1 9RT

July 2017

## Abstract

Vitamin D (VitD) deficiency has been implicated in the pathogenesis of multiple diseases including chronic kidney disease (CKD). VitD has direct effects on most cells in the innate and adaptive immune system including; $CD4^+$ T cells and dendritic cells (DCs) both of which express the vitamin D receptor (VDR). This thesis, divided into two distinct parts, dissects the effects of: a) *in vivo* repletion of VitD in a placebo controlled, double blinded clinical trial in CKD patients. Here we hypothesised that repletion with cholecalciferol in VitD insufficient/deficient adult patients would ameliorate systemic inflammation. And the effects of b) VitD treatment of $CD4^+$ T cells *in vitro* using multiple techniques to delineate the mechanisms influencing cytokine regulation. Here we hypothesised that VitD treatment of $CD4^+$ T cells would, through binding of liganded VDR, lead to epigenetic modifications affecting genes involved in the regulation of cytokine production. *In vivo* we show that VitD repletion in VitD-deficient and insufficient patients with early stage CKD has immunoregulatory effects on circulating myeloid DCs by reducing expression of HLA-DR (a marker of mature DC phenotype). *In vitro* we identify a novel signaling pathway in $CD4^+$ T cells, induced by VitD. The hallmark effect of VitD on $CD4^+$ T cells was the induction of an immunoregulatory phenotype characterized by inhibited Th1 and Th17 cytokines and induction of the anti-inflammatory cytokine IL-10, a process we show to be regulated by induction of IL-6 and subsequent STAT3 signalling. We further show that these processes are genetically regulated by histone modifications driven by liganded VDR, both at putative enhancer and promoter sites. These findings, most notably, have implications for dysregulated immunoregulation in the setting of inflammatory skin diseases and the development of novel therapeutics for the treatment of these conditions.

## Declaration

The work presented here is my own and all experiments were performed by myself, with input acknowledged in contributions section.

Reuben McGregor

## Dedication

This work is dedicated to my mother and father, and my family as a whole. Without their constant support and love, without the upbringing of questioning and debate, and without their guidance this thesis would never have been possible. You all have my eternal gratitude and love.

“It doesn't matter how beautiful your theory is, it doesn't matter how smart you are, it doesn’t matter what your name is. If it doesn't agree with experiment, it's wrong.”

Richard Feinman

# Table of contents

# Table of figures

# Table of tables

## Acknowledgements

I would like to thank my supervisors; Professor Giovanna Lombardi and Dr Behdad Afzali for their invaluable guidance and support, both academic and pastoral throughout my PhD. I would like to thank Dr Behdad Afzali for the patience he has shown me as I navigated the emotional and professional maze that is a PhD. Thank you for showing me that a supervisor can be a friend as well as a guide and I sincerely hope our paths will cross again. I would like to thank Professor Giovanna Lombardi for not only supervision, but an open office and smile whenever it was needed, and for trusting in me time and time again, when things did not always seem to be going in the right direction. I would also like to thank my mentor, supervisor and dear friend Dr Estefania Nova Lamperti without whom I would almost certainly have lost my way. Besides the academic rigor and experimental pride you have shown me, your friendship and diversions from work ensured my time at Guy's Hospital were thoroughly enjoyable, inside and outside the lab. I am sure our futures hold joint professional and personal adventures.

I would also like to thank Professor Claudia Kemper and Professor Paul Lavendar for all their input into the development of my project, both practically and intellectually, and again, I hope we can stay in contact for many years to come.

I would like to thank Dr Giovanni Povoloeri and Dr Estefani Nova Lamperti for their friendship and help, in and out of the lab. We laughed, we cried, we kept each other sane. We will stay friends forever after all we have been through.

I would like to thank every member of the immunoregulation lab for making my time here so enjoyable, despite the trials and tribulations we have sailed through together. It would be impossible to name everybody who made this thesis possible in so many ways, but I thank you all for the help, no matter how insignificant it may have seemed you have all contributed to the this thesis and my sanity.

A special thanks to all my friends (you know who you all are) who, despite the neglect I have shown whilst finishing and writing up, have housed me, fed me and entertained me. These years would have been hard to bear without you all.

Finally, I would like to thank Charlotte, we explored life, academia and the world together and without you it would not have been half as exhilarating. Let’s keep exploring!

## Contributions

Project expenses were funded by supervisors Professor Giovanna Lombardi and Dr Behdad Afzali and in part by the NIHR PhD scholarship awarded to me. General intellectual input into experimental design were significantly contributed to by supervisor Dr Behdad Afzali and post-doctoral researcher and mentor Dr Estefania Nova Lamperti. General intellectual input and project guidance were substantial from primary supervisor Professor Giovanna Lombardi.

Collection of trial samples and storage was orchestrated by Dr Nihil Chitalia and Dr Debasish Banerjee. Direction of trial was orchestrated by Professor David Goldsmith. Processing and storage of *in vivo* clinical trial samples was started by Dr Nihil Chitalia with the rest being completed by me following commencement of PhD. All analysis was carried out by Reuben McGregor with contributions for statistical data analysis from PhD candidate Charlotte Jelleyman, University of Leicester.

Experimental procedures and day to day *in vitro* work were also carried with substantial advice and guidance from Dr Estefania Nova Lamperti, with additional guidance on image stream analysis help from P.J Channa form the flow cytometry core, KCL.

ChIP-seq experimental procedures were carried out with substantial contribution and reagents from, Professor Paul Lavendar and Dr Audrey Kelley. Data analysis of ChIP-seq experiments using Galaxy was self-taught. Analysis using Ea-Seq was self-taught but with guidance from program designer Professor Mads Lerdrup, University of Copenhagen. Motif analysis using HOMER was self-taught with guidance from Dr Majid Kazemian, National Institute of Health, Bethesda. General ChIP-seq analysis advice were also given by supervisor Dr Behdad Afzali, who also provided invaluable advice on where to find advice on data analysis.

Writing of, and presentation of data in, this thesis was carried out by me, with invaluable and significant input from supervisor Dr Behdad Afzali. Thesis was corrected and finalized with input from both supervisors Dr Behdad Afzali and Professor Giovanna Lombardi and Dr Estefania Nova Lamperti.

## Abbreviations

| Abbreviation | Meaning |
|---|---|
| 1,25 VitD | 1,25-dihydroxy vitamin D |
| 25 VitD | 25-hydroxy vitamin D |
| Ac | Acetylation |
| APCs | Antigen presenting cells |
| bp | basepairs |
| CAMP | Cathelicidin antimicrobial peptide |
| CKD | Chronic kidney disease |
| CRP | C-reactive protein |
| CV | Coefficient of variation |
| CVD | Cardiovascular disease |
| DBD | DNA- binding domain |
| DBP | Vitamin D binding protein |
| DC, mDC, moDC | Dendritic cell, myeloid dendritic cell, monocyte derived dendritic cell |
| Don (number) | Donor |
| DR | Direct repeat |
| DRIPS | VDR interacting proteins |
| ER | Oestrogen receptor |
| ESKD | End stage kidney disease |
| FACS | Fluorescence-activated cell sorting |
| FCB | Fluorescent cellular barcoding |
| FGF23 | Fibroblast growth factor 23 |
| FMO | Fluorescence minus one |
| H(number) | Histone(number) |
| HAT | Histone acetyl-transferase |
| HDAC | Hostone-deacetylase |
| IFN | interferon |
| IL | Interleukin |
| IL-10R | Interleukin 10 receptor |
| IL-6R | Interleukin 6 receptor |
| K | Lysine |
| kDa | Kilodaltons |
| LBD | Ligand-binding domain |
| LCL | Lymphoblastoid cell line |
| MB | Mega base |
| me | methylation |
| MFI | Mean fluorescence intensity |
| MHC | Major histocompatibility complex |
| MS | Multiple sclerosis |
| mVDR | Membrane vitamin d receptor |
| NHR | Nuclear hormone receptor |
| NK | Natural killer |

| | |
|---|---|
| OSs | Observational studies |
| p | Phospho |
| PBMC | Peripheral blood mononuclear cells |
| PPAR | Peroxisome proliferator-activated receptor |
| PR | Progesterone receptor |
| PTH | Parathyroid hormone |
| RAR | Retinoic acid receptor |
| RARα | Retinoic acid receptor alpha |
| RCTs | Randomised control trials |
| RXR | Retinoid x receptor |
| TB | Tuberculosis |
| TCR | T cell receptor |
| TF | Transcription factor |
| Th | T helper |
| TLR | Toll-like receptor |
| Toc | Tocilizumab |
| TR | Thyroid receptor |
| Tr1 | Type 1 regulatory cell |
| Treg | T-regulatory cell |
| tss | Transcriptional start site |
| U.V | Ultraviolet |
| VDR | Vitamin D receptor |
| VDRE | Vitamin D response element |
| VitD | Vitamin D |

# 1. GENERAL INTRODUCTION

## 1.1 Vitamin D hormone

Hormones are secreted signalling molecules that usually act at a significant distance from the cell producing them, relying on the circulatory apparatus for transport to their sites of action (Tomkins and Martin, 1970). The steroid hormones are critically important as regulators of physiological processes. In general, steroids are divided into two broad categories depending on the site of synthesis of the mature hormone – either corticosteroids (synthesised in the cortex of the adrenal gland) or sex hormones (produced in the gonads) (Miller, 1988). They are structurally very similar but are sub-classified into five groups based on their physiological functions (**Table 1.1**) and by their use of specific steroid hormone receptors (Miller, 1988).

| Hormone group | Steroid hormone group | Physiological behavior |
|---|---|---|
| **Corticosteroids** | Mineralcorticoids | Instruct renal tubules to retain sodium |
| | Glucocorticoid | Named for carbohydrate mobilizing properties, but have many other effects |
| **Sex hormones** | Estrogens | Induce female secondary sexual characteristics |
| | Androgens | Induce male secondary characteristics |
| | Progesterins | Essential for reproduction |

**Table 1.1 |Steroid Hormone Groups|**

The prototypical member of a sixth group, the seco-steroids (“broken ring”) which share structural and functional characteristics with the corticosteroids and sex hormones, is vitamin D (VitD), whose role in disease was elucidated by a series of observations. Sir Edward Mellandby, concerned with the high incidence of rickets in the United Kingdom, identified a factor in cod liver that could cure rickets. At the same time Huldshinsky and Chick *et al.* found that children suffering from rickets could also be cured by exposure to summer sunlight or artificially produced U.V light (reviewed in (DeLuca, 2014)). With these two pieces of information Professor Steenbock, with a series of animal experiments, correctly concluded that an inactive lipid in the diet and skin could be converted by UV light into an active substance able to prevent and cure

rickets (antirachitic) (Steenbock, 1924). The actual identification of VitD and its structure was not achieved until the 1940's. These discoveries led to the elimination of rickets as a major medical disease in the developed world. However, following the second world war an outbreak of idiopathic hypercalcemia, attributed to food fortification with VitD, resulted in skepticism over VitD supplementation for health. The discovery of the VitD endocrine system in 1970 and subsequent re-classification of VitD as a hormone re-stimulated interest in the field of VitD biology. The resurgence of interest in VitD was also, in part, due to the discovery that it functions through a nuclear receptor found in many tissues and cells not related to calcium or bones (Bhalla et al., 1983). Since then VitD has been heralded by some researches as the panacea of human disease, whilst others remain skeptical about the use of the pro-hormone beyond amelioration of bone-mineral health (Theodoratou et al., 2014). VitD supplementation is often suggested by clinical investigators, using epidemiological measures, as evidence for VitD playing a role in the suppression of many diseases. However, there remain very few adequately powered trials able to prove a cause-and-effect relationship in any human disease, except rickets. In this introduction I will describe both the synthesis and metabolism of VitD, its described biological functions (with emphasis on the immune system) and the possible implications of these functions for human disease.

## 1.2 Vitamin-D physiology/endocrinology

VitD is a fat-soluble steroid pro-hormone that requires several enzymatic steps for activation and inactivation. It is essential for both the absorption and regulation of calcium and thus plays a central role in bone mineralization and metabolism. There are two environmental sources of VitD, Vitamin $D_2$ (or Ergocalciferol) is a dietary component present in some plants and mushrooms, whilst most Vitamin $D_3$ (Cholecalciferol) is synthesized via photo-conversion from 7-dehydrocholesterol in the skin when exposed to UVB radiation from sunlight (Lehmann et al., 2001). The structural similarities between these pro-hormones and their biosynthetic pathways are shown in **Figure 1.1 a**. A small proportion of Vitamin $D_3$ can also be obtained from the diet with

the vast-majority coming from animal products (such as eggs and liver) and the highest source being fatty fish.

These pro-hormones are then carried in the bloodstream and undergo hydroxylation catalyzed by the enzymes CYP27A1 (also known as 25 vitamin D hydroxylase) or CYP2R1 in the liver to produce 25-hydroxy vitamin D (25 VitD), the major form of VitD circulating in the bloodstream. 25 VitD is further hydroxylated in the kidneys, catalyzed by the tightly regulated CYP27B1 enzyme (also known as 1-$\alpha$ vitamin D hydroxylase), to the hormone 1,25-dihydroxy vitamin $D_3$ (1,25 VitD) which is the most biologically active form. These chemical reactions are shown in **Figure 1.1 b**. Most VitD products are transported through the circulation by D-binding protein (DBP – also known as group-specific component globulin) (Omdahl et al., 2002), 1,25 VitD is lipid soluble and freely diffusible across cell membranes, thus not requiring transporter-mediated internalization. Metabolic inactivation of 1,25 VitD occurs in target tissues, as well as the kidneys through a chain of enzymatic reactions catalyzed via hydroxylation by CYP24A1 (Kong et al., 1999). These processes are summarized in **Figure 1.2**.

In response to low serum levels of calcium and/or phosphate, the parathyroid gland release parathyroid hormone (PTH) which stimulates gene transcription of *CYP27B1* (Hewison et al., 2000) in the kidneys, leading to increased circulating levels of 1,25 VitD. This increases circulating levels of calcium concentration through several mechanisms, including increased renal and intestinal absorption of calcium and enhanced osteoclast activity in the bone, which resorb skeletal calcium and release it into circulation. Serum levels of the active metabolite 1,25 VitD are so tightly regulated under normal circumstances that the levels are practically invariant. Both PTH and reduced serum calcium induce CYP27B1 gene transcription. Conversely 1,25 VitD acts in a negative feedback loop to inhibit both CYP27B1 transcription as well as PTH production and aids in its own degradation through activation of CYP24A1 gene transcription (**Figure 1.2**) (reviewed in (DeLuca, 2008; McGregor et al., 2014))**.** In addition (and independently of calcium levels), high serum concentrations of phosphate drives 1,25 VitD induced release of fibroblast growth factor 23 (FGF23) from osteocytes (Lanske et al., 2014). FGF23 adds a further layer of control as it inhibits CYP27B1 gene

transcription and activates CYP24A1. Thus 1,25 VitD represses PTH and, in concert with elevated phosphate, induces FGF23. Together these mechanisms protect from hypercalcemia and hyperphosphatemia which are both drivers of ectopic calcification.

There is also evidence to suggest that cells outside of the kidneys can express CYP27B1 protein, particularly cells of the immune system (Adams et al., 2014), establishing a potential for paracrine or autocrine function of VitD within immune cells (Adams and Hewison, 2012). Indeed, *in vitro* studies using different immune cells have shown that CYP27B1 is able to catalyze local conversion of 25 VitD to 1,25 VitD. However, the physiological consequences of this extra renal 1,25 VitD production remains controversial. Mouse knockout models have, in general, concluded that the expression of CYP27B1 in healthy mice is limited to kidneys without additional stimulus (Vanhooke et al., 2006).

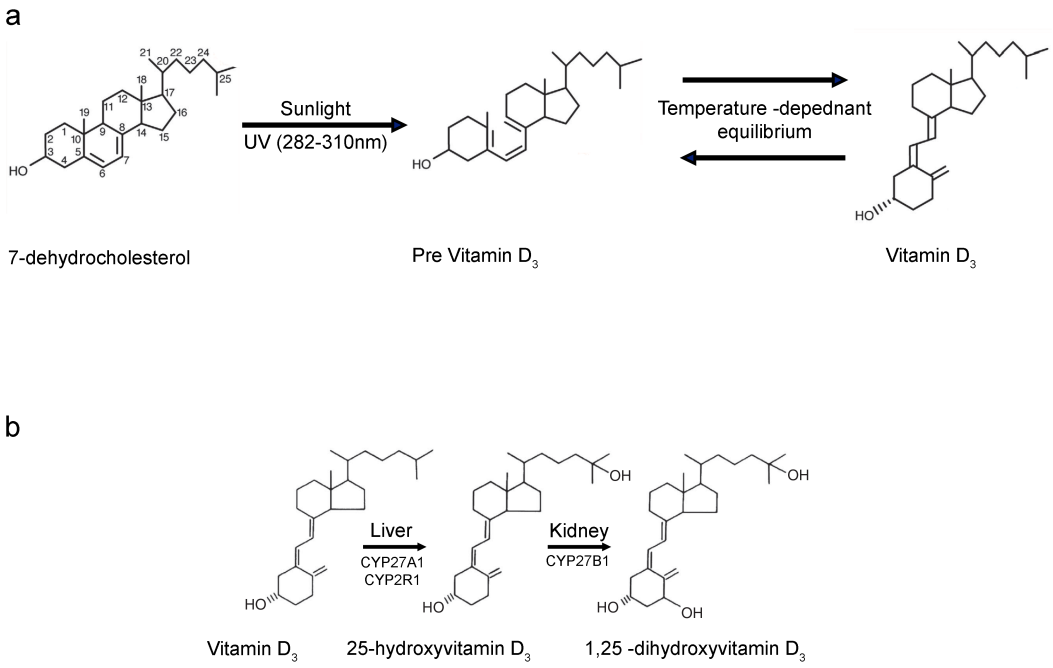


**Figure 1.1 |Structural representation showing activation of Vitamin D|**
(a) Conversion of 7-dehydroxycholesterol to pre-Vitamin $D_3$ by UV light at a wavelength of 282 – 310 nm, leading to open ring ("seco-steroid") structure. Equilibrium between different isomers, pre-Vitamin $D_3$ and Vitamin $D_3$ is a temperature dependent process. (b) Vitamin $D_3$ is subsequently converted to 25-hydroxyvitmain $D_3$ (25 ViD) through activity of either CYP27A1 or CYP2R1 present mainly in the liver, but also in cells of the immune system. Final activation to biologically active 1,25-dihydroxy vitamin $D_3$ (1,25 VitD) is then catalyzed by CYP27B1 present mainly in the kidney, but also cells of the immune system (modified from (DeLuca, 2014)).

a

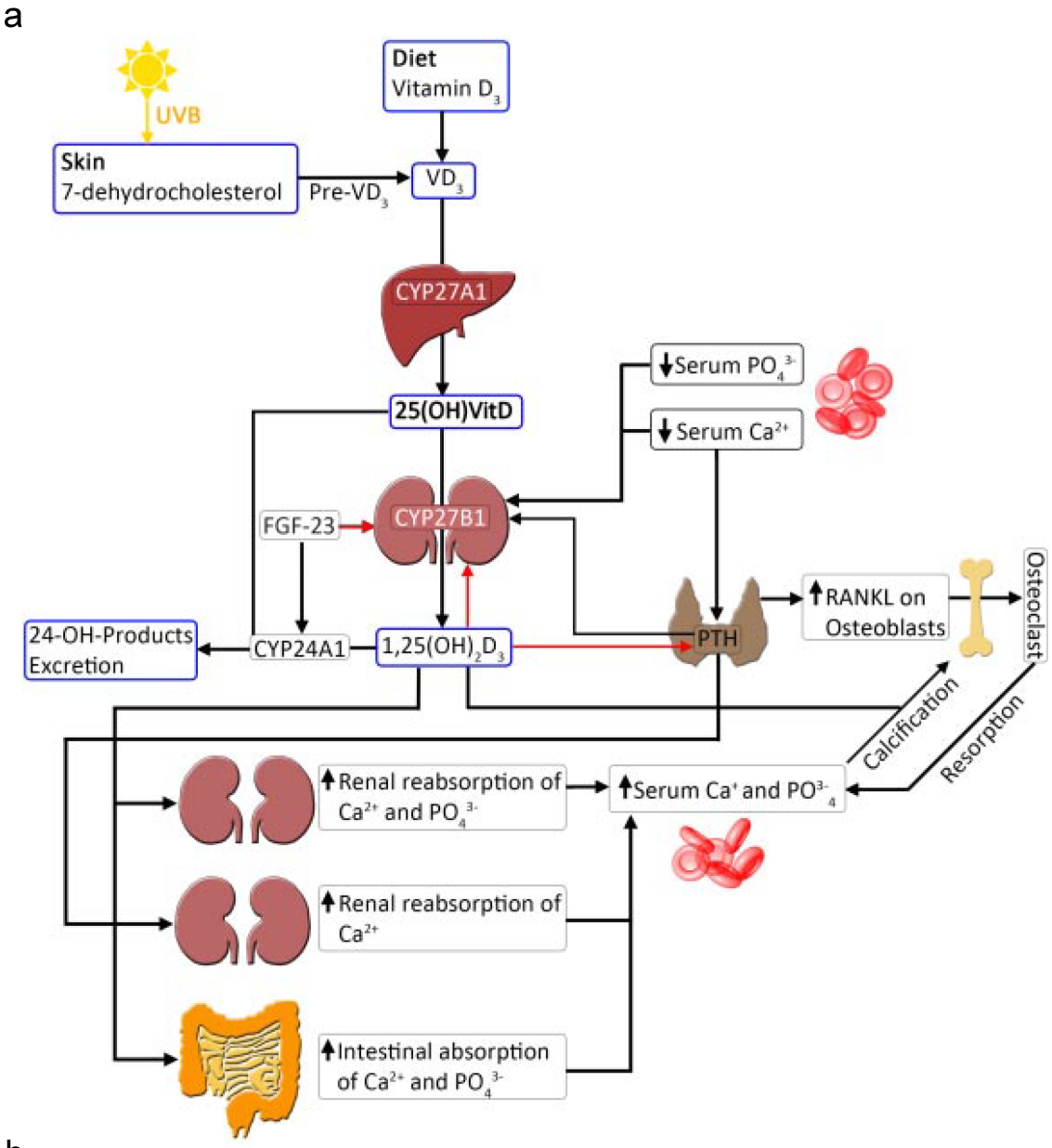


b

| Enhancing CYP27B1 | Inhibiting CYP27B1 |
|---|---|
| Hypocalcemia | FGF-23 |
| Hypophosphatemia | $1,25(OH)_2D_3$ |
| PTH | Dietary calcium intake* |
| Dietary calcium intake* | |

**Figure 1.2 | Effects of vitamin D on mineral biology and feedback control over VitD activation|**

(a) Schematic showing biogenesis of VitD. $VitD_3$ derived from either the diet or UVB irradiation in the skin is metabolized to 25(OH) VitD (25 VitD) in the liver through an enzymatic reaction catalyzed by CYP27A1. 25(OH) VitD is subsequently metabolized to the active form $1,25(OH)_2D_3$ (1,25 VitD) in the kidneys by CYP27B1. Both 25 VitD and 1,25 VitD are converted by CYP24A1 to 24 hydroxylated products and excreted. CYP27B1 is tightly regulated: a drop in serum calcium levels is detected by the parathyroid gland and results in secretion of parathyroid hormone (PTH). Both PTH and reduced serum calcium and phosphate concentration directly stimulate CYP27B1 transcription, and thus increased 1,25 VitD production. 1,25 VitD, in a negative feedback loop, down-regulates its own production by inhibiting CYP27B1 transcription as well as PTH production. 1,25 VitD has multiple systemic effects which ultimately result in restoration of serum calcium levels, as well as re-calcification of bones. FGF-23 is produced by osteocytes and decreases circulating concentrations of 1,25 VitD, through induction of CYP24A1 and suppression of CYP27B1. In the schematic, black arrows represent induction, red arrows represent inhibition. (b) factors controlling CYP27B1 activity. * a low calcium diet reduces extra-renal CYP27B1, particularly in the colon, and enhances renal CYP27B1.

## 1.3 Genomic actions of Vitamin D

VitD is estimated to regulate 3% of the human genome (Haussler et al., 1998) with the majority of 1,25 VitD effects being mediated through intracellular binding to the Vitamin D3 receptor (VDR) (Carlberg and Polly, 1998), a ligand-dependent transcription factor (TF). Binding promotes heterodimerisation with the retinoid X receptor (RXR) and subsequent binding of the VDR-RXR heterodimer to VitD response elements (VDREs) within the promoters or enhancers of VitD responsive genes (Carlberg and Polly, 1998).

RXRs dimerise in a ligand-dependent manner with the VDR, as well as several other nuclear receptors, with different functional outcomes (Lefebvre et al., 2010). Association with RXR is necessary for high affinity DNA binding of VDR. RXR heterodimers bind to motifs that consist of direct repeats (DR) containing the heptameric sequence AGGTCA. In most cases, DNA binding motifs of the RXR-VDR heterodimers are DR of the DR3 type (containing 3 spacer nucleotides between the DR motifs), whereas RXR- retinoic acid receptor alpha (RAR$\alpha$) dimers bind to DR2/5 type motifs (Lefebvre et al., 2010). The binding motif of VDR is shown in **Figure 1.3**, where it is contrasted with the related RAR$\alpha$ binding motif.

It has also been suggested that VitD has biological functions independent of regulating *de novo* gene transcription, through membrane VitD receptors. This possibility is based on data showing rapid activation (within minutes) of non-genomic signal transduction pathways upon stimulation with 1,25 VitD, thus leading to the speculation of a membrane VDR (mVDR) (Marcinkowska, 2001). However, this receptor has yet to be cloned.

### 1.3.1 The Vitamin D receptor, molecular mechanisms

The VDR is a member of the nuclear hormone receptor (NHR) superfamily. Nuclear receptors are intracellular transcription factors that regulate the activity of gene networks (Carlberg and Campbell, 2013). The VDR belongs to the Thyroid/Retinoid (class II) family, which also includes the thyroid receptor (TR), retinoic acid receptor (RAR) and the peroxisome proliferator–activated receptor (PPAR). These receptors

typically function as heterodimers generally associating with the RXR then binding to specific response elements in DNA. Nuclear hormone receptors share two highly conserved domain structures, a C-terminal ligand-binding domain (LBD) and a highly-conserved DNA-binding domain (DBD). The DBD, as the name suggests, docks the receptor to the specific response elements on genomic DNA.

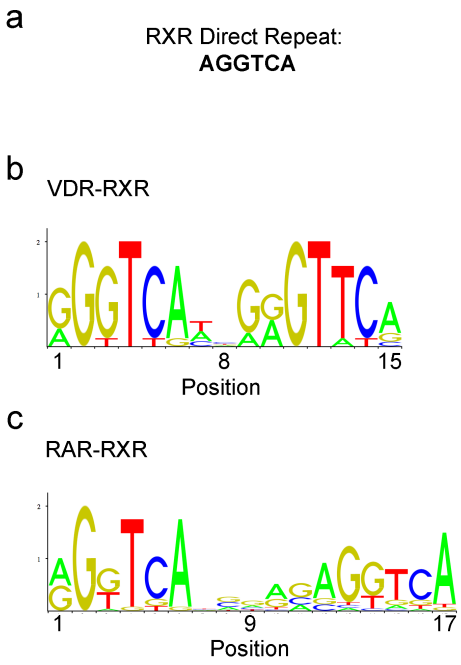


**Figure 1.3|RXR heterodimer binding motifs|**
(a) Direct repeat (DR) heptameric DNA sequence for RXR (b) Example of use of DR type DNA motif in VDR-RXR heterodimer and (c) in RAR-RXR heterodimer. Logos show schematic representation of frequency of nucleotides at each position in motifs, where frequency is proportional to size of nucleotide at given positions.

The LBD not only contains a binding pocket specific for cognate ligand (or hormone) but also contains a ligand-regulated transcriptional activation function (AF-2), which acts to recruit co-activating proteins such as TFIIB, a key component of the basic transcriptional apparatus required for gene transcription (MacDonald et al., 1995). These co-activating proteins can interact with transcriptional activation machinery as well as chromatin re-modelling proteins (Haussler et al., 2011). For example, direct ligand-dependant binding

of VDR and the histone acetyl-transferase (HAT) SRC-1 has been demonstrated (Masuyama et al., 1997). The structural domains of the VDR are shown in **Figure 1.4 a**.

Most NHR family members also contain amino acid sequences located N-terminally to the DBD. These domains have a transcriptional activation function-1 domain (AF-1). In contrast to the relatively conserved AF-2 sequence within the LBD, the AF-1 sequence shows less than 15% conservation even within subgroups. This lack of sequence homology both within AF-1, and more generally in the N-terminal region, may help explain how closely related steroid receptors can differentially regulate gene promoters containing the same binding sequences *in vivo*.

As mentioned in section 1.3, the VDR-RXR heterodimer typically recognises a specific sequence (known as a VDRE) comprised of two hexameric nucleotide half sites separated by three base-pairs known as "DR3" binding sites (Kerner et al., 1989; Umesono et al., 1991) (**Figure 1.3**). The VDR itself has little transcriptional activity so requires recruitment of a group of co-regulatory proteins to form a co-regulatory complex (McKenna and O'Malley, 2002). Within this complex at least one of the components will contain a VDR-interacting member and usually comprises numerous sub-units. The complex can include enzymes with ATPase activity that can modify the nucleosome structure, enzymes with histone modifying abilities (such as SRC-1 and p300 (Masuyama et al., 1997), and "mediator complexes" that aid in recruitment of RNA polymerases (such as TFIIB (MacDonald et al., 1995). The recruitment of the complex seems to be gene specific, with specific VDREs in specific genes leading to the recruitment of a co-regulatory complex consisting of different proteins (Pike et al., 2012). Close to 22,000 non-overlapping VDR peaks are specified by public ChIP-seq (depending on cell type and context). The observation that 75% of these peaks are cell-type specific (Tuoresmäki et al., 2014), in combination with expression data showing that different sets of genes are up and downregulated in response to VitD treatment (Pálmer et al., 2003; Suzuki et al., 2006; Wang et al., 2005; White et al., 2005), suggest a highly cell-type specific mode of action for VitD. Thus, each cell type will have a unique VDR "cistrome" (the binding sites on the genome for a specific transcription factor under specific conditions, in a given cell type). In osteoblasts, the cistrome consists of

approximately 1200 sites under basal conditions, which increased to 8000 sites following stimulation with 1,25 VitD (Meyer et al., 2010). Although the binding sites present in the absence of 1,25 VitD largely overlap with those present after 1,25 VitD stimulation, the data indicates occupancy at a select set of loci do not require ligand activation (Meyer et al., 2010), which is in contrast to other steroid receptors. Interestingly, these loci seem to have a lower rate of DR3-type sequences compared to 1,25 VitD dependent loci (Heikkinen et al., 2011) and are associated with VDR repressed genes, such as CYP27B1 (Turunen et al., 2007). Genome wide analysis of VDR loci combined with new insights from the ENCODE (2012) project confirm observations that the VDR is equally likely to bind upstream and downstream of the target transcriptional start site (tss), that VDR binding can occur at great distances (up to 1 mega base (MB) from genes tss) from regulated genes (Carlberg, 2014) and binding sites are located in both intergenic and non-coding intronic or intragenic regions (Ramagopalan et al., 2010).

### 1.3.2 The Vitamin D receptor, isotypes

Multiple isoforms of NHRs can be derived from separate genes, as with the RAR and RXR. In contrast, some NHR isoforms are generated through differential promoter usage or alternative splicing. This is seen in variant forms of both the progesterone receptor (PR) (Kastner et al., 1990) and PPARs (Elbrecht et al., 1996). Receptor isoforms can show important differences in function. In the case of the PR the isoforms exhibit striking differences in promoter specificity.

The human *VDR* gene contains a promoter and 6 regulatory regions (exons 1a-1f), as well as exons 2-9, which encode the full-length 48kDa protein (**Figure 1.4 a**). The VDR differs from other NHRs in that it has a short N-terminal region (also referred to as the A/B domain) of just 23 amino acids. Several isoforms of the VDR have previously been reported in the literature. One such isoform is the VDRB1 isoform, which is a splice variant of the canonical VDR expressed by an alternative start site within intron 1d, leading to a 50aa extension of the A/B domain **(Figure 1.4 b**). The isoform was identified in intestinal and kidney cell lines as well as human kidneys. This isoform shows different

transcriptional potential (transcription of CYP24A1 by VDRB1 is lower than by VDRA on the rat 24-hydroxylase promoter), compared to the canonical VDRA form (Sunn et al., 2001). Additionally, there is a less well-characterised 75kDa (kDa) VDR present in non-activated lymphocytes (Diaz et al., 2011), which is contradictory to the dogma of the VDR being expressed solely in activated immune cells. Finally, there is indirect evidence suggesting the existence of a membrane bound 64.5 kDa VDR, identified in chick intestinal epithelium, able to block 1,25 VitD rapid signaling (through protein kinase C) in rat chondrocytes (Nemere et al., 1998). As of yet, there is little evidence to suggest that these alternative isoforms differ dramatically in their function to the canonical VDR.

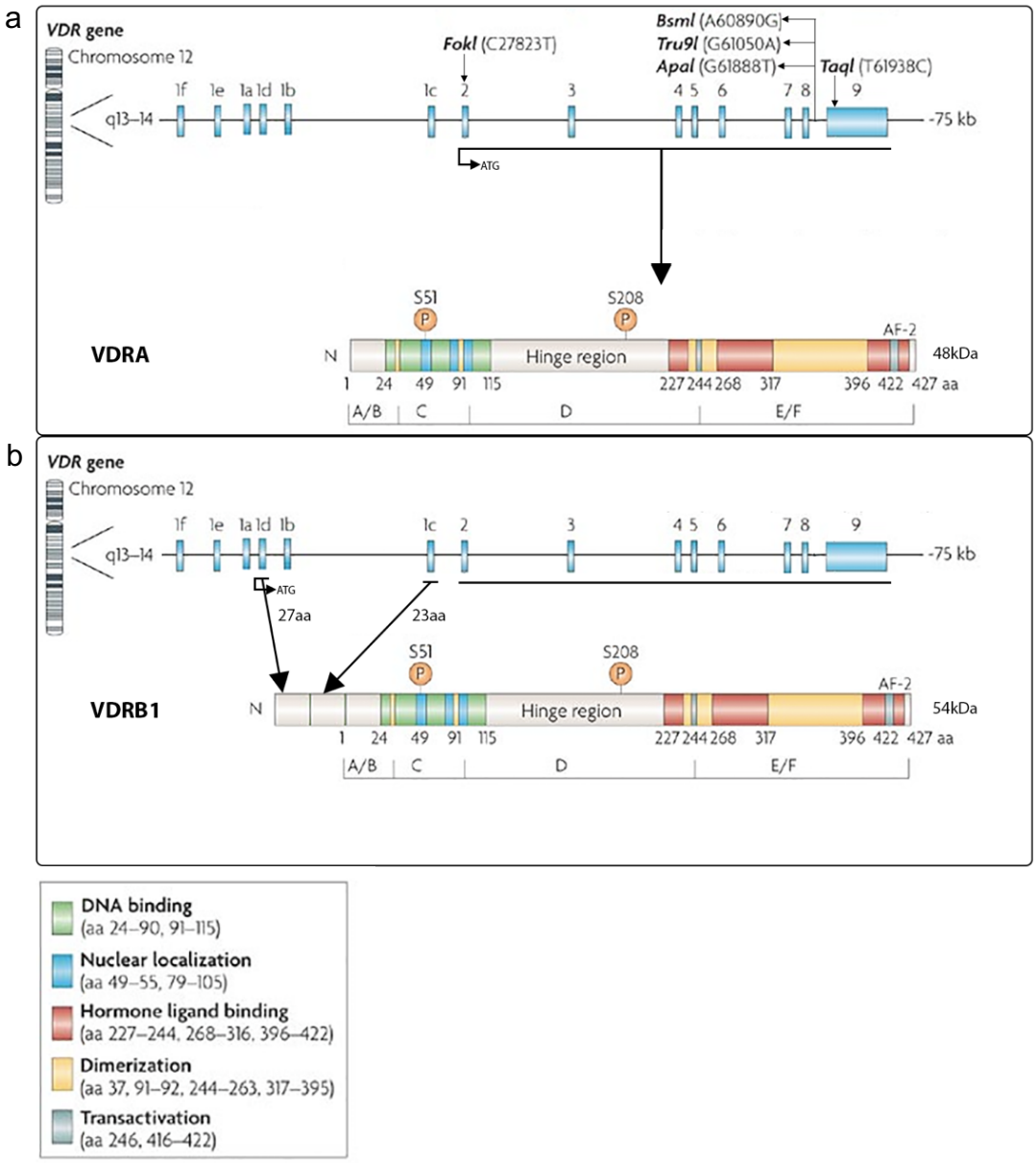


**Figure 1.4|The VitD Receptor (VDR)|**

(a) The VDR gene located on chromosome 12q has 6 regulatory regions, 1a-1f and exons 2-9 which encode the canonical VDR-A isotype, which has 6 broad domains (A-F). Functional domains are colour coded and consist of the highly-conserved DNA binding (green) and hormone ligand-binding domain (red). VDR bound to ligand can be stabalised by phosphorylation of serine 51 by protein kinase C and serine 208 by casein kinase II. Ligand bound VDR allows interaction of AF-2 region with stimulatory co-activators. Non-synonymous (*FokI*) and synonymous (*BsmI*, *ApaI*, *TaqI* and *Tru9I*) single-nucleotide polymorphisms (SNPs) have been identified in *VDR* and their location indicated on the gene map. (b) An alternative start site within exon 1d and subsequent alternative splicing, leads to generation of a 50 amino acid addition to the N-terminus of the VDR extending the A/B domain. This isoform is known as VDR-B1 which is 54kDa as opposed to the canonical 48kDa VDR-A. Figure adapted from (Deeb et al., 2007)

### 1.3.3 The Vitamin D receptor and the epigenome

Epigenetics is a term denoting the set of processes that alter gene activity without altering DNA sequences. Maintenance of normal functioning of cellular processes is highly dependent on the interactions between different epigenetic mechanisms. These include DNA methylation and histone modifications, discussed in more detail below.

Genomic DNA is intimately associated with chromatin, forming structures known as nucleosomes. At a given promoter or enhancer, the structure arising from DNA methylation and/or histone modifications establishes whether the chromatin is accessible (active) or non-accessible (repressed) to transcription factors and associated gene transcription machinery. The close association of genomic DNA and nucleosomes, referred to as chromatin, therefore has an intrinsic repressive potential (Razin, 1998). Thus, epigenetic marks on genomic DNA provide stable and long lasting regulatory "decisions" about gene expression, as is observed in terminally differentiated cells (Mohn and Schübeler, 2009), representing a form of cellular "decision" for phenotype, especially as daughter cells "inherit" epigenetic information from parent cells. Despite the long-lasting potential of these modifications, some regions of the epigenome respond to environmental stimuli and signals (such as 1,25 VitD signalling through VDR) in a highly dynamic but regulated fashion (Fetahu et al., 2014).

One way to assess global genome accessibility, is to determine regions of the genome that are nucleosome depleted, and therefore accessible using a technique called FAIRE-seq (Formaldehyde-Assisted Isolation of Regulatory Elements) (Giresi et al., 2007). The only study assessing this in relation to VitD is a time-course FAIRE-seq on THP-1 cells (Seuter et al., 2013) (a human monocyte cell line). In this study 87.4%, of the 1034 most prominent VDR ChIP-seq peaks aligned with regions of open chromatin. More interestingly, however, at 165 of these loci there was a strong 1,25 VitD-dependent increase in chromatin accessibility observed within as little as two hours of treatment. This is a strong indication that VitD/VDR can alter the epigenetic accessibility of loci in a targeted manner.

#### 1.3.3.1 Vitamin D and DNA methylation

The most studied epigenetic mark is DNA methylation which occurs on the cytosine of CpG (cytosine followed by guanaine, used to distinguish the single stranded linear sequence from CG base pairing) sequences (Bird, 1980). Regions of DNA with high frequencies of CpG sites are known as CpG islands and hyper-methylation at these regions usually indicates a transcriptionally inactive chromatin state (Herman and Baylin, 2003). The majority of epigenetic methylation studies have been carried out in the field of cancer biology and very few have looked at the effect of VitD on this process. One such study has shown that treatment of a triple-negative breast cancer cell line (one that does not express the oestrogen receptor (ER), PR or Her2/neu), MDA-MB-231, with 1,25 VitD reduced the methylation at the promoter of the e-cadherin promoter (Lopes et al., 2012). A second study showed demethylation of the PDZ-LIM domain-containing protein 2 promoter, which led to increased protein expression (Vanoirbeek et al., 2014). Additionally, site specific methylation of the p21 promoter was observed in epithelial cell lines, in a cell line specific manner (Doig et al., 2013). In summary, VitD can regulate specific DNA methylation processes but the mechanisms require further investigation.

#### 1.3.3.2 VitD and Histone modifications

Chromatin is a complex of chromosomal DNA associated with proteins in the nucleus. Within the chromatin, genomic DNA is wrapped around histone proteins in units called nucleosomes. A single nucleosome has 147 basepairs (bp) of DNA coupled with an octomeric core of histone proteins. These consist of a pair of H3-H4 histone dimers and a pair of H2A-H2B dimers (**Figure 1.5**). In the process of wrapping, the histones tails are left exposed and these N-terminal tails can undergo post-translational modifications which allow nucleosomes to shift, the chromatin to relax and genes to become activated (Campos and Reinberg, 2009). In this way histone modifications can act as identifiers for sites of transcription factor activity (Bernstein et al., 2007). Histone modifications are complex. They can occur on different histone proteins (H1 to H5), at different histone tail residues (such as lysine, arginine and serine) and positions, can

involve different chemical modifications (methylation, acetylation or phosphorylation) and can involve different degrees of methylation (mono, di and/or trimethylation). A particular set of permutations at a given location contribute to a "histone-code" which will ultimately fine-tune the expression of a gene, or set of genes (Jenuwein and Allis, 2001). In general, histone acetylation (ac) of a lysine (K) residue is associated with transcriptional activation whereas the effect of histone methylation (me) depends on the amino acid location and type as well as the degree of methylation (**Figure 1.5** and **Table 1.2**). Methylation of Histone 3 (H3) at K4 is linked to transcriptional activation whereas methylation of H3 at K9 or K27 (H3K9me and H3K27me, respectively) as well as H4 at K20 (H4K20me) is associated with transcriptional repression (Fetahu et al., 2014). More recently, H3K27Ac has been shown to distinguish "active" enhancers from "poised" enhancers containing only H3K4me1 in embryonic stem cells. These poised enhancers are not associated with active gene expression but remain in an accessible state awaiting external cues to become active and initiate gene transcription (Creyghton et al., 2010).

Active 1,25 VitD bound to VDR can both transactivate and transrepress target genes. These opposing functions probably ustilise different mechanisms and rely on specific VDRE motifs (Fetahu et al., 2014). Typically, non-liganded VDR forms complexes with co-repressor proteins such as histone-deacetylases (HDACs) (Malinen et al., 2008) whereas 1,25 VitD bound VDR interacts instead with acetyl histone-transferases (HATs) (Fetahu et al., 2014). Many of the members of the co-regulatory complex, including SRC1, 2 and 3 p300 and CBP, recruited by VDR, have lysine acetyltransferase activity, and treatment of THP-1 cells with 1,25 VitD leads to increased H3K27Ac in the promoter of many VitD target genes (Seuter et al., 2013). Additionally, in MDA-MB453 breast cancer cells treatment with 1,25 VitD regulates the expression of P21 in a process involving both histone acetylation (H3K9ac) and methylation (H3K4me2) (Saramäki et al., 2009).

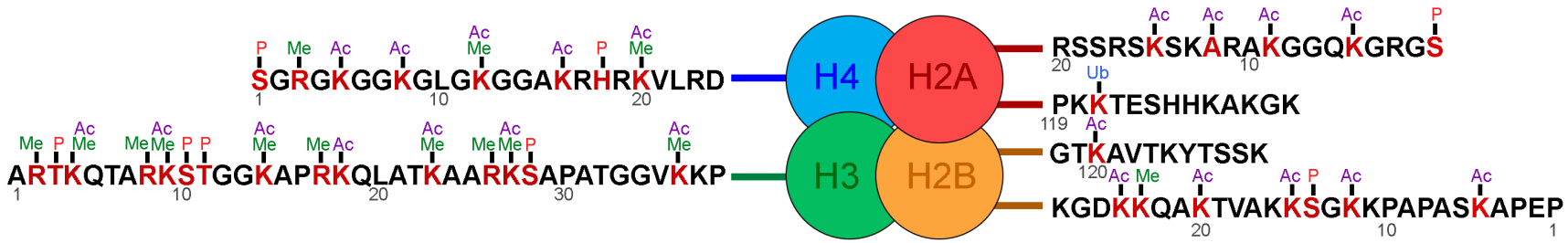


**Figure 1.5|Representation of histone modifications|**
The main four modifications; Acetylation, methylation, ubiquitination and phosphorylation color coded as shown in key, of the four core histones; H4, H3, H2A and H2B (based on (Rodríguez-Paredes and Esteller, 2011)).

| Type of modification | Histone | | | | |
|---|---|---|---|---|---|
| | **H3K4** | **H3K9** | **H3K14** | **H3K27** | **H2BK5** |
| mono-methylation | activation | activation | | activation | activation |
| di-methylation | | repression | | repression | |
| tri-methylation | activation | repression | | repression | |
| acetylation | | activation | activation | activation | |

**Table 1.2|Examples of histone modifications|**
A non-exhaustive list of methylation and acetylation changes on histone tails and their effect on chromatin.

## 1.4 Vitamin-D in the immune system

A study carried out over a century ago showing that an epidermal form of tuberculosis (TB) could be cured using light irradiation, coupled with the discovery U.V light promotes epidermal synthesis of VitD, heralded the beginning of interest on the effects of VitD in the immune system (Møller et al., 2005). Interest in these studies soon dwindled with the advent of antibiotics. In 2006, a seminal paper in the field revealed that pathogens induced an intracrine VitD system. The paper by Liu *et al.* indicated that monocytes activated via toll-like receptor (TLR) 1 and TLR2 upregulated the expression of both the VDR and CYP27B1 and subsequent treatment with 1,25 VitD induced the expression of the antimicrobial peptide cathelicidin as well as CYP24A1, leading to intracellular pathogen killing (Liu et al., 2006). This confirmed earlier observations of extra-renal production of 1,25 VitD from 25 VitD, leading to elevated serum 1,25 VitD in patients with granulomatous diseases (Kallas et al., 2010). Combined with early observations of VDR expression in haematopoietic cells (Bhalla et al., 1983), these findings supply strong evidence to suggest that the most biologically active form of VitD (1,25 VitD) can both be produced by cells of the immune system and that these cells subsequently respond to the 1,25 VitD to combat disease.

The VDR is ubiquitously expressed in immune cells, including activated $CD4^+$ and $CD8^+$ T lymphocytes as well as cells of the innate immune system, such as macrophages and dendritic cells (DCs). Immune cells not only express the VDR but many (including T cells, monocytes and DCs) contain the machinery for producing biologically active 1,25 VitD through inducible expression of the CYP27B1 (Provvedini et al., 1983). These findings, along with strong epidemiological evidence linking VitD deficiency to multiple autoimmune diseases, suggest a physiological role for VitD in immune homeostasis. Experimentally, VitD metabolites, particularly 1,25 VitD, have multiple effects on immune system functioning that are both antimicrobial and immunoregulatory. Thus, VitD seems to play a dichotomous role inducing intracellular antimicrobial actions of macrophages and monocytes (Rook et al., 1986), whilst simultaneously working to regulate adaptive immune responses (via multiple mechanisms reviewed in (Hewison, 2012)).

### 1.4.1 Immunoregulatory actions

VitD has clear effects on immune system functioning, classically characterised by inhibition of proliferation (Lemire et al., 1985; Rigby et al., 1984), interleukin (IL)-2 (Bhalla et al., 1986) and interferon (IFN)-γ production by $CD4^+$ T cells (Rigby et al., 1987) and reduced cytotoxicity of $CD8^+$ T cells (Meehan et al., 1992). While VitD also enhances IL-4 production by $CD4^+$ T cells (Boonstra et al., 2001; Mahon et al., 2003), its ability to enhance regulatory T cell differentiation is particularly important. Not only does VitD induce differentiation of suppressive $FoxP3^+$ regulatory T cells (Tregs) (Chambers and Hawrylowicz, 2011), the most critical of immunoregulatory T cells for the prevention of autoimmune diseases in humans, but also IL-10-producing $FoxP3^-$ type 1 regulatory T cells (Tr1 cells) (Mora et al., 2008) as well as IL-10 producing B cells (Heine et al., 2008). The immunomodulatory effects of VitD are mediated through both direct effects on adaptive immune cells and indirectly through modification of antigen presenting cells (APCs) function (Griffin et al., 2001; Mahon et al., 2003; Mora et al., 2008).

#### 1.4.1.1 Immunoregulatory actions on antigen presenting cells

DCs play a central role in the initiation, magnitude and quality of the adaptive immune response and are known as the "professional" APCs of the immune system. DCs constitutively express the VDR (Brennan et al., 1987). During DC differentiation from monocytes they decrease expression of the monocytic marker CD14, a process that is inhibited by 1,25 VitD leading to impaired ability to stimulate T cells (Penna and Adorini, 2000). VitD not only inhibits the maturation and antigen-presenting capacity of DCs but induces them to behave in a "tolerogenic" manner, preferentially stimulating naïve T cells both *in vitro* and *in vivo* (Farias et al., 2013) to mature into $FoxP3^+$ Tregs and Tr1 cells and enhancing the suppressive activity of these regulatory T cells. This effect is achieved by decreasing surface expression of major histocompatibility complex II (MHC-II)(for example HLA-DR) as well as co-stimulatory molecules (CD40, CD80 and CD86) (Griffin et al., 2001). In addition, inhibition of DC-derived IL-12 production by VitD is also of great relevance, as IL-12 is a central mediator in T-helper (Th)1 differentiation, a cell population intimately associated with inflammatory outcomes in multiple diseases

(Moss et al., 2004). In a similar fashion, 1,25 VitD reduces the APC and T cell stimulatory capacities of monocytes and macrophages (Almerighi et al., 2009) as well as inhibiting their production of pro-inflammatory cytokines, notably IL-1, IL-6, TNF-$\alpha$, IL-8 and IL-12 (Almerighi et al., 2009; D'Ambrosio et al., 1998; Giulietti et al., 2007).

#### 1.4.1.2 Direct immunoregulatory actions on T cells

T cells do not constitutively express the VDR, but its expression is dramatically increased upon activation via the T cell receptor (TCR) (stimulation through CD3/CD28) (Essen et al., 2010) or by triggering downstream signalling molecules through PMA/ionomycin (Baeke et al., 2010a). However, expression levels and kinetics of VDR activation vary between stimulation conditions (which may explain conflicting results regarding T cell proliferation (Lacey et al., 1987; Rigby et al., 1984)). Another confounding factor in the study of the response of T cells to VitD is its differential effects in memory (characterized by CD45RO expression) and naïve (characterized by CD45RA expression) T cells. Memory T cells are the major target of VitD. Naïve T cell proliferation is largely unaffected and the suppressive effect of VitD on cytokine production is delayed in this population (Müller and Bendtzen, 1993). Although some claim lower expression of VDR in naïve cells (Mora et al., 2008) this has never been directly assessed. What is clear is that T cells do not express the VDR at baseline and require activation to upregulate the receptor, and naïve cells primed by activation through CD3/CD28 and rested for 24h retain expression of the VDR (Essen et al., 2010). However, the kinetics of VDR upregulation in naïve vs memory T cells has not been tested. A final complication is that very few studies of direct VDR expression and effect of VitD on T cells distinguish between $CD4^+$ and $CD8^+$ T cells. Thus, all results mentioned above need to be interpreted with the caveat that effects from $CD8^+$ T cells cannot be excluded.

VitD directly alters cytokine production from $CD4^+$ T cells. In general, 1,25 VitD inhibits the production of pro-inflammatory cytokines such as IL-2, IFN-$\gamma$, IL-17 and IL-21, which are predominantly produced by Th1 and Th17 lineages (Boonstra et al., 2001; Jeffery et al., 2009; Mahon et al., 2003). Effects on Th2 cytokines is less clear with indications of both inhibition of Th2 cytokines (Staeva-Vieira and Freedman, 2002) and

induction of GATA-3 (the master transcription factor responsible for Th2 cell fate) as well as Th2 cytokines (Boonstra et al., 2001). Additionally, in concert with the induction of Tregs through VitD-mediated tolerogenic DC production, VitD seems to have a direct effect on Treg generation. Indeed, VitD is able to induce FoxP3 (the master transcription factor responsible for regulatory T cell fate), CTLA-4 and IL-10 from T cells in the absence of APCs (Barrat et al., 2002; Jeffery et al., 2009). Interestingly, both publications showed little effect of VitD treatment on $CD4^+$ T cell proliferation, which is contrary to the classical effects of inhibition of proliferation (Rigby et al., 1984), suggesting that the *in vitro* model may not reflect *in vivo* effects. Surprisingly, the ability of VitD to increase CTLA-4 expression is actually increased in the presence of Th17 skewing conditions (Jeffery et al., 2015). Additionally, a VitD analogue (TX527) is able to trigger the emergence of $CD4^+CD25^{high}CD127^{low}$ Treg phenotype, a phenotype associated with "classical Tregs" and strong immunosuppressive ability (Baeke et al., 2011).

VitD also has a profound effect on the migratory signature of $CD4^+$ T cells by inducing expression of appropriate chemokine receptors. These imprint both a skin-homing phenotype including (CCR4 and CCR10 (Baeke et al., 2011; Sigmundsdottir et al., 2007)) and impart the ability to migrate to sites of inflammation (by inducing CCR5, CXCR3, and CXCR6 (Baeke et al., 2011)).

### 1.4.2 Antimicrobial actions on monocytes and macrophages

Monocytes and macrophages are central players of the innate immune compartment, whose role is to detect and eliminate pathogens, acting as a first line of defence. VitD is known to be vital as a mediator of the innate immune response, enhancing antimicrobial properties of innate immune cells (Agrawal and Yin, 2014).

Monocyte activation with IFNγ or LPS, results in up-regulation of both CYP27B1 as well as the VDR (Fabri et al., 2011). Autocrine engagement of the VDR results in production of natural anti-microbial peptides, such as cathelicidin antimicrobial peptide (CAMP) and β-defensin 4 (DEFB4) (Wang et al., 2004), enhancing innate immune clearance of pathogen. Production of CAMP is further increased by the presence of pro-

inflammatory IL-17, synergising to remove inciting pathogens. Likewise, active 1,25 VitD can activate other innate immune cells, such as monocytes and macrophages, promoting proliferation and secretion of highly inflammatory IL-1 (Baeke et al., 2010b).

Though a direct mechanistic link has been reported between VitD and clearance of tuberculosis (see section 1.4), a process involving VitD effects on monocytes and increased antimicrobial peptide cathelicidin (see section 1.4) (Liu et al., 2006), indirect evidence of benefits of VitD for clearance of other types of infections also exists. Epidemiological evidence links VitD deficiency with increased rates of respiratory infections (Ginde et al., 2009; Laaksi et al., 2007) as well as suggestions of epidemic winter influenza being a result of VitD deficiency . These studies indicate a role for VitD in clearance of a range of infections and the mechanism is likely to be through antimicrobial action like those seen in tuberculosis infection. But this has not been experimentally proven.

## 1.5 Implications for disease

VitD metabolism allows immune cells to autonomously modulate their own responses (see section 1.2), but to achieve optimal functioning of this autocrine/paracrine loop, availability of 25 VitD is crucial. The optimum level of VitD is still a matter of debate. VitD status is most commonly determined by measuring 25 VitD in serum. There are several pitfalls in the measurement of VitD (McGregor et al., 2014) and some disagreement over definitions of VitD status in humans (Hewison, 2012). For several years VitD status was defined based on the absence or presence of rachitic bone disease and a cut-off serum level of <20 nM (8 ng/mL) was used. Since then, various studies have led to the endorsement of the term “Vitamin D insufficiency” to define people with sub-optimal levels of VitD but who do not have rachitic bone disease. In the UK, it is accepted that 25 VitD concentrations of <50 nM represent VitD deficiency, 50–75 nM insufficiency, >75 nM VitD repletion with 75–150 nM optimal VitD status. What is also clear is that for different clinical and biological readouts this value may vary considerably. A recent report by the institute of medicine (IOM) defined insufficiency as subjects with suboptimal VitD status (<75 nM serum 25 VitD) who did not have

rachitic bone disease, which in turn is termed deficiency (<20 nM 25 VitD) (reviewed in (Holick, 2009)).

Nonetheless, VitD sufficiency has been associated with a reduced risk of many cancers and insufficiency is associated with multiple sclerosis (Sotirchos et al., 2016), inflammatory bowel disease (Dadaei et al., 2015), type 1 diabetes and rheumatoid arthritis (Hong et al., 2014). VitD also prevents acute graft rejection after liver, kidney and heart transplantation (Stein and Shane, 2011). Human trials of VitD repletion in allograft rejection are limited. In kidney transplant recipients calcitriol (another name for 1,25 VitD) supplementation was associated with fewer episodes of acute cellular rejection (Tanaci et al., 2003) as well as reduced requirement for glucocorticoid treatment (Uyar et al., 2006). Reduced co-stimulatory (CD80 and CD28) and HLA-DR in kidney transplant recipients suggests a mechanism for allograft survival (Ahmadpoor et al., 2009). Finally, VitD deficiency is implicated as a risk factor for cardiovascular disease (CVD) (Gunta et al., 2013) and CKD (Sterling et al., 2012). These data suggest a link between VitD status and a range of disorders that are either mediated or exacerbated by the immune system.

### 1.5.1 Vitamin D in chronic kidney disease

As described in section 1.2, normal functioning of the kidneys is crucial for the synthesis of 1,25 VitD. Adding to this, VitD deficiency (measured by 25 VitD in serum) is high in patients with CKD, with estimates ranging anywhere from 20 to 85% depending partly on stage of disease (Ali et al., 2009; Satirapoj et al., 2013). Strong associations have been found between VitD deficiency and all-cause mortality in patients with CKD (Jayedi et al., 2017). It is becoming increasingly apparent that chronic low grade inflammation (a hallmark of CKD) is an important factor in the increased risk of mortality observed in CKD (Querfeld, 2013).

Few randomised placebo-controlled, double blind studies have examined the utility of VitD supplementation as a therapeutic in CKD, showing both that supplementation is safe and effective at maintaining sufficient serum 25 VitD levels as

well as decreasing inflammatory cytokine levels (Agrawal and Yin, 2014). Animal models have demonstrated the ability of VitD to control inflammation and thus prevent CKD (Tan et al., 2008). These models coupled with a plethora of *in vitro* data showing the immunomodulatory effect of VitD (discussed in section 1.4), support the notion of a mechanistic link between VitD supplementation in the immune system and beneficial outcomes in patients with CKD. To date no supplementation trials have demonstrated a direct link between VitD supplementation, the immune system and beneficial outcomes observed in CKD patients.

### 1.5.2 Issues in Vitamin D research

There are several issues that cloud the interpretation of clinical VitD research data. First, reliably assessing VitD status and activity is itself a challenge (Janssen et al., 2012). Measurement of serum 25 VitD concentration is widely used because this species has a 3-4 week half-life, whereas the biologically most active VitD species - 1,25 VitD - has a life-life of only hours. 25 VitD measurement is an indirect test as it does not measure the most active vitamin D species and does not accurately predict VitD concentrations in tissues. The biological function of VitD can also be modulated by polymorphisms in VitD binding protein and the VDR (see **Figure 1.4 a** for VDR polymorphisms), which are not accounted for in currently available trials. This is relevant because up to 3% of the human genome can be influenced by VitD (Bouillon et al., 2008), including steroid sensitivity (Nanzer et al., 2013). Additionally, there remains controversy over the accuracy of different VitD assays. Standardisation of assays has recently been improved but is still not perfect (Fraser and Milan, 2013). Second, as there is lack of consensus on what should constitute repletion in interventional trials, seasonal (UVB-driven) effects on study cohorts' serum VitD concentrations are important and relevant to patients with CKD, on dialysis or after renal transplantation (Elder, 2007).

Third, the species and route of administration of VitD treatment used in interventional studies is confounding. There are 6-8 different possible forms of VitD, including ergocalciferol, cholecalciferol, calcidiol, calcitriol, 1-alfacalcidol and paricalcitol, with almost no head to head studies comparing them. These VitD forms

have different affinities for the VDR, potencies, biological activities, and side-effect profiles (for a detailed discussion see (Kalantar-Zadeh and Kovesdy, 2009)). Further variables include the route (oral, intramuscular and intravenous – the latter confers greater bioavailability) and frequency of administration, whether daily, weekly or monthly. Additionally, although there is a high prevalence of VitD insufficiency, there is no consensus dosing strategy for VitD repletion.

Lastly, and most importantly, the optimum marker denoting biological VitD repletion has yet to be determined. Although biochemical markers (principally PTH and alkaline phosphatase) have traditionally been used to monitor repletion, the reliability and clinical relevance of PTH levels to infer changes in 25 VitD levels has been called into question (Boudville and Hodsman, 2006; McGregor et al., 2014).

## 1.6 Hypothesis and aims

Given the well-established, immunoregulatory actions of VitD and links of VitD deficiency with disease, this thesis delineates the mechanisms underlying its immune function both *in vivo* and *in vitro*. Individual hypotheses and aims will be provided for each chapter.

*In vivo*: We hypothesised that oral repletion with cholecalciferol in VitD insufficient/deficient adult patients with CKD stage 3b/4 over 52 weeks would ameliorate systemic inflammation. The work in this thesis focused solely on the *in vivo* effects of VitD on immune function

*In vitro:* We hypothesised that VitD treatment of $CD4^+$ T cells would, through binding of liganded VDR, lead to epigenetic modifications affecting genes involved in the regulation of cytokine production.

We aimed to test this hypothesis by:

a) Dissecting the signalling cascades induced by VitD treatment responsible for the regulation of cytokine expression, particularly IL-10, in $CD4^+$ T cells.

b) Studying the mechanisms underlying VitD induced IL-10 production, identified in a), and linking expression of the molecules involved to hypothesised epigenetic modifications induced by VDR binding.

# 2. MATERIALS AND METHODS

## 2.1 Clinical trial

### 2.1.1 Clinical trial design

Fifty adult patients (age 18-75) with "early" CKD (clinical stages 3b-4), mild CVD and hypovitaminosis D (serum 25 (OH)D levels between 12.5 to 75 nM) were recruited into the trial following institutional approval. Patients were excluded from recruitment if they met the following criteria: history of diabetes mellitus, total serum calcium ≥2.55 mmol/L, anaemia (Hb <10.0 g/dL or taking regular erythropoiesis stimulating agents), known malignancy, heart failure, uncontrolled hypertension (BP >150/90 mmHg despite medication), persistent hypertension during follow-up, significant valvular heart disease, conditions that may influence collagen metabolism such as recent (<6 months) surgery or trauma, fibrotic diseases or active inflammatory conditions, immunosuppressive medications, presence of arterio-venous fistula for dialysis access, and history of previous myocardial infarction.

Patients were randomized, in a double blinded fasion, to receive either cholecalciferol ($VitD_3$) or placebo. The trial schedule relevant for this thesis is shown in **Table 2.1**. Directly observed oral cholecalciferol (100,000 international units (IU)) was administered to the trial participants at 0, 4 ,8 ,12 ,24 and 42 weeks. This dose is proven to be safe and effective in CKD patients (Chandra et al., 2008). Serum 25 VitD (using isotope-dilution liquid chromatography–tandem mass spectrometry (ID-LC-MS/MS) with a stable-isotope-labelled internal standard (IS)) was measured at 0 and 52 weeks to monitor repletion. Blood was collected and peripheral blood mononuclear cells (PBMCs) isolated for immune studies at 0 weeks (prior to repletion) and 52 weeks. Trial schedule is represented in **Table 2.1.**

| Week | -2 | 0 | 4 | 8 | 12 | 24 | 42 | 52 |
|---|---|---|---|---|---|---|---|---|
| Oral $VitD_3$ 100,000 IU | | X | X | X | X | X | X | |
| PBMC collection | | X | | | | | | X |
| 25 VitD measurement (serum) | X | X | | | | | | X |

**Table 2.1|Patient visit protocol and investigation schedule|**
Planning and preparation was conducted in the first 4 weeks. Patient recruitment was started at week 4 at 3 hospital sites. VitD replacement was conducted over 42 weeks.

### 2.1.2 PBMC preparation

#### 2.1.2.1 PBMC isolation of patient Blood

Heparinised whole blood from patients was layered on lymphocyte separation medium (LSM 1077) (GE Healthcare), isolated as indicated in section 2.2.2 and re-suspended in 20 mL of complete RPMI 1640 (Gibco). Cells were counted on a haemaocytometer and viability determined by trypan blue exclusion and subsequently frozen (see section 2.1.2.2). For culture and/or FACS (Fluorescence-activated cell sorting) staining volume of PBMCs were then re-adjusted to desired number (1 x $10^5$ cells for memory assay, 2.5-5 x $10^6$ for FACS staining) in 10% AB plasma for culture and FACS buffer for FACS staining.

#### 2.1.2.2 Freezing PBMCs

For freezing 0.5mL PBMC's were mixed with 0.5mL of freezing medium, frozen at -80°C in a container containing isopropanol overnight and subsequently transferred to liquid nitrogen. Frozen PBMCs were retrieved from liquid nitrogen and immediately suspended in 15mL pre-warmed (37°C) 2% FCS and spun at 1800rpm for 5 min (min) at room temperature (RT). Cells were then washed (spun at 1800rpm for 5 min at RT) again in 15 mL 2% FCS and counted using haemaocytometer. Viability was determined by trypan blue exclusion.

### 2.1.3 Flow cytometry

Following thawing, cells where re-adjusted to 5 x $10^6$ for intracellular staining, 2.5 x $10^6$ for surface staining and fluorescence minus one (FMO) controls. Cells where first incubated with Zombie Yellow viability dye (Biolegend) according to manufacturer's protocol followed by Fc blocking in human serum for 20 min. Cells were then incubated with surface conjugated antibodies (4°C, 20 min, 100µl volume of FACS buffer) in the dark. Antibody concentrations were variable and defined determined in previous studies (see section 2.1.4). Cells only requiring surface staining where then washed (centrifuged at 1800rpm, 5 min) in 1mL MACS buffer and re-suspended in 300µl MACS buffer for acquisition.

For intracellular and FoxP3 staining, cells where then permeablised and fixed using FoxP3 transcription buffer staining set (eBioscience) as per manufacturers protocol. Cells where incubated with intracellular and transcription factor antibodies (4°C, 30 min, 100µl volume of Perm/Wash buffer) in the dark.

Samples were acquired by flow cytometry using a LSR Fortessa (BD biosciences). Routinely 100,000 cells were acquired using DIVA software version 7.6 (BD biosciences). Subsequent data analysis was done on FlowJo software (version 9.5.2). Graphpad Prism (version 6.0) and Excel (Microsoft).

### 2.1.4 Antibody staining panels

| Antibody | Panel | Source (Catalogue Number) | Volume per sample |
|---|---|---|---|
| **Pacific Blue Mouse anti-human CD4** | CD4 T cell | eBioscience (48-0048-42) | 3µL |
| **PE Mouse anti-human CD25** | CD4 T cell | BD Bioscience (341011) | 5µL |
| **PE-Cy7 Mouse anti-human CD45 RO** | CD4 T cell | BD Bioscience (560608) | 2µL |
| **AF700 Mouse anti-human CD45 RA** | CD4 T cell | Biolegend (304120) | 2µL |
| **PerCPCy5.5 Mouse anti-human CD127** | CD4 T cell | eBioscience (45-1278-42) | 5µL |
| **FITC Mouse anti-human FoxP3** | CD4 T cell | eBioscience (11-4776) | 3µL |

**Table 2.2|CD4 T cell antibody staining panel|**

| Antibody | Panel | Source (Catalogue Number) | Volume per sample |
|---|---|---|---|
| **APC Mouse anti-human CD56** | Leukocyte | eBioscience (17-0569-42) | 2µL |
| **AF700 Mouse anti-human CD20** | Leukocyte | eBioscience (56-0209-42) | 3µL |
| **PerCPCy5.5 Mouse anti-human CD3** | Leukocyte | eBioscience (45-0037-42) | 2µL |
| **PECy7 Mouse anti-human CD8α** | Leukocyte | Biolegend (25-0087-42) | 3µL |
| **FITC Mouse anti-human γδTCR** | Leukocyte | eBioscience (11-9959-42) | 2µL |

**Table 2.3|Leukocyte antibody staining panel|**

| Antibody | Panel | Source (Catalogue Number) | Volume per sample |
|---|---|---|---|
| **Pacific Blue Mouse anti-human CD16** | Myeloid | eBioscience (48-0168-42) | 2µL |
| **PE Mouse anti-human CD80** | Myeloid | BD Bioscience (341011) | 2µL |
| **PE-Cy7 Mouse anti-human HLA-DR** | Myeloid | eBioscience (25-9956-42) | 2µL |
| **AF700 Mouse anti-human CD20, CD56, CD3** | Myeloid | eBioscience (56-0209-42) Biolegend (318316) eBioscience (56-0037-42) | 2µL (each) |
| **PerCPCy5.5 Mouse anti-human CD11c** | Myeloid | Biolegend (337210) | 3µL |
| **FITC Mouse anti-human CD86** | Myeloid | Invitrogen (MHCD8601) | 2µL |

**Table 2.4|Myeloid antibody staining panel|**

### 2.1.5 Serum cytokine analysis

Patient serum was collected in plastic serum EDTA coated tubes (BD bioscience) and stored at -80°C in aliquots of 500µl. Serum samples were then thawed and analysed for seven cytokines using the (CBA) human TH1 TH2 TH17 kit (BD Biosceinces) as per manufacturers protocol. Samples were never thawed more than three times.

### 2.1.6 *In vitro* Generation of monocyte-derived DCs

PBMCs from healthy donors were separated as specified in section 2.2.2. Subsequently, highly purified $CD14^+$ monocytes were isolated using $CD14^+$ cell isolation kits (Miltenyi Biotech) according to manufacturer's instructions. Monocyte-derived DCs (mo-DCs) were generated by 5-day culture of $CD14^+$ monocytes cells in complete RPMI 1640 medium (Gibco-Invitrogen) supplemented with 50 ng/mL Granulocyte Macrophage-Colony Stimulating Factor (GM-CSF) and 800 U/mL IL-4 (all from Endogen), at 37°C in 5% $CO_2$. Monocytes were phenotyped at this point to ensure immature DC phenotype of $CD14^-$ $CD80^-$ $CD86^-$ and $HLA\text{-}DR^-$. Immature mo-DCs were then cultured for 48 hours with 1,25 dihydroxy Vitamin $D_3$ (10nM) (Enzo life sciences) or carrier (Ethanol, Sigma-Aldrich) in the presence of IL-4 (800 U/mL), GM-CSF (800 U/mL) (all from Endogen) and LPS (100 ng/mL, Enzo life sciences) to mature DCs.

### 2.1.7 Statistics

Data were analysed using Stata V.14 (StataCorp. 2015, Stata Statistical Software release 14. College Station, TX 77845). All outcomes were assessed using a 2 x 2 (treatment x time) repeated measures ANCOVA with age and sex as the covariates. Any significant interactions were followed up with paired samples t-test. Data are presented as mean $\pm$ standard error of the mean (SEM).

## 2.2 *In vitro*

### 2.2.1 Reagents

A list of reagents used in the basic science chapter are listed in **Table 2.5**. Unless otherwise stated, cells were obtained from leukocytes retained filtering cones (cones) from healthy volunteer blood donations (NHS Tooting blood bank). Cells were washed in MACs buffer (see **Table 2.5**) and maintained and cultured in X-VIVO 15 (Lonza) serum free medium. Where stated cells were also cultured in the same medium supplemented with 10% v/v human AB serum (HS) (Biosera).

| Reagent | Use | Composition |
|---|---|---|
| ***General*** | | |
| **MACs buffer** | Washing and staining cells | 0.5% bovine serum albumin (BSA) (Sigma-Aldrich)<br>2mM EDTA (Sigma-Alrdrich)<br>phosphate buffered saline (PBS) (Gibco) |
| **X-VIVO** | Culturing cells | X-VIVO (Lonza)<br>50IU/mL penicillin<br>50μg/mL streptomycin (Invitrogen)<br>2mM L-glutamine (PAA Labarotories)<br>Optional: 10% v/v human AB serum (Biosera) |
| ***ChIP-seq*** | | |
| **Buffer 1** | Cell lysis | 0.3M Sucrose (15mL - 1M fv 50mL)<br>60mM KCL (3mL - 1M fv 50mL)<br>15mM NaCL (150ul - 5M fv 50mL)<br>5mM MgCl2 (250ul - 1M fv 50mL)<br>0.1mM EGTA (10ul - 0.5M fv 50mL)<br>15Mm Tris-HCL (pH7.5) (750ul - 1M fv 50mL)<br>0.5mM DDT (20ul - 1.25M fv 50mL) |
| **Buffer 2** | Cell lysis | As buffer 1 with<br>0.4% IGEPAL-CA (200ul fv 50mL) |
| **Buffer 3** | Nuclei isolation | As buffer 1 with<br>1.2M Sucrose instead of 0.3M (20.5g fv 50mL) |
| **MNase Digestion Buffer** | MNase buffer | 0.32M Sucrose (16mL - 1M fv 50mL)<br>50mM Tris-Cl (pH 7.5) (2.5mL of 1M fv 50mL)<br>4mM MgCl2 (200ul - 1M fv 50mL)<br>1mM CaCl2 (50ul - 1M fv 50mL) |
| **MNase** | Digestion of chromatin into mono and di-nucleosomes | 10Units/ul in 50% glycerol (15,000U in 750ul sterile glycerol +750ul dH20) |
| **Stop solution** | Stop MNase digestion | 20mM EDTA (pH8.0) (2mL fv 50mL) |
| **Dialysis Buffer** | Final resuspension of ChIP material | 1mM Tris-Cl (pH 7.5) (50ul - 1M fv 50mL)<br>0.2mM EDTA (20ul - 0.5M fv 50mL) |
| **Wash buffer 1** | Washing beads | 20mM Tris.Cl pH 8.1 (1mL - 1M fv 50mL)<br>50mM NaCl (500ul - 5M fv 50mL)<br>2mM EDTA (200ul - 0.5M fv 50mL)<br>1% TX-100 (500ul neat fv 50mL)<br>0.1% SDS (500ul - 10% fv 50mL) |

| | | |
|---|---|---|
| **Wash buffer 2** | Washing beads | 10mM Tris.Cl pH 8.1 (500ul -1M fv 50mL)<br>150mM NaCl (1.5mL - 5M fv 50mL)<br>1 mM EDTA (100ul - 0.5M fv 50mL)<br>1% NP40 (500ul neat fv 50mL)<br>1% Na deoxycholate (0.5g fv 50mL)<br>250 mM LiCl (1.56mL - 8M fv 50mL) |
| **Elution Buffer** | Eluting bound DNA | 0.1M $NaHCO_3$ (500ul - 1M fv 50mL)<br>1% SDS (500ul -10% fv 5mLs) |
| **Modified RIPA buffer** | Buffer for immunoprecipitation | 140mM NaCl (1.4mL - 5M fv 50mL)<br>10mM Tris pH7.5 (500ul -1M fv 50mL)<br>1mM EDTA (100ul -0.5M fv 50mL)<br>0.5mM EGTA (50ul - 0.5M fv 50mL)<br>1% TX-100 (500ul neat fv 50mL)<br>0.01% SDS (50ul -10% fv 50mL)<br>0.1% sodium deoxycholate (50mg fv 50mL) |
| ***Clinical Trial*** | | |
| **Complete RPMI** | Cell culture | RPMI 1640 medium (Gibco) supplemented with 10% human serum male AB medium (Sigma-Aldrich), 100IU/mL penicillin (Invitrogen), 100µg/mL Streptomycin (Invitrogen), 2mM L-glutamine (Invitrogen) |
| **Freezing medium** | Cryopreservation of PBMCs | RPMI 1640 medium 2mL DMSO (20%),8mL FCS (80%)(0.5mL freezing medium +0.5mL cell suspension |

**Table 2.5|Reagents|**

Reagents separated into general reagents and ChIPseq specific reagents. Protease and phosphatase inhibitors (protease Inhibitors Cocktail, Sigma and phosphatase Inhibitors Cocktail Set II, Calbiochem) and sodium butyrate (0.5mM) is added to Buffers 1,2, 3, MNase buffer, dialysis buffer and modified RIPA buffer**.**

### 2.2.2 Separation of Peripheral Blood Mononuclear cells (PBMCs)

Leukodepletion cones (see section 2.2.1) were diluted 1 in 4 with sterile PBS and layered onto 15mL of lymphoprep (Axis-Shield) followed by centrifugation at 940 RCF at 20°C for 20 min, with slow acceleration and no brakes. PBMCs were collected by harvesting interface cells followed by two washes in PBS at 940 and 235 RCF respectively, for 10 min at 4°C with full acceleration and deceleration.

### 2.2.3 Selection of $CD4^+$ cells and subsets

#### 2.2.3.1 $CD4^+CD25^-$ T cells

RosetteSep Human $CD4^+$ enrichment cocktail (Stem Cell) was used to enrich for purified $CD4^+$ T cells from cones for both culture and pre-enrichment prior to sorting, as per manufacturers protocol. Briefly, cones where first diluted 1 in 2 and incubated at room temperature for 20 min with Rosettesep cocktail. Blood was then diluted a further 1 in 4 and $CD4^+$ Tcells separated as described for PBMCs (see 2.2.2) to a purity of 80-95%. $CD4^+$ T cells were subsequently depleted of $CD25^+$ T cells using CD25 positive selection (CD25 microbeads II, Human, Miltenyi Biotec) and collecting the unlabeled cells. Cells were rested over night before activation.

#### 2.2.3.2 $CD45RO^+$ memory cell isolation for ChIPseq

Memory $CD4^+$ T Cell isolation kit human (MiltenyiBiotec) was used to isolate memory $CD4^+$ T cells for ChipSeq analysis, following manufacturers protocol. Following culture period of 2 days, dead cells were removed using dead cell removal kit (Miltenyi biotechnology), before fixation and downstream ChIP-seq protocol (2.2.14).

#### 2.2.3.3 Cell sorting $CD4^+$, Naïve ($CD45RA^+$) and Memory ($CD45RO^+$) T cells

Following enrichment of $CD4^+$ T cells using rosettesep, cells were stained with antibodies against CD4, CD45RA and CD45RO for 30 min in MACS buffer at 4°C for 20 min. Following a wash in MACS buffer, cells were re-suspended at a concentration of $30x10^6$ cells per mL

before sorting using an ARIA (BD Bioscience) using a 70μm nozzle at 70 PSI into X-VIVO 15 media with human serum. Cells were sorted into $CD4^{+}CD25^{-}CD45RO^{-}CD45RA^{+}$ and $CD4^{+}CD25^{-}CD45RO^{+}CD45RA^{+}$ to a purity of >99% (Figure 2.1).

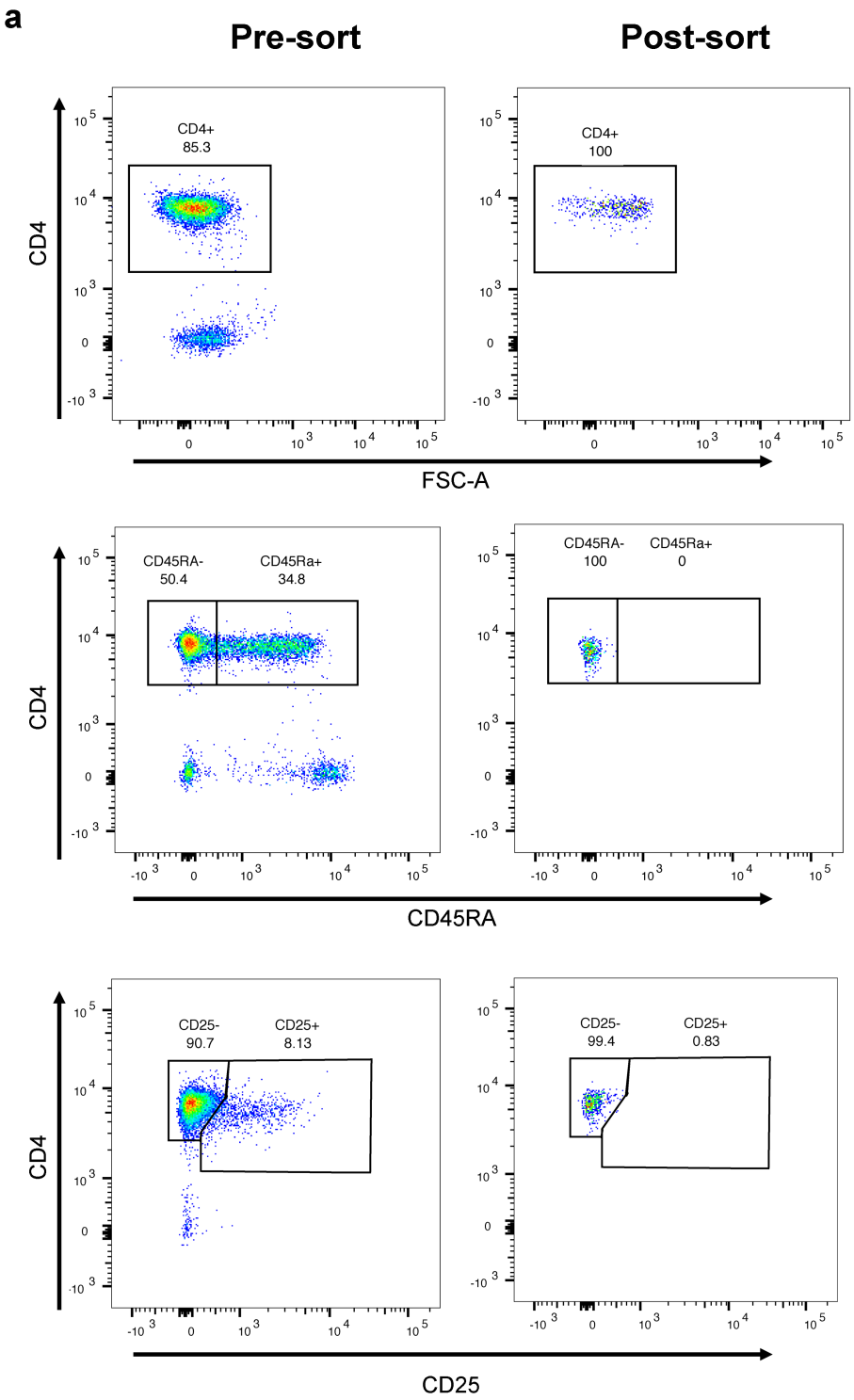


**Figure 2.1|CD4$^+$ T cell sorting purity|**
CD4$^+$ T cells were FACS sorted to purity of 99-100% (a) Representative flow cytometry plots showing pre- and post-sort purities of total CD4$^+$ T cells (top) memory T cells based on CD45RA negative (middle) and CD25 low T cells (bottom).

### 2.2.4 Culture conditions

Unless otherwise stated cells were cultured in X-VIVO 15 (Lonza) serum free medium supplemented with PSG (see 2.2.1). Typically, $CD4^+$ T cells were cultured in a 96 well u-bottomed plate (VWR) at a cell density of $10^6$ cells per mL in a total volume of 200μL. $CD4^+$ cells were activated using Dynabeads Human T-activator CD3/CD28 (Gibco), usually at a density of 1 bead per 4 cells. Cells were additionally cultured in the presence or absence of; 1α,25-Dihydroxyvitamin D3 (Enzo Life Sciences) reconstituted in 99.8% ethanol (Sigma-Aldrich), 99.8% ethanol as a carrier control, IL-6 (Biolegend), Tocilizumab (Toc) (a kind gift from Dr Ceri Roberts in Professor Leonie Taams lab) or STAT3 shRNA or inhibitor (see section 2.2.11 and 2.2.12).

### 2.2.5 Cytokine measurement

Supernatants from 96-well plates were removed, after brief centrifugation to pellet cells, and stored at -20°C. Supernatants were never thawed more than twice before cytokine analysis. Cytokines were quantified using either the Cytometric Bead Array (CBA) human/mouse TH1 TH2 TH17 kit (BD Biosceinces) or the Legendplex Th panel (BioLegend) following manufacturers protocol using a FACSCANTO II (BD) and analysed using FCAP Array™ software v3.0 (BD bioscience).

### 2.2.6 qPCR

Cells (typically 2-4x$10^5$) were lysed in 350 μl Trizol reagent (Ambion, Life Technologies) and RNA extracted using the Direct-zol RNA Miniprep kit (Zymo) with on column genomic DNA digestion, according to manufacturer's instructions. RNA concentration was assessed using a NanoDrop (NanoDrop) spectrophotometer. RNA was then reverse transcribed to cDNA using the qPCRBIO cDNA Synthesis Kit (PCR Biosystems) according to manufacturers protocol. qPCR was carried out in a 384-well plate using the ViiA7 real-time PCR system (Life technologies) and SYBR Green PCR Master Mix (Life Technologies) in a 20μl reaction volume containing 10ng of cDNA. All reactions were carried out in triplicate using *18s* and *UBC* (PrimerDesign) as housekeeping genes. Gene specific primers for IL-6 and VDR were QuantiTect primers from Qiagen (primer sequences not

provided). The cycling profiling was as follows: 10 min at 95°C, then 40 cycles of amplification (each cycle consisting of 15s at 95°C then 60s at 60°C), followed by melt curve analysis to ensure amplification of a single product. Comparative Ct method was used for analysis using the Viia7 software producing a ΔΔCt (relative quantity (RQ) compared to a reference sample).

### 2.2.7 Western blot

Whole cell extracts were prepared by cell lysis in RIPA buffer (Thermo Scientific), as per manufacturer's protocol, with added Protease Inhibitor Cocktail Set III (Calbiochem), at a 1 in 250 dilution. Protein concentration was quantified using quickstart protein assay (BioRad). Proteins were resolved by SDS-PAGE on 10% Tris-Glycine gels (Invitrogen) and electrotransferred onto polyvinylidene fluoride membranes (Immobilon, Millipore). Immunoblotting was performed according to standard protocols with initial blocking in PBS with 10% w/v clotting grade blocker (BioRad) or BSA (Sigma-Aldrich) 3% w/v and 0.1% v/v Tween20 (Sigma), followed by overnight incubation in primary antibodies: anti-VDR (clone D-6, Santa Cruz biotechnology) pSTAT3, STAT3 (Cell Signaling Technologies) followed by blocking and two hour incubation in appropriate HRP conjugated secondary antibodies: α-mouse, α-rabbit (TrueBlot antibodies, Rockland). Bound antibodies were detected using ECL-Plus reagents (Thermo Scientific) and visualized on an imageQUant LAS4000 mini (GE Healthcare). Blots were quantified using ImageStudioLite (LICOR).

### 2.2.8 Human Phospho-Kinase Antibody Array

Array was carried out as per manufacturers protocol. Briefly, $CD4^+CD25^-$ T cells from two donors were activated in the presence of ethanol-carrier and VitD, lysed and protein concentration was quantified using quickstart™ protein assay (BioRad). Lysates were normalized to a concentration of 800μg/mL using lysis buffer. Membranes dotted with biotlinylated anti phospho-protein antibodies were then blocked for one hour at room temperature before addition of lysates and overnight incubation at 4°C on a rocker. Following three washes in washing buffer detection antibody was added to membranes for two hours at room temperature on a rocker. Following another three washes

membranes were incubated with Streptavidin-HRP for 30 min at room temperature on a rocker. After final three washes, positive signal was detected using Chemi-Reagent Mix and visualised using an imageQuant LAS4000 mini (GE Healthcare) and quantified using ImageStudioLite (LICOR). Reference spots on each membrane were used to normalize signal across membranes.

### 2.2.9 Flow cytometry

All samples were acquired on LSRFortessa (BD) within 24 hours and data was analysed using FlowJo (LLC, v10.2). $10^6$ cells were stained for 30 min at 4°C, in 5mL polystyrene round bottom tubes (Falcon) in a final volume of 100μL MACS buffer. Following a wash in MACS buffer cells were acquired on a Fortessa (BD). Data was analysed using FlowJo v10 software. In general, dead cells were excluded using forward and side scatter area (FSC-A and SSC-A respectively) and singlets excluded using FSC-height (FSC-H) and FSC-width (FSC-W).

#### 2.2.9.1 Intracellular cytokine staining

Cells were activated with Phorbol 12-myristate 13-acetate (PMA) (50ng/mL, SIGMA), ionomicyn (1ug/mL, SIGMA), GolgiStop (1X, BD) and Brefeldin A (1X, BD) for 5 hours in fresh culture media at 37°C 5% $CO_2$. Cells were then washed in PBS, initially stained for surface molecules and then fixed and permeabilised using Cytofix/Cytoperm buffer (eBioscience), followed by a wash in Perm/Wash buffer (eBioscience) and incubation with intracellular antibodies for 30 min at 4°C. Finally, cells where washed and acquired as in section 2.2.9.

### 2.2.10 Mouse splenocyte isolation and activation

Spleens were obtained from C56BL/6 (B6) mice and homogenised (using the back end of a sterile syringe plunger) through a 70μm filter with PBS. 'Dynal Mouse $CD4^+$ Negative Isolation Kit' (Invitrogen) was used to isolate $CD4^+$ T cells from B6 splenocytes according to manufacturer's protocols. 200 x $10^5$ $CD4^+$ T cells where activated with 2 μg/mL plate-

bound mouse αCD3 (eBioscience) and 1 μg/mL soluble αCD28 (R&D systems) per well in a u-bottomed 96 well plate in the presence of ethanol (Sigma-Aldrich), 1,25 dihydroxy Vitamin $D_3$ (10nM) (Enzo life sciences) or LEAF Purified anti-mouse/rat CD126 (Biolegend).

### 2.2.11 STAT3 ShRNA

Memory $CD4^+$ T cells were sorted and rested overnight in media supplemented with 10% of human Serum (BioSera) at 37°C 5%$CO_2$. The next day, 5 x $10^6$ cells were washed twice with PBS and cell pellet was nucleofected with 10 nM *Silencer* Select STAT3 (s745) or Silencer Select Negative Control siRNA (ThermoScientific) using the Amaxa Human T Cell Nucleofector Kit (Lonza) and the Nucleofector 2b Device (Lonza) (U-014 program). After nucleofection, cells were rested in culture media at 37°C 5%$CO_2$ for 6 hours. Then, dead cells were removed with Ficoll-Hypaque density gradient centrifugation (Lymphoprep, Axis-Shield, Oslo, Norway) and 2 x $10^5$ cells were activated anti-CD3/CD28 beads (ThermoFisher) 4:1 ratio cell:bead for 72hrs at 37°C 5%$CO_2$. Cytokines were detected in the supernatants with BD Cytometric Bead Array and proteins were detected by western blot.

### 2.2.12 STAT3 inhibitor

Memory $CD4^+$ T cells were sorted and rested overnight in media supplemented with 10% of human Serum (BioSera, Nuaille, France) with at 37°C 5%$CO_2$. Next day, 2x$10^5$ cells were activated anti-CD3/CD28 beads (ThermoFisher) in a 4:1 ratio cell:bead for 72 hours at 37°C, 5%$CO_2$ with 1,25 dihydroxy Vitamin $D_3$ (10nM) (Enzo life sciences) or carrier (Ethanol, Sigma-Aldrich) in the presence of 150 nM Curcubitacin I, Cucumis sativus L. (Cat:238590 Millipore) or carrier (Ethanol, Sigma-Aldrich).

### 2.2.13 Image Stream

VDR and DAPI co-localisation was performed in memory $CD4^+$T cells stained with mouse anti-human VDR (clone D3, Santa Cruz), anti-mouse-AlexaFluor647 and DAPI. Data was

acquired on an ImageStream$^X$ system equipped with three lasers, running with Inspire software and analysed with IDEAS 3.0 software (all from AMNIS Corp, Seattle, WA, USA). Co-localisation between VDR and DAPI was assessed with specific features/masks within IDEAS 3.0. A minimum of 100.000 cell events were acquired per sample.

### 2.2.14 ChIP-seq

#### 2.2.14.1 Isolation of chromatin

20-30 x $10^6$ live memory $CD4^+$ T cells (isolated as in section 2.2.3.2) were pelleted and fixed in 10mL of 1% formaldehyde (Sigma-Aldrich) in PBS and let for 10 min to fix. 1mL of 1.25 M glycine was then added to neutralize fixation. Cells where then centrifuged at 1000 x g for 5 min and supernatant discarded.

To lyse cells and obtain pure nuclei the following procedure was carried out: Two mL of ice-cold buffer 1 was added to cell pellet and cells were gently re-suspended by pipetting. Two mL of ice-cold buffer 2 was subsequently added on top and tube gently inverted and incubated on ice for no more than 10 min. Two mL was then layered gently on top of 8 mL ice-cold buffer 3 and tubes covered in parafilm before centrifugation at 10,000 g for 20 min at 4°C. Supernatant was subsequently removed gently, ensuring pelleted nuclei did not encounter detergent in supernatant.

To separate chromatin into mononucleosomes the following procedure was carried out: nuclei from previous step were re-suspended in 500μl MNase buffer, pooled and added to 1.5 mL loBind micro-centrifuge tubes (Eppendorf) at which point an aliquot was removed to check nuclei integrity and number using 2% Trypan blue cell counting in haemocytometer. Chromatin was incubated with 100unit (U)/μL at 37°C for 10 min at which point 20μl stop solution was added and tubes placed on ice. Tubes were subsequently spun at 10,000 rpm for 10 min at 4°C and supernatant, containing primarily mononucleosomes, was transferred to fresh eppendorfs and stored at 4°C.

Chromatin was then sonicated: Pellet was re-suspended in 350ul sonication buffer and sonicated at 80% power, using a three mm probe for 10 seconds and put on ice. This sonication was repeated five times, each time returning the eppendorf to ice. Tubes were then spun at 10,000 rpm for 10 min at 4°C and supernatant collected in fresh eppendorfs

and volume brought to 500μl in sonication buffer and stored at 4°C. Pellet was re-suspended in 50μl dialysis buffer.

To reverse cross link chromatin, an aliquot of each chromatin fraction above (approx. 10% of each) was taken and added to a new eppendorf and 1μl 10μg/mL RNase A and NaCl at a final concentration of 250mM was added. Tubes were then incubated at 65°C for 4 hours after which tubes were cooled on ice and two μL 0.5 μg/mL proteinase K were added and incubated for a further 37°C for one hour. Quality and quantity of chromatin was checked with this fraction using a high sensitivity DNA chip (Agilent) on a 2100 Bioanalyzer (Agilent).

For histone modification ChIPseq (H3K27ac and H3K4me3) no cross linking was performed and no sonication was performed (native ChIPseq). After pelleting of live memory $CD4^+$ T cells, two mL of ice cold buffer 1 was added and procedure followed as above until sonication, which was skipped.

#### 2.2.14.2 Chromatin immunoprecipitation

10ug of samples containing mono-nucleosomes, and sample containing di-nucleosomes were mixed in a new eppendorf and volume made up to 500μl with modified RIPA buffer. To this, 5μg of respective antibody (H3K27Ac ab4729, polyclonal, Abcam/ H3k4me3 ab8580, polyclonal Abcam/ VDR, clone D-6, Santa Cruz biotechnology) and 25ul of magnetic protein G beads (Active Motif) was added and incubated overnight rotating at 4°C. Input was used as control and similarly contained 10ug of each chromatin fraction and was treated in identical fashion to ChIP material.

Eppendorf tubes were subsequently placed on a Dynal mag magnetic stand (Invitrogen, ThermoFisher) and left to clear for approximately two min. Supernatant was discarded and beads washed once with 800μl wash buffer 1, wash buffer 2 and finally buffer TE (pH 8.0), for two min discarding supernatant each time. Beads were then re-suspended in 100μl elution buffer for five min, before placing tubes in magnetic stand and supernatant, containing ChIPed material, transferred to new eppendorf tube.

#### 2.2.14.3 DNA extraction

Phenol:choloroform:isoamylalcohol in a ratio 25:24:1 was added in equal volumes to each sample and vortexed for 30 seconds and spun at 13,000 rpm for 15 min. The upper, aqueous layer was carefully collected in a new eppendorf and NaCl added to a final concentration of 250mM. 40μg of glycogen was then added to each sample along with an equal volume of iso-propanol, this solution was then mixed and left to precipitate over night at -80°C.

Samples were then thawed and spun at 13,000 rpm for 15 min at 4°C and supernatant discarded. 1mL of ice cold 70% ethanol was added to wash pellet and sample spun again at 13,000 rpm for 15 min at 4°C and supernatant discarded. Pellet was then left to air-dry at room temperature for approximately half an hour and pellet re-suspended in 30μl distilled water.

Samples were then checked for quality and quantity using a high sensitivity DNA chip (Agilent) on a 2100 Bioanalyzer (Agilent).

#### 2.2.14.4 Library prep and sequencing

Libraries were prepared using NEBNext ChIP-Seq Library Prep Reagent Set for Illumina (New England Biolabs) (**Figure 2.2**) as per manufacturers protocol. Briefly, 10ng of ChIP material, and input, were end repaired, 5' phosphorylated and cleaned up using AMPure XP Beards (Beckman Coulter). Samples then had 1 single Adenine (A) amino acid added to 3' ends and cleaned up again. NEBNEXT Adapters containing a single uracil were then ligated to the dA-tailed DNA and excised at uracil location using USER enzyme. Following another clean up, fragments were size selected for 300 bp fragments using AMPure XP Beards (Beckman Coulter). This step also serves to remove un-ligated adaptors. PCR enrichment of adaptor ligated DNA was then performed using NEBNext Multiplex Oligos for Illumina (New England Biolabs) for 15 cycles and product cleaned up as before.

Samples were then checked for quality and quantity using a high sensitivity DNA chip (Agilent) on a 2100 Bioanalyzer (Agilent) (**Figure 2.3 a and b**) and pooled libraries assessed for size by agarose gel electrophoresis (**Figure 2.3 c**)

Equimolar concentrations (4 nM) of each uniquely indexed sample were then loaded and run on Hiseq 2500 for 50 cycles using single-end run.

Sequencing of ChIP material was carried out by Biomedical Research Centre (BRC) genomics core at Guys and St Thomas's national institute for health research (NIHR) genomics core.

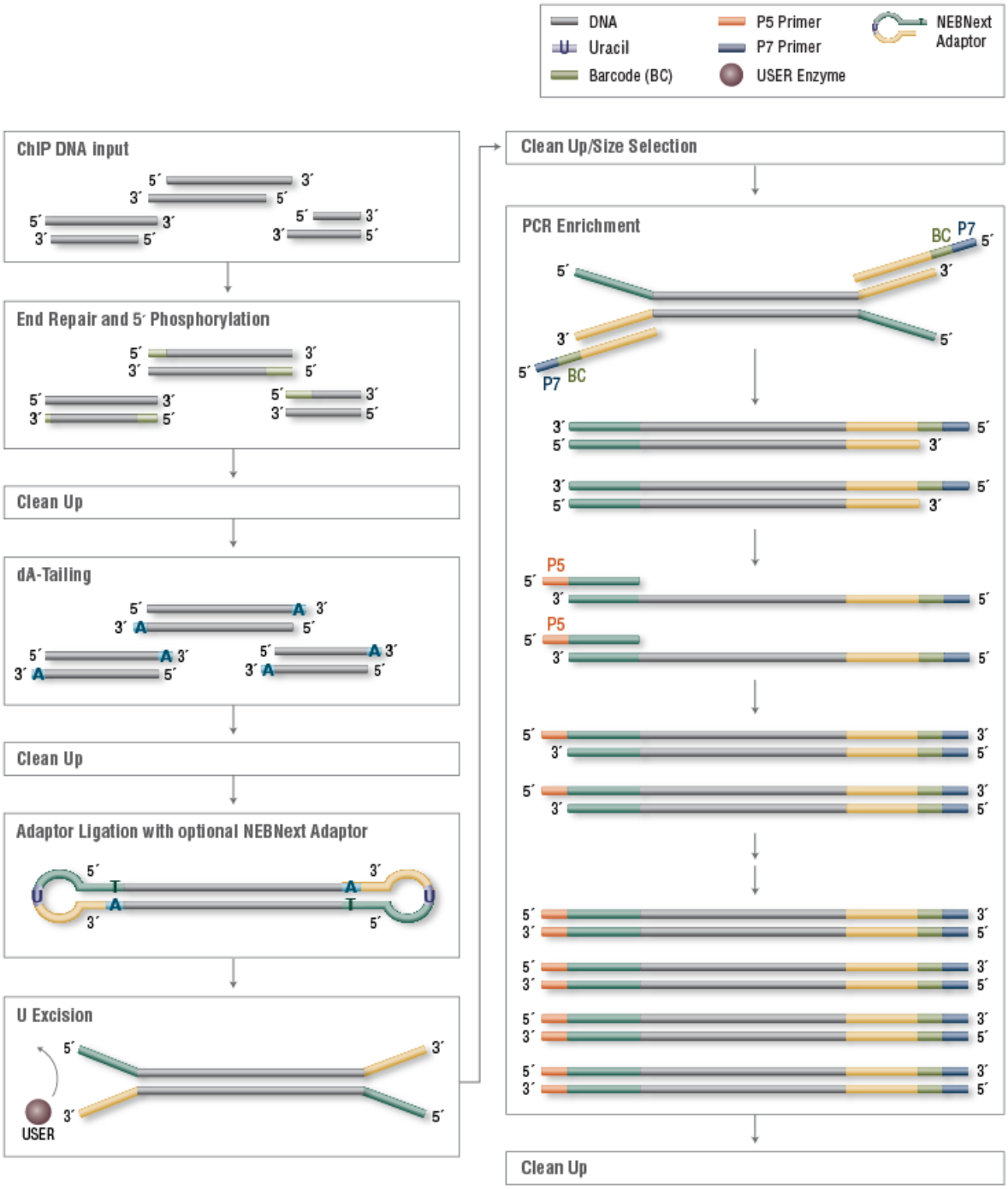


**Figure 2.2|ChIP DNA Library Preparation Workflow for Illumina|**
Workflow for ChIP library preparation using NEBNext ChIP-Seq Library Prep Reagent Set for Illumina (New England Biolabs) (taken from New England Biolabs website).

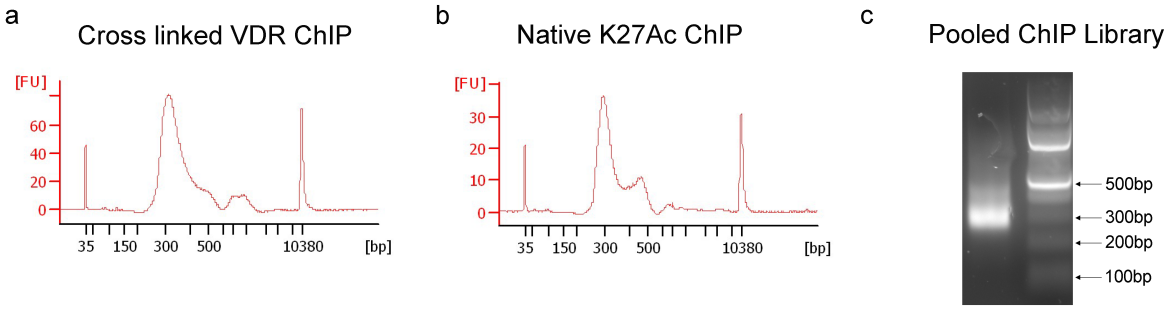


**Figure 2.3 |Example ChIP material quality control|**
(a) Quality and size distribution assessment of cross linked VDR ChIP material (b) Quality and size distribution assessment of native 27Ac ChIP material. (c) Pooled ChIP samples assessed for size by agarose gel electrophoresis.

#### 2.2.14.5 Analysis

Fastq files were obtained from the sequencing facility and analysed using the online next generation sequencing (NGS) analysis platform Galaxy (Afgan et al., 2016). FastQC (http://www.bioinformatics.babraham.ac.uk/projects/fastqc/) was used to assess quality of FastQ files (**Figure 2.4 a and b**). FastQ groomer (Blankenberg et al., 2010) was then used to convert files to FastQSanger format, required for many NGS tools. As quality of reads was lower and more variable GC content was observed at beginning of reads (**Figure 2.4 a**) trimmomatic (Bolger et al., 2014) was used with following parameters: Initial Illuminaclip step was used to cut adaptors. Sliding window operation was used. Sequences that dropped below a quality score of 20 were dropped and 5bp were cut from the start of every read. FastQC was then re-run to ensure quality of reads post-trimming (**Figure 2.4 b**). Bowtie2 (Langmead et al., 2009) was then used to map reads to reference genome hg19 (for entire workflow see **Figure 2.5 a**). Mapping statistics were checked and all files were mapped with an overall alignment rate of over 90%.

Bam files output from Bowtie2 were then uploaded into GalaxyDeeptools (Ramírez et al., 2014). The bamCoverage tool was used, normalising to coverage 1x or reads per genomic content (RPGC = (total number of mapped reads x fragment length) / effective genome size), to convert the bam files to bigwig format for viewing in Integrative Genomics Viewer (IGV) (Robinson et al., 2011). Diagnostics were run on bamfiles using both plotCoverage and plotPCA (following generation of matrix using multiple input bam files) (**Figure 2.5 b**).

Homer was used for peak-calling and motif analysis (Heinz et al., 2010). The following commands were run: makeTagDirectory was used to make tag directories from bam files. findPeaks was run using the following options; -style histone -size 1000. findMotifsGenome was run using the following options; -size given –mask. Peaks with total tag counts of lower than 20 were then excluded to filter out spurious peaks.

Bamfiles from Galaxy and filtered peaks from Homer were then imported into Easeq (Lerdrup et al., 2016) for downstream analysis and visualisation. As some sequence duplication was observed (**Figure 2.4 b**) only reads with unique positions were imported.

Prior to further analysis in Easeq all ChIP-seq signal from bamfiles were quantile normalised to ensure linear normalisation for local comparisons of ChIPseq.

Data from public repositories was accessed as sequence read archives (SRA) after which they were subjected to the same data analysis as above. One important difference was bedtools “genomecoveragebed” tool was used to convert to BedGraph and “begrpahtobigwig” to convert to BigWig and in the process normalised to reads per million mapped reads per kilobase (RPKM = number of reads per bin / (number of mapped reads (in millions) x bin length).

### 2.2.15 Data presentation and Statistical analyses

Figures were drawn using Photoshop CC 2017 (Adobe). Statistics were carried out using GraphPad for Mac software (Prism 7.0a). Data were typically grouped format and a two-way ANOVA with Sidak correction for multiple comparisons used. For comparison of two-groups only data, appropriate paired and unpaired parametric and non-parametric tests were carried out. For all data, p-values less than 0.05 were considered statistically significant.

a

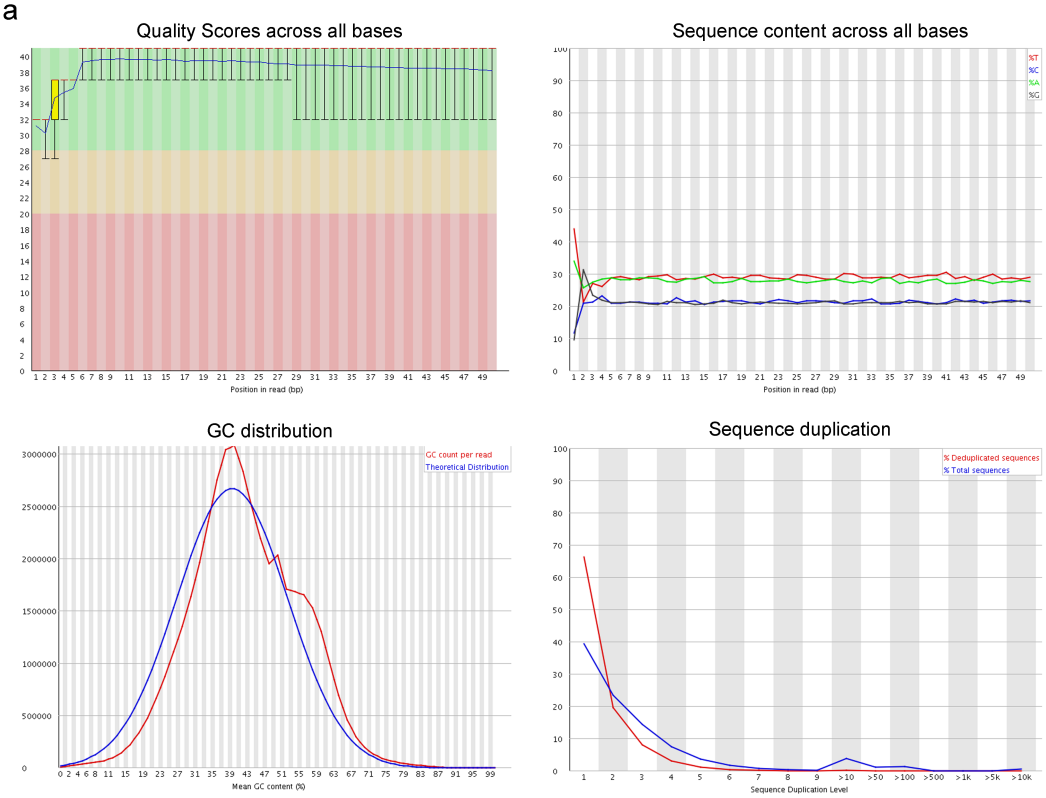


b

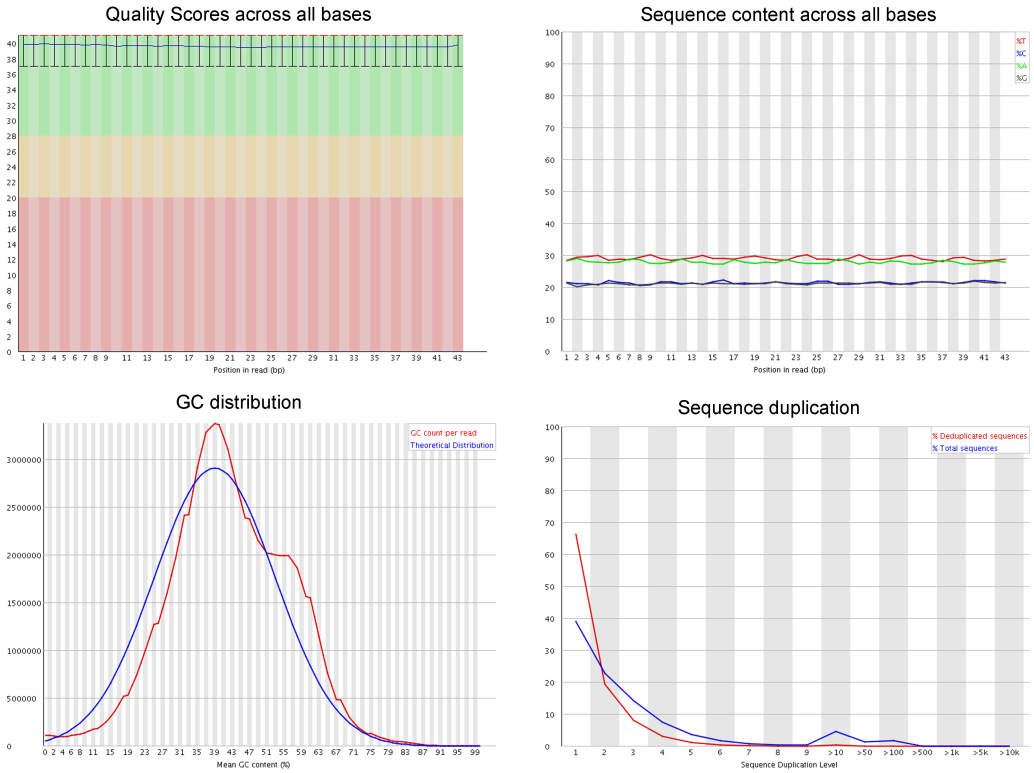


**Figure 2.4 |Select FastQC parameters|**
FastQ parameters before (a) and after (b) FastQ trimming.

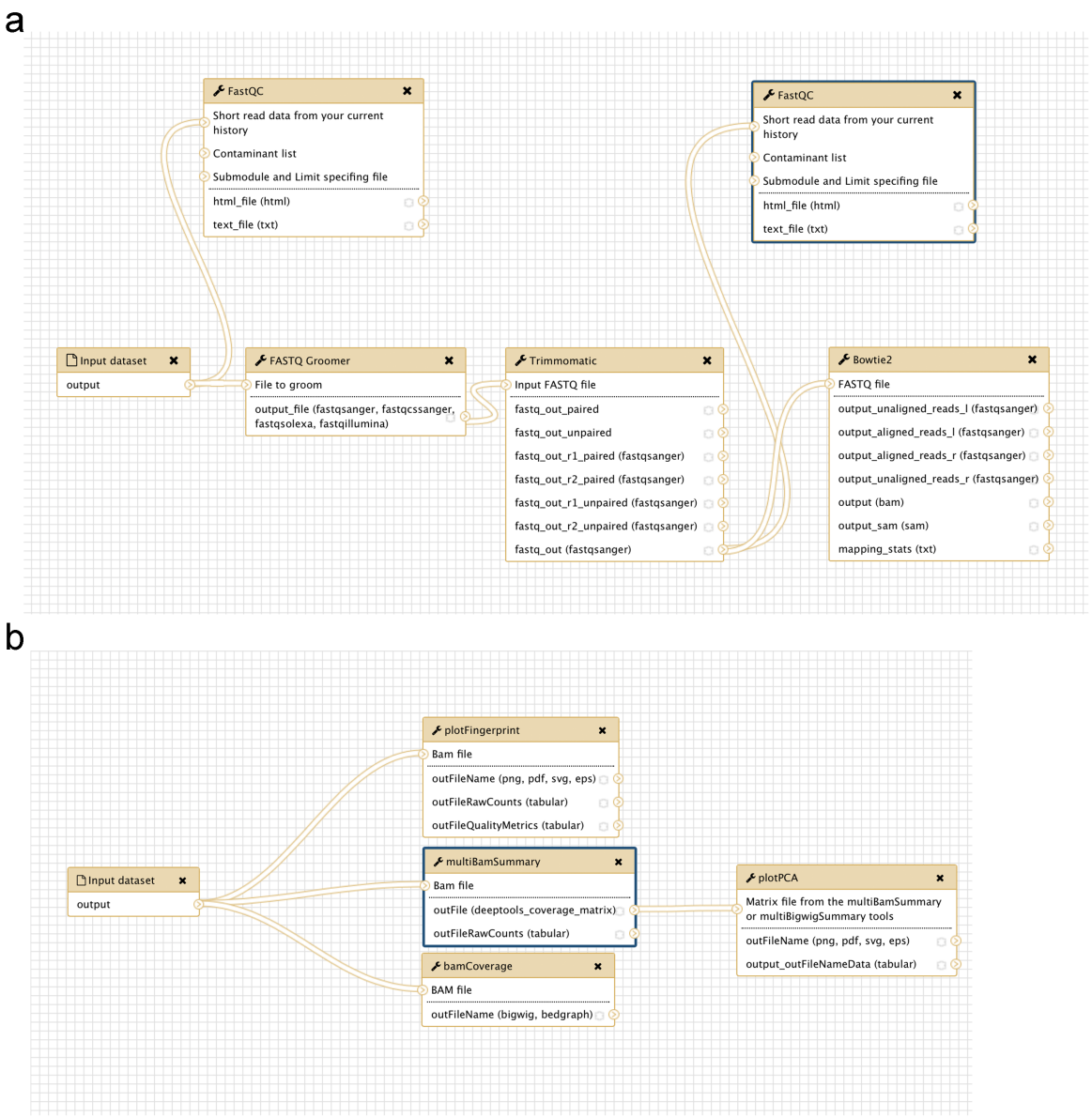


**Figure 2.5|Workflow for ChIPseq analysis in Galaxy|**
(a)Workflow from Fastq, through quality control using FastQC to mapping using Bowtie2 and (b) from bamfiles to bigiwig, coverage and PCA plots

#### 2.2.15.1 Pathway analysis using Metascape

Gene lists were input into Metascape (Tripathi et al., 2015) as multiple gene lists. KEGG, Gene ontology and Hallmark pathways were searched for enrichment of gene lists. Default parameters were selected for all other parameters.

# 3. IMPACT OF VITAMIN D SUPPLEMENTATION ON IMMUNE PHENOTYPE IN CHRONIC KIDNEY DISEASE - A RANDOMISED PLACEBO CONTROLLED TRIAL

## 3.1 Introduction

End stage kidney disease (ESKD) dramatically increases the risk of death. By far the most common cause of death is accelerated CVD with the second most common being infections. ESKD patients have a relative risk of CVD of up to 3.4 compared to the general population (Go et al., 2004). This can only partially be explained by the clustering of traditional CV risk factors (hypertension, hyperlipidaemia and obesity) in these patients (Schiffrin et al., 2007). The mechanistic link between CVD, infection and immune dysregulation is increasingly apparent (Jaber, 2005; Kato et al., 2008; Kimmel et al., 1998; Sterling et al., 2012; Stinghen et al., 2010; Vanholder and Ringoir, 1993). Thus, recent focus in the field has been on 'non-traditional' risk factors seen in patients with CKD, such as chronic inflammation, oxidative stress (Cachofeiro et al., 2008) and VitD deficiency (Inaguma et al., 2008) also discussed in section 1.5.1.

Patients with CKD are known to be deficient in both 25 and 1,25 VitD with several observational studies showing that treatment of patients with VitD analogues is associated with improved survival (Kalantar-Zadeh et al., 2006; Kimmel et al., 1998; Melamed et al., 2006; Teng et al., 2005). In addition, cross sectional studies have demonstrated an inverse relationship between 25 VitD levels and CVD in both the general (Dobnig et al., 2008; Martins et al., 2007) and CKD populations (Inaguma et al., 2008; Mehrotra et al., 2009). In observational studies, intervention with VitD supplementation improves survival in patients on dialysis (Wolf et al., 2007).

Given the immunoregulatory effects of VitD and its various analogues and their postulated involvement in multiple diseases involving the immune system, understanding the mechanisms driving VitD-induced immunomodulation is of great biological and clinical importance

## 3.2 Hypothesis and aims

We hypothesised that oral repletion with cholecalciferol ($VitD_3$) in VitD insufficient/deficient adult patients with CKD stage 3b/4 over 52 weeks would ameliorate

systemic inflammation. The work in this thesis focused solely on the *in vivo* effects of VitD on immune function.

In this chapter, we aimed to investigate the effects of $VitD_3$ repletion on immune functioning, in particular, regulatory and inflammatory components.

# Results

## 3.3 Immuno-monitoring

The primary outcome of the clinical trial is changes in cardiac structure following VitD repletion. Based on observations that CKD demonstrates a state of chronic inflammation and that VitD has pleiotropic immune functions, immune phenotyping of peripheral blood and cytokine measurements in serum were also measured as a secondary outcome. We were responsible for carrying out these immunological measures. Thus, this chapter will focus on these aspects.

### 3.3.1 Flow cytometry panel optimisation for immune-phenotyping

As patient samples were frozen and limited, immune-phenotyping panels of peripheral blood mononuclear cells (PBMCs) was first optimised on healthy control blood to ensure appropriate discrimination of all populations using appropriate controls.

#### 3.3.1.1 Optimisation of population discrimination and fluorescence minus one controls

Both the innate and adaptive immune systems are affected in CKD (Betjes, 2013) (see section 1.5.1). To study the effects of Vitamin D repletion on immune cells in our patient cohort, we immunophenotyped white blood cells to identify gross changes in frequencies of major populations of circulating immune cells. **Table 3.1** gives a summary of the effects of CKD on immune cell function and the predicted effects of VitD on these immune cells, based on available evidence. Using these as a guide, three flow cytometry panels were designed on healthy donor blood, as described in section 2.1.4. Cells were stained and analysed using the initial gating strategy indicated in **Figure 3.1.** Lymphocytes were first gated on for T cell and leukocyte staining panels (**Figure 3.1 a**). As DCs are present in both

lymphocyte and monocyte gates, both were gated for in the myeloid panel (**Figure 3.1 a**). Next, doublet (**Figure 3.1 b**) and dead cells (**Figure 3.1 c**) were excluded. To minimise the number of cells being used for *ex vivo* phenotyping, we sought to determine which controls were essential for accurate gating. Current guidelines suggest that the best way to determine the difference between no expression and low expression of a particular antigen is to measure it directly in a sample stained with all of the fluorophores used except for the fluorophore under question (Tung et al., 2004). These are known as FMO controls.

For T cells, markers such as CD4, CD45RA and CD45RO, could be accurately gated without FMO controls (**Figure 3.2 a and b**)**.** Similarly, Tregs were easily identified as $CD4^{+}CD25^{hi}CD127^{lo}$ T cells (**Figure 3.2 c**). Reliably discriminating between $FoxP3^{+}$ and $FoxP3^{-}$ human cells is difficult with an isotype control. Thus, $CD4^{+}CD25^{-}$ cells were used as internal negative controls, since these cells are $FoxP3^{-}$, as shown in (**Figure 3.2 d**). It is generally accepted in the field that resting, un-activated, human $CD4^{+}CD25^{-}$ T cells express minimal FoxP3.

| Immune cell | Phenotypic Markers in Antibody Panels | CKD/ESRD effect | Proposed Vit D effect/rationale for inclusion in panel |
|---|---|---|---|
| CD4 T cell | Memory ($CD45RO^+$)<br>Naïve<br>($CD45RA^+$) | Reduced numbers of T cells (due to increased apoptosis primarily in naïve T cells) (Litjens et al., 2006)<br>Increased TH1 and decreased TH2 response (Sui et al., 2009). | Block TH1 responses and promote TH2 responses (van Etten and Mathieu, 2005).<br>Increase Naïve T cell pool (Khoo et al., 2012). |
| CD8 T cell | $CD8^+$ | Reduced numbers (Betjes, 2013). | Inhibits T cell mediated cytotoxicity (Meehan et al., 1992). |
| Treg | CD127lo CD25high<br>FoxP3 expression | Decreased number and impaired function (Hendrikx et al., 2009; Meier et al., 2009). | Induces differentiation of Tregs (Talmor et al., 2008). |
| Monocytes | $CD14^+CD16^+$<br>$CD14^+CD16^-$ | Increased number of pro-inflammatory CD14+CD16+ monocytes (Scherberich et al., 2004)<br>Hyporeactivity/reduced intracellular killing (Ando et al., 2005). | Stimulate monocyte proliferation and increased bactericidal peptide and IL-1 production (Bhalla et al., 1986). |
| mDCs | $CD14^-$ HLA-$DR^+$ $CD11c^+$ | Numbers decreased (Hesselink et al., 2005)<br>Defect in up-regulation of co-stimulatory molecules (CD86) (Girndt et al., 2001) | Inhibit differentiation and maturation of DCs (Mora et al., 2008). Switch function to IL-10 production (Penna and Adorini, 2000). |
| NK cells | CD56bright<br>CD56dim | Poorly understood,<br>NK numbers decreased (Vacher-Coponat et al., 2008). | Poorly understood |
| B-cells | $CD20^+$ | Decreased numbers but effect poorly understood (Descamps-Latscha and Chatenoud, 1996).. | Decreased B-cell proliferation (Chen et al., 2007), but conflicting results of VDR expression in B-cells (Mora et al., 2008). |

**Table 3.1|Immune cells in phenotyping panels and effects of ESRD and vitamin D on their function|**

VitD, Vitamin-D; Treg, Regulatory T cells; TH, T-helper; NK cells, Natural Killer cells; mDC, myeloid dendritic cells; VDR, Vitamin D receptor.

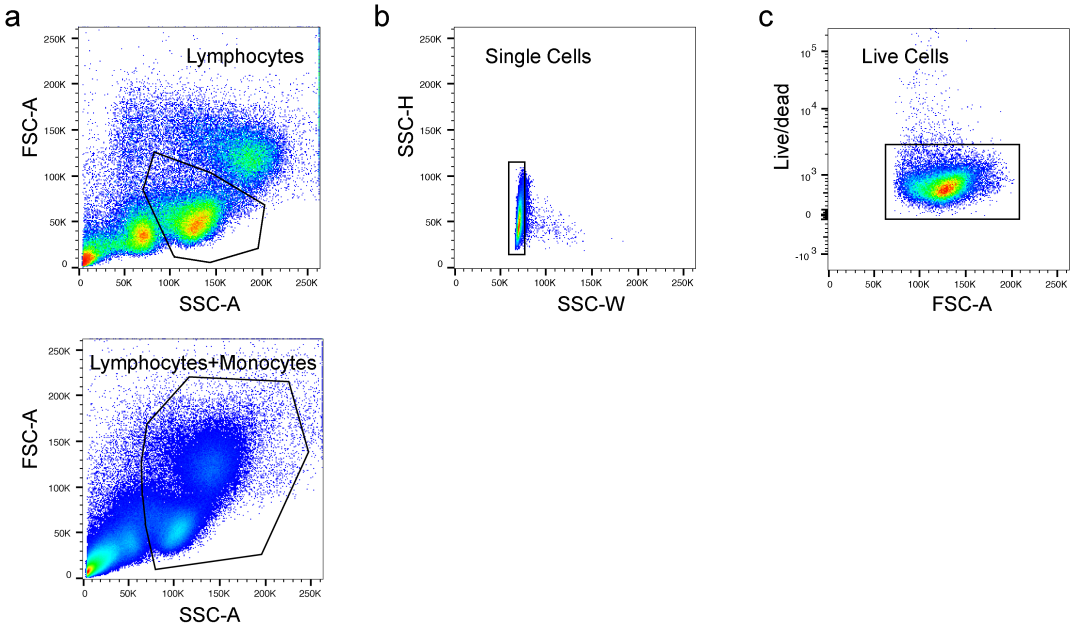


**Figure 3.1|Initial gating strategy for all flow cytometry panels|**
Flow cytometry plots demonstrating gating strategy used for initial gating from total cells. (a) FSC-A, size and SSC-A was used to discriminate lymphocytes for leukocyte and T cell panels, and lymphocytes and monocytes for myeloid panel. (b) Single cells were then gated to exclude doublets. (c) Live cells were gated based on negative staining of live/dead dye incorporation.

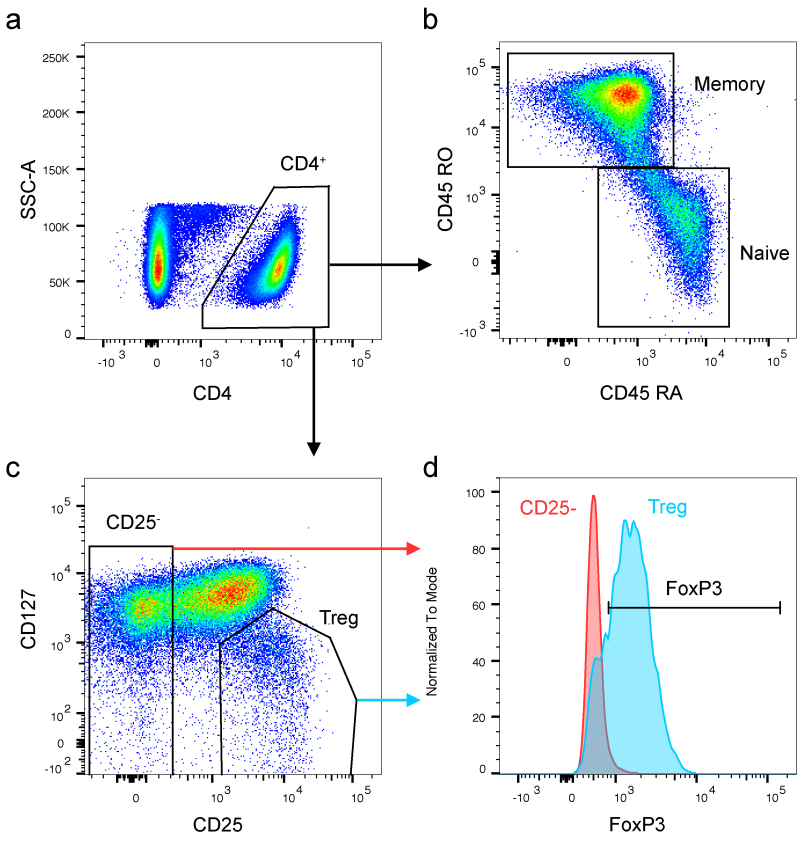


**Figure 3.2|T cell panel representative flow cytometry plots|**
Following lymphocyte gating in Figure 3.1 a: (a) $CD4^+$ T cells were initially gated on and used for subsequent gating. (b) Memory and naïve $CD4^+$ T cells where gated based on CD45RO and CD45RA expression respectively. (c) Tregs were gated based on high expression on CD25 and low expression of CD127. $CD25^-$ T cells were gated as a control for FoxP3 expression in panel (d). (d) FoxP3 gate was set based on expression in $CD25^-$ T cell expression and assessed in Tregs.

In the myeloid panel monocytes were gated into both classical $CD14^{+}CD16^{-}$ monocytes as well as the pro-inflammatory $CD14^{+}CD16^{+}$ monocytes (Ziegler-Heitbrock, 2007). FMOs are not necessary to identify the two populations as shown in (**Figure 3.3 a**). To identify myeloid dendritic cells (mDCs) lineage markers must first be excluded as both monocytes and lymphocytes are included in the FSC and SSC discrimination. To overcome this potential confounding factor, a dump gate was included, comprising of CD56 (natural killer (NK)-cells), CD3 (T cells) and CD20 (B-cells) (**Figure 3.3 b**). This is a flow cytometry technique in which all antigens that are to be excluded are labelled with the same fluorochrome and then excluded in one gate. In this case NK, T and B-cells were labelled with the AF700 fluorochrome, and all AF700 positive events excluded prior to further analysis. mDCs were subsequently selected as $CD14^{-}HLA^{-}DR^{+}CD11c^{+}$, none of which require FMOs, as all the populations are clearly identifiable and can be gated in an unbiased way (**Figure 3.3 c, d and e**).

Additionally, both mDCs and monocyte populations were analysed for levels of expression (using mean fluorescence intensity (MFI)) of CD80, CD86 and HLA-DR as markers of activation.

Finally, the lymphocyte panel was used to identify NK cells (both immature CD56 bright and mature CD56 dim (White et al., 2014), $CD4^{+}$ and $CD8^{+}$ T cells, B cells and $\gamma\delta$ T cells (**Figure 3.4**). No FMOs are needed, as all populations of cells are distinct.

#### 3.3.1.2 Fluorescent cell barcoding

In order to minimise variation in immune-phenotyping panels and reduce the time required for immune-phenotyping, multiplexing of samples by fluorescent cellular barcoding (FCB) was trialled (Krutzik and Nolan, 2006). FCB enables high throughput, high content flow cytometry. It does so by multiplexing samples (staining each sample with gradually higher FCB dye) prior to staining and acquisition on the cytometer, therefore one antibody cocktail is added to previously barcoded samples theoretically reducing variability as all clinical trial samples could be stained in one condition.

Barcoding has not previously been used for large surface staining panels and thus needed to be tested. FCB was successfully applied to PBMCs and 10 different samples

could be effectively discriminated with different concentrations of dye (**Figure 3.5 a**). However, when combined with other staining panels, although $CD4^+$ T cells could be accurately identified (**Figure 3.5 b**) the harsh fixatives used altered some cell surface antigens, such as CD45RA and CD45RO, leading to loss of surface staining (**Figure 3.5 c**). Different fixatives were trialled (ethanol, tween20, BD fix/perm, e-bioscience fix/perm) but were not able to overcome the technical challenge of barcoding while preserving all surface antigens (data not shown). Thus, FCB was discarded as an applicable flow cytometry technique in staining PBMC samples for the clinical trial.

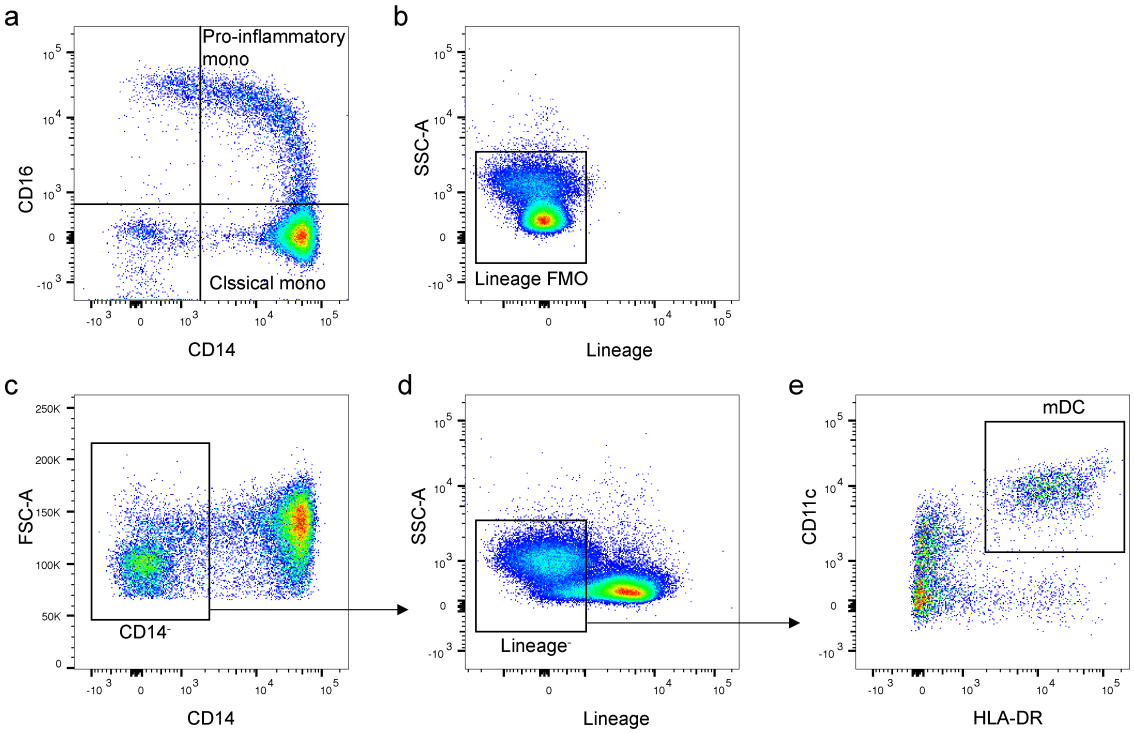


**Figure 3.3|Myeloid staining panel representative flow cytometry plots|**
Following lymphocyte + monocyte gating as in Figure 3.1 a: (a) classical monocytes (mono) were identified as $CD14^{+}CD16^{-}$, with pro-inflammatory monocytes being identified as $CD14^{+}CD16^{+}$. (b) FMO for lineage markers (CD20, CD56 and CD3) was used to set up lineage negative gate as used in (d). mDCs were identified as $CD14^{-}$ (c), $lineage^{-}$ (d) and $CD11c^{+}HLA\text{-}DR^{+}$ (e).

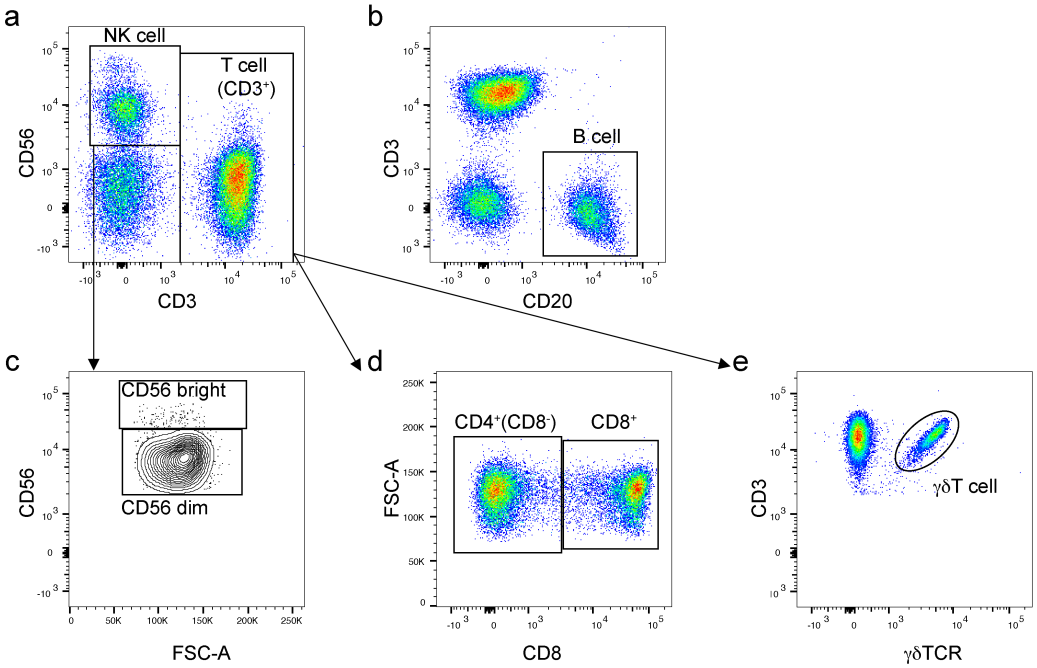


**Figure 3.4|Leukoctye staining panel representative flow cytometry plots|** Following lymphocyte gating as in Figure 3.1 a: (a) Natural Killer (NK) cells and T cells are gated on base don their expression of CD56 and CD3; T cells are identified as $CD3^+$ and NK cells as $CD3^-CD56^+$. (b) B cells are identified as $CD20^+CD3^-$ cells. (c) NK cells are further divided into $CD56^{bright}$ and $CD56^{dim}$ cells based on intensity of CD56. (d) Following gating on $CD3^+$ T cells from (a), CD4 T cells were identified as $CD8^-$ and CD8 T cells were identifies as $CD8^+$. (e) Following gating on $CD3^+$ T cells from (a) $\gamma\delta$ T cells were identified as $\gamma\delta$ $TCR^+$.

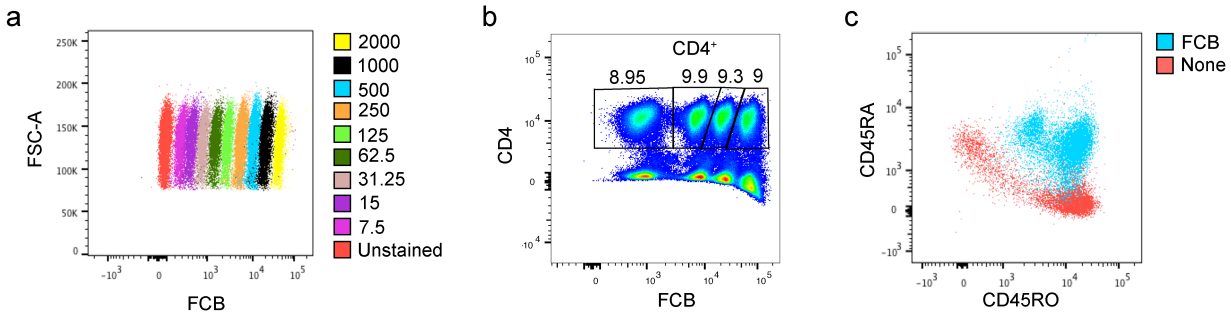


**Figure 3.5|Fluorescent cell barcoding|**
(a) PBMCs from different healthy control donors were labelled with indicated concentrations of FCB dye after fixation. (b) Representative flow cytometry plot of 4 barcoded samples stained with T cell staining panel and each individual sample gated for $CD4^+$ cells. (c) Flow cytometry plot comparing fixed (blue) for FCB experiment and unfixed (red) $CD4^+$ cells showing altered surface staining for CD45RO and CD45RA.

### 3.3.2 Minimisation of inter-assay variation as a confounding variable

Several factors can influence the inter-assay variability of flow cytometry, including laser strength and variability over time. To minimise inter-assay variability, application settings (allowing the same analysis setting to be used on every run) cytometer setup and tracking (CS&T) beads were used during acquisition. CS&T beads are composed of equal concentrations of dim, mid, and brightly dyed polystyrene beads which, critically, have low intrinsic coefficients of variation. These beads are used to set baseline 'target' laser settings, which are maintained by running the beads prior to every experiment to calibrate the laser voltages. This allows cytometer performance to stay the same every run.

To track the inter-assay variation over time, a healthy donor blood sample was frozen down into multiple aliquots and was run with every clinical trial sample and analysed in parallel with trial samples in every run (**Figure 3.6 a and b**). Coefficient of variation (CV) was calculated for both MFI of functional markers in myeloid cells and percentages of gated populations (**Table 3.2**). Most measures showed low variation however, some displayed higher variation. For example, γδT cells had a CV of 41.6%, which may indicate their susceptibility to freeze-thawing. In addition, all measures of MFI showed higher variation, due to the inherent measure variability. Due to this variability, paired samples (pre and post-repletion) for each patient were run on the same run to ensure day to day variation in experimental procedure would not be a major source of error.

### 3.3.3 Immune Phenotyping

At the time of writing thesis, 30 participants had been recruited, dosed and completed trial. On thawing, 19 of these patient samples were deemed to have useable PBMC samples both before and after repletion for flow cytometry analysis (defined as >20% lymphocytes and monocytes gated using FSC-A and SSC-A) (**Figure 3.7**). Nine of these were in placebo and ten were in cholecalciferol treatment group. Summary data for

patients at start of trial is shown in **Table 3.3**, with no significant differences in age, sex or kidney function (measured by glomerular filtration rate (GFR)).

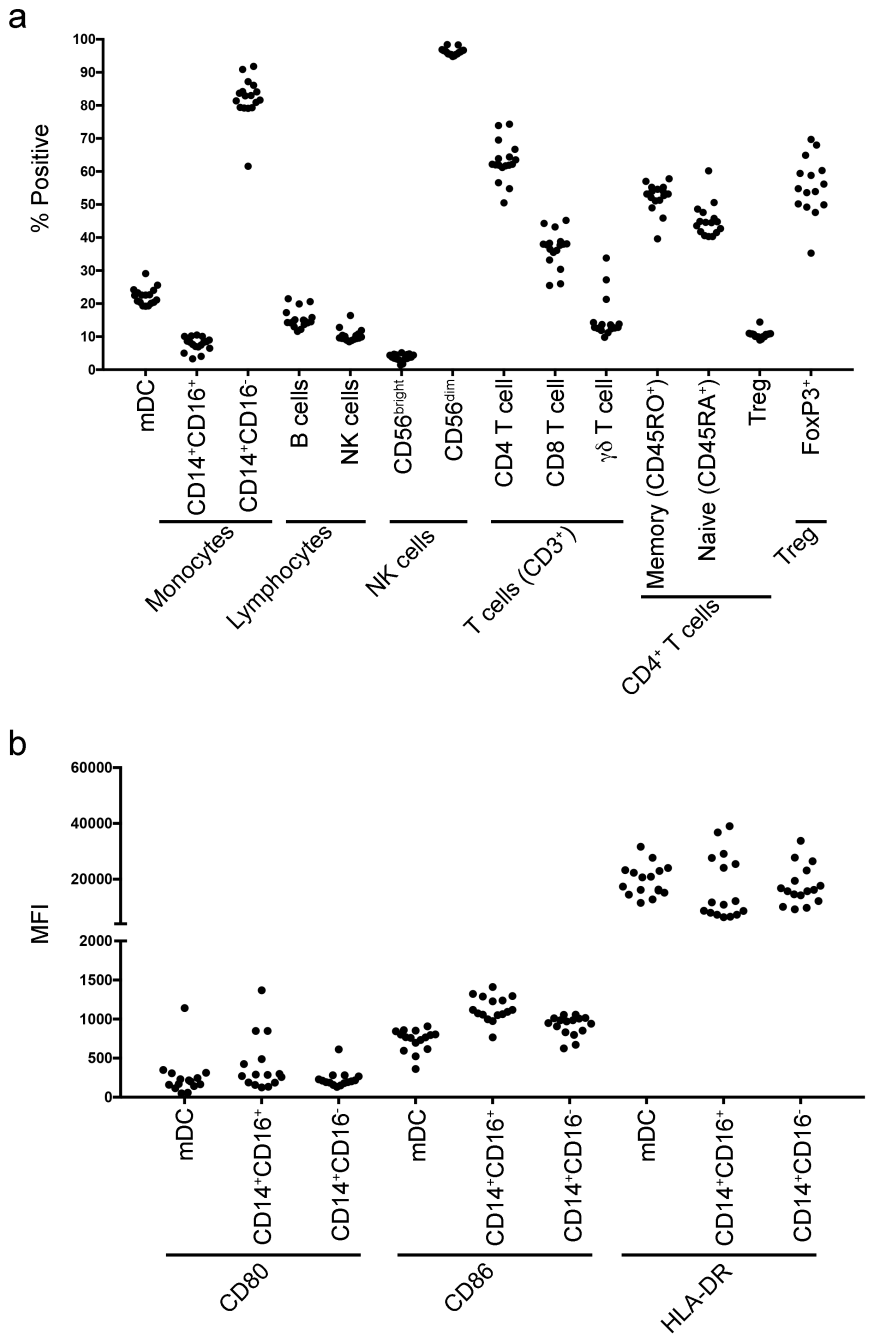


**Figure 3.6|Inter assay variability|**
Frequencies of leukocyte populations (a) and MFI of functional markers on myeloid cells (b) form multiple aliquots of a single healthy donor run in parallel with every pair of patient samples, over a 9-month period, in order to track variability of assay. mDC: myeloid dendritic cell.

| CD80 (MFI) | | | CD86 (MFI) | | | HLA-DR (MFI) | | |
|---|---|---|---|---|---|---|---|---|
| mDC | $CD14^+/CD16^+$ | $CD14^+/CD16^-$ | mDC | $CD14^+/CD16^+$ | $CD14^+/CD16^-$ | mDC | $CD14^+/CD16^+$ | $CD14^+/CD16^-$ |
| 46.42 | 69.13 | 49.10 | 19.51 | 14.15 | 14.10 | 28.44 | 68.15 | 39.35 |

| mDC(%) | $CD14^+/CD16^+$(%) | $CD14^+/CD16^-$ (%) | B-cells (%) | NK cells (%) | NKcells/CD56Bright (%) | NKcells/CD56Dim (%) | CD4 (%) | CD8 (%) | γδ T Cells (%) |
|---|---|---|---|---|---|---|---|---|---|
| 11.72 | 27.50 | 7.94 | 18.29 | 18.48 | 27.18 | 1.05 | 9.55 | 14.96 | 41.16 |

| $CD4^+CD45RA^+$ (%) | $CD4^+CD45RO^+$ (%) | Treg (%) | $TReg/FoxP3^+$ (%) |
|---|---|---|---|
| 8.53 | 11.09 | 11.24 | 15.78 |

**Table 3.2|Coefficients of variation for flow cytometry staining panels|**
Coefficients of variation for MFI in myeloid panel (top), for percentages of cell populations (middle and bottom). All from multiple aliquots of a single healthy donor run in parallel with every pair of patient samples, over a 9-month period, to track variability of assay. (*n* = 17, coefficient of variation as percentage)

| | Median [IQR]/number (%) | |
|---|---|---|
| | Placebo<br>*n*=9 | Cholecalciferol<br>*n*=10 |
| Sex (Male) | 7 (78) | 8 (80) |
| Age (Years) | 54 [49-59] | 51.5 [41-66] |
| Pre-trial GFR (mL/min) | 40 [36-42.5] | 30 [25-33] |

**Table 3.3|Basic patient characteristics at week 0 of trial|**

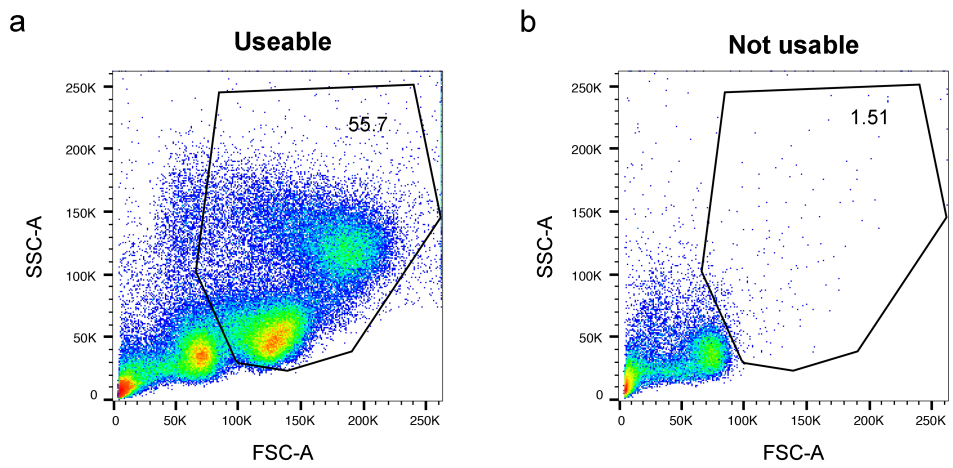


**Figure 3.7|Quality assessment of PBMC samples|**
Representative flow cytometry plots of PBMC sample deemed useable (a) and not useable (b) for flow cytometry analysis based on identification of monocyte and lymphocytes using FSC-A and SSC-A

### 3.3.4 Serum cytokine measurement

As the pathogenesis of CKD has been shown to involve cytokines, driving inflammation and potentially causing several adverse outcomes (Lam, 2009), we assessed the changes in serum cytokine levels of seven cytokines before and after 52 weeks of cholecalciferol treatment or placebo.

Most cytokines showed very low levels, with most being below the limit of detection, with only IL-6 and IL-17 showing consistently elevated levels and even those in only some patients (**Figure 3.8**). Although the elevated concentrations of serum IL-6 and IL-17 probably indicated some inflammation, no significant difference was observed in any cytokine between placebo or cholecalciferol treatment.

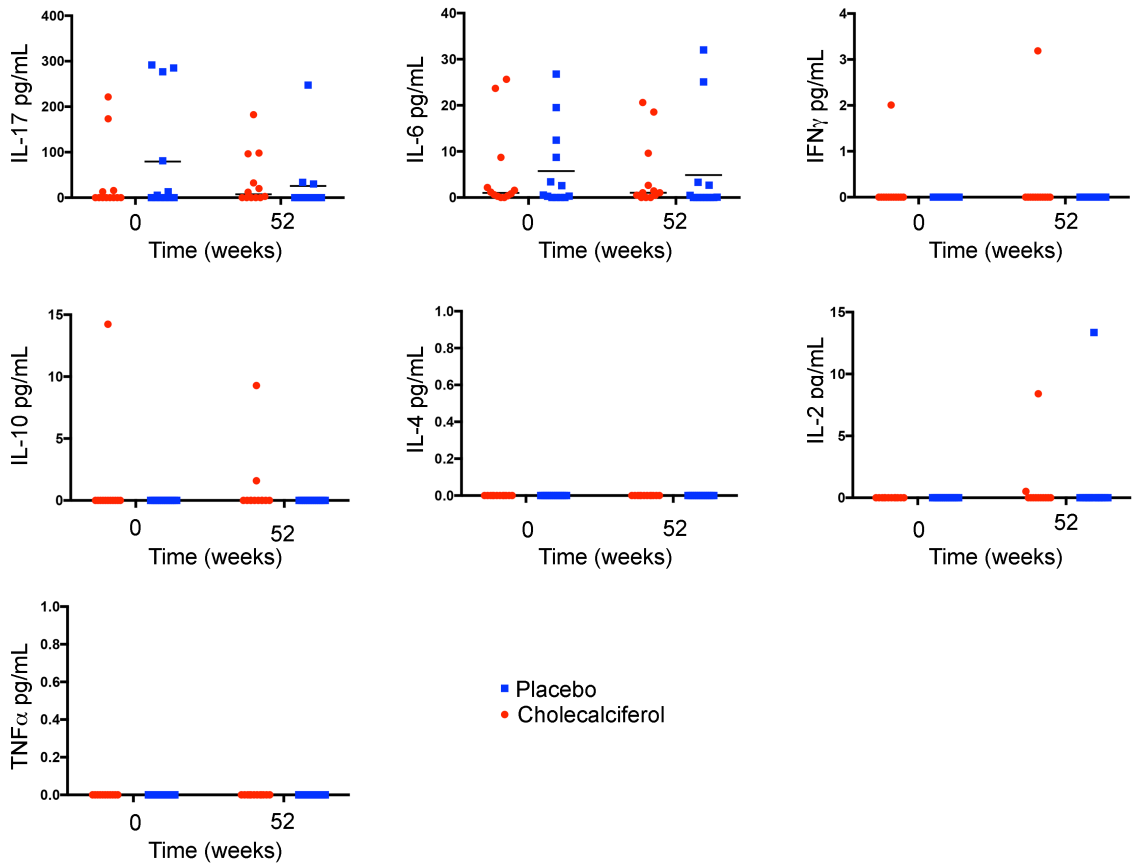


**Figure 3.8|Serum cytokines|**
Concentration of seven cytokines present in the serum of patients at week 0 and week 52 with either cholecalciferol (red circles) or placebo (blue squares) treatment. Line on graph represents the median. (Placebo *n* = 12, cholecalciferol *n* = 14)

### 3.3.5 Phenotyping data revealed significantly reduced HLA-DR expression on mDCs following cholecalciferol treatment

ANCOVAs, controlling for age and sex, were run on all phenotypic data as well as available 25 VitD levels.

Within the $CD4^+$ T cell compartment, no significant changes were seen in percentages of naïve, memory T cells nor Tregs (**Figure 3.9 a and b**). Additionally, no significant changes in $FoxP3^+$ percentage were seen (**Figure 3.9 b**). No significant changes were observed in percentages of any of the major leukocyte populations measured (**Figure 3.10**). Finally no significant changes were seen in percentages of $CD14^+CD16^+$ (**Figure 3.11 a**) or $CD14^+CD16^-$ monocyte populations (**Figure 3.12 a**), nor in their expression of CD80, CD86 and HLA-DR (**Figure 3.11 b and Figure 3.12 b**).

We noted a significant treatment x week interaction between cholecalciferol supplementation and VitD levels (**Figure 3.13 a**) as well as HLA-DR MFI expression on mDCs (**Figure 3.13 b**). However, there were no significant changes in actual percentages of mDCs nor expression of CD80 or CD86 on mDCs (**Figure 3.14 a**). Follow up t-tests confirmed 25 VitD levels were significantly increased in the cholecalciferol group at week 52 compared to week 0 ($p=0.036$, $t=2.836$), with a mean increase of 27.17 nmol/L, with no significant change observed in the placebo group over the same period. This indicates cholecalciferol treatment did lead to a significant increase in serum 25 VitD. Follow up t-tests also revealed the interaction for HLA-DR MFI was due to a significant decrease in HLA-DR expression in the cholecalciferol-treated group, which was not seen in the placebo group ($p=0.0106$, $t=3.214$) (**Figure 3.14 b**). Although levels of serum 25 VitD increased after treatment, levels reached a mean of 71.2 nM, still below the threshold at which VitD sufficiency is classified (>75nM). Not all 25 VitD levels were available for both time-points (**Figure 3.13 a**), which may reduce the magnitude of change seen in the overall study population.

In summary, serum levels of 25 VitD significantly increased and HLA-DR expression on mDCs significantly decreased in the cholecalciferol treatment group but not in the placebo group. As one of the main targets of VitD in a mixed immune population is DCs and the main effect is the generation of tolerogenic phenotype, with

low HLA-DR expression (Lyons et al., 2010; Marchal et al.), this effect is an indication that increasing serum levels of VitD can lead to a reduction in inflammatory status of circulating immune cells.

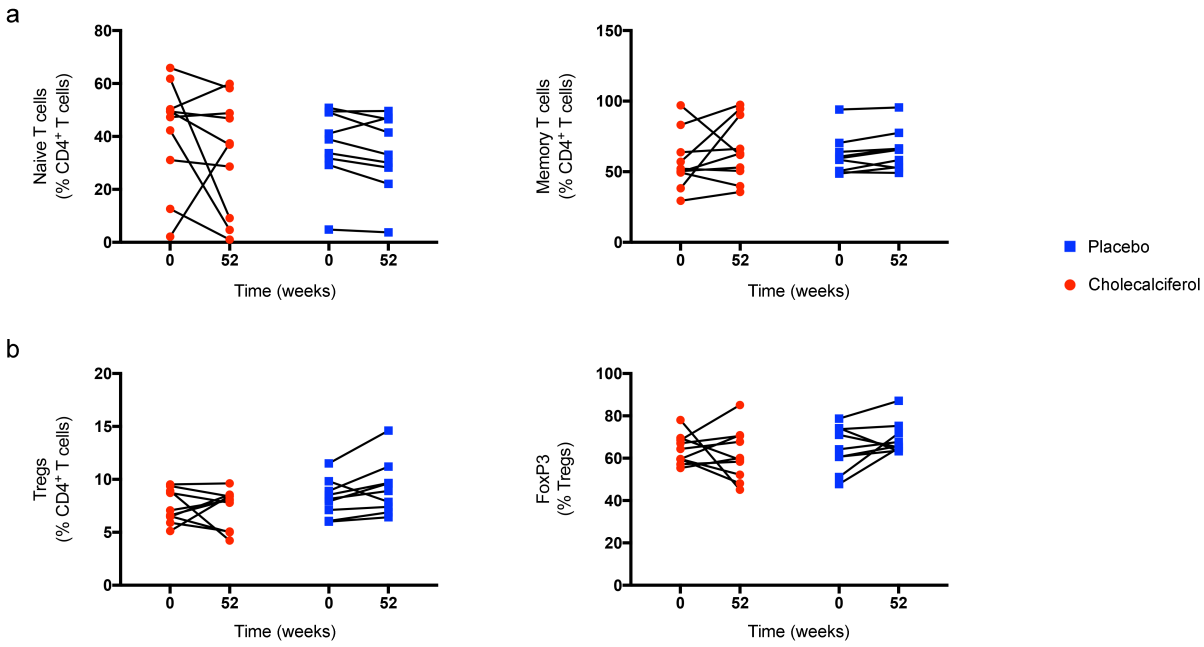


**Figure 3.9|Immune phenotype of T cells in clinical trial|**
Quantification of flow cytometry analysis showing (a) percentage of naïve ($CD45RA^+$) and memory ($CD45O^+$) $CD4^+$ T cells as well as (b) Tregs and FoxP3 in Tregs, in cholecalciferol (red circles) and placebo (blue squares) group, at week 0 and week 52. (*n* = 9 in placebo and *n* = 10 in cholecalciferol group)

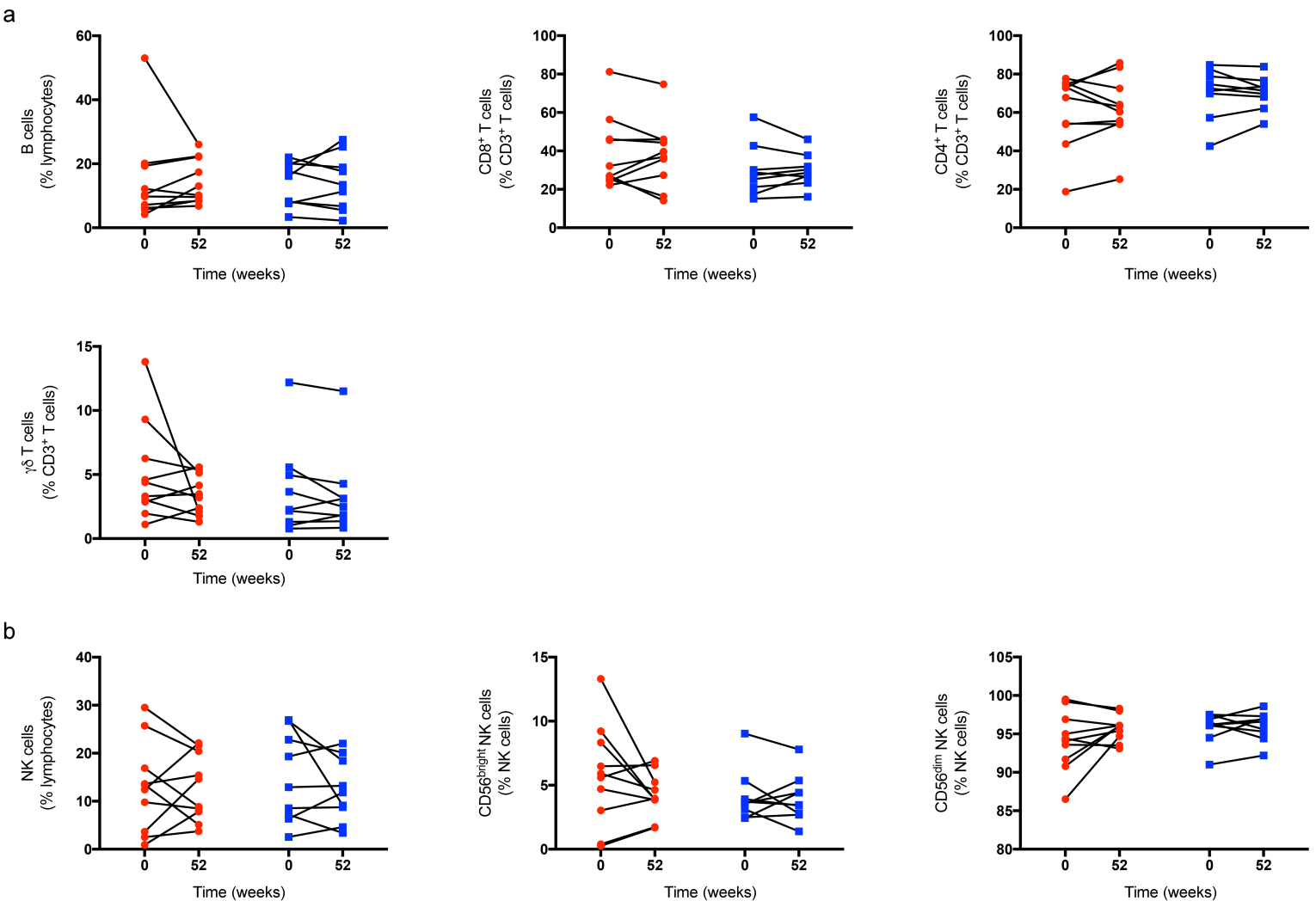
a
B cells
(% lymphocytes)
60
40
20
0
0
52
0
52
Time (weeks)
CD8+ T cells
(% CD3+ T cells)
100
80
60
40
20
0
0
52
0
52
Time (weeks)
CD4+ T cells
(% CD3+ T cells)
100
80
60
40
20
0
0
52
0
52
Time (weeks)
γδ T cells
(% CD3+ T cells)
15
10
5
0
0
52
0
52
Time (weeks)
b
NK cells
(% lymphocytes)
40
30
20
10
0
0
52
0
52
Time (weeks)
CD56bright NK cells
(% NK cells)
15
10
5
0
0
52
0
52
Time (weeks)
CD56dim NK cells
(% NK cells)
105
100
95
90
85
80
0
52
0
52
Time (weeks)

**Figure 3.10|Immune phenotype of leukocyte subsets in clinical trial|**
Quantification of flow cytometry analysis showing percentages of (a) B cells, $CD8^+$, $CD4^+$ and $\gamma\delta$ T cells; (b) NK cells both $CD56^{bright}$ and $CD56^{dim}$ populations, in cholecalciferol (red circles) and placebo (blue squares) group, at week 0 and week 52. (*n* = 9 in placebo and *n* = 10 in cholecalciferol group)

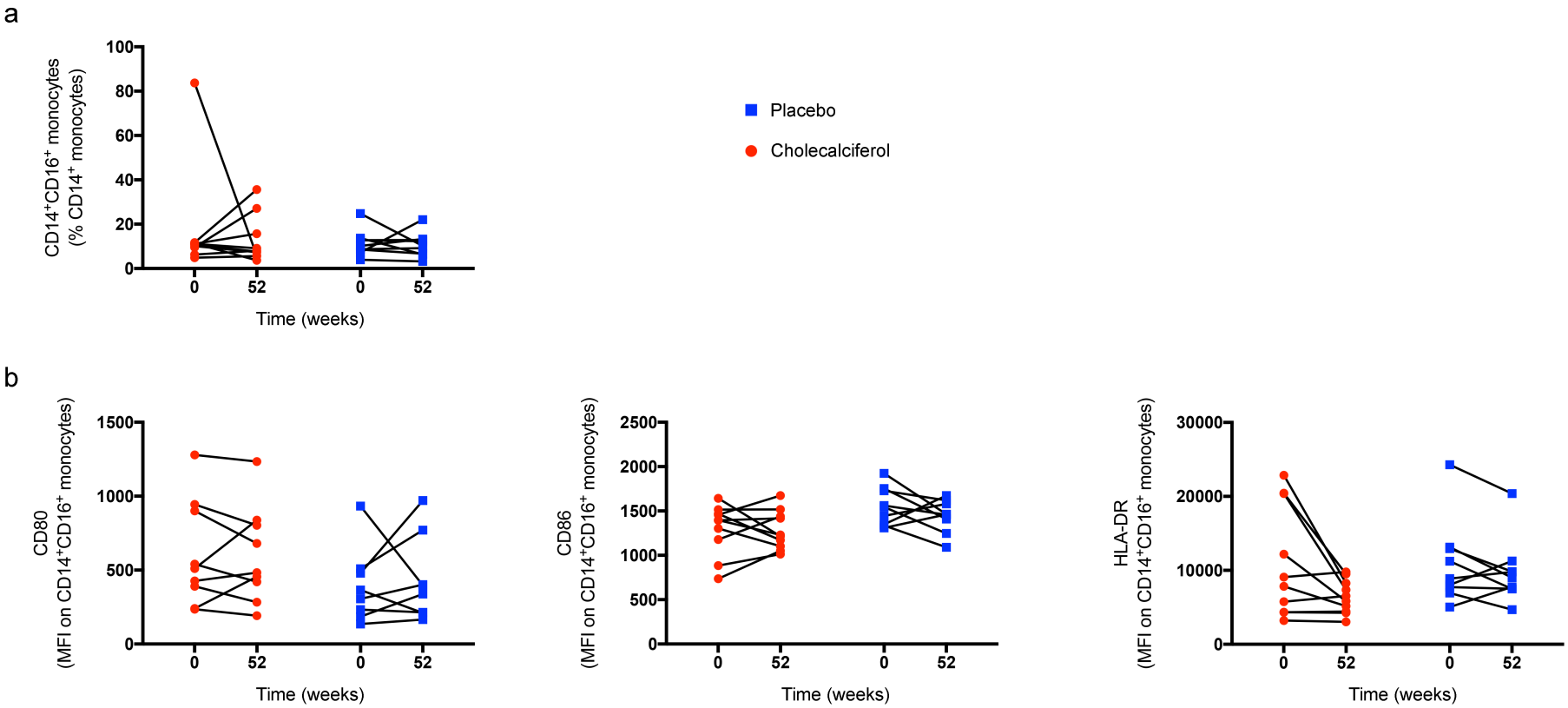


**Figure 3.11|Immune phenotype of CD14$^+$CD16$^+$ monocyte subsets in clinical trial|**
Quantification of flow cytometry analysis showing percentages of (a) CD14$^+$CD16$^+$ monocytes and (b) CD80, CD86 and HLA-DR MFI, in cholecalciferol (red circles) and placebo (blue squares) group, at week 0 and week 52. (*n* = 9 in placebo and *n* = 10 in cholecalciferol group)

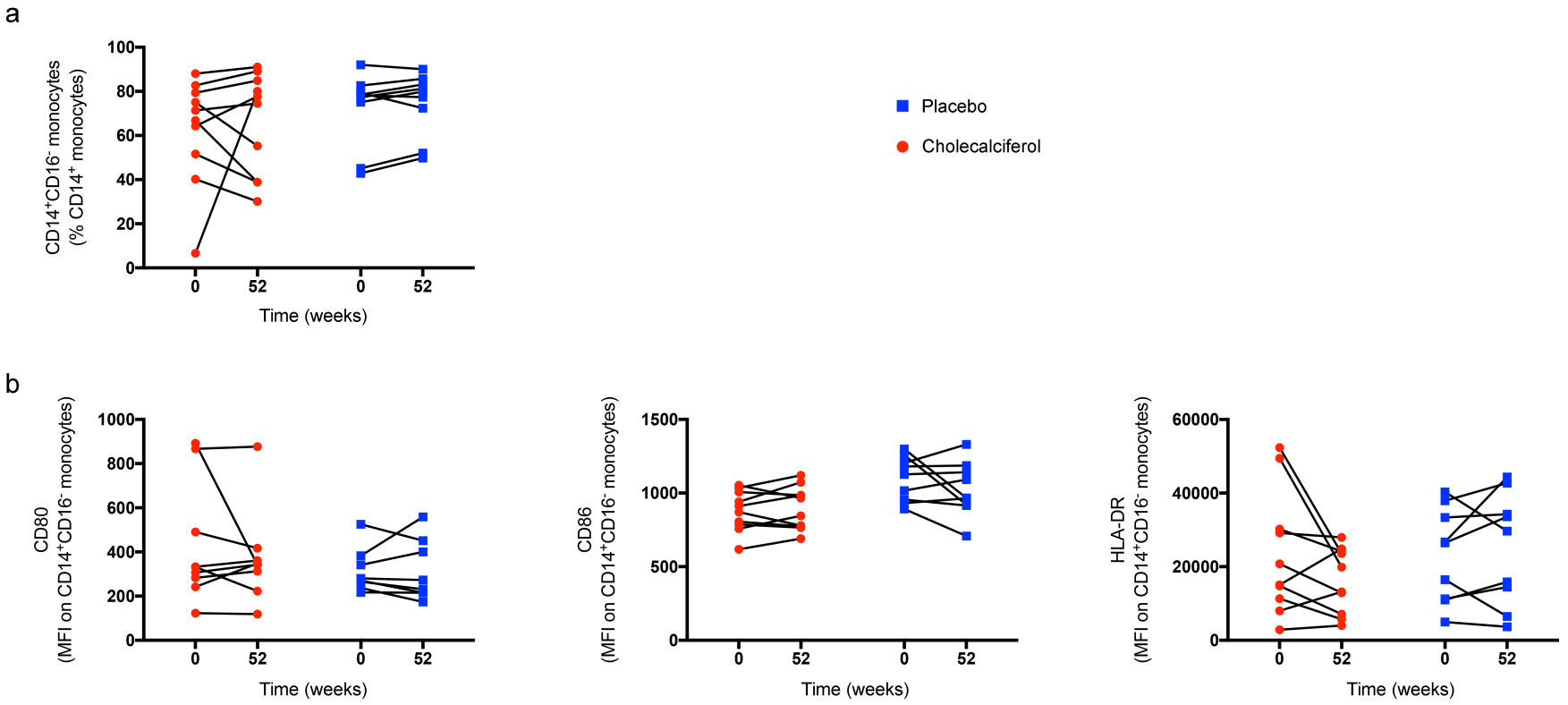


**Figure 3.12|Immune phenotype of CD14$^+$CD16$^-$ monocyte subsets in clinical trial|**
Quantification of flow cytometry analysis showing percentages of (a) CD14$^+$CD16$^-$ monocytes and (b) CD80, CD86 and HLA-DR MFI, in cholecalciferol (red circles) and placebo (blue squares) group, at week 0 and week 52. (*n* = 9 in placebo and *n* = 10 in cholecalciferol group)

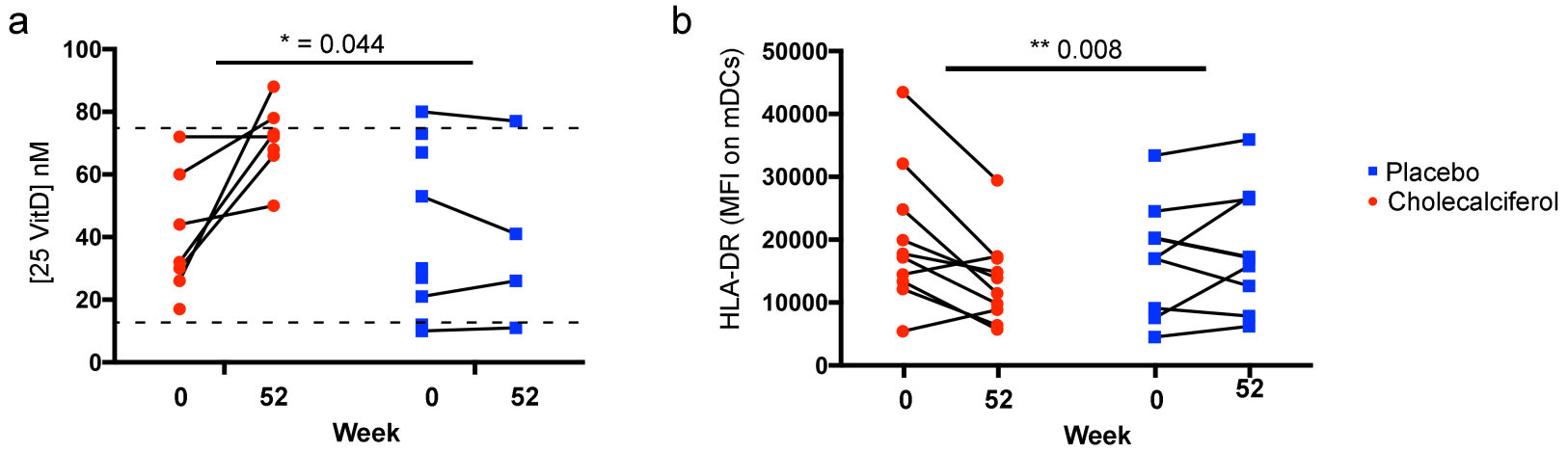


**Figure 3.13|Significant results from clinical trial|**
(a) Serum 25 VitD levels and (b) HLA-DR expression (MFI) on mDCs at weeks 0 and 52 in the placebo and cholecalciferol groups. 2x2 way ANCOVA, controlled for age and sex, showed significant treatment x week interaction, as indicated by p-values above graphs. Follow-up tests revealed (a) significant increase in 25 VitD levels in cholecalciferol group and (b) significant decrease in HLA-DR MFI on mDCs (myeloid dendritic cells) in cholecalciferol group. (a) Dotted lines represent insufficient range of 12.5-75 nM 25 VitD. (*n* = 9 in placebo and *n* = 10 in cholecalciferol group with *n* = 6 cholecalciferol and *n* = 4 placebo paired samples * $p \leq 0.05$, ** $p \leq 0.01$)

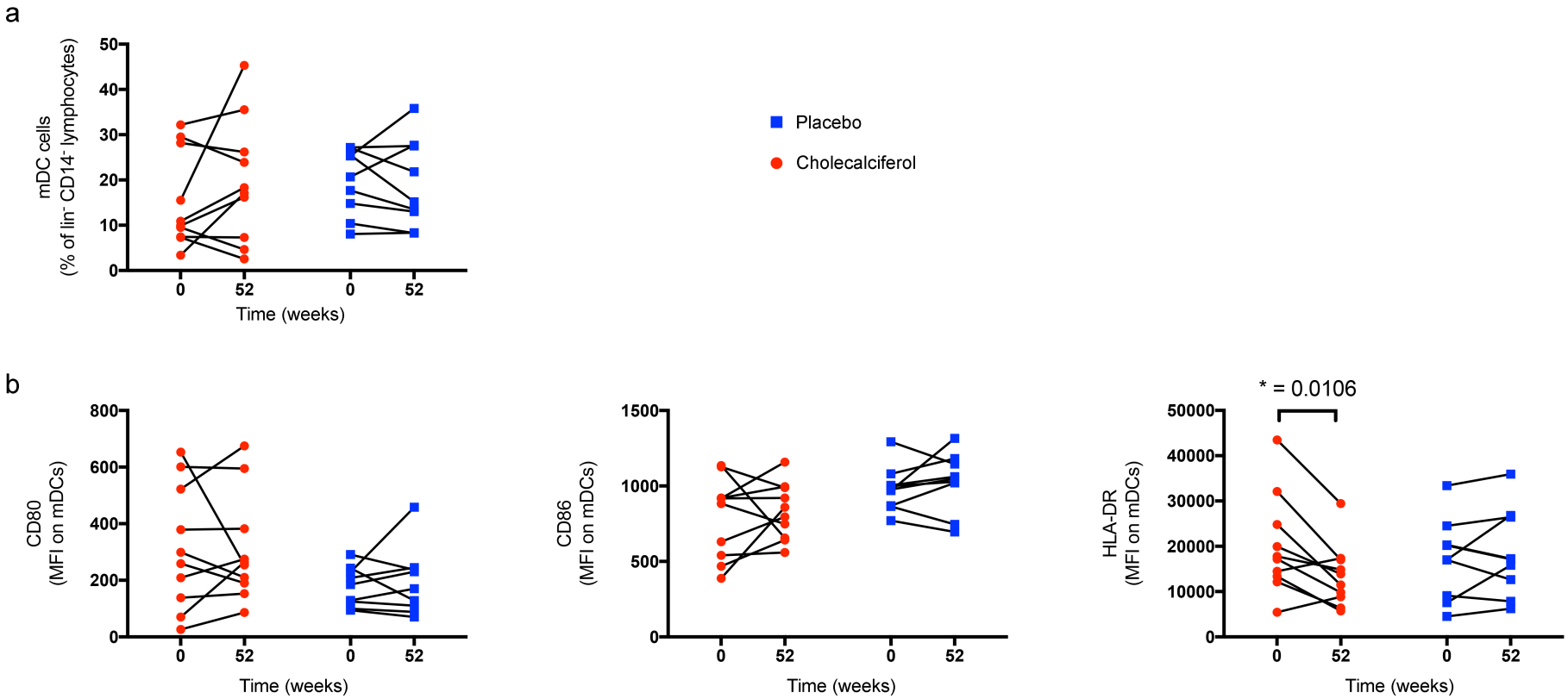


**Figure 3.14|Immune phenotype of mDCs$^-$ in clinical trial|**
Quantification of flow cytometry analysis showing percentages of (a) mDCs (myeloid dendritic cells) and (b) CD80, CD86 and HLA-DR MFI, in cholecalciferol (red circles) and placebo (blue squares) group, at week 0 and week 52. (*n* = 9 in placebo and *n* = 10 in cholecalciferol group, * $p \leq 0.05$)

### 3.3.6 Confirmation of inhibitory effect of *in-vitro* VitD treatment on DC maturation and HLA-DR expression

To confirm the ability of VitD to inhibit maturation of mDCs, by inhibiting up-regulation of co-stimulatory molecules, we turned to monocyte derived DCs (mo-DCs) as a model cell. Although mo-DCs differ in some ways from mDCs, mo-DCs are often used as an *in vitro* model for the study of mDCs as they share myeloid precursor lineage (Osugi et al., 2002). mo-DCs were matured by addition of LPS in the presence of carrier or 1,25 VitD and expression of CD80, CD86 and HLA-DR was measured. Maturation was evident in the absence of VitD by high expression of HLA-DR, CD80 and CD86 (**Figure 3.15**). VitD significantly inhibited this maturation of DCs by inhibiting expression of CD80, CD86 and HLA-DR during the maturation process (**Figure 3.15**). This confirmed the published data (Lyons et al., 2010; Marchal et al.) and our clinical trial data, that VitD can inhibit the maturation of mDCs, perhaps leading to DCs with reduced ability to activate immune responses through co-stimulation of T cells.

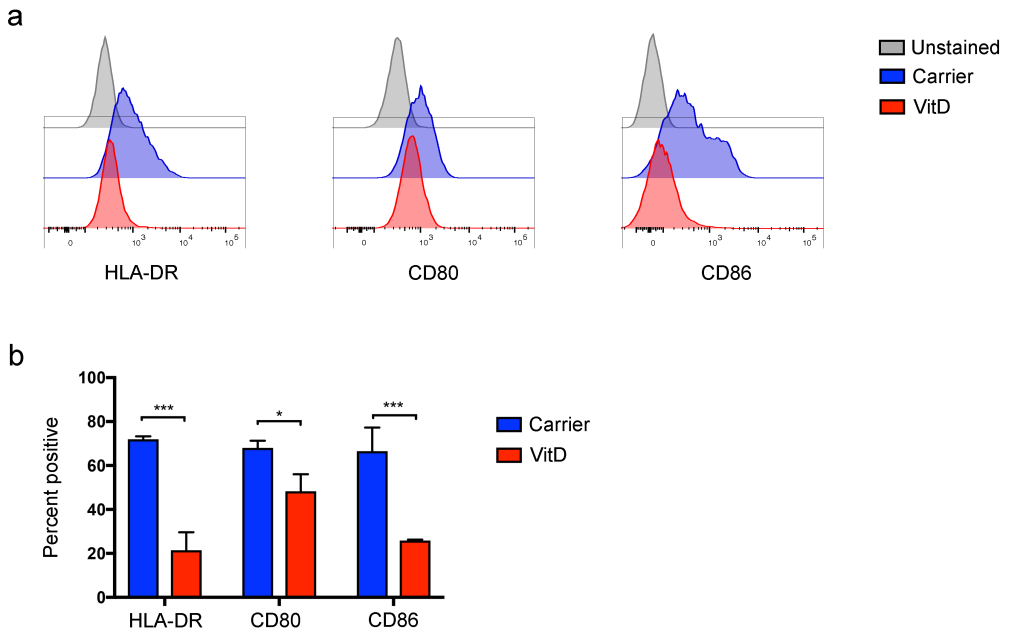


**Figure 3.15|Effect of VitD treatment during maturation of mo-DC on expression of co-stimulatory molecules|**
(a) Representative flow cytometry histograms showing expression of HLA-DR, CD80 and CD86 after maturation of mo-DCs (monocyte derived dendritic cells), matured in the presence of carrier or 1,25 VitD. (b) Cumulative data of expression of markers shown in (a). (*n* = 3, ANOVA, mean ± SEM * $p<0.05$, *** $p<0.001$).

## 3.4 Discussion

Although much has already been published on the *in vitro* effects of vitamin D on immune cells (see section 1.4), to the best of our knowledge no studies have carried out immune profiling testing the effect of VitD supplementation on circulating immune cell frequencies in a randomised, double blinded clinical trial setting. We have carried out a comprehensive analysis of the main immune cell subsets before and after VitD supplementation in a cohort of patients with early stage CKD and early CVD. The major findings of this chapter are that supplementation, in patients with early CKD, using cholecalciferol over a 52 week period is able to both significantly increase circulating levels of 25 VitD as well as reduce expression of HLA-DR on mDCs, with neither effect observed in the placebo group.

*In vitro* treatment of DCs with the active 1,25 VitD has consistently been shown to reduce HLA-DR expression (Marchal et al.; Mora et al., 2008), an effect further confirmed *in vitro* in this chapter. This effect ,along with reducing other co-stimulatory molecules (such as CD80 and D86), has been suggested to be one of the major immunoregulatory mechanism by which VitD indirectly leads to Treg generation (Chambers and Hawrylowicz, 2011). Lower HLA-DR expression is associated with an immature DC phenotype and a reduced ability to provide the co-stimulation required for appropriate effector T cell responses, preferentially generating Tregs instead (Adorini and Penna, 2009). Additionally, an activated mDC phenotype (notably increased HLA-DR expression), is one of the markers used as an indicator of immune activation in CKD populations (Pereira et al., 2010). Thus, a reduced HLA-DR expression observed following cholecalciferol treatment in our CKD cohort suggests an early reduction in inflammatory status of immune cells due to VitD repletion. These findings are in agreement with two studies in which calcitriol treatment was shown to reduce HLA-DR expression on both cells in the kidney (Özdemir et al., 2011) and PBMCs (Ahmadpoor et al., 2009) of renal transplant patients. In both studies, calcitriol treatment was associated with increased graft survival. Interestingly, we did not observe any decrease in other co-stimulatory molecules which suggests that reduction in HLA-DR expression may be one of the earlier changes induced by increased serum 25 VitD levels.

We did not observe any effect of VitD repletion on any other circulating immune cells. We also found no effect on the serum concentrations of any cytokines, though most of the cytokine fell below the detection range of the assays. Although CKD patients display chronic basal inflammation, the majority of studies have analysed patients with late stages of CKD and ESKD (Kato et al., 2008). Thus, the fact that we could not detect inflammatory cytokines in our cohort of relatively early (stage 3-4b) CKD patients may reflect the non-inflamed nature of our cohort. In fact, a recent meta-analysis of cholecalciferol treatment on the systemic inflammatory profile in adults free of acute inflammatory disease found no support of a beneficial effect of cholecalciferol on systemic IL-6 and C-reactive protein (CRP , a marker of systemic inflammation) (Calton et al., 2017). In fact this study suggested confounding effects of age, gender and sex, and most importantly a sub-group analysis indicated a serum 25 VitD level of ≥80 nM should be targeted in order to see changes in inflammatory status. As we aimed to achieve 75nM and a mean level of only 71.2 nmol/L was achieved, it may be that higher repletion levels may be required to see an effect on circulatory inflammatory status.

Interestingly, we also did not observe a significant change in immune cell frequencies over the 52-week trial period regardless of trial group. Although previous studies have found an effect of CKD on immune cell numbers and phenotype (see **Table 3.1**), CKD patients in these studies were usually compared to healthy control groups, or across stages of CKD. In addition, most of these studies looked at absolute cell numbers (Hendrikx et al., 2009; Hesselink et al., 2005; Litjens et al., 2006). Thus, future studies of this kind would benefit from including cell counts in the analysis of immune cell populations following VitD supplementation, which would increase the ability to detect changes.

In addition, previous studies have shown no significant difference in numbers of major white blood cell populations in CKD populations compared to healthy controls (Litjens et al., 2006), whilst others have observed differences in functional markers (Girndt et al., 2001; Sui et al., 2009). Specifically, VitD deficiency and increased frequencies of $CD4^{+}CD28^{null}$ cells in CKD patients have been correlated with accelerated atherosclerosis (Yadav et al., 2012). $CD4^{+}CD28^{null}$ T cells are a subset of helper T lymphocytes that are potential catalysts of inflammation in several inflammatory

disorders (Dumitriu, 2015). Thus, perhaps future trials should include more functional markers of VitD induced immuno-regulation rather than focusing on frequencies of circulating populations. Indeed, in this chapter HLA-DR expression on subsets was one such functional marker of VitD activity and the only maker identified as significantly altered due to VitD repletion.

### 3.4.1 Limitations

The clinical trial originally sought to recruit 50 participants, with 25 to be randomised to receive placebo and 25 cholecalciferol (see section 2.1.1). After discarding of unusable PBMC samples we were left with 9 in the placebo group and 10 in the cholecalciferol group for phenotypic analysis, at the time of writing this thesis. Recruiting fewer patients has the potential to reduce the power to detect significant changes. In hindsight, this trial may have been better conducted if PBMC samples had been phenotyped directly *ex vivo*, to bypass any effects of freeze thaw cycle. However, this would mean pre- and post-repletion samples could not be run on the same day. This would mean any assay variation may complicate downstream analysis.

The repletion regimen was 100,000 IU six times over the 52-week trial period (see section 2.1.1 and **Table 2.1**). This regimen was chosen as similar regimens have been proven safe and effective at increasing levels of 25 VitD from <50nmol to >75 nM (Chandra et al., 2008) in CKD patients. However, in this trial, although a significant increase in 25 VitD levels was seen, repletion above 75nM was only obtained in 2 participants receiving cholecalciferol. This may have been due to the differences in dosing. In the original trial 50,000 IU was given once a week for 12 weeks. To make the trial more feasible with less hospital visits (as cholecalciferol was directly observed) 100,000 IU was given at 0,4,8,12,24 and 42 weeks. The clinically relevant levels of 25 VitD are still debated (see section 1.5) so these cut-offs are somewhat arbitrary. Despite this the relatively modest repletion levels seen in this trial potentially hindered the ability to detect VitD induced effects on the immune system. However, successful repletion has been obtained using cholecalciferol in other trials using a monthly 100,000 IU dosing regimen (Jean et al., 2009). So perhaps dosing could have been monthly throughout the

trial, but as mentioned the feasibility would have been reduced with drop-outs increased and enrolment reduced, as more hospital visits would be required.

Although we do not currently have access to the clinical data (the trial is still blinded) preliminary analysis has revealed no difference in CKD or CVD outcomes analysed by independent collaborators. In addition, a recent randomised, placebo failure patients (Zittermann et al., 2017). These findings perhaps indicate that repletion needs to occur earlier. Our trial only recruited patients with early CKD (stage 3b-4), so perhaps repletion needs to be started earlier for the ant-inflammatory effects (like reduced HLA-DR expression) to influence clinical signs of disease. Opposing this view a different trial showed cholecaciferol repletion of stage 5 CKD and haemodialysis patients led to significantly less inflamed ventricles of the heart accompanied by reduced CRP levels (Kidir et al., 2015). However, several factors where differing in this trial design that could explain the different observations. This trial used a dose of 50,000 IU/week for 3 months and 73% of patients attained sufficient levels at end of trial, whereas in our current trial, as mentioned above, only two patients achieved sufficient levels. Additionally, we did not measure CRP levels as a measure of systemic inflammation, and this is something that can be incorporated into future trial designs. Finally, the trial was not placebo controlled and compared to patients on standard care, which was a strength of our clinical trial.

### 3.4.2 Future directions

We are awaiting clinical measures of the primary outcomes for this clinical trial to determine if the evidence of reduced inflammatory status of circulating mDCs correlates with any other measures of disease status and to determine whether oral VitD repletion in patients with early CKD and CVD improves any parameter of cardiovascular disease, all of which will be carried out in independent labs blinded. In this context, a recent meta-analysis of 28 high quality randomised control trials (RCTs) and observational studies (OSs) with over 220,000 CKD patients, showed no significant benefit in RCTs of VitD treatment in all-cause mortality or cardiovascular mortalities. However, this contrasted with OSs in which VitD treatment was significantly associated with reductions in all-cause mortality and cardiovascular mortalities (Lu et al., 2017). This points towards a more

general feature in the field of VitD research, where there seems to be a disconnect with OSs generally showing beneficial effects of replete levels of serum VitD, and RCTs generally showing no beneficial effect of repletion using VitD. This disconnect is probably due in part to the known issues of VitD research discussed in section 1.5.2.

Additionally, we have to date only received serum samples from 12 placebo and 14 cholecalciferol participants for cytokine analysis and do not have full paired 25 VitD levels yet. Thus, the trial has not yet been completed and we hope upon completion, further analysis could yield more disease specific results.

# 4. VITD SIGNALLING INDUCED IL-10 IN AN IL-6 AND STAT-3 DEPENDENT MANNER, THROUGH EPIGENETIC MODIFICATIONS

## 4.1 Introduction

Although no differences were observed in $CD4^+$ T cells in the clinical trial it is known that VitD has pleiotropic functions in the immune system including direct effects on $CD4^+$ T cells (see section 1.4). One of the best studied effects of VitD on $CD4^+$ T cells is its ability to regulate cytokine production, classically inducing anti-inflammatory IL-10, even under Th17 skewing conditions, and inhibiting pro-inflammatory IFNγ and IL-17 (Dankers et al., 2016). However, the mechanisms by which VitD, through binding to VDR, influences cytokine production are poorly understood, particularly in T cells. In fact no publications have suggested a mechanism by which vitamin D induces IL-10 production from $CD4^+$ T cells, with one study identifying a VDR binding site upstream of the IL-10 promoter as a mechanism for VitD induced IL-10 production in monocytes (Matilainen et al., 2010). Only one study has investigated genome-wide VDR binding locations in $CD4^+$ T cells (Handel et al., 2013) and did not treat the cells with active 1,25 VitD, but compared ChIPseq signal of cells coming from VitD sufficient vs deficient participants. Given the reported ability of VitD bound to VDR to recruit enzymes capable of remodelling chromatin (intro chapter 5.2.3.2 VitD and Histone modifications) and thus influencing epigenetic landscapes, it seems likely that this is a key mechanism by which VitD could influence gene transcription in $CD4^+$ T cells. In fact, VDR ChIPseq data from $CD4^+$ T cells show enrichment of VDR binding sites or chromatin marks associated with transcriptional regulation (H3K27Ac, H3K4me1, H3K4me2, H3K4me3 and H3K9Ac) and poor enrichment for repressive chromatin marks (H3K9me3) (Handel et al., 2013). Supporting this observation, VDR ChIPseq in lymphoblastoid cell lines (LCLs) following 1,25 VitD treatment indicate that enrichment of VDR binding sites are far greater at H3K4me3 and H3K27Ac sites when compared with H3K4me1 sites (Ramagopalan et al., 2010). In line with this, Joshi *et al.* showed that IL-17 production from human $CD4^+$ T cells was dependent on decreased NFAT binding upstream of the IL-17 tss through recruitment of HDACs and reduced H4 acetylation (Joshi et al., 2011).

Very few studies have assessed the direct influence of VitD on specific epigenetic chromatin marks and the result of these marks on gene expression/cellular

phenotype. To date, the bulk of evidence points towards histone acetylation as the primary epigenetic effect of VitD, with only a few studies suggesting VitD may also affect DNA methylation (Fetahu et al., 2014; Nemere et al., 1998). This is likely one of the key mechanisms by which VitD imprints a specific phenotype on cells, altering genomic responsiveness to additional stimuli. As discussed in section 1.3.1 it seems that the VDR cistrome is largely cell-specific with only a few loci being shared in all models studied to date. These loci could represent a core set of regions acting as entry points for the VDR into the genome, which can then propagate the various pleiotropic functions of VitD, each of which may be cell-type specific. The large number of loci identified by ChIP-seq in several different cell lines and activation conditions are probably far more than are needed to explain the physiological actions of 1,25 VitD. There may therefore be some noise associated with these dataa. It is therefore likely that to draw robust conclusions in relation to the physiological actions of VitD in a given cell environment several parallel approaches should be gainfully employed, notably: 1) Monitoring of genomic VDR loci by ChIP-seq 2) genome wide assessment of chromatin accessibility ChIP-seq using histone modifications or ATAC-seq and 3) assessment of magnitude of gene expression changes resulting from VDR binding to open chromatin using RNA-seq or microarray. This will be of particular interest in primary cells in health and disease. We have tried to do apply some of these approaches in this thesis as outlined below.

## 4.2 Hypothesis and aims

We hypothesised that VitD treatment of $CD4^+$ T cells would, through binding of liganded VDR, lead to epigenetic modifications affecting genes involved in the regulation of cytokine production.

We aimed to test this hypothesis by:

a) Dissecting the signalling cascades induced by VitD treatment responsible for the regulation of cytokine expression, particularly IL-10, in $CD4^+$ T cells.

b) Studying the mechanisms underlying VitD induced IL-10 production, identified in a), and linking expression of molecules involved to hypothesised epigenetic modifications induce by VDR binding.

## 4.3 VitD induces IL-10 in CD4$^+$ T cells through an IL-6 signalling cascade

### 4.3.1 T cell activation and VitD transcriptionally regulate expression of the VDR

As discussed, the genomic actions of VitD are dependent on liganding of the VDR (see section 1.3.1). Therefore, to study how VitD functions in T cells, we first determined the dynamics of VDR expression in CD4$^+$ T cells in the presence and absence of VitD. CD4$^+$ T cells were polyclonally activated through TCR, with anti-CD3/CD28 ligation, either in the presence of the biologically active form of VitD (1,25 VitD) or carrier control (ethanol), and expression of VDR protein assessed by qPCR and Western blot (**Figure 4.1**).

As previously reported (Kongsbak et al., 2014), VDR was not expressed in un-activated CD4$^+$ T cells but induced after activation at both mRNA (**Figure 4.1 a**) and protein level (**Figure 4.1 b**). VDR protein expression progressively increased over time with both carrier- and VitD-treatment, but the presence of VitD significantly increased VDR protein expression relative to carrier alone (**Figure 4.1 b**). As with protein expression, T cell activation induced *VDR* mRNA expression in a manner also augmented by the presence of VitD (**Figure 4.1 a**). Collectively, these data demonstrate that T cell activation is necessary for expression of VDR protein and that VitD transcriptionally regulates VDR protein expression in these cells.

### 4.3.2 Liganding of VDR by VitD induces nuclear translocation

To confirm that liganding of the VDR in activated CD4$^+$ T cells leads to nuclear localisation of the receptor, implying genomic effects, we imaged sub-cellular localisation of the VDR using ImageStream (**Figure 4.2**). The VDR in activated CD4$^+$ T cells treated with carrier alone was preferentially localised within the cytoplasm whereas in the presence of VitD the VDR was preferentially localised within the nucleus, evidenced by overlap with DAPI DNA stain (**Figure 4.2 a-c**). To confirm these findings, we immunoblotted for VDR and appropriate housekeeping proteins in nuclear and cytoplasmic extracts of the same cells. As expected, VDR was highly expressed in nuclear extracts of VitD-treated cells (**Figure 4.2 d**), indicating nuclear translocation induced by VDR-liganding.

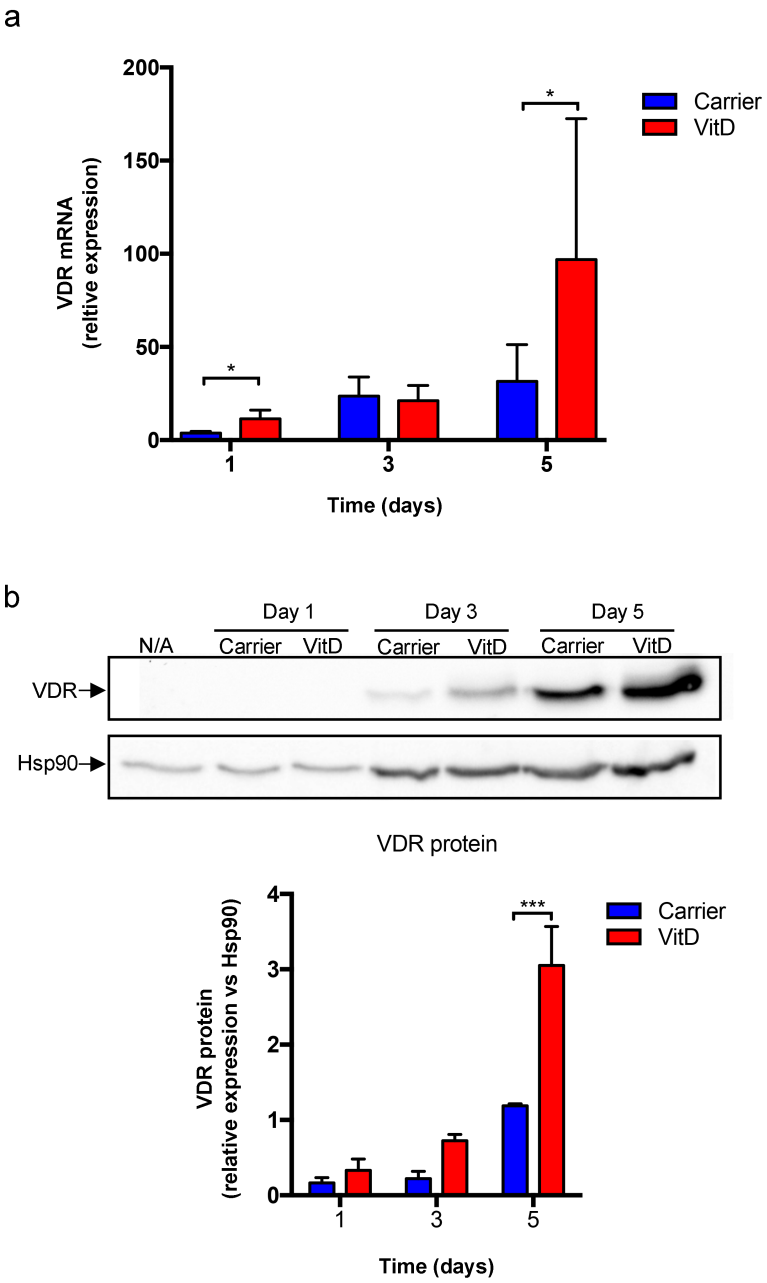


**Figure 4.1|VDR dynamics in polyclonally activated CD4$^+$ T cells|**
VDR mRNA (a) and protein (b) expression, measured at the time points shown following polyclonal activation. Shown in (a) are cumulative data from multiple experiments; shown in (b) are a representative blot (top) and quantification of VDR:Hsp90 ratio from multiple experiments (bottom). N/A = non-activated. All experiments carried out on bulk CD4$^+$ T cells as specified in materials and methods section 2.2.3.1. (*n* = 3 independent experiments in each panel; bar graphs indicate mean ± SEM throughout; 2-way ANOVA with follow up t-tests; * $p < 0.05$; *** $p < 0.001$.)

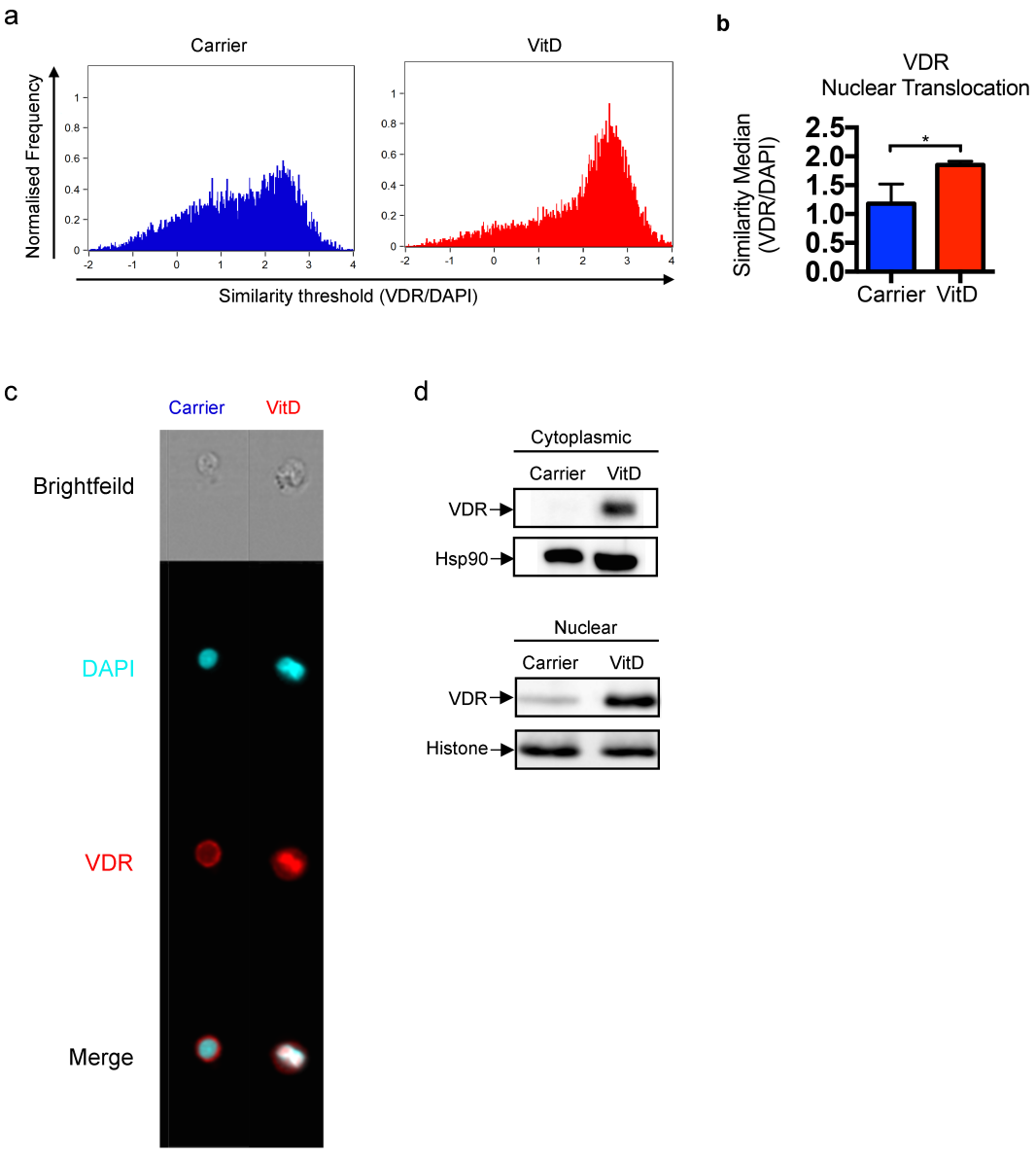


**Figure 4.2|VDR localisation in polyclonally activated CD4$^+$ T cells|**
(a) Co-localisation of VDR and DAPI (as indicated by similarity threshold (VDR/DAPI) on x –axis) in carrier and VitD treated CD4$^+$ T cells after polyclonal activation, measured on day 2. (b) Representative frequency histograms indicating overlap between VDR and DAPI in the entire population, and cumulative data from 3 experiments (b). (c) Shown are representative ImageStream images depicting stains for VDR and DAPI in carrier and VitD-treated cells. (d) Immunoblots for VDR and housekeeping proteins in nuclear and cytoplasmic extracts of carrier and VitD treated CD4$^+$ T cells after polyclonal activation, measured on day 2. All experiments carried out on bulk CD4$^+$ T cells as specified in materials and methods section 2.2.3.1.(*n* = 3 independent experiments in each panel; bar graphs indicate mean ± SEM throughout; 1-way ANOVA with follow up t-tests; * $p < 0.05$.)

### 4.3.3 VitD induces IL-6 production from $CD4^+$ T cells

Having established the time course of VDR expression (section 4.3.1), we assessed the effects of VitD on proliferation, cell survival and effector function (measured by cytokine production) of highly pure sorted $CD4^+$ $CD25^-$ T cells (from here on referred to as $CD4^+$ T cells) after 3 days polyclonal activation. For these and subsequent experiments, $CD4^+$ T cells were FACS sorted to >99% purity. Representative pre- and post-sort purities are shown in section 2.2.3.3 (**Figure 2.1**)

We saw no effect of VitD, compared to carrier alone, on the proliferation of $CD4^+$ T cells nor cell viability during culture (**Figure 4.3 a**). Thus, we concluded that any effect we observe on effector function was independent of any effect on proliferation or cell death.

VitD significantly decreased concentrations of IFN$\gamma$ and reduced IL-17 concentrations in culture supernatants, whilst having no effect on IL-4, TNF-$\alpha$ or IL-2 (**Figure 4.3 b**). At the same time, there was a substantial increase in concentrations of IL-10 in culture supernatants (**Figure 4.3 b**). We were surprised to observe substantial and significantly increased concentrations of IL-6 in VitD-treated culture supernatants (**Figure 4.3 b**).

IL-6 is a cytokine not normally associated with T cells. To confirm this observation and to determine whether IL-6 induction from $CD4^+$ T cells was transcriptionally regulated, we performed a time course experiment, measuring *IL6* mRNA in carrier and VitD-treated $CD4^+$ T cells and IL-6 protein concentrations in the culture supernatants of those cells. Sustained induction of *IL6* mRNA in the presence of VitD was evident as early as 1 day of culture, and IL-6 protein as early as 3 days (**Figure 4.3 c**). In addition, we performed intracellular staining for IL-6 and found a greater percentage of $CD4^+$ T cells treated with VitD expressing IL-6 than carrier alone (**Figure 4.3 d**). Collectively, these data indicate significant production of IL-6 from a highly pure (>99%) population of $CD4^+$ T cells, when polyclonally activated in the presence of VitD.

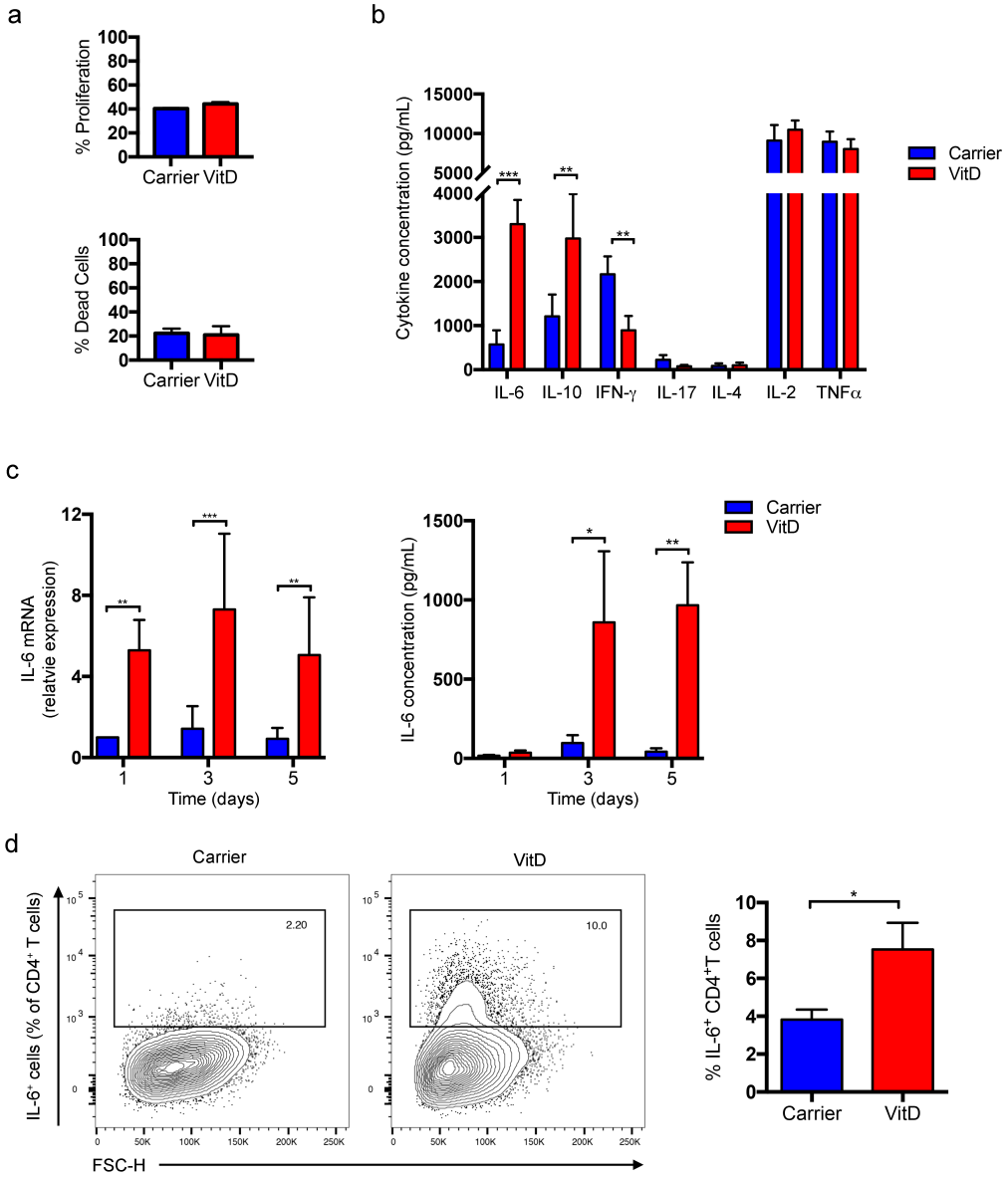


**Figure 4.3|VitD supresses pro-inflammatory cytokine production and increases IL-6 and IL-10 production in polyclonally activated sorted CD4$^+$ T cells|**

(a) Cell death by live/dead stain and proliferation as assessed by CFSE incorporation in polyclonally activated CD4$^+$ T cells in presence of carrier or VitD after 3 days culture. (b) Cytokine concentrations in supernatants of T cell cultures after 5 days of polyclonal activation with carrier or VitD; (c) *IL6* mRNA, fold change compared to day 1 carrier (left) and IL-6 protein concentration in matched supernatants (right) at days 1, 3 and 5 in carrier and VitD treated cultures; (d) Representative flow cytometry plot (left) and cumulative data (right) of intracellular IL-6 expression in T cells treated with carrier or VitD (assay carried out on day 3). Bar graphs show cumulative data (mean ± SEM). All experiments carried out on bulk CD4$^+$ T cells as specified in materials and methods section 2.2.3.1 (From *n* = 3 (a-c) and *n* = 4 (d) independent experiments; 1 way –ANOVA in a, b and, d and 2-way ANOVA in c with follow up t-tests; * $p < 0.05$, ** $p<0.01$, *** $p<0.001$.)

### 4.3.4 Despite increased IL-10 production, VitD does not skew T cells towards FoxP3$^+$ T regulatory or Foxp3$^-$ Tr1 phenotype

IL-10 is a cytokine that can be produced by most CD4$^+$ T cell lineages as part of the auto-regulatory phase of their life cycle. It has previously been particularly attributed to a population of regulatory cells designated as Tr1 (see below) and can also be produced by some FoxP3$^+$ regulatory T cells (Tregs) (Hawrylowicz and O'Garra, 2005; Saraiva and O'Garra, 2010).

VitD has been reported to act directly on T cells to induce a Treg phenotype (Chambers and Hawrylowicz, 2011). Since we saw suppression of IFN-$\gamma$ and IL-17 in culture supernatants and enhanced IL-10, we next assessed the phenotype of CD4$^+$ T cells activated in the presence of VitD to determine whether we had generated induced Tregs. Tregs can be identified by constitutively high expression of CD25, which is normally only transiently expressed upon T cell activation, and the expression of lineage specific transcription factor FoxP3 (Povoleri et al., 2013; Torgerson and Ochs, 2007). VitD significantly increased percentage of FoxP3$^+$ cells at both 3 days and 5 days following activation, but did not increase FoxP3 MFI (**Figure 4.4 a and b**). This contrasts with CD25, which did not show an increased frequency but did show a dramatic and significant increase in MFI after treatment with VitD (**Figure 4.4 a and c**). As both FoxP3 and CD25 are general markers of activation in CD4$^+$ T cells (Kmieciak et al., 2009), and thus do not necessarily denote classical Treg generation, maintenance of FoxP3 expression, rather than expression, is more indicative of true Treg phenotype (Rudensky, 2011). To assess this, following 5 days of activation in the presence of VitD, T cells were removed from $\alpha$CD3/CD28 stimulus and rested in fresh media for a further 2 days and expression of FoxP3 and CD25 re-measured. VitD treated cells showed a significantly higher frequency of CD25 (**Figure 4.4 c**) and a significantly lower FoxP3 MFI than carrier-treated cells (**Figure 4.4 b**). This suggests that both CD25 and FoxP3 expression in VitD treated cells is transient, in keeping with activation markers, rather than a true regulatory phenotype.

Tr1 cells are a type of FoxP3$^-$ regulatory T cells that are characterised by the ability to produce high levels of IL-10. These cells are said to be identifiable by their expression of CD49b and LAG-3 (Gagliani et al., 2013). As VitD-treated cells produced high levels of

IL-10 and only showed transient upregulation of FoxP3 we checked if VitD was skewing T cells to a Tr1 phenotype. In fact, VitD treatment led to a significantly decreased frequency of CD49b expression and fewer $CD49b^{+}LAG\text{-}3^{+}$ double positive cells (**Figure 4.4 d and e**).

Combined, these results suggest that VitD treatment, in our experimental setup, is not inducing a classical Treg or Tr1 phenotype. However due to the induced IL-10 and inhibited IFN$\gamma$ (section 4.3.3), it is likely that the cells have transitioned from a pro- to an anti-inflammatory phenotype.

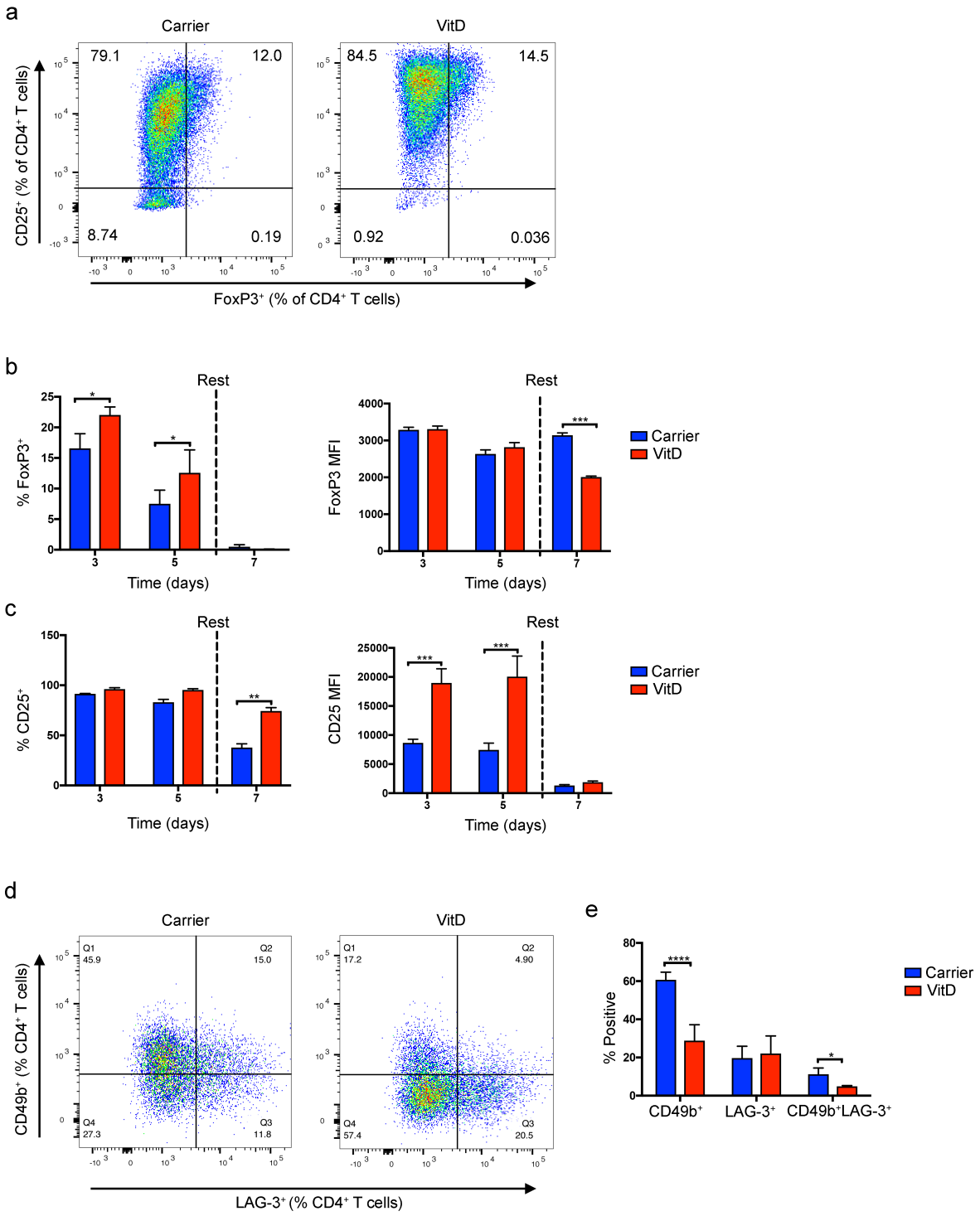
a
Carrier
VitD
79.1
12.0
8.74
0.19
84.5
14.5
0.92
0.036
CD25+ (% of CD4+ T cells)
FoxP3+ (% of CD4+ T cells)
b
Rest
% FoxP3+
Time (days)
FoxP3 MFI
Carrier
VitD
c
% CD25+
CD25 MFI
d
Q1 45.9
Q2 15.0
Q4 27.3
Q3 11.8
Q1 17.2
Q2 4.90
Q4 57.4
Q3 20.5
CD49b+ (% CD4+ T cells)
LAG-3+ (% CD4+ T cells)
e
% Positive
CD49b+
LAG-3+
CD49b+LAG-3+

**Figure 4.4|Phenotype of VitD treated T cells|**
(a) Representative flow cytometry plots showing CD25 and FoxP3 expression after 3 days in activated $CD4^+$ T cells, with carrier and VitD treatment (b) Quantification of cumulative data from (a), showing FoxP3 percentage in total $CD4^+$ T cells and MFI in $FoxP3^+$ $CD4^+$ T cells at day 3, day 5 and after removal of $\alpha$CD3/CD28 beads and resting for 2 days. (c) Quantification of cumulative data from (a), showing CD25 percentage and MFI in total $CD4^+$ T cells at day 3, day 5 and after removal of $\alpha$CD3/CD28 beads and resting for 2 days. (d) Representative flow cytometry plot showing CD49b and LAG-3 expression in activated $CD4^+$ T cells, with carrier and VitD treatment. (e) Quantification of cumulative data from (d), showing CD49b and LAG-3 percentage as well as $CD49b^+LAG\text{-}3^+$ double positive cells. All experiments carried out on bulk $CD4^+$ T cells as specified in materials and methods section 2.2.3.1. (*n* = 3 independent experiments in all panels; all bar graphs show mean ± SEM; comparisons were carried out throughout using 2-way ANOVA for panel b and c, and 1-way ANOVA for e, and follow up t-tests; * $p<0.05$, ** $p<0.01$, *** $p<0.001$, ****$p<0.0001$.)

### 4.3.5 VitD induces IL-10 production via IL-6 production in $CD4^+$ T cells

We observed induction of both IL-6 and IL-10 in VitD-treated $CD4^+$ T cells. To determine whether this is a dose-dependent or independent effect, we measured concentrations of cytokines in the supernatants of $CD4^+$ T cells treated with increasing concentrations of VitD. This revealed that the effect of VitD on cytokine production is dose-dependent, with maximal effect on IL-6 and IL-10 at 1 to 10nM and maximal inhibition of IFNγ occurring at 100nM (**Figure 4.5 a**). Interestingly at higher concentrations (50-100nM) of VitD both the IL-6 and IL-10 response decreased, whereas the IFNγ response reduced at each increase VitD dose (**Figure 4.5 a**). Since both IL-10 and IL-6 showed an almost identical response to activation in the presence of VitD, and were strongly linearly correlated to each other ($r^2$=0.92, p=0.0025) (**Figure 4.5 b**), we speculated that the production of IL-6 and IL-10 could be mechanistically linked.

We first determined the expression of the IL-6 and IL-10 receptors (IL-6R and IL-10R, respectively) and found that both receptors are expressed on $CD4^+$ T cells (**Figure 4.5 c**, and representative FACS plots in **Figure 4.6**). Following TCR activation *ex vivo*, in both carrier and VitD-treated conditions there was an initial drop in IL-6R expression from baseline, which gradually returned to baseline over 5 days (**Figure 4.5 c**). Intriguingly, IL-6R expression in VitD-treated cells was lower in VitD-treated cells, after 5 days, compared to carrier alone, as might be expected if the receptor is shed or internalised following receptor-ligand interaction (**Figure 4.5 c**). IL-10R expression, in contrast, gradually increased during *in vitro* culture and remained similar between carrier and VitD-treated cells throughout (**Figure 4.5 c**). These observations suggested that IL-6 induced by VitD may be the driver of IL-10 production in VitD-treated cells. To test this, we blocked the IL-6R using tocilizumab (Toc) during culture with VitD. Toc is a humanised monoclonal antibody directed against the IL-6R (Jones et al., 2011). Thus, it blocks both membrane bound and soluble IL-6R, inhibiting IL-6R signalling both *in situ* and *in trans* (Mihara et al., 2011). When IL-6 signalling was blocked, at each concentration of VitD, IL-10 production was also significantly inhibited (**Figure 4.7 a**), suggesting that IL-6R signal transduction drives IL-10 production. Interestingly, the simple addition of exogenous IL-6 to cultures of activated $CD4^+$ T cells in the absence of

VitD did not induce the production of IL-10 from carrier treated cells (**Figure 4.7 b**), suggesting that the concurrent presence of VitD is a requisite. Addition of IL-6 to cultures of VitD-treated cells did not augment IL-10 production, suggesting that the IL-6R is already fully saturated in this scenario (**Figure 4.7 b**).

Collectively, these data indicate that VitD treatment induces IL-6 and primes $CD4^+$ T cells to produce IL-10 in response to IL-6; additionally, VitD treatment saturates the ability of a cell to respond to the IL-6 signal, such that additional exogenous IL-6 has no additive effect on IL-10 production.

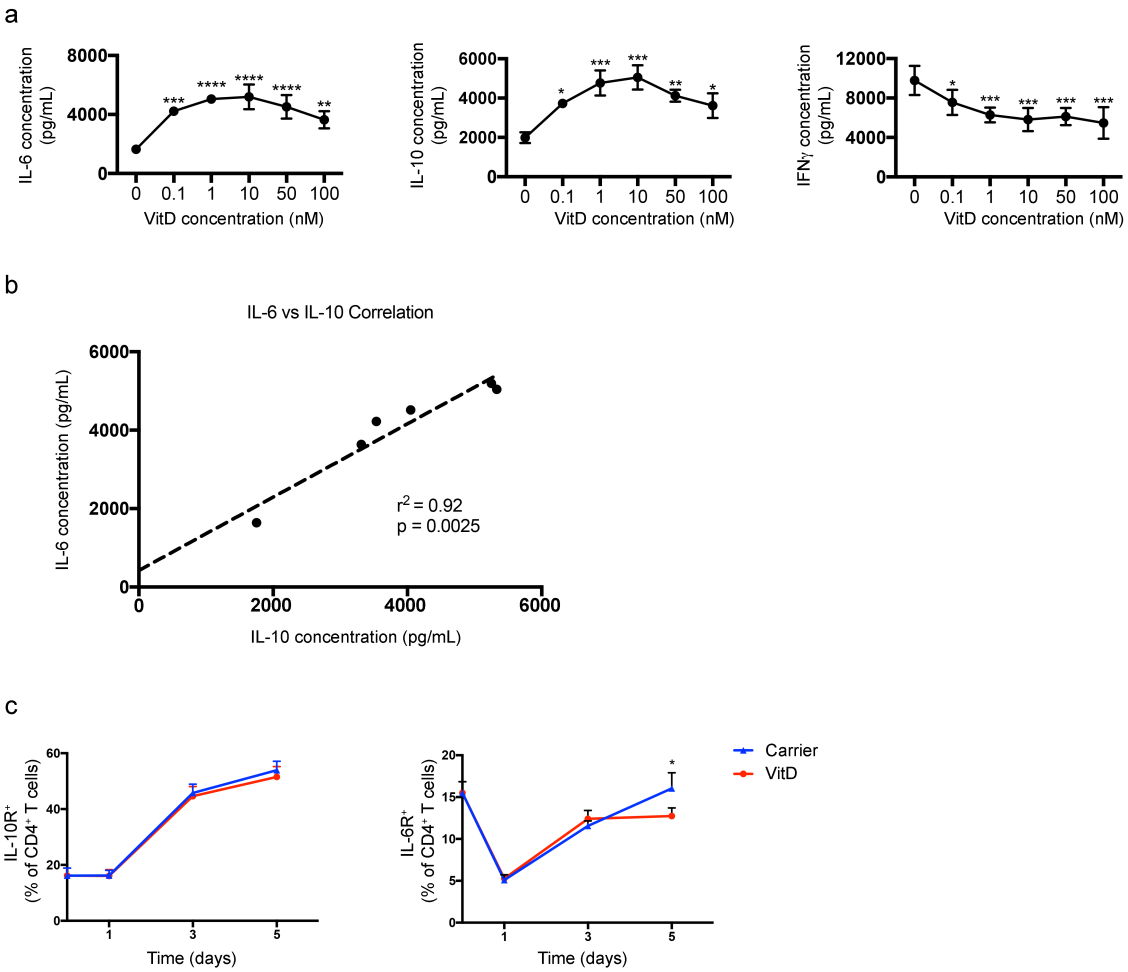


**Figure 4.5|VitD effect on IL6 and IL-10 production and receptor expression in activated CD4$^+$ T cells|**

(a) Concentration of IL-6, IL-10 and IFN-γ in culture supernatants of CD4$^+$ T cells treated with different concentrations of VitD; (b) Correlation between mean IL-6 and mean IL-10 concentrations in (a). (c) Quantification of cumulative data showing IL-10R and IL-6R expression at baseline, day 1, day 3 and day 5 in activated CD4$^+$ T cells, with carrier and VitD treatment. Representative FACT plots are shown in **Figure 4.6**. Line graphs show mean ± SEM throughout; (*n* = 3 independent experiments for each panel, compared using 2-way ANOVA and follow up t-tests; * p<0.05, ** p<0.01, *** p<0.001, ****p<0.0001). Significance in a is compared to 0nM VitD. All experiments carried out in sorted memory CD4$^+$ T cells as specified in materials and methods section 2.2.3.3.

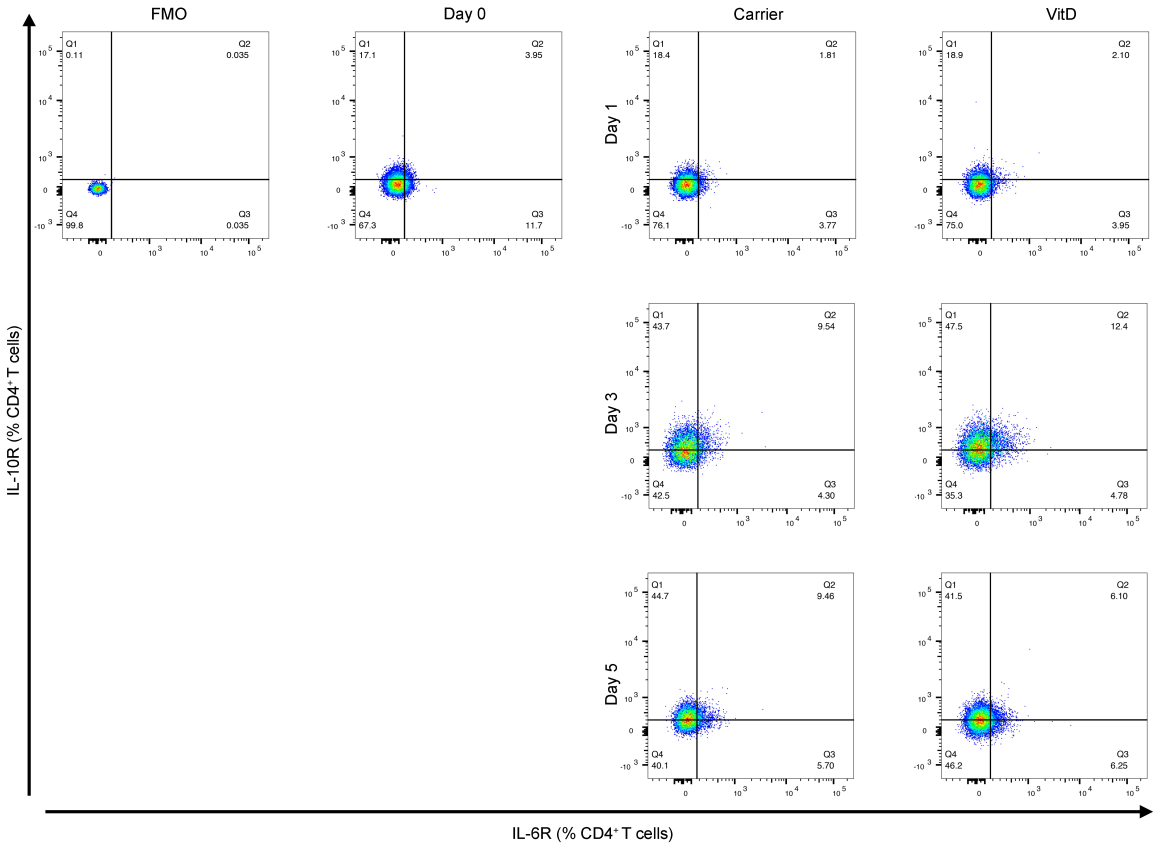


**Figure 4.6|IL-6R and IL-10R representative FACS plots|**
Representative FACS plots of time-course experiment on $CD4^+$ memory T cells. Quantification shown in **Figure 4.5 c**. FMO (fluorescence minus one) control was used to set up gating strategy, as indicated in top left. Percentages of $CD4^+$ T cells shown at day 0 and at Day 1, Day 3 and Day 5 activation with αCD3/CD28 beads in the presence of Carrier control or VitD. All experiments carried out in sorted memory $CD4^+$ T cells as specified in materials and methods section 2.2.3.3

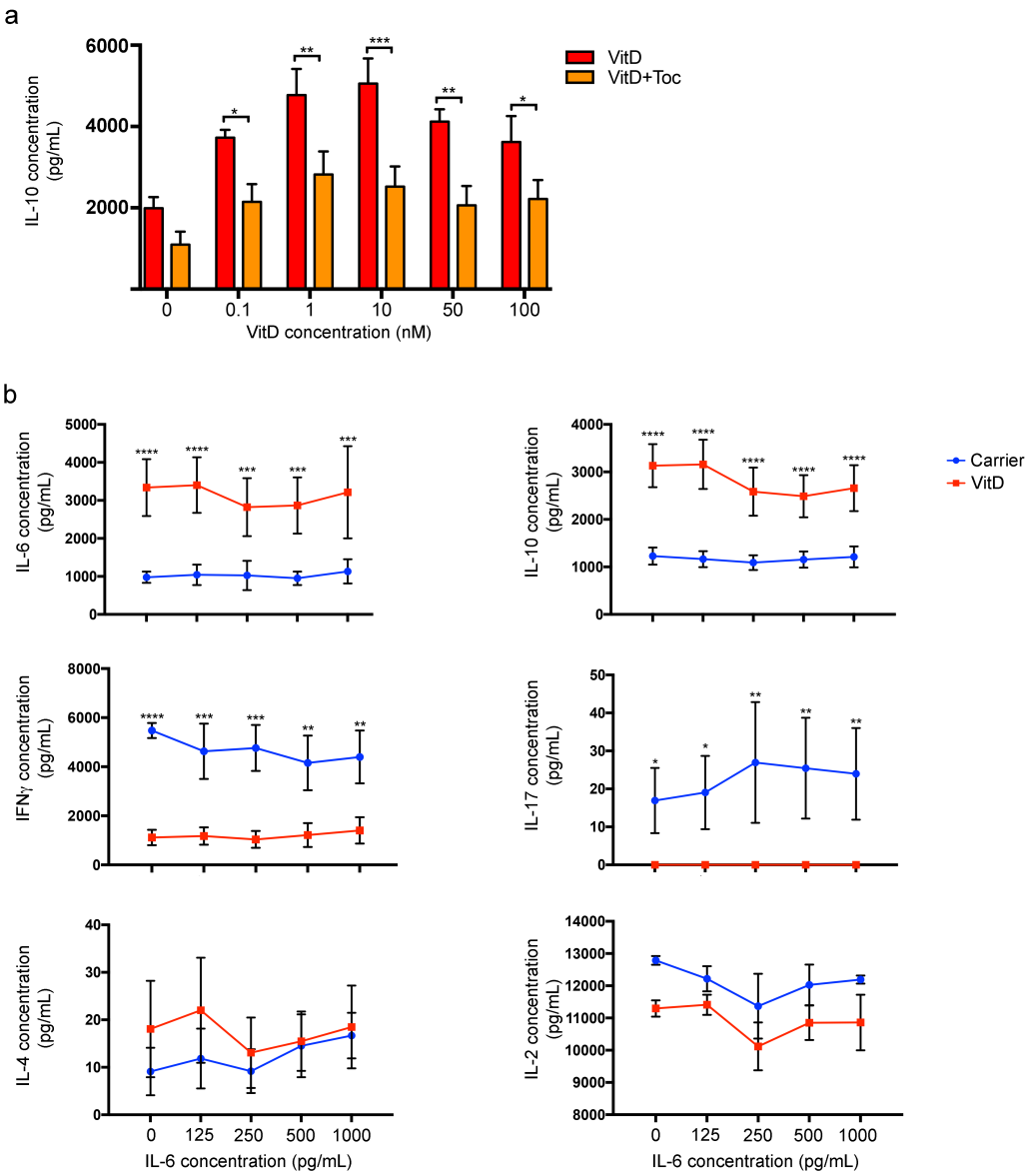


**Figure 4.7|IL-6R blockade inhibits IL-10 production which is not further increased by exogenous IL-6|**

(a) IL-10 culture supernatant concentrations with and without IL-6R blockade using tocilizumab (Toc). (b) Effect of exogenous IL-6 addition. Dose escalation of IL-6 from 0 to 1000 pg/mL at day 3 in polyclonally activated T cells, in the presence of carrier and VitD. Line and bar graphs show mean ± SEM throughout (*n* = 3 independent experiments for each panel, compared using 2-way ANOVA and follow up t-tests; * p<0.05, ** p<0.01, *** p<0.001, ****p<0.0001). Significance in b) is compared to respective carrier treatment.)

### 4.3.6 VitD mediated signalling largely occurs in memory CD4$^+$ T cells

To determine whether antigen experience or T cell maturity plays a role in the observed signalling loop, we FACS sorted naïve and memory CD4$^+$ T cells and tested their *in vitro* response to VitD. We found that memory T cells were the dominant population producing IL-10 in response to VitD and that the pattern of cytokine secretion was similar to that observed in bulk CD4$^+$ T cells – IL-6 and IL-10 were induced together, with blockade of the IL-6R inhibiting the IL-10 response (**Figure 4.8 a**). In naïve T cells, although this cytokine pattern was mirrored, we saw a much lower induction of IL-6 than in memory T cells and almost negligible IL-10 production (**Figure 4.8 b**). In memory cells, there was a significant reduction in IFN$\gamma$ and IL-17 in the presence of VitD, but no effect on these cytokines was observed in the presence of Toc (**Figure 4.8 a**). In naïve T cells this effect was mirrored but again at much lower concentration (**Figure 4.8 b**). Interestingly, measurement of cytokines in naïve CD4$^+$ T cells was restricted to day 3, as at day 5 substantial cell death was observed in the wells. Since the effect of VitD was largely restricted to memory populations of CD4$^+$ T cells, we conjecture that IL-10 production in this context is involved in the auto-regulatory/shut-down part of the life cycle of T cells.

### 4.3.7 The VDR-induced IL-6-dependent IL-10 signalling loop is not mirrored in murine splenic CD4$^+$ T cells

Many of the basic mechanistic studies of VitD in T cells *in vivo* have been carried out in mice (Cantorna et al., 2015), including some suggestions that IL-6 signalling may play a role in the induction of IL-10 from naïve T cells (McGeachy et al., 2007; Stumhofer et al., 2007). We thus sought to determine whether the observed VitD-IL-6-IL-10 signalling loop in human CD4$^+$ T cells also exists in mouse CD4$^+$ T cells. CD4$^+$ T cells from wild type C56Bl/6 (B6) mice were polyclonally activated with $\alpha$CD3/CD28 in the presence of VitD or carrier and supernatants assessed for cytokine concentrations. While we observed a substantial increase in IL-10 concentrations induced by VitD, IL-6 was actually suppressed by VitD (**Figure 4.9 a**). IL-6R blockade had no effect on production of any

cytokine measured (**Figure 4.9 a**). Interestingly, there was also no reduction of IFNγ in the presence of VitD (**Figure 4.9 a**). These results suggest that the mechanism for VitD induced IL-10 production in murine $CD4^+$ T cells may be different to human $CD4^+$ T cells.

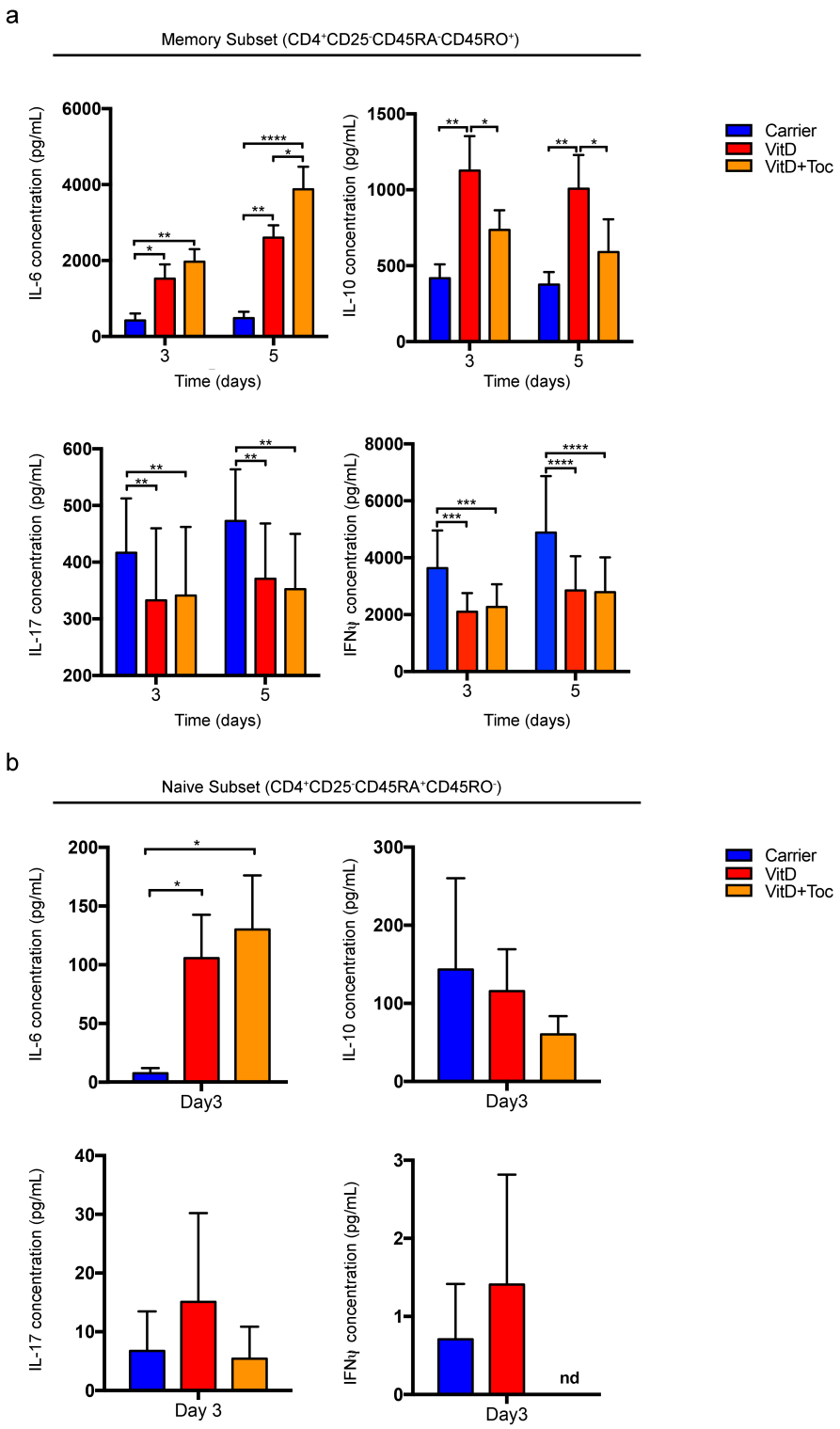


**Figure 4.8|VitD effect on cytokine production from memory and naïve CD4$^+$ T cell compartments|**

Cytokine concentrations in supernatants of activated FACS-sorted memory (CD25$^-$ CD45RA$^-$CD45RO$^+$) (a) and naïve (CD25$^-$CD45RA$^+$CD45RO$^-$) (b) CD4$^+$ T cells at day 3 and 5 in the presence of carrier, VitD and VitD plus Toc. Bar graphs show mean ± SEM throughout (*n* = 3 independent experiments for each panel, compared using 2-way ANOVA and follow up t-tests; * p<0.05, ** p<0.01, *** p<0.001, ****p<0.0001).

a

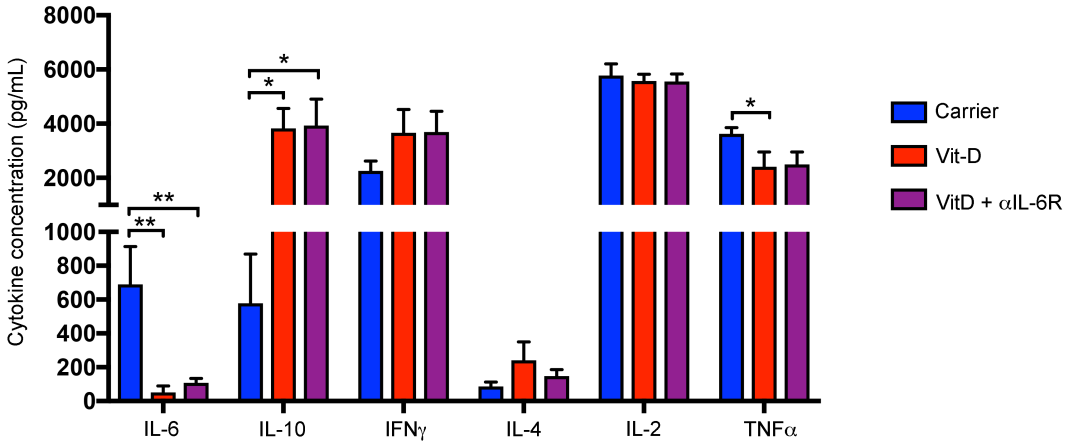


**Figure 4.9|VitD treatment inhibits IL-6 production from mouse CD4$^+$ splenocytes, with no effect with IL-6R blockade|**

(a) Concentrations of seven cytokines (IL-17 was not detectable) in culture supernatants after 5 days of polyclonal activation of murine CD4$^+$ T cells, in the presence of carrier, VitD or VitD and αIL-6R. Bars show mean ± SEM. (*n* = 4; comparisons were made using 2-way ANOVA and follow up t-tests; * $p < 0.05$, ** $p < 0.01$). Experiments carried out in mouse CD4$^+$ T cells from solenocyte origin as specified in section 2.2.10.

### 4.3.8 $CD4^+$ T cell responses to VitD can be entirely self-contained

In experiments presented so far, we used the active form of VitD (1,25 VitD) throughout. A substantial body of published literature shows that T cells have the capacity to express CYP27B1 and convert 25 VitD to 1,25 VitD (Correale et al., 2009; Kongsbak and Essen, 2014; Kongsbak et al., 2014; Sigmundsdottir et al., 2007), the rate limiting enzyme in the activation of 25 VitD to its active form, 1,25 VitD (see section 1.4). This suggests that T cells could have the capacity both to activate VitD and respond to it by inducing IL-10. To explore this possibility, we cultured $CD4^+$ T cells in the presence or absence of 25 VitD (25(OH)VitD), at physiological concentrations, with and without activation through CD3/CD28. We observed that production of both IL-6 and IL-10 occurred with 25 VitD in the same manner as with the active form of the vitamin, although only in activated memory $CD4^+$ T cells (**Figure 4.10 a**). Additionally, IFN$\gamma$ and IL-17 were both significantly inhibited in a dose dependent manner in the presence of 25(OH)$D_3$ (**Figure 4.10 b**), with little effect seen on IL-4, IL-2 and TNF$\alpha$ (**Figure 4.10 c**). These results are very similar to those observed in the presence of 1,25 VitD. This suggests memory $CD4^+$ T cells both activate 25 VitD to 1,25 VitD and respond to it, and that the presence of the VDR is essential (i.e. T cell activation) for biological activity of the VitD signalling loop.

In summary, these results show that IL-6 signalling is crucial for VitD induced IL-10 production in human memory $CD4^+$ T cells, an effect which does not affect other T cell cytokines.

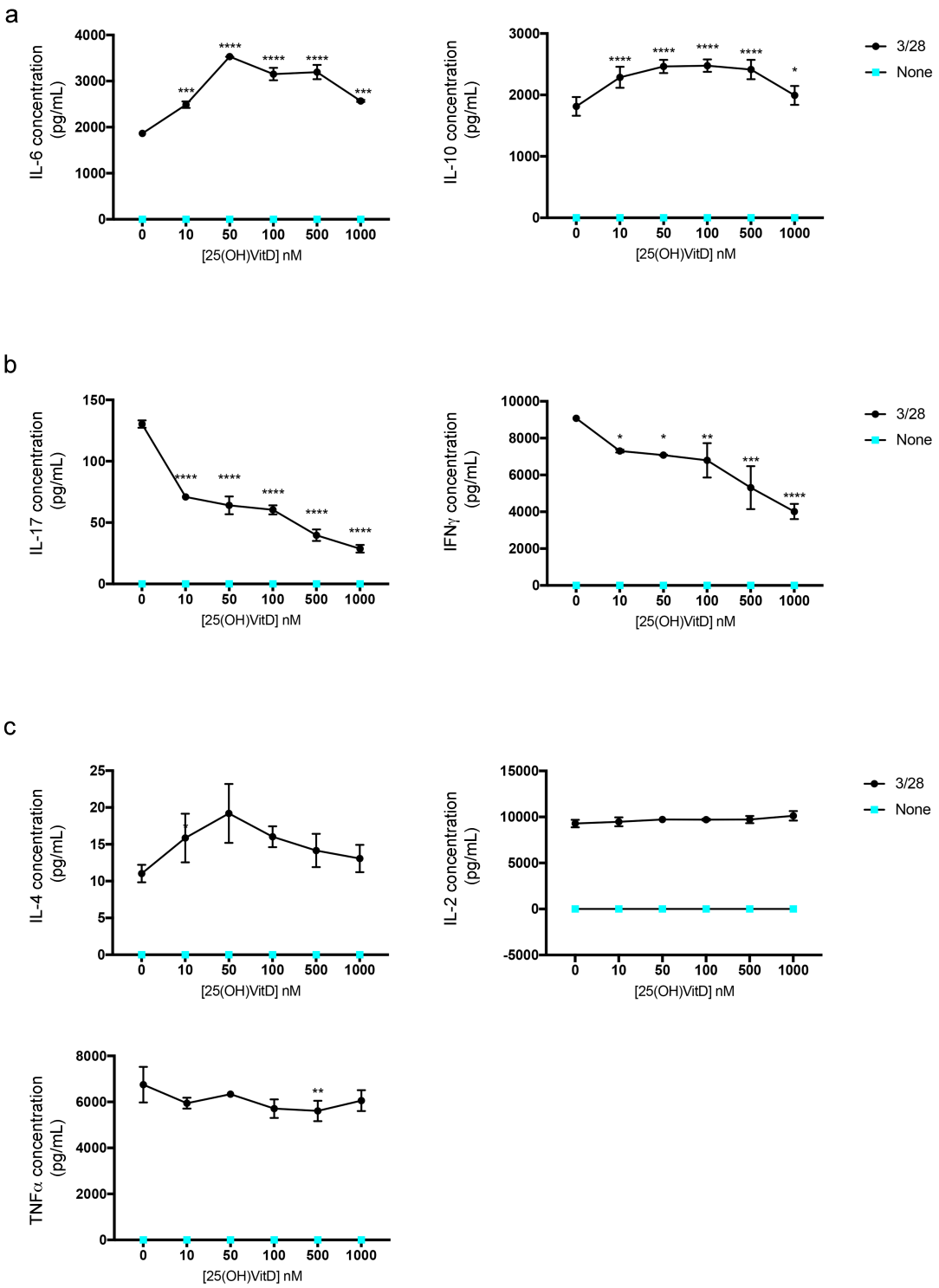


**Figure 4.10|25(OH)VitD affects T cells in the same manner as 1,25(OH)$_2$D$_3$|**
Concentrations of (a) IL10, IL-6 (b) IL-17 IFNγ and (c) IL-4 IL-2 and TNFα in culture supernatants of T cells activated (black circles) or not (turquoise squares) in the presence of escalating doses of 25(OH)VitD. Line graphs show mean ± SEM. (*n* = 3 independent experiments; comparisons made using 2-way ANOVA and follow up t-tests; *p<0.05, **p<0.01, *** p<0.001, ****p<0.0001). Significance is compared to 0nM VitD. All experiments carried out in memory CD4$^+$ T cells. All experiments carried out in sorted memory CD4$^+$ T cells as specified in materials and methods section 2.2.3.3

## 4.4 Signalling and genomic mechanisms driving IL-6, IL-10 signalling loop in memory CD4$^+$ T cells

We have thus far identified a novel mechanism underlying VitD induced IL-10 production from CD4$^+$ T cells, which involved IL-6 signalling. We next sought to determine the signalling and genomic mechanisms driving these observations.

### 4.4.1 Phosphorylation of STAT3, downstream of IL-6R engagement, is responsible for IL-10 production in CD4$^+$ T cells

We sought to determine the downstream signals responsible for driving IL-10 production. We initially carried out a phospho(p)-kinase antibody array for 43 phosphorylated signalling proteins on lysates of cells activated in the presence of active VitD (**Figure 4.11 a and b**, and **Appendix 1** and **Appendix 2**). Of the phosphorylated proteins assayed, phosphorylated pS63-c-Jun, pY705-STAT3, pT183/pY185, pT221/pY223-Jnk-1/2/3 and pT183-AMPK$\alpha$1 were consistently increased and pHsp60 decreased in VitD-treated cells compared to carrier. Importantly, these results are exploratory and further validated in the next section by western blot.

The IL-6R is coupled to STAT3 (and to a lesser extent STAT1) activation via gp130 and activation of recruited JAK proteins (JAK1, JAK2 and Tyk2), although this process is usually rapid, transient and not sustained (Braun et al., 2013). IL-10 signal transduction also uses STAT3. Thus, these data are consistent with signal transduction via both IL-6R and IL-10R. To confirm the sustained pYSTAT3 signal and determine whether there is more STAT3 phosphorylation or simply more STAT3 in VitD treated cells, we immunoblotted for total and pY705-STAT3 (hereafter simply called pSTAT3) in lysates of VitD treated cells. Although low level phosphorylation of STAT3 was evident at 3 days following TCR activation in isolation, addition of VitD significantly increased pSTAT3 (**Figure 4.12 a and b**). Additionally, total STAT3 protein was significantly induced in presence of VitD (**Figure 4.12 a and b**), suggesting that the observed increased pSTAT3 is at least in part due to increased total STAT3 expression induced by VitD. With the addition of Toc (blocking the IL-6R), phosphorylation of STAT3 was completely abrogated, indicating that sustained phosphorylation of STAT3 is a direct consequence

of IL-6R engagement (**Figure 4.12 a and b**) and not the result of IL-10. Importantly, Toc did not reverse elevation of STAT3 protein (**Figure 4.12 a and b**), indicating that STAT3 induction is independent of IL-6R engagement and a predicate of VitD treatment itself. These findings contrasted with phosphorylation of c-Jun which, though significantly increased in the presence of VitD, was sustained in the presence of IL-6R blockade (**Figure 4.12 a and b**), suggesting that IL-6 binding to IL-6R does not lead to phosphorylation of c-Jun, but increased total c-Jun expression is induced by VitD treatment.

We then validated the role of pSTAT3 signalling in IL-10 production by using a specific inhibitor of STAT3, (Curcubitacin I, (Blaskovich et al., 2003)). In the presence of the STAT3 inhibitor VitD induced significantly less IL-10 production from $CD4^+$ T cells (**Figure 4.13 a**), without affecting IL-6 production. Since chemical STAT3 inhibitors are not 100% specific to STAT3, we also used a parallel strategy by knocking down STAT3 using RNA interference. IL-10 production in response to VitD was substantially inhibited in STAT3-silenced T cells (**Figure 4.13 b**). Interestingly, an increase in IL-6 was also observed (**Figure 4.13 b**). We confirmed approximately 50% knockdown of total STAT3 was achieved using shRNA (**Figure 4.13 c and d**). These effects were mirrored in the pSTAT3 levels.

These data confirm that VitD-dependent IL-6 production induces IL-10 production from primary human memory $CD4^+$ T cells, through a signalling loop in which STAT3 is a key signalling protein.

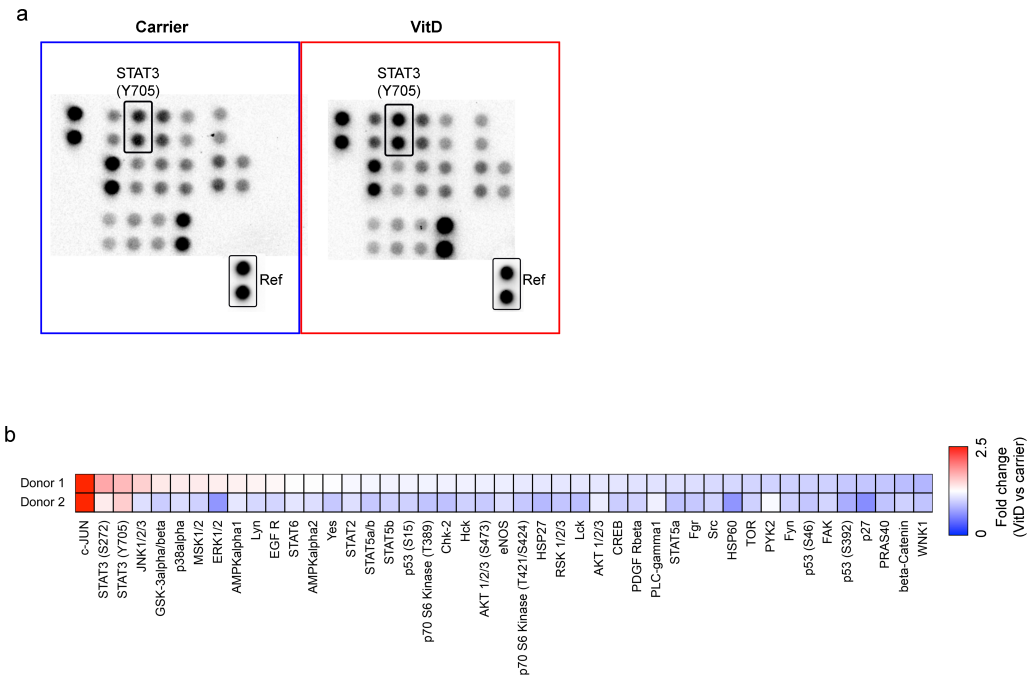


**Figure 4.11|p-STAT3 signalling is responsible for VitD induced IL-10 production|**
(a) Representative image of membrane B of phospho-kinase antibody (array of 43 kinases in duplicate spots) from polyclonally activated $CD4^+$ memory T cells with carrier and VitD at day 3. Location of STAT3 phosphorylated at lysine 705 and reference spot (to which all spots are normalized) are indicated. The complete blot, plus membrane A are shown, for completeness, in Appendix 1 and Appendix 2. (b) Heatmap of fold change between carrier and VitD treatment of all 43 kinases. All experiments carried out in sorted memory $CD4^+$ T cells as specified in materials and methods section 2.2.3.3 (*n* = 2 independent experiments)

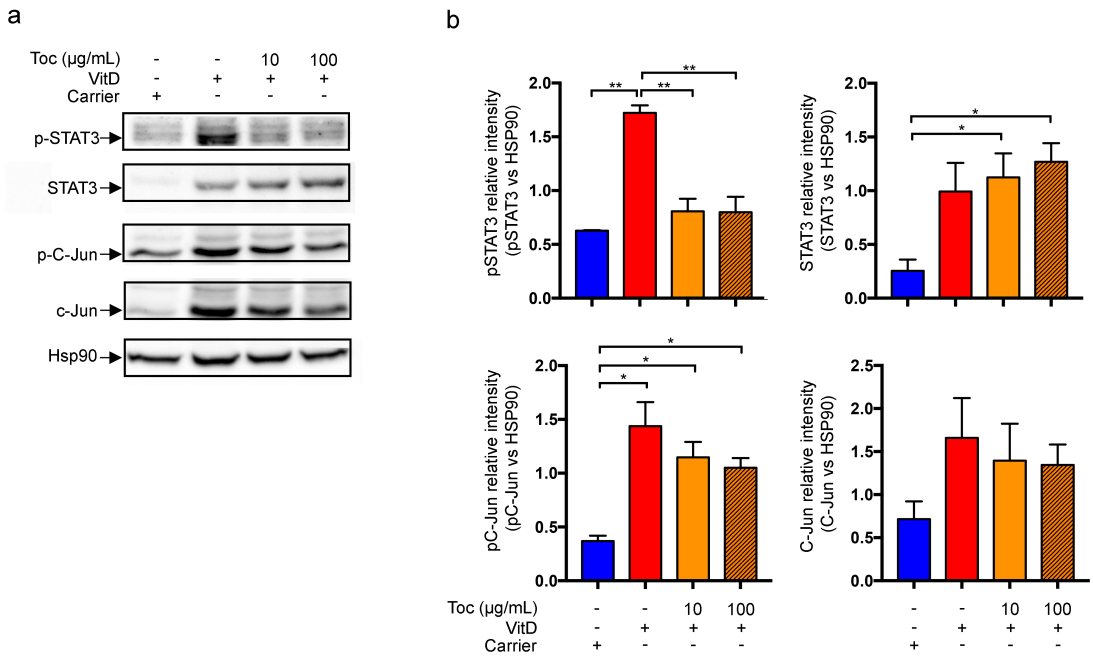


**Figure 4.12|STAT3 but not c-Jun is directly phosphorylated as response to IL6R engagement|**

(a) Western blot of polyclonally activated memory $CD4^+$ T cells, in the presence of carrier or VitD with and without Toc at the concentrations shown. Western blot for phosphorylated and total c-Jun as well as phosphorylated and total STAT3 with Hsp90 as loading control. Representative image (a) and quantification of cumulative data (b). All experiments carried out in sorted memory $CD4^+$ T cells as specified in materials and methods section 2.2.3.3. (Data are from *n* = 3 independent experiments; comparisons made using 1-way ANOVA and follow up t-tests; *p<0.05, **p<0.01).

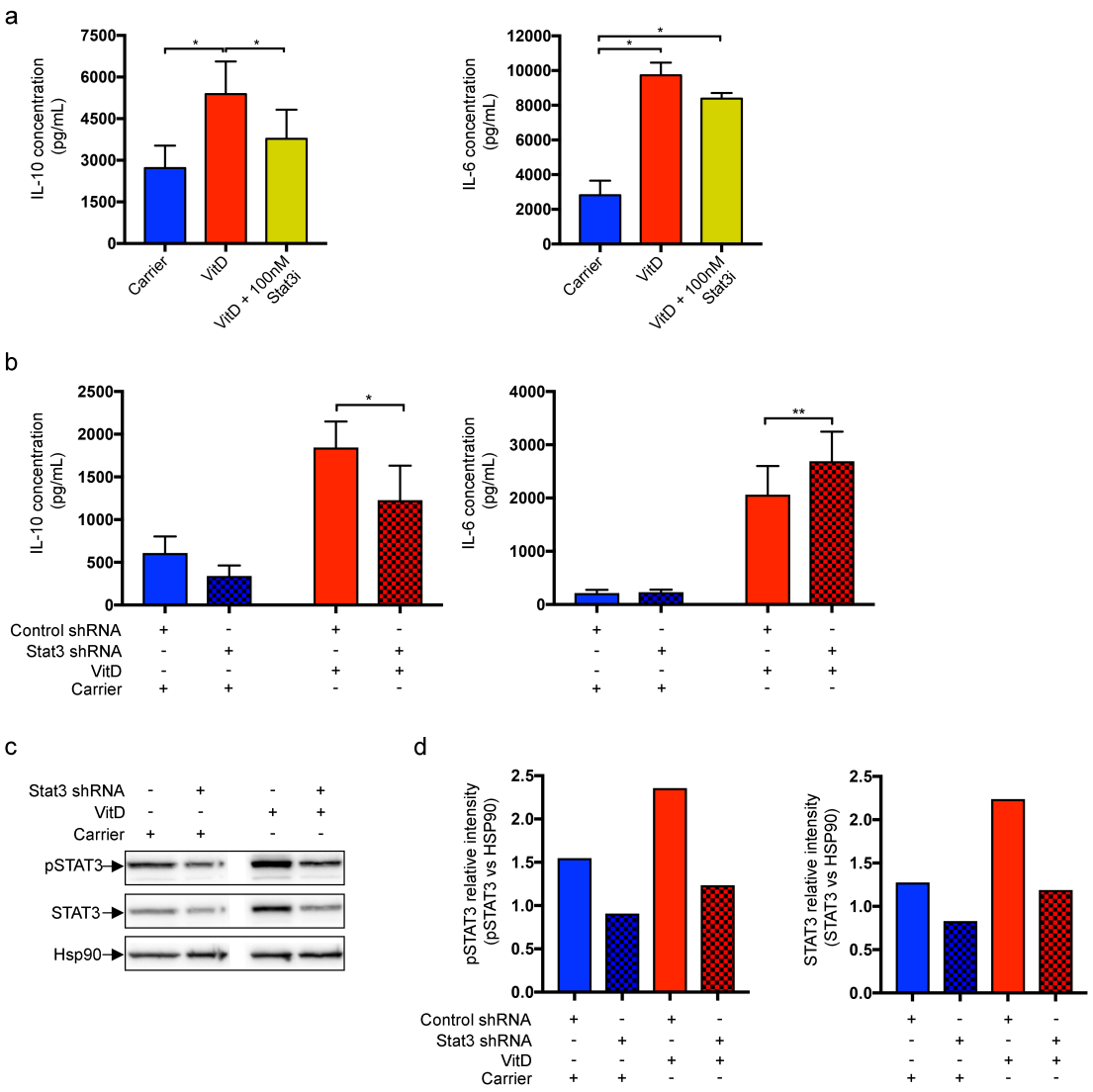


**Figure 4.13|STAT3 plays an important role in IL-6 induced production of IL-10|**
(a) IL-10 and IL-6 levels in supernatant after 3 days of polyclonal activation of memory $CD4^+$ T cells in the presence of carrier or VitD with and without STAT3 inhibitor at 100nM, added at day 1 following activation. *n* = 3 independent experiments; comparisons made using 2-way ANOVA and follow up t-tests; *p<0.05. (b) IL-10 and IL-6 production from polyclonally activated $CD4^+$ T cells with and without STAT3 or control shRNA. (*n* = 3 independent experiments; comparisons made using 2-way ANOVA and follow up t-tests; *p<0.05, **p<0.01). (c-d) Representative Western blot (c) and quantification (d) after polyclonal activation of $CD4^+$ T cells, in the presence of carrier or VitD, with and without STAT3 or control shRNA. (*n* = 1 experiment). All experiments carried out in sorted memory $CD4^+$ T cells as specified in materials and methods section 2.2.3.3.

### 4.4.2 Assessment of epigenetic histone modifications induced by VitD using ChIPseq

From our previous observations, we hypothesised that VitD would directly regulate both total STAT3 production (see section 4.4.1) and the ability of IL-6 to induce IL-10. As VitD has been shown to affect gene regulation through recruitment of a diverse set of transcriptional machinery, primarily altering histone modifications (see section 1.3.3) (Fetahu et al., 2014), it followed that the mechanism underlying the observed signaling loop could be epigenetic modifications induced by VitD. Thus, to delineate the molecular mechanisms of VitD function in $CD4^+$ T cells and identify how the observed IL-10 production is regulated, we next carried out ChIP-seq for VDR and the histone marks; H3K4me3 and H3K27Ac, in carrier- or VitD-treated cells.

#### 4.4.2.1 VDR antibody quality control

As ChIP-seq is an expensive and long experiment, we first wanted to validate the use of the VDR antibody in ChIP experiments. To do so we carried out a ChIP-qPCR experiment on known enhancer regions of the CYP24A1 genes, known to be bound and activated by VDR/RXR binding (Pike and Meyer, 2012). We first scanned the upstream region of the CYP24A1 gene for possible RXR/VDR binding motifs using JASPAR motif scanning (Mathelier et al., 2014) for the VDR/RXR motif shown in (**Figure 4.14 a**). The prediction successfully identified the canonical VDRE elements VDREp and VDREd. (Figure 4.12 b). In addition these site lie in regions of highly conserved regions, as identified by mammalian GERP scores (Cooper et al., 2005) just upstream of the CYP24A1 tss (**Figure 4.14 b**). We then carried out a ChIP qPCR on a region that spanned both the VDREp and VDREd regions of the genome and found that in $CD4^+$ memory cells treated with VitD, VDR binding was enriched to the VDRE regions compared to IgG control (**Figure 4.14 c**).

Thus, we concluded that the VDR antibody was probably suitable for ChIP techniques such as ChIP-seq.

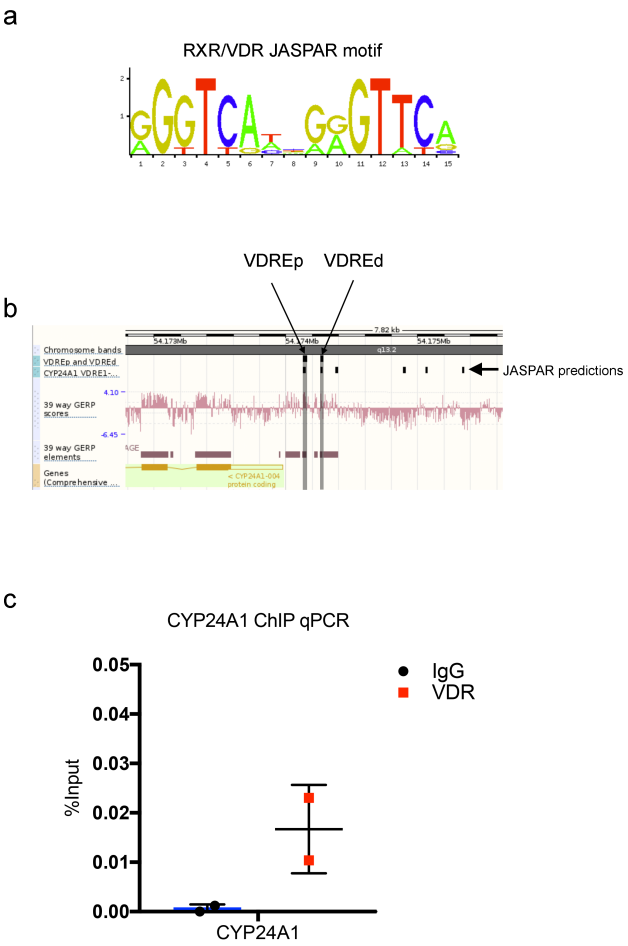


**Figure 4.14 |VDR ChIP qPCR|**
(a) RXR/VDR motif used by JASAPAR for motif searching. Logo show schematic representation of frequency of nucleotides at each position in motifs, where frequency is proportional to size of nucleotide at given positions. (b) Genome view using ENSEMBL genome browser (Yates et al., 2016). Black bars on top row show genomic location of canonical VDREp and VDREd enhancer sites. Black bars on second row show predicted binding regions using JASPAR motif search. The pink histograms and pink bars represent conservation of genomic sequence between all mammalian species with sequenced genomes. A positive value on the histogram represents positive enrichment which is then represented as a pink bar below. (c) Enrichment of VDR binding by ChIP qPCR, represented as % enrichment compared to input. IgG in black circles compares to VDR in VitD treated $CD4^+$ memory T cells as red squares. (*n = 2*). Experiments carried out on bead isolated memory $CD4^+$ T cells as specified in materials and methods section 2.2.3.2.

#### 4.4.2.2 ChIP-seq quality control

Following sequencing we first checked if the ChIP had been successful, i.e. if reads were enriched to specific regions of the genome. We used "Deeptools" (Ramírez et al., 2016) to plot fingerprints for each of the ChIP-seqs. This software splits the genome into genomic regions (bins, set here to 50bp) and counts the number of reads per bin. An ideal input, with a uniform distribution of read alignments, would result in a diagonal line. A very specific and strong ChIP enrichment, on the other hand, would result in a large portion of reads accumulating in just a few bins and the resulting plot showing a steep rise toward the right-most edge. VDR showed similar distribution to its cross-linked input control (**Figure 4.15 a**) with little enrichment to specific bins, suggesting no enrichment for VDR from ChIP – i.e. an unsuccessful ChIP in all donors. H3K27Ac showed increased enrichment to specific bins and diverged from its native input control (**Figure 4.15 b**), as would be expected for a broad peak histone modification. H3K4me3 showed strong enrichment to specific bins suggesting more narrow peaks enriching to genomic bins (**Figure 4.15 c**). This suggests H3K4me3 denotes reads at narrower segments of the genome compared to H3K27Ac which are broader in nature.

These results suggested that VDR ChIP had not worked and that H3K27Ac has broader enrichment compared to H3K4me3, as expected. To confirm these results a principle component analysis was carried out on all ChIP-seq samples from both donors. Both native and cross-linked inputs controls clustered together with VDR ChIP-seq (**Figure 4.15 d**). Combined with fingerprint analysis showing that inputs and VDR displayed low enrichment to specific bins, this confirms that VDR ChIP was unsuccessful. All H3K27Ac samples clustered together but separated from H3K4me3 clusters (**Figure 4.15 d**), though these clusters were closer in the principle components to each other than to input controls, suggesting closer similarity between regions enriched for H3K27Ac and H3K4me3 than to inputs, as would be expected.

In summary, both histone modification ChIP-seqs were successful. As VitD, through actions of VDR, primarily effects histone modifications, especially acetylation (Fetahu et al., 2014), downstream analysis was confined to histone modifications.

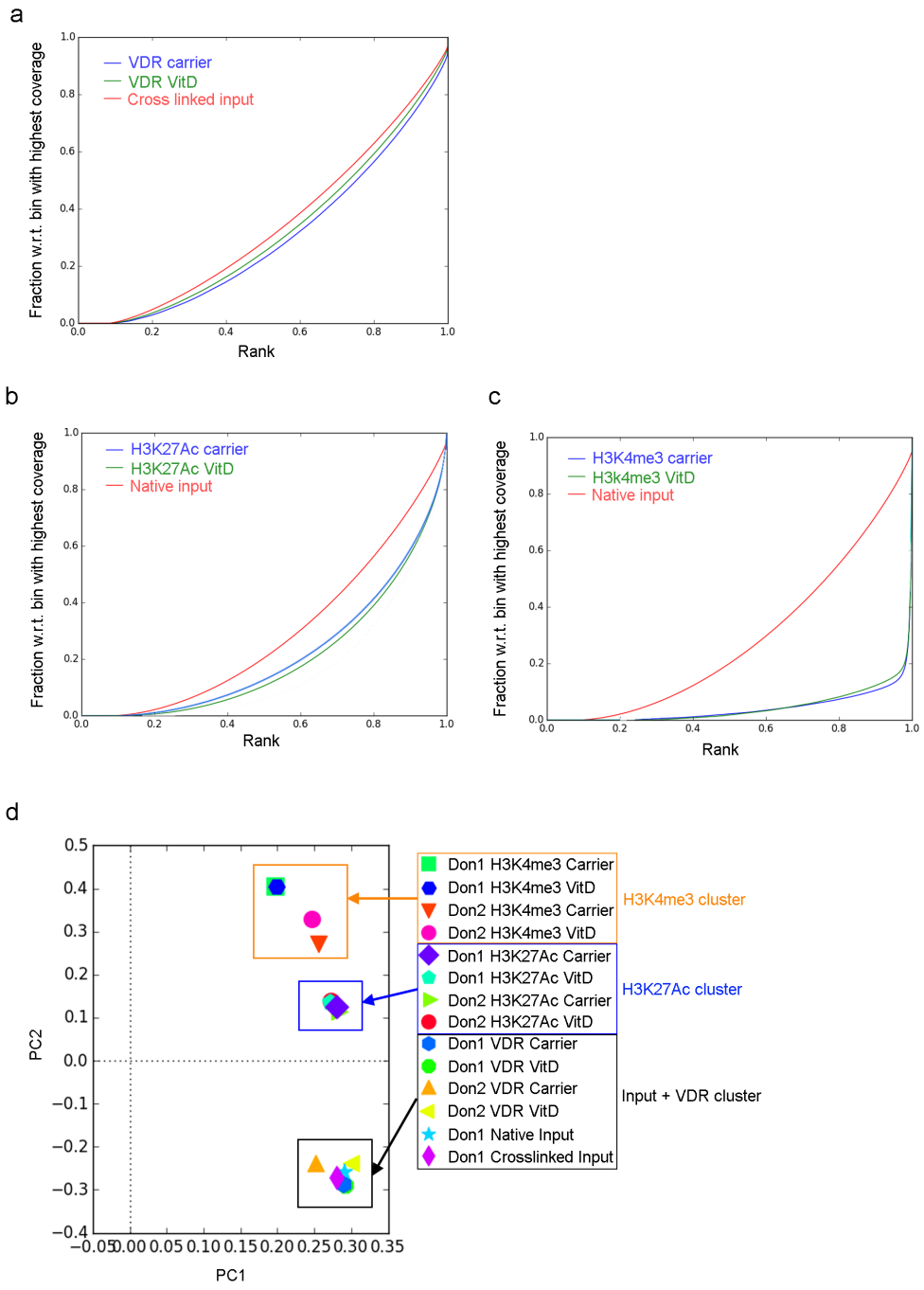


**Figure 4.15|Assessment of ChIP quality|**
Fingerprint of ChIP enrichment to 50bp genomic windows (bins) in one representative donor, for VDR with cross-linked input (a), H3K4me3 with native input (b) and H3K27Ac with native input (c). Plots show per-base coverage of reads overlapping a bin. Values are sorted according to their rank (the bin with the highest number of reads has the highest rank), with the cumulative sum plotted. (d) Principle component analysis (PCA) with all conditions and donors combined. H3K4me3 cluster indicated by orange box, H3K27Ac clusters indicated by blue box and VDR and input clusters indicated by black box. Experiments carried out on bead isolated memory $CD4^+$ T cells as specified in materials and methods section 2.2.3.2.

#### 4.4.2.3 VitD alters the $CD4^+$ T epigenome

We next analysed H3K4me3 and H3K27Ac ChIP-seq peaks in carrier and VitD treated cells. There was a total of 25,583 H3K4me3 peaks in donor 1 (Don1) and 28,731 in donor 2 (Don2), with 23,965 common peaks (**Figure 4.16 a**). A total of 25,712 H3K27Ac peaks were evident in Don1 and 35,760 in Don2, with 21,862 common peaks (**Figure 4.16 c**). This indicates good reproducibility of peak identification between two biological replicates. Within the common H3K4me3 peaks, a strong correlation was identified in ChIP-seq signal, in both carrier and VitD treatment conditions (**Figure 4.16 b**) and unsupervised clustering of ChIP-seq signal showed very similar cluster formation between both donors and treatments (**Figure 4.16 b**). For H3K27Ac a good correlation was also observed in ChIP-seq signal from peaks in common between donors in VitD treated cells (**Figure 4.16 d**). A lower correlation was observed in carrier treated cells and clustering indicated ChIP-seq signal from Don2 with carrier treatment was not consistent with VitD treated H3K27Ac ChIP-seq signal (**Figure 4.16 d**). For this reason, Don1 was used for downstream analysis and key results confirmed in Don2.

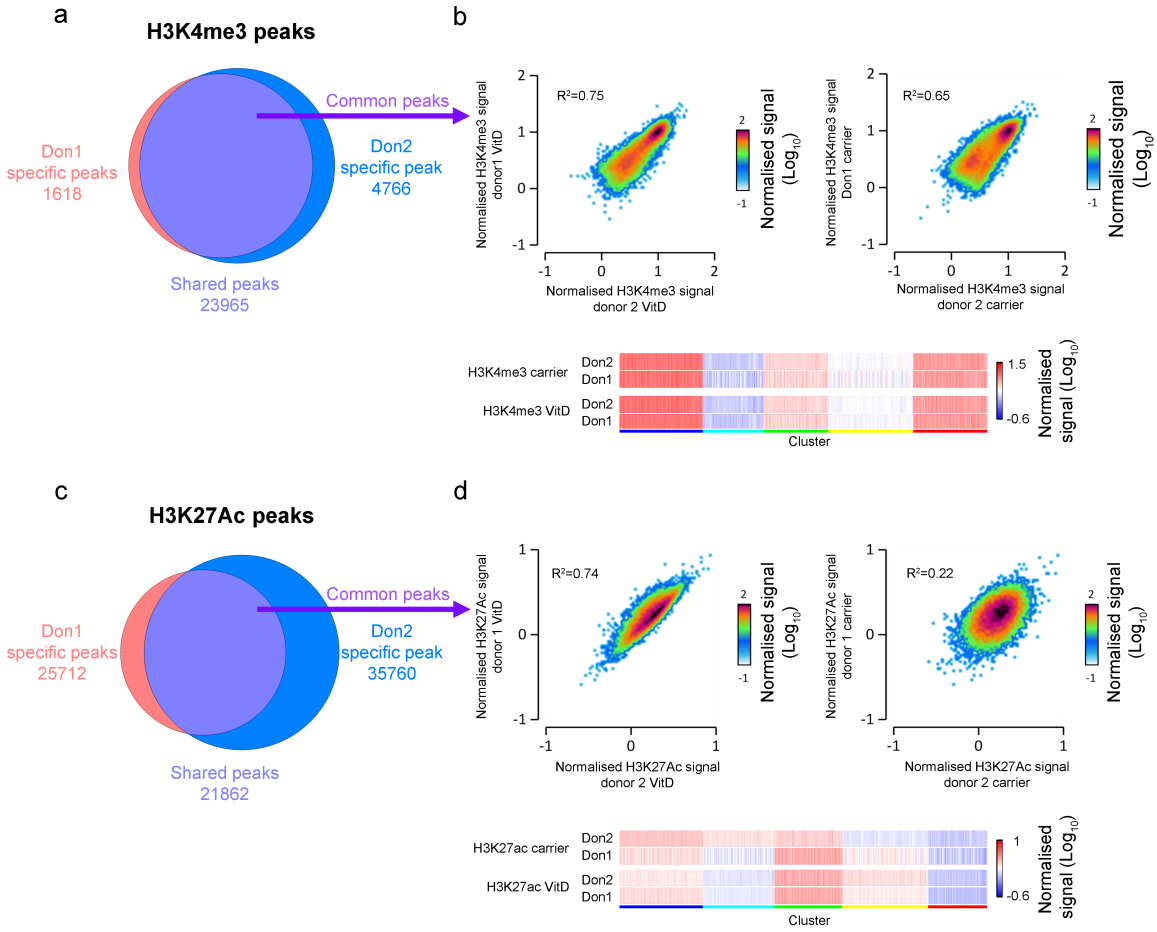


**Figure 4.16|Donor variability in H3K4me3 and H3K27Ac ChIPseq|**
(a) Proportionate Venn diagram showing overlap between merged H3K4me3 peaks of both carrier and VitD conditions, compared between two donors, with peaks in Donor 1 (Don1) in red, peaks in Donor 2 (Don2) in blue and overlapping peaks in purple. (b) Normalised ChIP signal of common H3k4me3 peaks from (a) were compared in scatter plot and correlation reported as $R^2$. All common peaks were then clustered (k-means clustering, k=5) and signal in clustered peaks compared by heatmap. (c) Proportionate Venn diagram showing overlap between merged H3K27Ac peaks of both carrier and VitD conditions, compared between two donors, with peaks in Don1 in red, peaks in Don2 in blue and overlapping peaks in purple. (d) Normalised ChIP signal of common H3k27Ac peaks from (c) were compared in scatter plot and correlation reported as $R^2$. All common peaks were then clustered (k-means clustering, k=5) and signal in clustered peaks compared in a heatmap. Experiments carried out in bead isolated memory $CD4^+$ T cells as specified in materials and methods section 2.2.3.2.

#### 4.4.2.3.1 VitD induces H3K27 acetylation at putative enhancer sites enabling STAT3 and IL-6 transcription

H3K27Ac is a marker of promoter and enhancer activity. We first determined whether VitD treatment alters the overall distribution of H3K27Ac peaks in the genome. The genome, as a whole, consists of predominantly distal intergenic regions, which have no assigned function in our analysis, with the majority of the rest being intronic regions (**Figure 4.17 a**). Most H3K27Ac peaks in our ChIP-seqs were located within introns of genes, with increased localisation to promoters compared to genomic background, but we saw no difference between VitD and carrier-treated cells (**Figure 4.17 a**). Interestingly, this is similar to VDR localisation following treatment with VitD (increased VDR binding occurs in intronic regions following VitD treatment) (Ramagopalan et al., 2010). Thus, VitD does not globally alter the overall distribution of H3K27Ac activity in the genome.

We next compared H3K27Ac peak signal intensities of carrier and VitD treated cells. 966 peaks were induced (1.5 fold increased compared to carrier) and 793 peaks were repressed (1.5 fold decreased compared to carrier) by VitD treatment (**Figure 4.17 b and c**). We analysed the DNA sequences corresponding to induced and repressed H3K27Ac sites for binding motifs of known transcription factors. VDR (DR3 type) was identified as having the highest motif frequency within VitD induced peaks (**Figure 4.17 d and e** and **Table 4.1**) and showed no enrichment in VitD repressed peaks (**Figure 4.17 d and e** and **Table 4.2**). Among the VitD-induced H3K27Ac sites, the next five enriched TF motifs were those of AP1 family members, including Jun (**Table 4.1**). The Jun-AP1 motif was the most enriched motif within VitD repressed peaks (**Table 4.2**). Other notable motifs enriched within the repressed loci included sequences corresponding to IRFs and interferon stimulated response elements (ISRE) (**Figure 4.17 d and e, and Table 4.2**).

Peaks were then assigned to the closest RefSeq genes. *IL6* and *STAT3* were both associated with H3K27Ac peaks induced by VitD treatment. The H3K27Ac peak assigned to *IL6* was approximately 100kb upstream of the *IL6* tss (**Figure 4.17 f**). In contrast, the *STAT3* peak lay within an intron approximately 90kb downstream of the tss (**Figure 4.17 f**). Both peaks contained VDR sequence motifs, predicting binding of VDR. We therefore

next assessed VDR binding from publically available VDR ChIP-seq in unstimulated vs VitD stimulated lymphoblastoid cell line (LCL) (GSM558636). Additionally, as VDR recruits histone acetylases (HATs), such as p300 (Haussler et al., 2011; 2013), we also aligned p300 ChIP-seq from another lymphoblastoid cell line (GM12878 cell line)(GSM1817183). Not only was there a strong VDR binding peak in VitD treated cells (but not unstimulated cells) at exactly the site of increased H3K27Ac (and predicted DR3 VDR motif) upstream of the *IL6* promoter, but p300 binding was also identified nearby (**Figure 4.17 f**). At the *STAT3* intronic H3K27Ac peak, p300 loading was clearly identified, with weak VDR binding peaks also present (**Figure 4.17 f**). Interestingly, there was clear binding of p300 and VDR at the tss of *STAT3* as well as H3K27Ac peaks, but this region of acetylation was not increased by addition of VitD.

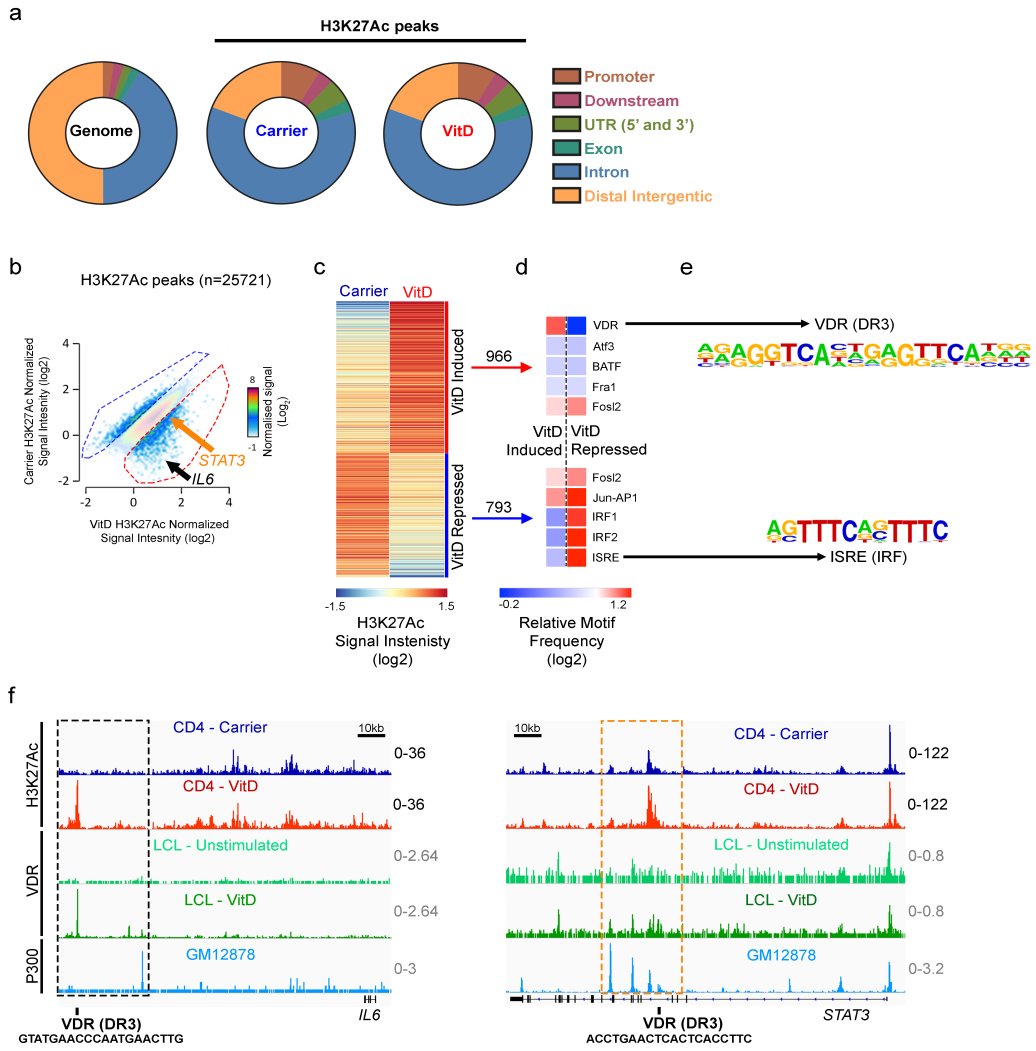


**Figure 4.17|Direct VitD induced H3K27 acetylation at enhancer sites as mechanism for observed protein expression|**

(a) Distribution of all H3K27Ac peaks in carrier treated (middle), and peaks that in VitD treated cells (right), as compared to overall genomic distribution (left) of gene features. (b) Intensity of H3K27Ac signal in carrier treated compared to VitD treated cells in scatter plot. Peaks 1.5 times induced (blue gate) and repressed (red gate) by VitD treatment are marked. Location of IL-6 (black) and STAT3 (orange) enhancer peaks are shown with coloured arrows. (c) Heatmap showing H3K27Ac peak intensities (quantile normalised) of VitD induced and repressed peaks. (d) Heatmap showing enriched transcription factor motifs in VitD induced (top) and repressed (bottom) H3K27Ac peaks. Enrichment of top 5 motifs are shown. (e) Top enriched motif from VitD induced (top), and repressed (bottom) peaks, VDR and ISRE respectively (f) H3K27Ac tracks in VitD treated and carrier treated $CD4^+$ T cells, with VDR tracks from unstimulated and VitD treated lymphoblastoid cell line (LCL) in green and p300 track from GM12878 cell lines in light blue. Track heights are shown with RPKM normalisation in black and RPGC normalisation in grey. Highlighted in box are locations of *IL6* (black) and *STAT3* (orange) putative enhancers. Beneath both sets of tracks are shown VDR (DR3) binding motifs identified in (d). Experiments carried out in bead isolated memory $CD4^+$ T cells as specified in materials and methods section 2.2.3.2.

| Motif name | Consensus | P-value | q-value | Target sequences with Motif | | Background sequences with Motif | | Motif enrichment (fold) |
|---|---|---|---|---|---|---|---|---|
| | | | | Number | % | Number | % | |
| VDR(NR),DR3 | ARAGGTCANWGAGTTCANNN | 1.00E-45 | 0 | 303 | 34.99% | 7469.5 | 15.25% | 2.29 |
| Fosl2(bZIP) | NATGASTCABNN | 1.00E-35 | 0 | 322 | 37.18% | 9240.8 | 18.87% | 1.97 |
| Fra1(bZIP) | NNATGASTCATH | 1.00E-33 | 0 | 443 | 51.15% | 15287.4 | 31.22% | 1.64 |
| Atf3(bZIP) | DATGASTCATHN | 1.00E-32 | 0 | 487 | 56.24% | 17774.5 | 36.29% | 1.55 |
| BATF(bZIP) | DATGASTCAT | 1.00E-31 | 0 | 479 | 55.31% | 17434.6 | 35.60% | 1.55 |
| Jun-AP1(bZIP) | GATGASTCATCN | 1.00E-31 | 0 | 248 | 28.64% | 6555.2 | 13.39% | 2.14 |
| AP-1(bZIP) | VTGACTCATC | 1.00E-25 | 0 | 499 | 57.62% | 19557.1 | 39.93% | 1.44 |
| Bach2(bZIP) | TGCTGAGTCA | 1.00E-12 | 0 | 173 | 19.98% | 5630 | 11.50% | 1.74 |
| Ets1-distal(ETS) | MACAGGAAGT | 1.00E-07 | 0 | 241 | 27.83% | 9893.3 | 20.20% | 1.38 |
| bZIP:IRF(bZIP,IRF) | NAGTTTCABTHTGACTNW | 1.00E-06 | 0 | 310 | 35.80% | 13588.9 | 27.75% | 1.29 |
| Bach1(bZIP) | AWWNTGCTGAGTCAT | 1.00E-05 | 0.0001 | 52 | 6.00% | 1486.7 | 3.04% | 1.97 |
| EWS:FLI1-fusion(ETS) | VACAGGAAAT | 1.00E-04 | 0.0003 | 362 | 41.80% | 17020.7 | 34.76% | 1.20 |
| MafK(bZIP) | GCTGASTCAGCA | 1.00E-04 | 0.0005 | 153 | 17.67% | 6252.8 | 12.77% | 1.38 |
| NF-E2(bZIP) | GATGACTCAGCA | 1.00E-04 | 0.0008 | 50 | 5.77% | 1528.5 | 3.12% | 1.85 |
| IRF:BATF(IRF:bZIP) | CTTTCANTATGACTV | 1.00E-04 | 0.0008 | 109 | 12.59% | 4182.7 | 8.54% | 1.47 |
| SpiB(ETS) | AAAGRGGAAGTG | 1.00E-04 | 0.001 | 193 | 22.29% | 8364.5 | 17.08% | 1.31 |
| ETS1(ETS) | ACAGGAAGTG | 1.00E-04 | 0.0012 | 551 | 63.63% | 27993.8 | 57.16% | 1.11 |
| PU.1(ETS) | AGAGGAAGTG | 1.00E-04 | 0.0014 | 335 | 38.68% | 15930.9 | 32.53% | 1.19 |
| ETS:RUNX(ETS,Runt) | RCAGGATGTGGT | 1.00E-03 | 0.0024 | 87 | 10.05% | 3289.7 | 6.72% | 1.50 |
| RFX(HTH) | CGGTTGCCATGGCAAC | 1.00E-03 | 0.003 | 65 | 7.51% | 2302.4 | 4.70% | 1.60 |

**Table 4.1|H3K27Ac VitD induced peaks|**

Motif analysis. Top 20 Significantly enriched motifs in H3K27Ac peaks induced by VitD

| Motif Name | Consensus | P-value | q-value | Target sequences with Motif | | Background sequences with Motif | | Motif enrichment (fold) |
|---|---|---|---|---|---|---|---|---|
| | | | | Number | % | Number | % | |
| Jun-AP1(bZIP) | GATGASTCATCN | 1.00E-40 | 0 | 225 | 31.08% | 6018.1 | 12.23% | 2.54 |
| Fosl2(bZIP) | NATGASTCABNN | 1.00E-39 | 0 | 284 | 39.23% | 8891.5 | 18.07% | 2.17 |
| IRF2(IRF) | GAAASYGAAASY | 1.00E-38 | 0 | 183 | 25.28% | 4297.6 | 8.73% | 2.90 |
| IRF1(IRF) | GAAAGTGAAAGT | 1.00E-35 | 0 | 227 | 31.35% | 6507.9 | 13.23% | 2.37 |
| ISRE(IRF) | AGTTTCASTTTC | 1.00E-35 | 0 | 136 | 18.78% | 2705.5 | 5.50% | 3.41 |
| Fra1(bZIP) | NNATGASTCATH | 1.00E-33 | 0 | 427 | 58.98% | 18039.2 | 36.66% | 1.61 |
| BATF(bZIP) | DATGASTCAT | 1.00E-28 | 0 | 447 | 61.74% | 20191.6 | 41.04% | 1.50 |
| bZIP:IRF(bZIP,IRF) | NAGTTTCABTHTGACTNW | 1.00E-28 | 0 | 441 | 60.91% | 19834.8 | 40.31% | 1.51 |
| AP-1(bZIP) | VTGACTCATC | 1.00E-26 | 0 | 460 | 63.54% | 21372.9 | 43.44% | 1.46 |
| Atf3(bZIP) | DATGASTCATHN | 1.00E-26 | 0 | 442 | 61.05% | 20268.5 | 41.19% | 1.48 |
| Bach2(bZIP) | TGCTGAGTCA | 1.00E-22 | 0 | 164 | 22.65% | 4935.5 | 10.03% | 2.26 |
| IRF4(IRF) | ACTGAAACCA | 1.00E-17 | 0 | 357 | 49.31% | 16531.2 | 33.60% | 1.47 |
| ETS1(ETS) | ACAGGAAGTG | 1.00E-17 | 0 | 467 | 64.50% | 23930.6 | 48.63% | 1.33 |
| Etv2(ETS) | NNAYTTCCTGHN | 1.00E-15 | 0 | 452 | 62.43% | 23289.2 | 47.33% | 1.32 |
| Ets1-distal(ETS) | MACAGGAAGT | 1.00E-13 | 0 | 219 | 30.25% | 9075.3 | 18.44% | 1.64 |
| EWS:FLI1-fusion(ETS) | VACAGGAAAT | 1.00E-13 | 0 | 311 | 42.96% | 14531 | 29.53% | 1.45 |
| IRF:BATF(IRF:bZIP) | CTTTCANTATGACTV | 1.00E-13 | 0 | 177 | 24.45% | 6813 | 13.85% | 1.77 |
| PU.1:IRF8(ETS:IRF) | GGAAGTGAAAST | 1.00E-13 | 0 | 192 | 26.52% | 7684.2 | 15.62% | 1.70 |
| RUNX-AML(Runt) | GCTGTGGTTW | 1.00E-13 | 0 | 384 | 53.04% | 19334.5 | 39.29% | 1.35 |

**Table 4.2|H3K27Ac VitD repressed peaks|**

Motif analysis. Top 20 Significantly enriched motifs in H3K27Ac peaks repressed by VitD.

As the enhancer sites within the *STAT3* intron and upstream of the *IL6* tss are putative and novel we confirmed the VitD induced induction of H3K27 acetylation at these sites in a second donor. This was particularly important as there was great donor variability observed in H3K27Ac ChIP-seq signal in carrier treated conditions (section 4.4.2.3). Despite this donor variability, H3K27 acetyation upstream of both the *IL6* tss regions (**Figure 4.18 a**) and within the *STAT3* intron (**Figure 4.18 b**) were significantly induced by VitD treatment in both donors.

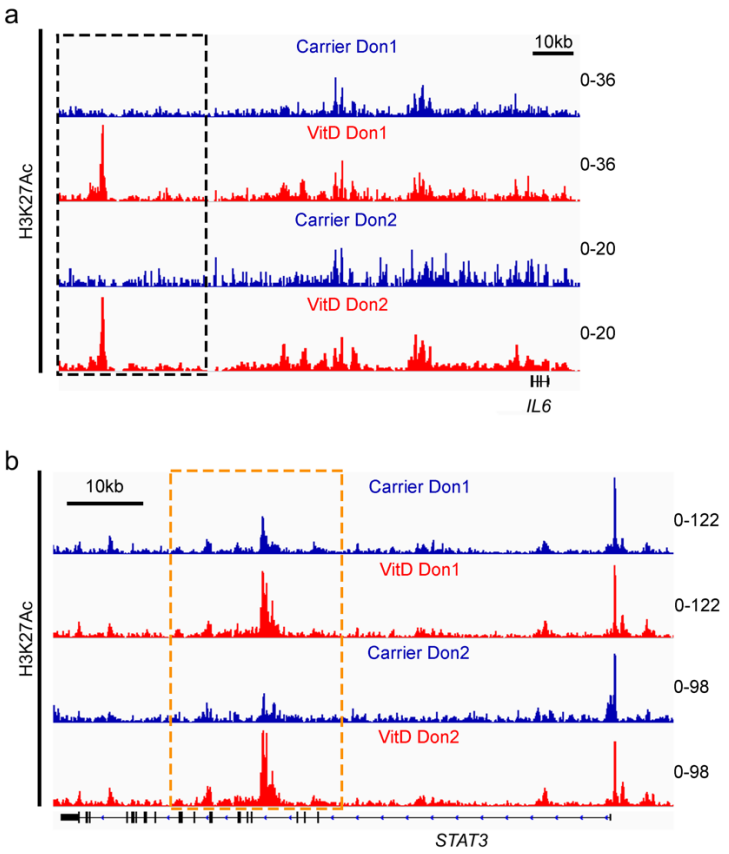


**Figure 4.18|Confirmation of two putative enhancer sites in second donor|** H3K27Ac tracks in VitD treated and carrier treated $CD4^+$ T cells, tracks heights are shown (RPGC normalisation). Highlighted in box are locations of (a) IL-6 (black) and (b) STAT3 (orange) putative enhancers, shown in Donor1 (Don1) at top and Donor 2 (Don2) at bottom. Experiments carried out in bead isolated memory $CD4^+$ T cells as specified in materials and methods section 2.2.3.2.

#### 4.4.2.3.2 VitD represses H3K4 methylation at tss for IFNγ and induces H3K4 methylation at tss for IL-10

Using H3K4me3 as a marker of promoter activity we found that, like H3K27Ac, VitD did not change overall distribution of peaks in relation to gene features (**Figure 4.19 a**). As expected, H3K4me3 showed substantially increased association with promoter regions compared to H3K27Ac (**Figure 4.19 a**).

Signal intensity was compared between carrier and VitD treatment in all 25,583 identified peaks, and 3,667 peaks induced (1.5 fod increased compared to carrier) by VitD treatment, and 3,896 peaks repressed (1.5 fold decreased compared to carrier) by VitD were found (**Figure 4.19 b**). TF motif analysis of these DNA sequences showed strong enrichment for CTCF motifs and the related CTCFL motif in K4me3 VitD induced regions (**Table 4.3**) and, as before, IRF sequences in K4me3 down-regulated areas (**Table 4.4**). Interestingly, motif analysis did not identify VDR as a significantly enriched motif in either VitD induced (**Table 4.3**) or repressed H3K4 tri-methylation peaks (**Table 4.4**).

We next assigned H3K4me3 peaks to genes. *IL10* had an associated H3K4me3 peak induced by VitD whereas *IFNG*, the gene encoding IFNγ, had an H3K4me3 peak that was repressed by VitD (**Figure 4.19 b**). We again visualised tracks and aligned VDR ChIPseq data from LCL (GSM558636)**.** VDR binding by ChIP-seq corresponded to the same H3K4me3 locus induced by VitD (**Figure 4.19 c**). As we had earlier shown a causal link between pYSTAT3 signalling and IL-10 production (**section 4.4.1**), we performed *in-silico* analysis for predicted STAT3 motif binding sites and identified a putative STAT3 site at this *IL10* associated H3K4me3 peak (**Figure 4.19 c**). To further clarify STAT3 binding we analysed a STAT3 ChIP-seq track (GSM1227212) and found that STAT3 does, indeed, bind at this locus (**Figure 4.19 c**).

H3K4 trimethylation at the *IFNG* promoter was substantially reduced following VitD treatment (**Figure 4.19 b and c**). No VDR binding was identified at this site, either *in silico* or with publically available datasets, suggesting that reduced promoter activity at *IFNG* is not directly due to VDR binding.

In summary, total STAT3 and IL-6 expression in primary $CD4^+$ T cells is induced by opening of novel enhancer regions by direct VDR binding and we see evidence from LCLs

HAT p300 recruitment. Following phosphorylation of STAT3, through IL-6 signalling, pSTAT3 binds to the proximal regulatory region (promoter) of *IL10*, whose enhanced gene transcription in the context of VitD is reflected by increased H3K4 tri-methylation.

*IL6* was also identified as having 1.5 fold increased H3K4me3 signal, and when visualised clear induction was seen at tss of the *IL6* gene in both donors **(Figure 4.20 a**). However, neither VDR binding motifs nor VDR peaks in LCLs were identified within the region of increase H3K4me3 (**Figure 4.20 a**). Thus, the increased H3K4me3 supports our previous findings of increased IL-6 expression by an active promoter, but this is likely not due to liganded or un-liganded VDR effects but due to indirect mechanism.

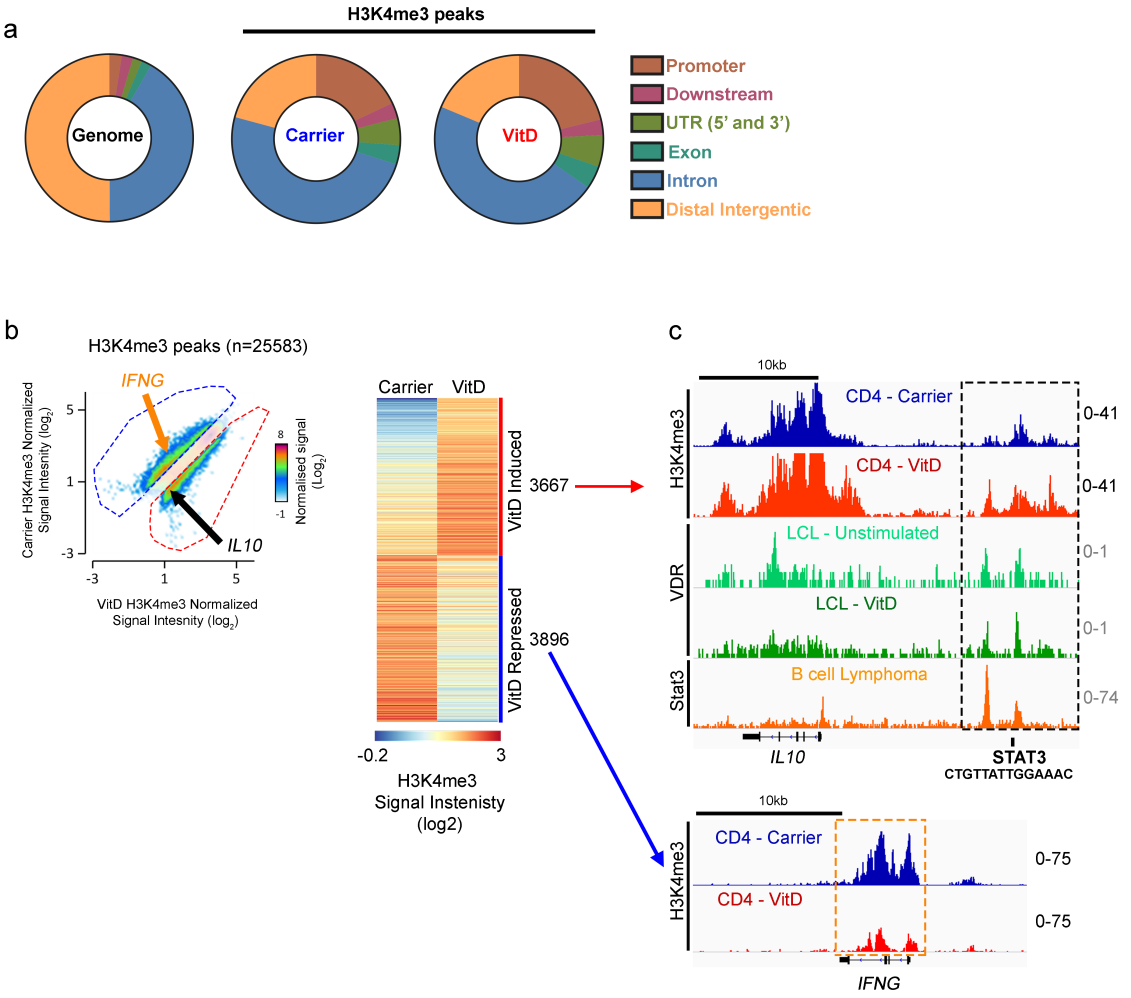


**Figure 4.19|Opening of chromatin by H3K4 tri methylation in VitD-treated cells and STAT3 binding to *IL10* promoter region|**

(a) Distribution of all H3K4me3 peaks in carrier treated (middle), and peaks that in VitD treated cells (right), as compared to overall genomic distribution (left) of gene features. (b) Intensity of H3K4me3 signal in carrier treated compared to VitD treated cells in scatter plot (left). Peaks 1.5 fold induced (blue gate) and repressed (red gate) by VitD treatment are marked. Location of IL-6 (black) and STAT3 (orange) peaks are represented as coloured spots. Signal intensity at VitD induced (red vertical line and arrow) and repressed (blue vertical line and arrow) peaks represented in heatmap, with numbers of peaks indicated above arrows (ChIP signal is quantile normalised). (c) H3K4me3 tracks in VitD treated and carrier treated $CD4^+$ T cells, with VDR tracks from unstimulated and VitD treated lymphoblastoid cell line (LCL) in green and STAT3 track from B cell Lymphoma cell line in orange. Tracks heights are shown with RPKM normalisation in black and RPGC normalisation in grey. Highlighted in box are locations of *IL10* (black) and *IFNG* (orange) promoter regions. The site of an *in-silico* predicted STAT3 binding motif is shown beneath the *IL10* locus. Experiments carried out in bead isolated memory $CD4^+$ T cells as specified in materials and methods section 2.2.3.2.

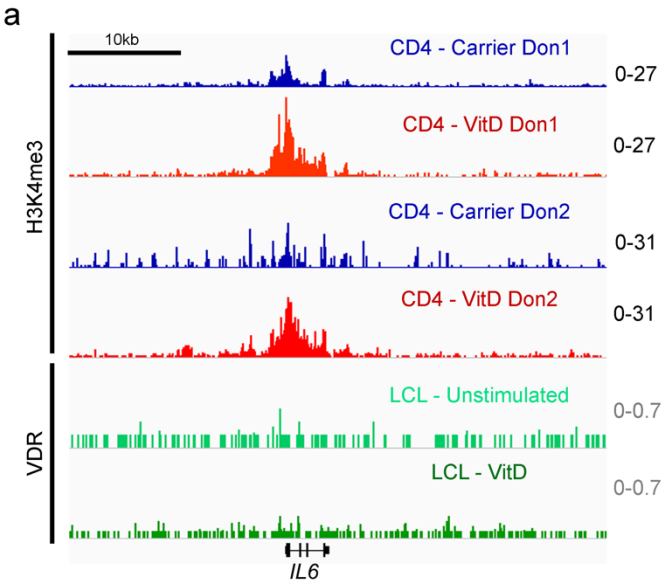


**Figure 4.20|K4me3 induced at IL-6 tss with no VDR binding|**
(a) H3K4me3 tracks from two donors (Donor 1, Don1; Donor 2, Don2) in VitD treated and carrier treated $CD4^+$ T cells, with VDR tracks from unstimulated and VitD treated lymphoblastoid cell line (LCL) in green. Tracks heights are shown with RPKM normalisation in black and RPGC normalisation in grey. Experiments carried out in bead isolated memory $CD4^+$ T cells as specified in materials and methods section 2.2.3.2.

| Motif name | Consensus | P-value | q-value | Target sequences with Motif | | Background sequences with Motif | | Motif enrichment (fold) |
|---|---|---|---|---|---|---|---|---|
| | | | | Number | % | Number | % | |
| CTCF(Zf) | AYAGTGCCMYCTRGTGGCCA | 1.00E-123 | 0 | 964 | 27.10% | 5214.1 | 12.33% | 2.20 |
| BORIS(Zf) | CNNBRGCGCCCCCTGSTGGC | 1.00E-80 | 0 | 1595 | 44.84% | 12533.9 | 29.64% | 1.51 |
| Sp1(Zf) | GGCCCCGCCCCC | 1.00E-15 | 0 | 1741 | 48.95% | 17847.7 | 42.20% | 1.16 |
| E2F6(E2F) | GGCGGGAARN | 1.00E-08 | 0 | 2233 | 62.78% | 24526.7 | 57.99% | 1.08 |
| E2F4(E2F) | GGCGGGAAAH | 1.00E-06 | 0 | 1963 | 55.19% | 21580.3 | 51.03% | 1.08 |
| Klf9(Zf) | GCCACRCCCACY | 1.00E-05 | 0.0005 | 1736 | 48.81% | 19126 | 45.22% | 1.08 |
| RFX(HTH) | CGGTTGCCATGGCAAC | 1.00E-04 | 0.0015 | 310 | 8.72% | 2936.3 | 6.94% | 1.26 |
| Rfx2(HTH) | GTTGCCATGGCAACM | 1.00E-04 | 0.0031 | 328 | 9.22% | 3167.3 | 7.49% | 1.23 |
| Jun-AP1(bZIP) | GATGASTCATCN | 1.00E-04 | 0.0031 | 407 | 11.44% | 4028.1 | 9.52% | 1.20 |
| X-box(HTH) | GGTTGCCATGGCAA | 1.00E-04 | 0.0031 | 285 | 8.01% | 2707.6 | 6.40% | 1.25 |
| Mef2c(MADS) | DCYAAAAATAGM | 1.00E-03 | 0.0051 | 589 | 16.56% | 6091.7 | 14.40% | 1.15 |
| Fosl2(bZIP) | NATGASTCABNN | 1.00E-03 | 0.0078 | 549 | 15.43% | 5675.6 | 13.42% | 1.15 |
| Mef2a(MADS) | CYAAAAATAG | 1.00E-03 | 0.0201 | 613 | 17.23% | 6467.3 | 15.29% | 1.13 |
| Mef2b(MADS) | GCTATTTTTGGM | 1.00E-03 | 0.0216 | 1067 | 30.00% | 11688.8 | 27.64% | 1.09 |
| HOXD13(Homeobox) | NCYAATAAAA | 1.00E-02 | 0.051 | 1199 | 33.71% | 13316.9 | 31.49% | 1.07 |
| Lhx1(Homeobox) | NNYTAATTAR | 1.00E-02 | 0.0672 | 1233 | 34.66% | 13750.5 | 32.51% | 1.07 |
| Bach2(bZIP) | TGCTGAGTCA | 1.00E-02 | 0.0672 | 359 | 10.09% | 3711.6 | 8.78% | 1.15 |
| Fra1(bZIP) | NNATGASTCATH | 1.00E-02 | 0.0672 | 767 | 21.56% | 8347.8 | 19.74% | 1.09 |
| E2F1(E2F) | CWGGCGGGAA | 1.00E-02 | 0.0761 | 1349 | 37.93% | 15143.7 | 35.81% | 1.06 |
| CTCF(Zf) | AYAGTGCCMYCTRGTGGCCA | 1.00E-123 | 0 | 964 | 27.10% | 5214.1 | 12.33% | 1.13 |

**Table 4.3|H3K4me3 VitD induced peaks|**

Motif analysis. Top 20 significantly enriched motifs in H3K4me3 peaks induced by VitD.

| Motif name | Consensus | P-value | q-value | Target sequences with Motif | | Background sequences with Motif | | Motif enrichment (fold) |
|---|---|---|---|---|---|---|---|---|
| | | | | Number | % | Number | % | |
| IRF2(IRF) | GAAASYGAAASY | 1.00E-298 | 0 | 1240 | 35.57% | 5278.9 | 11.54% | 3.082 |
| IRF1(IRF) | GAAAGTGAAAGT | 1.00E-244 | 0 | 1454 | 41.71% | 7990.8 | 17.47% | 2.388 |
| ISRE(IRF) | AGTTTCASTTTC | 1.00E-239 | 0 | 897 | 25.73% | 3385.3 | 7.40% | 3.477 |
| Ets1-distal(ETS) | MACAGGAAGT | 1.00E-100 | 0 | 1430 | 41.02% | 11245 | 24.58% | 1.669 |
| PU.1:IRF8(ETS:IRF) | GGAAGTGAAAST | 1.00E-83 | 0 | 1230 | 35.28% | 9588.5 | 20.96% | 1.683 |
| EWS:FLI1-fusion(ETS) | VACAGGAAAT | 1.00E-70 | 0 | 1898 | 54.45% | 18084.3 | 39.53% | 1.377 |
| ETS(ETS) | AACCGGAAGT | 1.00E-68 | 0 | 1062 | 30.46% | 8320.8 | 18.19% | 1.675 |
| Elk1(ETS) | HACTTCCGGY | 1.00E-67 | 0 | 1493 | 42.83% | 13220.8 | 28.90% | 1.482 |
| GABPA(ETS) | RACCGGAAGT | 1.00E-64 | 0 | 2327 | 66.75% | 24009.9 | 52.48% | 1.272 |
| Elk4(ETS) | NRYTTCCGGY | 1.00E-60 | 0 | 1492 | 42.80% | 13536.9 | 29.59% | 1.446 |
| IRF4(IRF) | ACTGAAACCA | 1.00E-53 | 0 | 1920 | 55.08% | 19217.4 | 42.00% | 1.311 |
| ELF1(ETS) | AVCCGGAAGT | 1.00E-52 | 0 | 1337 | 38.35% | 12106.6 | 26.46% | 1.449 |
| bZIP:IRF(bZIP,IRF) | NAGTTTCABTHTGACTNW | 1.00E-51 | 0 | 2129 | 61.07% | 22099.7 | 48.30% | 1.264 |
| Etv2(ETS) | NNAYTTCCTGHN | 1.00E-47 | 0 | 2498 | 71.66% | 27379.9 | 59.84% | 1.198 |
| PU.1(ETS) | AGAGGAAGTG | 1.00E-47 | 0 | 1726 | 49.51% | 17123.6 | 37.43% | 1.323 |
| Fli1(ETS) | NRYTTCCGGH | 1.00E-44 | 0 | 2516 | 72.17% | 27794 | 60.75% | 1.188 |
| ETS1(ETS) | ACAGGAAGTG | 1.00E-43 | 0 | 2550 | 73.15% | 28364.6 | 62.00% | 1.180 |
| IRF:BATF(IRF:bZIP) | CTTTCANTATGACTV | 1.00E-43 | 0 | 931 | 26.71% | 7916.3 | 17.30% | 1.544 |
| ETV1(ETS) | AACCGGAAGT | 1.00E-33 | 0 | 2771 | 79.49% | 32214.5 | 70.41% | 1.129 |
| IRF2(IRF) | GAAASYGAAASY | 1.00E-298 | 0 | 1240 | 35.57% | 5278.9 | 11.54% | 1.166 |

**Table 4.4|H3K4me3 VitD repressed peaks|**

Motif analysis. Top 25 Significantly enriched motifs in H3K4me3 peaks repressed by VitD

#### 4.4.2.3.3 Preferential VDR binding occurs at active enhancers

As we used published VDR ChIP-seq data, we next wanted to ascertain the level of agreement between out VDR motif prediction within sites of histone modifications and this published ChIP-seq data on a global genomic scale. To do so we first identified the proportion of VDR peaks from both un activated and activated LCLs (*n* = 3,049) that were present within regions of both H3K4me3 and H3K27Ac (*n* = 35,195). We found that around half (1,455) of LCL VDR peaks lay within regions of H3K4me3 and H3K27Ac (**Figure 4.21 a**). The vast majority of these 1,455 VDR peaks (1,289) were correctly identified as VDR motifs (**Figure 4.21 b**) validating our data.

Having identified histone modifications at putative enhancer sites we next assessed the overall distribution of VDR binding sites in relation to enhancers and promoters. Active enhancers were defined as regions of H3K27Ac more than 3kb from tss of genes, and active promoters as regions of H3K4me3 within 3kb of tss. Of the 1,289 VDR peaks in LCLs that overlapped with VDR motifs, 735 localised to active enhancers, with only 549 localising to active promoters (**Figure 4.21 c**). This suggests that VDR binding to enhancers, as identified for *STAT3* and *IL6*, is a general feature and not restricted to the pathway identified.

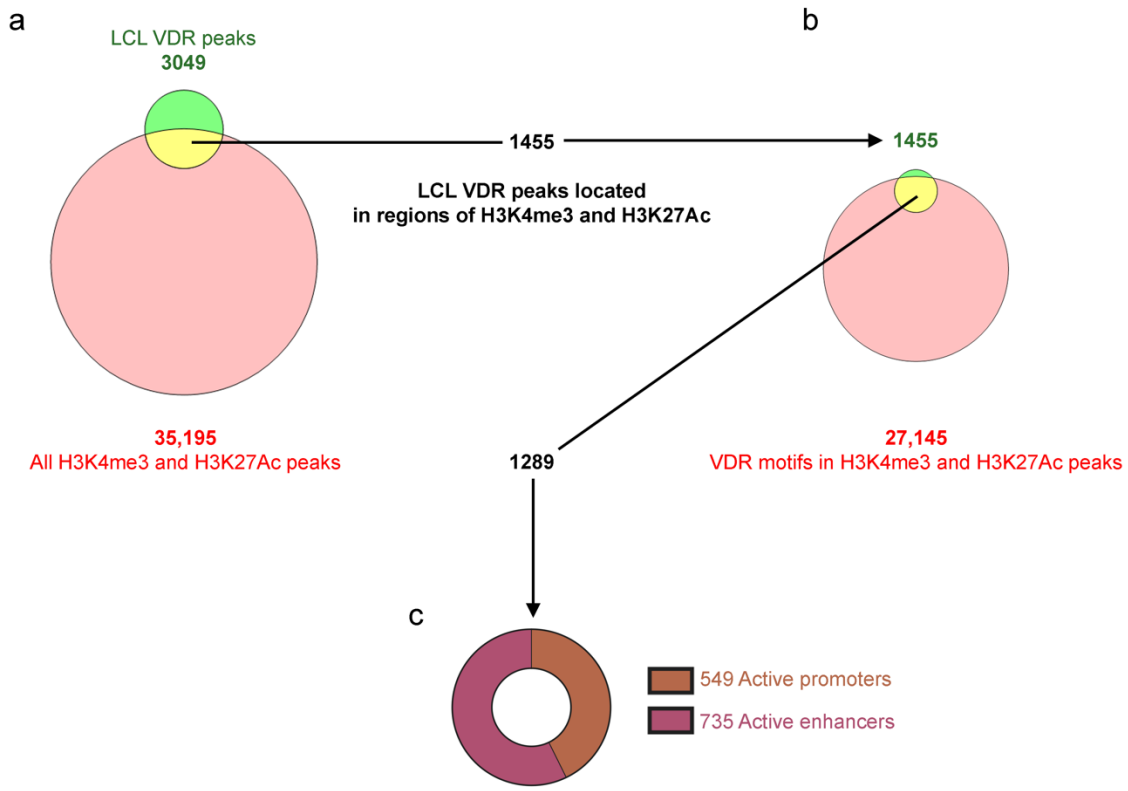


**Figure 4.21 |VDR peak localization in active enhancers and promoters|**
(a) Overlap of VDR peaks in LCLs and H3K4me3 and H3K27Ac peaks. (b) Overlap of VDR peaks in LCLs and H3K4me3 and H3K27Ac peaks with predicted VDR motifs in H3K4me3 and H3K27Ac peaks. (c) Proportion of common peaks from (b) that localise to active promoter and active enhancers.

#### 4.4.2.4 Pathway analysis of genes with predicted VDR binding sites supports epigenetic modifications by VitD involved in key immunological processes

We next wanted to gain a broader insight into the functional role played by epigenetic changes induced by VitD treatment in $CD4^+$ T cells. Peaks with predicted VDR binding motifs were assigned to closest genes. Assigned genes with VDR motifs from VitD induced, repressed (as previously defined) and unaffected genes were then subjected to pathway enrichment analysis using "Metascape" (Tripathi et al., 2015).

##### 4.4.2.4.1 Pathway analysis of genes with VDR binding sites and unaltered epigenetic states

We first determined the function of genes and biological pathways corresponding to genes unaffected by VitD treatment (thus, genes regulated by histone modification and

VDR binding, that are part of the core transcriptional programme in $CD4^+$ T cells). VDR Binding motifs within H3K27Ac and H3K4me3 peaks unaffected by VitD (neither induced nor repressed) were annotated to genes and subjected to pathway analysis. We used Circos plots in **Figure 4.22 a** to visualise the relationship between annotated genes in both H3K4me3 and H3K27Ac unaffected regions. In this Figure, genes present in both genesets are joined by purple lines and genes sharing the same functional annotation or pathway (KEGG, gene ontology and hallmark gene-sets) are joined by blue lines. Approximately 50% of annotated genes were found within both H3K27Ac and H3K4me3 regions (**Figure 4.22 a**). As such, it was not surprising that there was high commonality between pathways (high density of blue links in the Circos plot) (**Figure 4.22 a**).

Pathways were then clustered based on the top 20 most significantly enriched (**Figure 4.22 b**). The majority of significantly enriched pathways were shared between genes annotated to both histone marks (**Figure 4.22**). In addition, the vast majority of pathways involved modulation of immune cell function, including "T cell receptor signalling pathway", "T cell activation" and "cytokine signalling in the immune system" (**Figure 4.22 b**). Interestingly, one of these pathways was gene ontology (GO) pathway for "covalent chromatin modification" which included *EP300,* the gene encoding p300.

These results suggest that VDR binding in regions which do not lead to H3K4me3 or H3K27Ac changes, still target key immune system and T cell processes, perhaps by other mechanisms than the histone modifications.

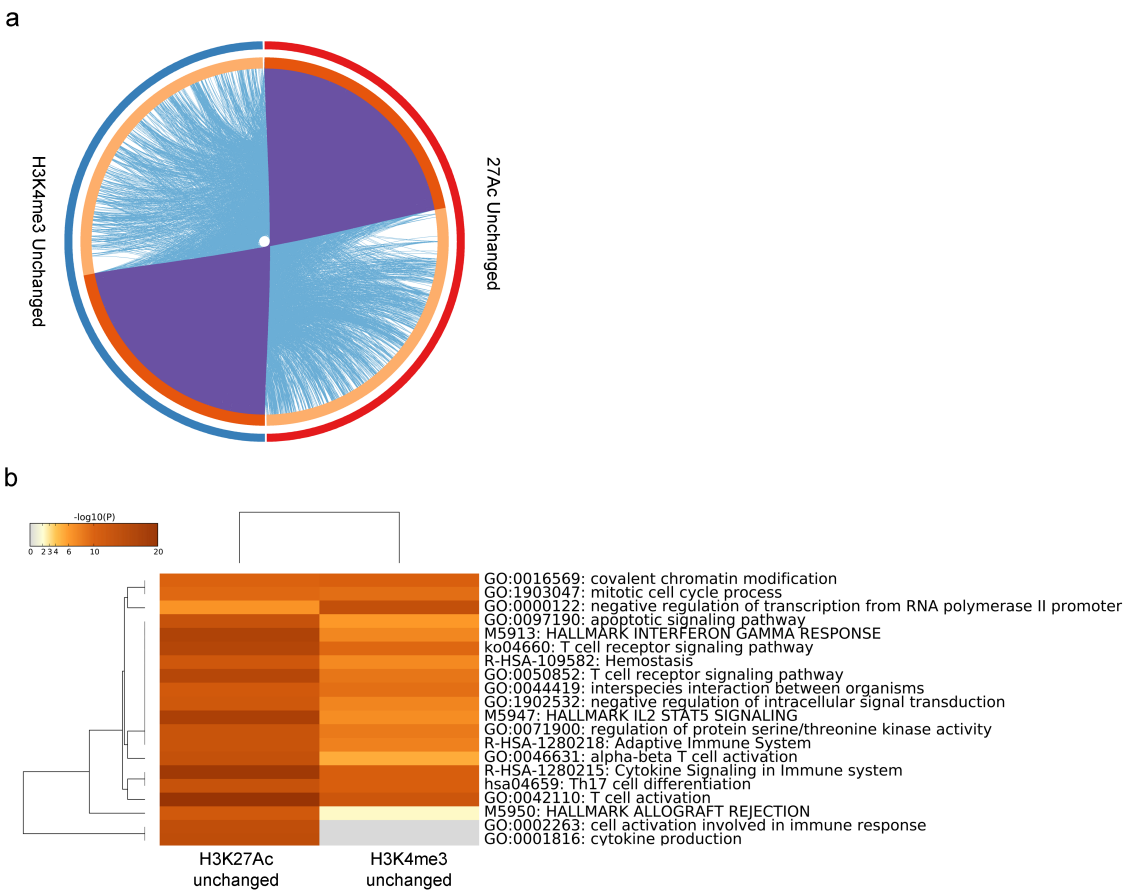


**Figure 4.22|Pathway analysis of genes with predicted VDR binding with unchanged H3K27Ac peak and H3K4me3 peaks|**

(a) Circos plot shows how genes from unchanged H3K27Ac (red) and H3K4me3 (blue) gene lists overlap. On the outside arcs represents the identity of each gene list**.** On the inside arcs represents a gene list, where each gene has a unique location in the arc. Dark orange colour represents the genes that appear in multiple lists and light orange colour represents genes that are unique to that gene list. Purple lines link the same gene that are shared by multiple gene lists. Blue lines link the different genes where they fall into the same ontology term (all terms are statistically significantly enriched). (b) Heatmap of statistically significant pathways from unchanged H3K427Ac and H3K4me3 gene lists. Significant terms are hierarchically clustered into a tree based on Kappa-statistical similarities among their gene memberships. The heatmap cells are coloured by their p-values. The term with the best p-value within each cluster was chosen as its representative term and displayed in a dendrogram.

#### 4.4.2.4.2 Pathway analysis of genes with VDR binding sites and altered H3K27Ac

We next carried out the same analysis, but with regions that showed either VitD induced or repressed H3K27Ac. Encouragingly very few (<15) VitD induced and repressed H3K27Ac peaks were concurrently assigned to the same gene (**Figure 4.23 a**). Many more genes with VDR motifs showed increased, rather than repressed, H3K27Ac signal following VitD treatment (**Figure 4.23 a**), consistent with data from section 4.4.2.3.1 in which we identified VDR as the most significantly enriched motif in H3K27Ac VitD induced peaks. Most of the top 20 significantly enriched pathways were not shared between induced and repressed gene lists, indicating differential acetylation of genes in specific pathways induced by VitD (**Figure 4.23 b**). The "IFNγ response" pathway was identified as statistically enriched in H3K27Ac VitD repressed gene list. We therefore visualised the ChIP-seq signal at each of the regions annotated to genes identified in this pathway. Dramatic decrease in signal was observed at each of the regions with VitD treatment (**Figure 4.23 d**). The "IL-6 Jak STAT3 signalling" pathway was also statistically enriched within H3K27Ac VitD induced genes and genes contributing to this pathway, including *STAT3* and *IL6,* were present as identified in pathways in section 4.4.2.3.1. Another 13 genes were also identified and H3K27Ac signal intensity at these regions also visualised. In contrast to the IFNγ response pathway, dramatic increase of signal at each of these loci was observed with VitD treatment (**Figure 4.23 d**). Interestingly *IL10* was also identified as having a significantly increased H3K27Ac mark, which we showed in section 4.4.2.3.2 as also having a VitD induced H3K4me3 induction.

The majority of pathways identified shared genes, as indicated by tight clustering and multiple links in the pathway network analysis (**Figure 4.23 c**). Interestingly the two pathways that separate from this network originate from H3K27Ac VitD repressed gene lists. Members of the IFNγ response pathway and regulation of cytokine production pathway are separated from other pathways in the network layout (**Figure 4.23 c**).

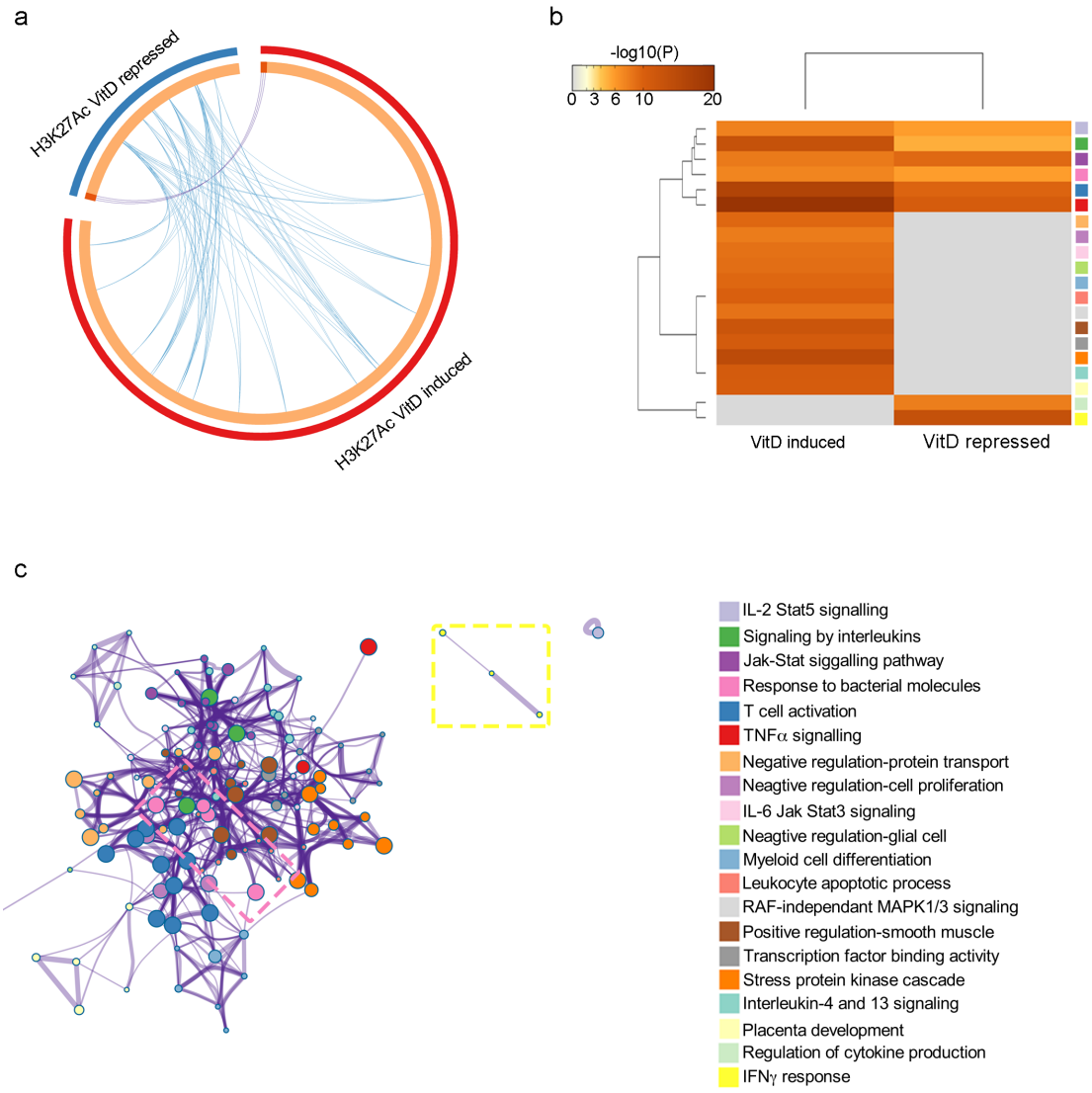
a
H3K27Ac VitD repressed
H3K27Ac VitD induced
b
-log10(P)
0 3 6 10 20
VitD induced
VitD repressed
c
IL-2 Stat5 signalling
Signaling by interleukins
Jak-Stat siggalling pathway
Response to bacterial molecules
T cell activation
TNFα signalling
Negative regulation-protein transport
Neagtive regulation-cell proliferation
IL-6 Jak Stat3 signaling
Neagtive regulation-glial cell
Myeloid cell differentiation
Leukocyte apoptotic process
RAF-independant MAPK1/3 signaling
Positive regulation-smooth muscle
Transcription factor binding activity
Stress protein kinase cascade
Interleukin-4 and 13 signaling
Placenta development
Regulation of cytokine production
IFNγ response
d
IFNγ response pathway
IL-6 Jak STAT3 signalling pathway
GPR18 GDNF PDE4B SNTB1 AKAP13 CMPK2 STAT4 OASL
CD59 IL6R NOD2 IL2RA ITGAM CSF1 STAT1 STAT3 TNFRSF1A EDN1 IL10 CD38 MAP3K7 IL6
H3K27Ac Carrier
H3K27Ac VitD
0 1
Normalised H3K27Ac signal (log2)
-1 0 1 2
Normalised H3K27Ac signal (log2)

**Figure 4.23|Pathway analysis of genes with predicted VDR binding at induced and repressed H3K27Ac peaks|**
(a) Circos plot shows how genes from H3K27Ac induced (red) and H3K27Ac repressed (blue) gene lists overlap. On the outside arcs represents the identity of each gene list**.** On the inside arcs represents a gene list, where each gene has a unique location in the arc. Dark orange colour represents the genes that appear in multiple lists and light orange colour represents genes that are unique to that gene list. Purple lines link the same gene that are shared by multiple gene lists. Blue lines link the different genes where they fall into the same ontology term (all terms are statistically significantly enriched). (b) Heatmap of statistically significant pathways from H3K27Ac induced and H3K27Ac repressed gene lists. Significant terms are hierarchically clustered into a tree based on Kappa-statistical similarities among their gene memberships. The heatmap cells are coloured by their p-values. The term with the lowes p-value within each cluster was chosen as its representative term and display in a dendrogram with colours representing the term as found in key below in (c)**.** (c) Network layout of a subset of representative terms from the full cluster. Each term is represented by a circle node, where its size is proportional to the number of input genes that fall into that term, and its colour represent its cluster identity (indicated on right in key). Terms with a similarity score > 0.3 are linked by an edge with the thickness of the edge representing the similarity score. (d) Heatmaps showing quantile normalised H3K27Ac ChIP-seq signal from carrier and VitD treated $CD4^+$ T cells of genes within pathways from (b) and (c), ordered from smallest to largest signal difference in carrier vs VitD. IFN$\gamma$ response pathway is highlighted in (c) by dashed yellow line and IL-6 Jak STAT3 pathway by pink dashed line.

#### 4.4.2.4.3 T cell activation pathway

The most significantly enriched Gene Ontology pathway in the geneset of VitD-induced H3K27 acetylation with VDR motifs, was the T cell activation pathway ($p=1.25x10^{-9}$), which represents a key pathway in our experimental context. Significant increases in H3K27Ac signal after treatment with VitD in all 43 members of this pathway were evident (**Figure 4.24 a**), including some of the genes encoding the key proteins differentially regulated in our study: *IL6, IL10* and *STAT3* (**Figure 4.24 a**). As discussed in section 1.4.1.2, one of the key immunoregulatory molecules consistently induced by VitD is CTLA-4 (Barrat et al., 2002; Jeffery et al., 2009). In our ChIP-seq, *CTLA4* was associated with an enhancer (H3K27Ac) region strongly induced by treatment with VitD and bound by VDR approximately 30kb up-stream of the *CTLA4* tss, and coinciding with an *in silico* predicted VDR(DR3) binding motif in T cells (**Figure 4.24 b**). Similarly, CD38, an activation marker induced by VitD (Handel et al., 2013) that functions as an ectoenzyme to regulate calcium signaling (Quarona et al., 2013) was also identified as having an associated VDR-bound H3K27Ac region strongly induced by treatment with VitD (**Figure 4.24 b**). This enhancer locus was present 20kb up-stream of the *CD38* tss and also coincided with an *in silico* predicted VDR(DR3) binding site and VDR ChIPseq peak in LCLs (**Figure 4.24 b**). As this molecule has only recently been shown to be induced by VitD in $CD4^+$ T cells, we verified induction of CD38 in 2 donors by flow cytometry (**Figure 4.24 c**).

In summary, we have identified two further putative enhancer sites, induced by treatment with VitD, upstream of key molecules in the T cell activation pathway.

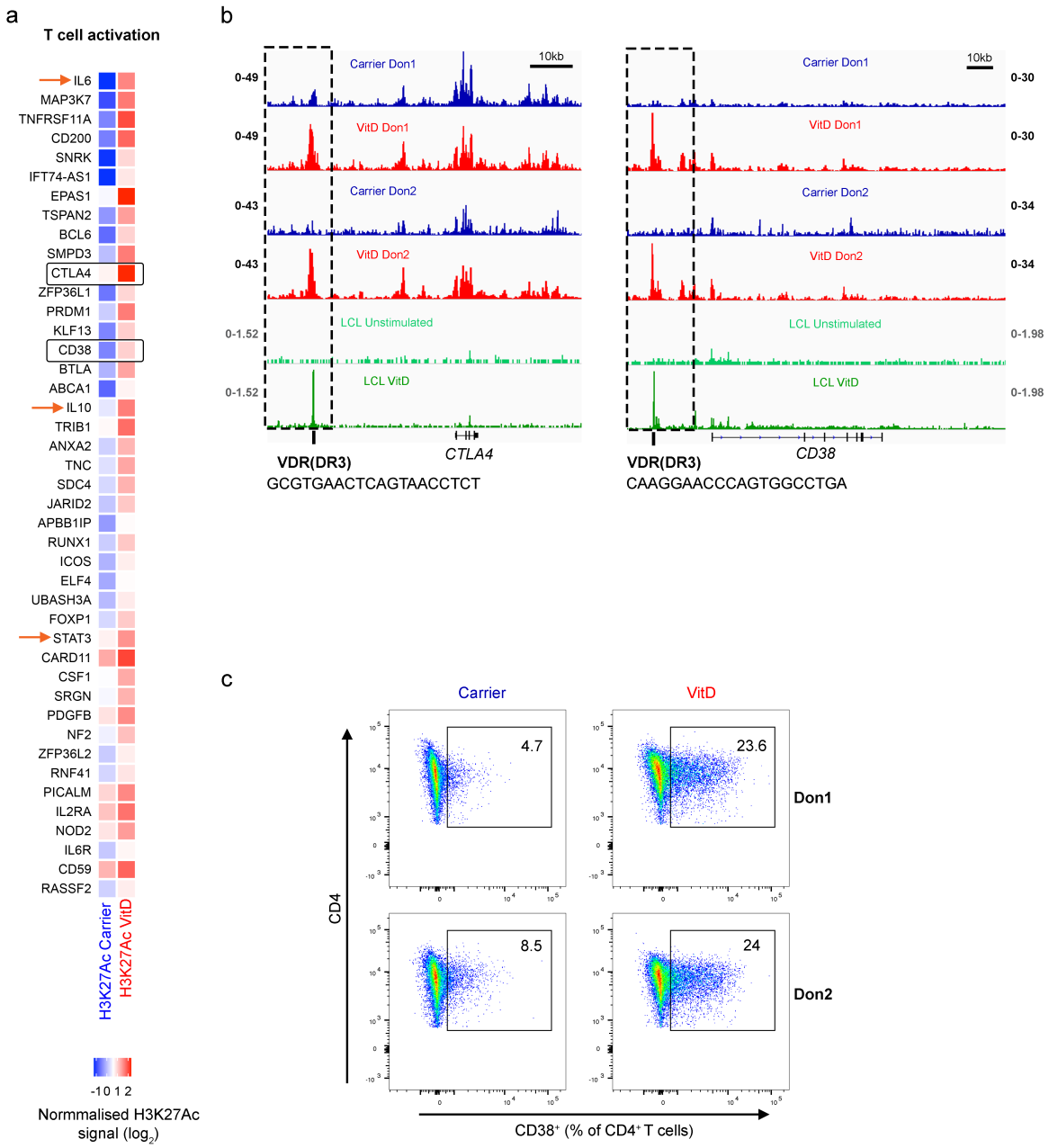


**Figure 4.24|Altered enhancer landscapes in genes associated with T cell activation genes|**

(a) Heatmap showing quantile normalised H3K27Ac ChIP-seq signal from carrier and VitD treated $CD4^+$ T cells of genes within the T cell activation pathway GO term, ordered from smallest to largest signal difference in carrier vs VitD. Indicated by orange arrows are *IL6*, *IL10* and *STAT3* and genes encoding CTLA-4 and CD38 in black boxes. (b) H3K27Ac tracks from two donors (Donor 1, Don1; Donor 2, Don2) in VitD treated and carrier treated $CD4^+$ T cells, with VDR tracks from unstimulated and VitD treated lymphoblastoid cell line (LCL) in green. Tracks heights are shown with RPKM normalisation in black and RPGC normalisation in grey. Highlighted in box are locations of *CTLA4* and *CD38* putative enhancers. Beneath both sets of tracks are shown VDR(DR3) binding motifs from *in silico* prediction. (c) Flow cytometry plots of CD38 expression from 2 donors.

#### 4.4.2.4.4 Pathway analysis of genes with VDR binding sites and altered H3K4me3

For H3K4me3 similar numbers of genes were identified from VitD induced and repressed gene lists (**Figure 4.25 a**). Again, the majority of the top 20 significantly enriched pathways were not shared between induced and repressed gene lists, indicating differential methylation of genes in specific pathways induced by VitD (**Figure 4.25 b**). Most of the significantly enriched pathways originate from the repressed H3K4me3 gene list in response to VitD. The "IFNγ response" pathway was identified as statistically enriched in H3K4me3 VitD repressed gene list (**Figure 4.25 b**), as with the H3K27Ac VitD repressed gene list. When signal at regions annotated to genes was visualised as in section 4.4.2.4.2, dramatic reduction at each of the regions was observed with VitD treatment (**Figure 4.25 d**). This shows common pathways being repressed by different epigenetic marks. However, only one member of the "IFNγ response" H3K4me3 VitD repressed pathway (**Figure 4.25 d**) is the same as from the H3K27Ac VitD repressed gene list (**Figure 4.23 d**). Thus, although common pathways are targeted, different members of the pathway are affected. Pathways specific for H3K4me3 VitD modifications cluster very tightly with many links (**Figure 4.25 c**). This suggests that genes targeted by VitD induced H3K4me3 modifications are within similar inter-connected pathways, and hence histone modifications are targeted.

In summary, pathway analysis of histone modifications, specifically containing VDR binding sites, identified other members of the IL-6 signalling cascade, supporting the findings mechanistically linking VitD induced histone modifications with IL-6 signalling in the induction of IL-10.

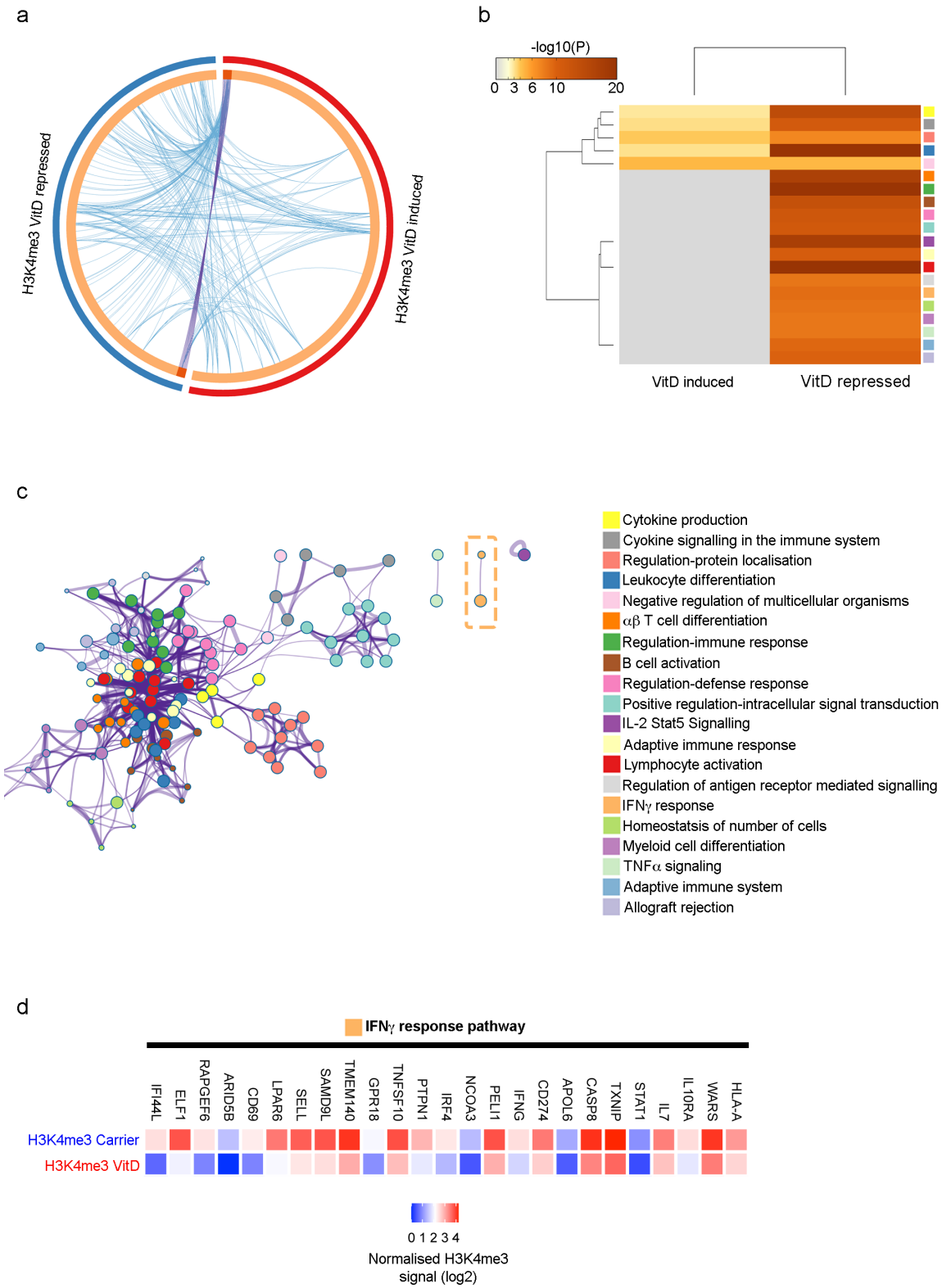
a
H3K4me3 VitD repressed
H3K4me3 VitD induced
b
-log10(P)
0 3 6 10 20
VitD induced
VitD repressed
c
Cytokine production
Cyokine signalling in the immune system
Regulation-protein localisation
Leukocyte differentiation
Negative regulation of multicellular organisms
αβ T cell differentiation
Regulation-immune response
B cell activation
Regulation-defense response
Positive regulation-intracellular signal transduction
IL-2 Stat5 Signalling
Adaptive immune response
Lymphocyte activation
Regulation of antigen receptor mediated signalling
IFNγ response
Homeostatsis of number of cells
Myeloid cell differentiation
TNFα signaling
Adaptive immune system
Allograft rejection
d
IFNγ response pathway
IFI44L
ELF1
RAPGEF6
ARID5B
CD69
LPAR6
SELL
SAMD9L
TMEM140
GPR18
TNFSF10
PTPN1
IRF4
NCOA3
PELI1
IFNG
CD274
APOL6
CASP8
TXNIP
STAT1
IL7
IL10RA
WARS
HLA-A
H3K4me3 Carrier
H3K4me3 VitD
0 1 2 3 4
Normalised H3K4me3
signal (log2)

**Figure 4.25|Pathway analysis of genes with predicted VDR binding at induced and repressed H3K27Ac peaks|**
(a) Circos plot shows how genes from H3K4me3 induced (red) and H3K4me3 repressed (blue) gene lists overlap. On the outside arc represents the identity of each gene list**.** On the inside arcs represents a gene list, where each gene has a unique location in the arc. Dark orange colour represents the genes that appear in multiple lists and light orange colour represents genes that are unique to that gene list. Purple lines link the same gene that are shared by multiple gene lists. Blue lines link the different genes where they fall into the same ontology term (all terms are statistically significantly enriched). (b) Heatmap of statistically significant pathways from H3K4me3 induced and H3K4me3 repressed gene lists. Significant terms are hierarchically clustered into a tree based on Kappa-statistical similarities among their gene memberships. The heatmap cells are coloured by their p-values. The term with the lowest p-value within each cluster was chosen as its representative term and display in a dendrogram with colours representing the term as found in key below in (d)**.** (c) Network layout of a subset of representative terms from the full cluster. Each term is represented by a circle node, where its size is proportional to the number of input genes that fall into that term, and its colour represent its cluster identity (indicated on right in key). Terms with a similarity score > 0.3 are linked by an edge with the thickness of the edge representing the similarity score. (d) Heatmaps showing quantile normalised H3K4me3 ChIP-seq signal from carrier and VitD treated $CD4^+$ T cells of selected genes within pathways from (b) and (c), ordered from smallest to largest signal difference in carrier vs VitD. IFNγ response pathway is highlighted in (c) by dashed orange line.

## 4.5 Discussion

VitD has both direct and indirect effects on $CD4^+$ T cells (see intro 5.5.1 immunoregulatory actions) with the majority of studies reporting that VitD is able to directly influence cytokine production (Cantorna et al., 2015). Despite the well characterised effects of VitD as an inducer of the anti-inflammatory cytokine IL-10 and inhibitor of pro-inflammatory cytokines, especially IL-17 and IFNγ, the mechanisms underlying these effects are not well defined. In this chapter, we uncover a novel mechanism by which VitD induces IL-10 production, through a signalling loop involving IL-6 and downstream pSTAT3 signalling. In addition, we suggest that this is driven at the epigenetic level by liganded VDR induced histone modifications.

VitD has direct effects on $CD4^+$ T cells through the expression of VDR, which is only present following TCR activation (Provvedini et al., 1983). In fact, our results of VDR time-course are mirrored in an elegant study by Essen *et al.* in which VDR was observed to be expressed only following activation through TCR, but not in un-activated T cells, and to increase daily over the 3 day experiment (Essen et al., 2010). In addition, they found nuclear localisation of VDR only after 2 days' polyclonal activation. However, Essen *et al.* study dynamics of VDR expression and localisation were not assessed after addition of VitD and key experiments were carried out in bulk T cells without discrimination of $CD4^+$ and $CD8^+$. We have performed a more comprehensive spatio-temporal analysis of VDR expression in $CD4^+$ T cells, confirming increased expression and nuclear translocation of VDR following TCR activation in the presence of 1,25 VitD. Supporting our findings Kongsbak *et al.* have reported the redistribution of VDR to the nucleus in $CD4^+$ T cells after treatment with both 25 and 1,25 VitD by Western blot (Kongsbak et al., 2014).

We show some evidence, using surrogate markers, to suggest we are not generating classical Tregs or Tr1 Tregs, however, without directly assessing regulatory function, we cannot rule out the possibility that these cells are a type of induced Treg. This is especially true as most definitions of induced Tregs include reduced IFNγ and IL-17, enhanced FoxP3 expression and increased expression of CD25. Nonetheless, these cells will undoubtedly supress effector T cell responses in a suppression assay, probably

due to decreased pro-inflammatory cytokines and IL-10 expression. In addition, although we did not test expression of CTLA-4, it has been shown to be induced by VitD in similar conditions to ours and to contribute to T cell regulation in cultures with monocytes, where it maintains its B7 trans-endocytosis properties (Jeffery et al., 2015; 2009). In fact Jeffery *et al.* show that IL-2 is the main driver of FoxP3 expression in the context of VitD treated $CD4^+$ T cells (Jeffery et al., 2009). This is important as we show that FoxP3 is not maintained following resting of VitD treated cells, but this would have been in a milieu of low IL-2, which may be needed to maintain FoxP3. However, the fact that the effect is mainly in memory cells suggests that, instead of generating an induced regulatory cell, we are seeing the effect of VitD on the self-regulation of the T cell life cycle.

In line with our findings of a dose response to VitD in both IL-10 and IL-6, Urry *et al.* showed that lower concentrations of 1,25 VitD induced higher $IL\text{-}10^+$ $CD4^+$ T cells with higher concentrations of 1,25 VitD preferentially inducing FoxP3 expression, with little co-expression of both IL-10 and FoxP3 (Urry et al., 2012). In fact, they show that IL-10 in this context can impair FoxP3 expression induced by 1,25 VitD. This data suggest that VitD can support two phenotypically distinct subpopulations of $CD4^+$ T cell; at lower concentrations $CD4^+FoxP3^-IL10^+$ and at higher concentrations $CD4^+FoxP3^+IL10^-$ cells, both populations being suppressive (although their suppressive mechanisms were IL-10-dependent and IL-10-independent, respectively). This data, with our data, suggest a model where as an immune response develops, 1,25 VitD concentrations increase and signals in $CD4^+$ T cells, and innate and adaptive immune responses could be attenuated by IL-10-dependent and IL-10-independent mechanisms, respectively (Hayes et al., 2015). This is in line with gradual increase in VDR expression following activation shown in this thesis and suggests an auto-regulatory switch as an immune response develops. This model is speculative and needs to be studied in more detail at different time points and with different sub-populations of $CD4^+$ T cells.

We initially observed IL-6 production from a highly pure, sorted population of $CD4^+$ T cells. IL-6 is not classically thought to be a cytokine produced by T cells, with its production usually linked to stromal cells and cells of the innate immune system (Tanaka et al., 2014). This led to some speculation of contamination by monocytes in our

cultures. However, a sorting purity of over 99% along with the observation that IL-6 production was not induced in the sorted $CD4^+$ naïve T cell compartment removed this doubt. Additionally, in line with our results, previous findings have suggested IL-6 production from $CD4^+$ T cells (Zubiaga et al., 1990). However, isolation methods in this early study could not rule out contamination by innate immune cells.

IL-6 is a pleiotropic cytokine, with almost all stromal and all cells of the immune system being capable of producing it (Hunter and Jones, 2015). IL-6 is classically known for its importance in lineage commitment of Th17 cells. Indeed, IL-6 signalling in the presence of TGF-$\beta$ promotes differentiation of Th17 cells, with expression of their key transcription factor, ROR$\gamma$t, and expression of the pro-inflammatory cytokine IL-17 (Ivanov et al., 2006), which is implicated in the pathogenesis of many autoimmune diseases including arthritis (Jones et al., 2013). However, studies have showed that IL-6 is able to polarise Th2 cells and the inhibit Th1 responses (Rincón et al., 1997). In cells other than Th17 cells, it seems that IL-6 does not directly influence lineage commitment, but rather the inflammatory context in which IL-6 signalling is induced is important (Hunter and Jones, 2015). Our finding that IL-6 leads to IL-10 production, only in the presence of VitD, leads to the question of which context this response is important *in vivo*.

Two studies have reported IL-6 promoting the production of IL-10 in murine T cells. The first of these showed, in the context of experimental autoimmune encephalomyelitis (EAE, the mouse model for multiple sclerosis (MS)), treatment of myelin reactive $CD4^+$ T cells with TGF$\beta$ and IL-6 unexpectedly abrogated their pathogenic function (McGeachy et al., 2007). In this study, they linked the anti-inflammatory effects of IL-6 to concurrent IL-10 production in Th17 cells. The limitation of this paper is that the pathogenic role of Th17 cells in EAE is dependent on IFN$\gamma$ production and so additional factors other than the IL-10 are also involved. The second paper showed that IL-6 and IL-27, independently of each other, induce the production of IL-10 from $CD4^+$ T cells in a STAT3 dependent manner (Stumhofer et al., 2007). However, both studies were carried out in murine $CD4^+$ T cells, which in our system did not lead to IL-6 mediated IL-10 production, suggesting that either different mechanisms to induce IL-10 exist in mice and in humans, or that the context of the IL-6 signal is important, which differs in

circulating blood $CD4^+$ T cells from humans and mice. Another study reported 1,25 VitD treatment of $CD4^+$ T cells from healthy controls and Crohn's disease patients led to an increased IL-6 and IL-10 production (Bartels et al., 2007), speculating that IL-6 may lead to the increased IL-4 also observed, thus skewing cells to a Th2 like lineage. They point to evidence of IL-6 infusion leading to plasma IL-10 production in humans, where the authors conclude that physiological concentrations of IL-6 induce an anti-inflammatory rather than pro-inflammatory response in humans (Steensberg et al., 2003). These studies provide some evidence of the ability of IL-6 to induce anti-inflammatory IL-10 production from $CD4^+$ T cells, with the studies suggesting the relevance *in vivo* being with the gut environment and the brain. Our findings suggest the presence of VitD could be another, distinct, mechanism by which IL-6 is able to drive IL-10 production. Additionally, we propose the source of IL-6 can be $CD4^+$ T cells themselves and that this can be self-contained. Several studies have shown that $CD4^+$ T cells have the ability, and express the enzymes necessary, to convert 25 VitD to 1,25 VitD (but not $VitD_3$ to 25 VitD) (Correale et al., 2009; Kongsbak and Essen, 2014; Kongsbak et al., 2014; Sigmundsdottir et al., 2007), supporting our finding that addition of 25 VitD nearly exactly mirrors the cytokine response seen from T cells, but at physiological concentrations. As 25 VitD also shows some affinity for the VDR, we cannot rule out direct 25 VitD VDR interactions. However, 25 VitD has several hundred times lower affinity for VDR (Ritter et al., 2006) than 1,25 VitD and thus physiological concentrations at which we added 25 VitD are unlikely to have substantial ability to bind VDR. Together, these observations build a convincing argument for the context specific, anti-inflammatory role of IL-6 in $CD4^+$ T cells, through its induction of IL-10. Importantly we show that VitD is indispensable in this signalling cascade.

One major limitation of this part of the thesis was the inability to stain for IL-10 and IL-6 within our $CD4^+$ T cells. This would have given us the ability to gain a deeper insight into which sub-populations are responsible for producing IL-6, and which population respond to this IL-6 through IL-10 production. IL-6 is classically a cytokine secreted by the innate immune system and thus most protocols for intracellular staining are not optimised for $CD4^+$ T cells, which hampered our ability to use this as an experimental readout. IL-10 was also difficult for us to measure and in the future, we

envisage using an IL-10 capture assay, as this assay is more sensitive and would allow us to subsequently stain for IL-6 in these cells. With these results, we could truly verify if the signalling loop was working in an autocrine/paracrine fashion, as well as which sub-populations are involved. Both of these questions are key to further understand the context in which the mechanism might be important.

The organ in the body subjected to the highest levels of both 25 and 1,25 VitD is the skin. Not only is this the site of $VitD_3$ photo-production (see section 1.2) but keratinocytes possess both enzymes needed to convert $VitD_3$ to 1,25 VitD (Vantieghem et al., 2006). Additionally, the skin contains an abundance of memory $CD4^+$ T cells, which play a critical role in the pathogenesis of skin diseases such as psoriasis (Cai et al., 2012). Importantly several lines of evidence suggest that IL-6 and IL-10 are beneficial in the context of skin immunity. Overexpression of IL-6 specifically in the skin of mice did not lead to enhanced epidermal proliferation as expected, but resulted in a thicker protective skin layer, with an otherwise normal program of differentiation. This led the authors to conclude that the role of IL-6 in the skin may be to provide increasing protection from injury stimuli or infection. On the other hand, IL-6 deficient mice display impaired cutaneous wound healing (Gallucci et al., 2000; Lin et al., 2003). Topical VitD and UVB therapy are well established treatments for psoriasis with induction of IL-10 suggested as a mechanism (Asadullah et al., 1998). Finally, subcutaneous injection of IL-10 in patients with psoriasis has been shown to be safe and clinically effective in treatment of psoriasis (Asadullah et al., 1999).

Although UVB is known to induce VitD and VitD is known to lead to production of IL-10 in the skin, no mechanism linking the two have been proven. The results in this chapter suggest a link between the protective effects of cutaneous IL-6 and the success of VitD and UVB therapy in treatment of psoriasis. In accordance with these observations, despite the success of the IL-6R blocking antibody Toc to treat inflammatory arthritis (Jones et al., 2011), case reports have emerged of onset of psoriasis following clinical therapy with anti-IL-6R (Toc) (Laurent et al., 2010; Wendling et al., 2012). Thus, the results of the novel signalling cascade provided in this chapter reinforce a link between anti-inflammatory actions of VitD, the production of IL-6 and IL-10, both of which have beneficial effects in the context of skin immunity, and the

beneficial effects of UVB and VitD in treatment of psoriasis. The model beginning to emerge could work at multiple levels. Firstly, when T cells become activated in the skin, and thus in the presence of an abundance of 25 VitD, they can convert this to 1,25 VitD. Individuals with skin conditions such as psoriasis may lack VitD, and thus UVB therapy and topical VitD treatment can bypass this deficiency. In addition, individuals with polymorphisms in the VDR locus (see section 1.3.2 and **Figure 1.4 a** for VDR polymorphisms) show susceptibility to psoriasis (Lee et al., 2012). Our results suggest that expression of the VDR is then gradually increased leading to IL-6 production, which itself has a protective role in the context of skin tissue repair, and subsequently IL-10 production, which along with inhibition of IFN$\gamma$ and IL-17 lead to a strong anti-inflammatory $CD4^+$ T cell signal. Thus, when this signalling process is interfered with by treatment with Toc, the skin is one of the major organs effected. Importantly, the VDR is only induced after activation of T cells and thus may give recruited T cells time to respond to stimuli (infection or damage) before being switched to a pro-wound healing and anti-inflammatory status. Interestingly, we have seen unpublished RNAseq data, from $CD4^+$ T cells isolated from the skin vs peripheral blood $CD4^+$ T cells, showing that skin resident T cells express the VDR without the need for activation. This suggests that tissue resident $CD4^+$ T cells would be able to respond more rapidly to the presence of 1,25 VitD, perhaps in order to maintain tolerance to microbiota. Th1 (O'Garra and Vieira, 2007) and THh17 (McGeachy et al., 2007) lineages have been shown to produce IL-10 at later stages in their life cycle to avoid out of control immune responses. Indeed mice lacking IL-10 clear infection with Toxoplasma gondi (Nishikawa et al., 2001) and Trypanosoma cruzi (Hunter et al., 1997) more rapidly but later die of severe tissue damage due to uncontrolled Th1 responses. As a result, the idea of T cell intrinsic IL-10 production as an auto-regulatory loop has recently gained momentum (Cope et al., 2011), and we suggest VitD may be instrumental in this pathway in certain contexts.

In this chapter, we next showed that induction of IL-10 by IL-6 is STAT3 dependent. Although STAT3 phosphorylation is directly downstream of IL-6R engagement, phosphorylation of STAT3 is usually rapid and transient (minutes to hours) (Braun et al., 2013) and not expected to be sustained for days as we have shown in this chapter. More recent evidence, on the other hand, suggests IL-6 signalling in naïve T cells

is reduced to 50% after 4 hours, but in memory $CD4^+$ T cells it is maintained (Jones et al., 2016), supporting our findings. We have also shown that the sustained pSTAT3 signal is dependent on total STAT3 expression which is induced by VitD. This may explain the sustained nature of the observed pSTAT3 signal. In line with discussion of the described pathway being important in skin immunology, a GWAS study identified psoriasis susceptibility loci in the STAT3 locus (Tsoi et al., 2012).

Multiple lines of evidence suggest that the mechanism by which VitD imprints cell specific phenotypes is through altering epigenetic histone modifications (see section 1.3.3.2). In support of this, available VDR ChIP-seq data shows liganded VDR recruitment to sites regulated by histone modifications, specifically H3K27Ac and H3K4me3 (Handel et al., 2013; Ramagopalan et al., 2010). However, no studies have directly probed histone modification alterations at multiple loci, on a large scale, following VitD treatment, in any cell type. The finding in this chapter that the most enriched motif in regions of increased H3K27 acetylation in VitD treated cells, is a strong indication that this is the main mechanism by which liganded VDR controls cell specific gene regulation. Indeed, VDR ChIP-seq peaks from LCLs were preferentially located at sites of active enhancers. Whilst the VDR motif was not enriched at sites of H3K4 tri methylation, pathway analysis of genes associated with VDR binding and tri methylation clearly pointed to targeted histone modifications within specific pathways such as the IFN$\gamma$ response pathway. In fact, the pathway analysis of both H3K27Ac and H3K4me3 alterations targeted by VDR binding both yielded networks with not many separated nodes. This suggests that histone modifications targeted by liganded VDR are mechanistically linked in $CD4^+$ T cells.

We show clear evidence in this chapter that the VitD induced signaling pathway identified, is largely regulated by direct liganded VDR binding, leading to histone modifications. VDR ChIP-seq unfortunately did not work, and quality control suggested that this was at the stage of immunoprecipitation with VDR antibody. As the antibody clone (C-20) used for previous VDR ChIP-seq experiments (Handel et al., 2013; Ramagopalan et al., 2010) had been discontinued, we used the manufacturers recommended replacement (D-6) which was available in highly concentrated form for ChIP experiments. We will attempt to repeat the VDR ChIP-seq experiments in the future (see section 4.5.2). Using a parallel approach, we were able to use both motif

identification and published VDR ChIP-seq data to provide strong validation of VDR binding. We identified putative enhancers, marked by strong H3K27 acetylation, of both *IL6* and *STAT3* at which loci VDR binding and predicted VDR binding motifs were clearly present in 1,25 VitD stimulated, but not untreated, cells. It is correct to admit that binding of VDR at the putative *STAT3* enhancer was less clear than at the *IL6* enhancer locus, *in silico* predicted VDR binding motif was apparent. It is possible that time-course and the cell specific context would be important to see this effect more clearly.

As we observed clear H3K27 acetylation and it is known that VDR recruits HATs, such as p300 (Haussler et al., 2011; 2013), we also observed HAT P300 recruitment form published ChIP-seq data close to the loci of increased acetylation. Interestingly one of the pathways shown to be targeted by VDR binding in both H3K27Ac and H3K4me3 unchanged regions was covalent chromatin modifications, and one of the genes annotated to this pathway was *EP300,* the gene encoding p300. This suggest that VDR regulates the histone acetyltransferase that it recruits upon DNA binding, but not through altering levels of histone modifications.

In the context of basal occupancy (non liganded VDR occupancy), VDR is most enriched at promoter regions (Ramagopalan et al., 2010). For IL-10 we found increased H3K4tri methylation closer to the *tss* of the *IL10* gene and VDR binding was evident in both untreated and VitD treated cells. VDR binding at this promoter region may not require VitD but increased methylation here requires VitD. This could be due to differential recruitment of histone modifying enzymes in the presence of VitD ligand compared to un-liganded VDR. H3K27Ac was also increased at this same location but as H3K4me3 is a mark of enhancer activity, this is probably not an enhancer site. Therefore, opening of the locus by increased H3K4 tri-methylation and H3K27Ac would enable pSTAT3 binding at this region which would be epigenetically inaccessible in the absence of VitD. We suggest in this chapter that VDR, unlike a classical TF, achieves its immuneregulatory function through epigenetic modifications, opening up specific loci for other TFs to drive transcription.

A summary diagram of our proposed mechanism of IL-10 production through histone modifications is presented in **Figure 4.26**. It is important to note that this is a working a model and many of the aspects remain to be confirmed experimentally,

however this thesis has made important observations that suggest the key aspects of the mechanism presented. In a context devoid of 1,25 VitD, or low levels of available 25 VitD to convert to 1,25 VitD, chromatin at both enhancers upstream of *STAT3* and *IL6*, as well as promoter region of *IL10,* are tightly packed around nucleosomes and hence inaccessible to core transcriptional machinery and co-activators (**Figure 4.26 a and b**). In addition, this closed chromatin state leads to masking of TF binding sites (**Figure 4.26 b**). We show evidence suggesting VDR is bound at the *IL10* promoter even in the absence of 1,25 VitD, but in the un-liganded state does not alter chromatin structure (**Figure 4.26 b**). We present data to show that 25 VitD can be converted to 1,25 VitD by $CD4^+$ T cells which then becomes available to bind to the VDR which translocates to the nucleus (**Figure 4.26 a**). Here it binds to VDR(DR3) motifs at *IL6* and *STAT3* enhancer sites, leading to recruitment of HAT enzymes, as well as both HAT and histone methyltransferase (HMT) enzymes at the promoter region of *IL10* (**Figure 4.26 c**). This leads to H3K27 acetylation and H3K4 tri-methylation, and ultimately accessible chromatin state (**Figure 4.26 c**). Recruitment of co-activator complex and core transcriptional machinery (including RNA polymerase II (RNA pol II)) would then lead to expression of IL-6 and STAT3 (**Figure 4.26 d**). IL-6 binding to IL-6R then leads to phosphorylation of STAT3 and subsequent pSTAT3 binding at promoter region of *IL10.* This leads to recruitment of co-activator complex and core transcriptional machinery at active *IL10* promoter region, marked by increased H3K37Ac and H3K4me3. This finally leads to expression of IL-10 protein (**Figure 4.26 c**).

It seems that there are three possible mechanism by which VDR can induce transcriptional changes, at the epigenetic level, in our study. The predominant mechanism is by binding and activating enhancer sites with no change or H3K4me3, as is the case for CTLA-4. In this case CTLA-4 already displayed active promoter state with high H3k4me3 in the presence of carrier (data not shown). The same can occur but with increase H3K4me3 at the tss not induced by VDR, as is the case for IL-6. Finally, un-liganded VDR can be bound near tss of genes and upon liganding, VDR can lead to H3K27Ac and H3K4me3 near tss.

Although using histone modifications as markers of active genome enhancers as done here (using H3K27Ac as a mark of active enhancers and promoters, and H3K4me3

as a mark of active promoters) is widely used, it is not without its limitations. For example, 41% of mesodermal enhancers in *D. melanogaster* embryos were not predicted by H3K27 acetylation (Bonn et al., 2012). In addition, there is no evidence of a mechanistic link between chromatin modifications and active enhancers, with little evidence for H3K27Ac being sufficient or necessary for transcription (Pengelly et al., 2013). As such this is one of the major limitations to this body of work. Further verification of enhancer activity could be carried out at these putative enhancer sites using plasmid based systems. In these systems putative enhancer regions are typically placed up or downstream of reporter genes and activity detected by expression of reporter gene (techniques nicely reviewed in (Shlyueva et al., 2014)). However, the need for this is somewhat negated as we have already assessed protein expression of the key molecules involved.

In summary, this chapter has presented mechanistic evidence of a VitD dependent signalling loop leading to production of IL-10 (through an IL-6 and STAT3 dependent mechanism) mediated through VitD driven histone modifications. This mechanism is most likely to occur in the context of cutaneous immunology, though this still needs further investigation.

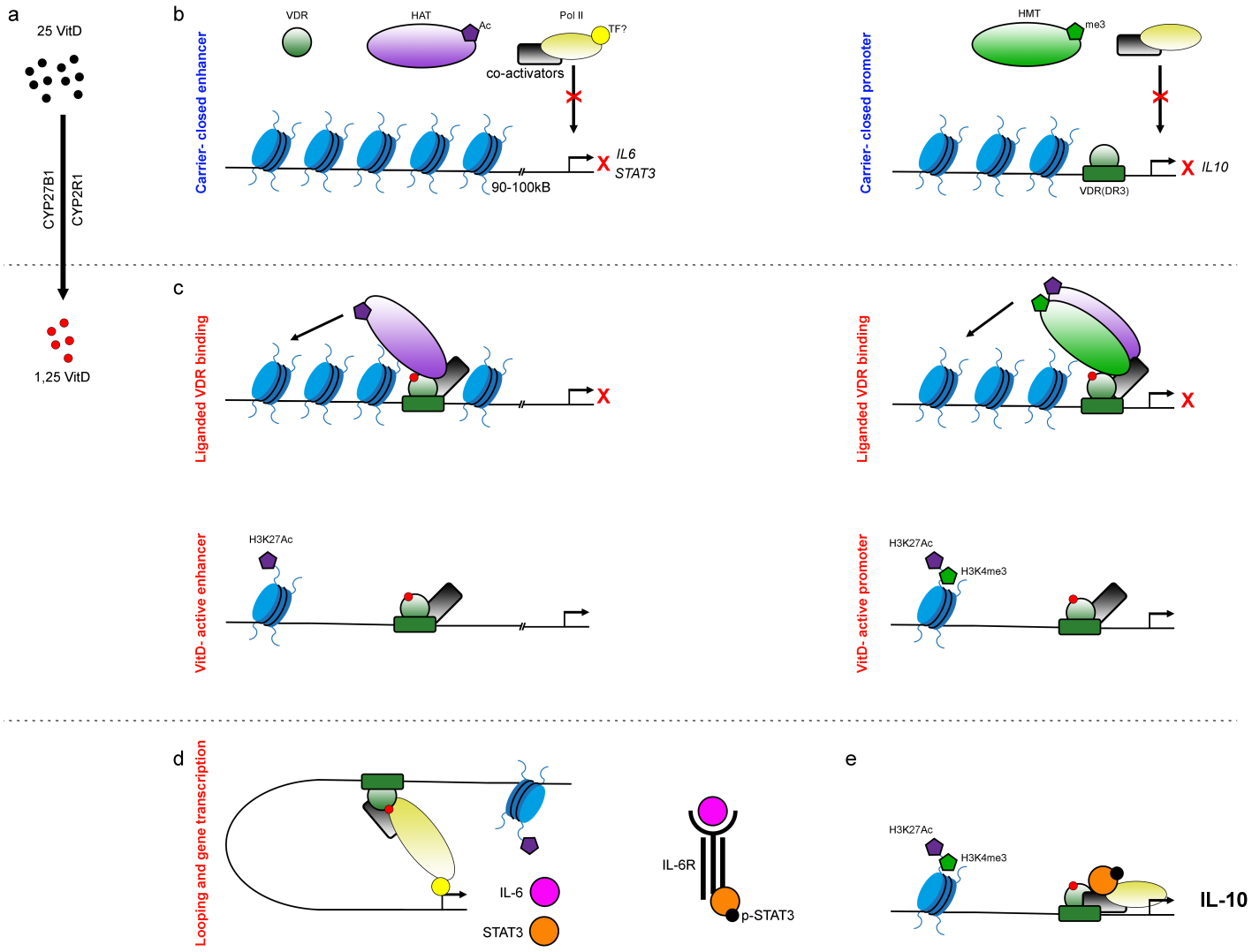
a
25 VitD
CYP27B1
CYP2R1
1,25 VitD
b
Carrier- closed enhancer
VDR
HAT
Ac
Pol II
TF?
co-activators
IL6
STAT3
90-100kB
Carrier- closed promoter
HMT
me3
IL10
VDR(DR3)
c
Liganded VDR binding
VitD- active enhancer
H3K27Ac
Liganded VDR binding
VitD- active promoter
H3K27Ac
H3K4me3
d
Looping and gene transcription
IL-6
STAT3
IL-6R
p-STAT3
e
H3K27Ac
H3K4me3
IL-10

**Figure 4.26|Proposed mechanism of IL-10 production in polyclonally activated $CD4^+$ T cells|**
(a) 25 to 1,25 VitD conversion probably occurs in $CD4^+$ T cells through action of CYP27B1 or CYP2R1. (b) In the absence of 1,25 VitD chromatin is in a closed, tightly condensed, state at *IL6* and *STAT3* enhancers. Similarly, at promoter of *IL10,* chromatin is in closed state. However un-liganded VDR is already bound at the *IL10* promoter. This closed state means access to promoters of core transcriptional machinery (including classical TF, and co-activators, which recruit RNA pol II) to tss (indicated by black arrow on genome) is reduced. Additionally, little IL-6 is produced in this context and thus the IL-6R is un-engaged. (c) Upon liganding of the VDR by 1,25 VitD, liganded VDR binds to VDR(DR3) motifs and recruits HAT enzymes which lead to observed increase in H3K27Ac at enhancer sites. This leads to de-construction of nucleosomes and creation of active enhancers upstream of the *STAT3* and *IL6* locus at promoter sites, liganding of VDR leads to recruitment of bot HAT and HMT enzymes which leads to H3K27Ac and H3K4me3 near promoter sites. This also leads to de-construction of nucleosomes and creation of active promoter at *IL10* locus. (d) Active enhancer induced by VDR binding lead to recruitment of unknown TF and core transcriptional machinery ultimately leading to looping of chromatin and STAT3 and IL-6 transcription and protein expression. IL-6 binding to IL-6R then leads to the phosphorylation of STAT3. As there is an accessible chromatin state upstream of the *IL10* tss, p-STAT3 can bind and lead to recruitment of core transcriptional machinery and ultimately IL-10 protein production. VDR = vitamin D receptor, HAT = Histone acetyl transferase, Ac = acetyl group, Pol II = RNA polymerase II, TF? = Unknown transcription factor, IL6-R = IL-6 receptor, HMT = histone methyl transferase, me3 = trimethyl group.

### 4.5.1 Conclusion

The data in this chapter could have implications for both our basic understanding of VitD mechanisms of $CD4^+$ T cell immunology and future therapy of diseases, such as psoriasis and other skin conditions.

Understanding how VitD mechanistically carries out its effects on immune cells is lacking. Thus, this chapter adds significant insight into the direct effect of VitD on $CD4^+$ T cells. The clarification that VitD directly effects the epigenetic landscape of T cells verifies previous data suggesting this is the case. Our pathway could also suggest a more general mechanism by which immune cells limit overt pro-inflammatory reactions. In the presence of substantial inflammation, T cells, as well as other immune cells, could utilise 25 VitD from circulation or in tissue as a signalling mechanism to prevent over activation of other $CD4^+$ T cells. This mechanism may then be dysfunctional in the context of VitD deficiency, implicating many more auto-immune diseases. Previous VDR ChIP-seq data (Handel et al., 2013; Ramagopalan et al., 2010) have consistently found regions bound by VDR interacting with disease associated genes. As speculation still exists regarding the involvement of VitD in diseases, studies showing direct evidence of VitD mechanistically linked to immune cell function will help clarify this involvement.

The suggestion stemming from this data of involvement of this signalling loop in cutaneous immunology are potentially far reaching. The mechanism underlying the potency of UVB therapy in psoriasis is still not known, and though it likely involves non VitD related pathways, we here propose a new mechanism linking the two. Obvious direct implications suggest care in using anti IL-6R medication such as Toc as this may lead to cutaneous side effects. Additionally, IL-6 has been shown to have both pro and anti-inflammatory effects and we here suggest a context specific anti-inflammatory role. Thus, therapeutics for inflammatory cutaneous conditions could target specific parts of our identified pathway whilst, somewhat counterintuitively, taking care not to inhibit IL-6 or STAT3 signalling.

### 4.5.2 Future directions

There remain two major outstanding questions in relation to the work in this chapter. The first question is whether the histone modifications observed lead to actual transcriptional alterations. We have assessed the final protein expression of the key molecules in our signalling pathway, this will need to be clarified on a global scale. Otherwise other pathway level changes identified by histone ChIP-seq remain speculative. We have already begun RNA-seq experiments to assess the transcriptional changes due to VitD treatment and to see whether these align with histone modifications observed. Unfortunately, preliminary RNA-seq experiments showed substantial donor variability in expression of transcripts at both baseline and after VitD treatment. We are therefore focusing on adding extra donors to the dataset, or targeting the transcripts identified to a pre-validated panel, which would also have the advantage of avoiding technical issues that can arise from RNA-seq library preparation, including PCR bias. On this question, our data would be substantiated if we could obtain reliable VDR ChIP-seq data to show whether liganded VDR is required for the observations and compare it to basal VDR occupancy. We are considering repeating the VDR ChIP-seq with a validated antibody or using alternative strategies, including CUT&RUN (Skene and Henikoff, 2017).

The second, and more pertinent, outstanding question is the *in vivo* context of our observation. In this discussion we have speculated, based on published data, that this VitD induced signalling loop ultimately leading to IL-10 production would be most likely to occur in the skin. The observation of psoriasis onset after treatment of arthritis patients with Toc is the most substantial evidence that led us to this hypothesis. We already have preliminary data taken from immunofluorescence of healthy skin sections suggesting UV light irradiation leads to substantial increase in pSTAT3, IL-6 and IL-10 not observed in non-UV treated skin samples. The ideal scenario would be to obtain biopsies from healthy and psoriatic skin, both before and after UVB therapy, or topical VitD treatment. However, having explored this, psoriasis biopsies are difficult to obtain and are highly sought after. Thus, we have concluded that initially showing the mechanism is present in healthy skin following UV or VitD treatment is sufficient. This skin is more

easily obtained as large amounts are available following skin removal from bariatric surgery.

# 5. Overall conclusions

This thesis has explored the mechanisms of VitD induced immune-regulation *in vitro* and *in vivo*. Both results chapters present evidence for anti-inflammatory roles of VitD, both in the context of repletion in a diseased population and direct actions on *in vitro* treatment of $CD4^+$ T cells.

Whilst ample evidence exists linking VitD deficiency with many chronic diseases, repletion studies with clinical outcomes have shown variable results. Thus, though basic science studies on VitD in immune cells clearly show broad reaching effects of the hormone, this has not translated into therapeutic benefits which has cast doubt over the clinical usefulness of VitD repletion (Peterlik, 2012) and suggesting the extra-renal VitD system is more complex than initially thought. Given the known issues in VitD research (see section 1.5.2) a better understanding of the mechanism underlying the immunoregulatory effects of VitD would be of great benefit in deciphering the specific effects of VitD on immune cells, which could help focus future research.

The research presented here has uncovered that increased VitD levels achieved through dietary repletion is sufficient to affect immune cells phenotypically. The reduced HLA-DR expression observed on mDCs is a hallmark anti-inflammatory VitD effect *in vitro.* Whether this change leads to clinical benefits remains to be seen, but regardless could be used in the future as an early biomarker of anti-inflammatory activity of VitD *in vivo*.

We also show that VitD induced phenotypic changes in $CD4^+$ T cells correspond to a change from pro-inflammatory to anti-inflammatory function. That significant epigenetic alterations were also evidenced as part of these immunoregulatory effects suggests a more general predicate of VitD in regulation of gene expression. This would suggest VitD has the ability to imprint stable regulatory decisions about gene expression on immune cells. Additionally, we present evidence for a novel pathway responsible for IL-10 production. We suggest that this may be a more general mechanism by which $CD4^+$ T cells self-limit immune reactions. This observation is in line with the main population affected being memory cells, as these would be the main cell subset found at sites of inflammation and tissues, which would need regulating. This hypothesis needs further

investigation, but if confirmed could additionally link VitD deficiency with uncontrolled immune activation. In this context without sufficient 25 VitD in circulation for signalling, $CD4^+$ T cells would lose the ability to imprint self-limiting programmes, and thus lead to over-activation of T cell driven immune responses.

In conclusion, we have shown VitD can fundamentally influence immune responses at multiple levels. Though the work presented here remains to be clarified in disease settings, the data is novel and justifies further research into the multifaceted roles of VitD in the immune system.

# References


Adams, J.S., and Hewison, M. (2012). Extrarenal expression of the 25-hydroxyvitamin D-1-hydroxylase. Arch. Biochem. Biophys. *523*, 95–102.

Adams, J.S., Rafison, B., Witzel, S., Reyes, R.E., Shieh, A., Chun, R., Zavala, K., Hewison, M., and Liu, P.T. (2014). Regulation of the extrarenal CYP27B1-hydroxylase. J. Steroid Biochem. Mol. Biol. *144 Pt A*, 22–27.

Adorini, L., and Penna, G. (2009). Induction of tolerogenic dendritic cells by vitamin D receptor agonists. Handb Exp Pharmacol *188*, 251–273.

Afgan, E., Baker, D., van den Beek, M., Blankenberg, D., Bouvier, D., Čech, M., Chilton, J., Clements, D., Coraor, N., Eberhard, C., et al. (2016). The Galaxy platform for accessible, reproducible and collaborative biomedical analyses: 2016 update. Nucleic Acids Res. *44*, W3–W10.

Agrawal, D., and Yin, K. (2014). Vitamin D and inflammatory diseases. *Volume 7*, 69–87.

Ahmadpoor, P., Ilkhanizadeh, B., Ghasemmahdi, L., Makhdoomi, K., and Ghafari, A. (2009). Effect of active vitamin D on expression of co-stimulatory molecules and HLA-DR in renal transplant recipients. Exp Clin Transplant *7*, 99–103.

Ali, F.N., Arguelles, L.M., Langman, C.B., and Price, H.E. (2009). Vitamin D deficiency in children with chronic kidney disease: uncovering an epidemic. Pediatrics *123*, 791–796.

Almerighi, C., Sinistro, A., Cavazza, A., Ciaprini, C., Rocchi, G., and Bergamini, A. (2009). 1Alpha,25-dihydroxyvitamin D3 inhibits CD40L-induced pro-inflammatory and immunomodulatory activity in human monocytes. Cytokine *45*, 190–197.

Ando, M., Shibuya, A., Yasuda, M., Azuma, N., Tsuchiya, K., Akiba, T., and Nitta, K. (2005). Impairment of innate cellular response to in vitro stimuli in patients on continuous ambulatory peritoneal dialysis. Nephrol. Dial. Transplant. *20*, 2497–2503.

Asadullah, K., Döcke, W.D., Ebeling, M., Friedrich, M., Belbe, G., Audring, H., Volk, H.D., and Sterry, W. (1999). Interleukin 10 treatment of psoriasis: clinical results of a phase 2 trial. Arch Dermatol *135*, 187–192.

Asadullah, K., Sterry, W., Stephanek, K., Jasulaitis, D., Leupold, M., Audring, H., Volk, H.D., and Döcke, W.D. (1998). IL-10 is a key cytokine in psoriasis. Proof of principle by IL-10 therapy: a new therapeutic approach. J. Clin. Invest. *101*, 783–794.

Baeke, F., Korf, H., Overbergh, L., van Etten, E., Verstuyf, A., Gysemans, C., and Mathieu, C. (2010a). Human T lymphocytes are direct targets of 1,25-dihydroxyvitamin D3 in the immune system. J. Steroid Biochem. Mol. Biol. *121*, 221–227.

Baeke, F., Korf, H., Overbergh, L., Verstuyf, A., Thorrez, L., Van Lommel, L., Waer, M., Schuit, F., Gysemans, C., and Mathieu, C. (2011). The vitamin D analog, TX527,

promotes a human CD4+CD25highCD127low regulatory T cell profile and induces a migratory signature specific for homing to sites of inflammation. J. Immunol. *186*, 132–142.

Baeke, F., Takiishi, T., Korf, H., Gysemans, C., and Mathieu, C. (2010b). Vitamin D: modulator of the immune system. Curr Opin Pharmacol *10*, 482–496.

Barrat, F.J., Cua, D.J., Boonstra, A., Richards, D.F., Crain, C., Savelkoul, H.F., de Waal-Malefyt, R., Coffman, R.L., Hawrylowicz, C.M., and O'Garra, A. (2002). In vitro generation of interleukin 10-producing regulatory CD4(+) T cells is induced by immunosuppressive drugs and inhibited by T helper type 1 (Th1)- and Th2-inducing cytokines. J Exp Med *195*, 603–616.

Bartels, L., Jørgensen, S., Agnholt, J., Kelsen, J., Hvas, C., and Dahlerup, J. (2007). 1,25-dihydroxyvitamin D3 and dexamethasone increase interleukin-10 production in CD4+ T cells from patients with Crohn's disease. Int Immunopharmacol *7*, 1755–1764.

Bernstein, B.E., Meissner, A., and Lander, E.S. (2007). The mammalian epigenome. Cell *128*, 669–681.

Betjes, M.G.H. (2013). Immune cell dysfunction and inflammation in end-stage renal disease. Nat Rev Nephrol *9*, 255–265.

Bhalla, A.K., Amento, E.P., and Krane, S.M. (1986). Differential effects of 1,25-dihydroxyvitamin D3 on human lymphocytes and monocyte/macrophages: inhibition of interleukin-2 and augmentation of interleukin-1 production. Cell. Immunol. *98*, 311–322.

Bhalla, A.K., Amento, E.P., Clemens, T.L., Holick, M.F., and Krane, S.M. (1983). Specific high-affinity receptors for 1,25-dihydroxyvitamin D3 in human peripheral blood mononuclear cells: presence in monocytes and induction in T lymphocytes following activation. J. Clin. Endocrinol. Metab. *57*, 1308–1310.

Bird, A.P. (1980). DNA methylation and the frequency of CpG in animal DNA. Nucleic Acids Res. *8*, 1499–1504.

Blankenberg, D., Gordon, A., Kuster, Von, G., Coraor, N., Taylor, J., Nekrutenko, A., Galaxy Team (2010). Manipulation of FASTQ data with Galaxy. Bioinformatics *26*, 1783–1785.

Blaskovich, M.A., Sun, J., Cantor, A., Turkson, J., Jove, R., and Sebti, S.M. (2003). Discovery of JSI-124 (cucurbitacin I), a selective Janus kinase/signal transducer and activator of transcription 3 signaling pathway inhibitor with potent antitumor activity against human and murine cancer cells in mice. Cancer Res. *63*, 1270–1279.

Bolger, A.M., Lohse, M., and Usadel, B. (2014). Trimmomatic: a flexible trimmer for Illumina sequence data. Bioinformatics *30*, 2114–2120.

Bonn, S., Zinzen, R.P., Girardot, C., Gustafson, E.H., Perez-Gonzalez, A., Delhomme, N., Ghavi-Helm, Y., Wilczyński, B., Riddell, A., and Furlong, E.E.M. (2012). Tissue-specific analysis of chromatin state identifies temporal signatures of enhancer activity during embryonic development. Nat. Genet. *44*, 148–156.

Boonstra, A., Barrat, F.J., Crain, C., Heath, V.L., Savelkoul, H.F., and O'Garra, A. (2001). 1alpha,25-Dihydroxyvitamin d3 has a direct effect on naive CD4(+) T cells to enhance the development of Th2 cells. J. Immunol. *167*, 4974–4980.

Boudville, N.C., and Hodsman, A.B. (2006). Renal function and 25-hydroxyvitamin D concentrations predict parathyroid hormone levels in renal transplant patients. Nephrol. Dial. Transplant. *21*, 2621–2624.

Bouillon, R., Carmeliet, G., Verlinden, L., van Etten, E., Verstuyf, A., Luderer, H.F., Lieben, L., Mathieu, C., and Demay, M. (2008). Vitamin D and human health: lessons from vitamin D receptor null mice. Endocr. Rev. *29*, 726–776.

Braun, D.A., Fribourg, M., and Sealfon, S.C. (2013). Cytokine response is determined by duration of receptor and signal transducers and activators of transcription 3 (STAT3) activation. J. Biol. Chem. *288*, 2986–2993.

Brennan, A., Katz, D.R., Nunn, J.D., Barker, S., Hewison, M., Fraher, L.J., O'Riordan, JL (1987). Dendritic cells from human tissues express receptors for the immunoregulatory vitamin D3 metabolite, dihydroxycholecalciferol. Immunology *61*, 457–461.

Cachofeiro, V., Goicochea, M., de Vinuesa, S.G., Oubiña, P., Lahera, V., and Luño, J. (2008). Oxidative stress and inflammation, a link between chronic kidney disease and cardiovascular disease. Kidney Int Suppl S4–S9.

Cai, Y., Fleming, C., and Yan, J. (2012). New insights of T cells in the pathogenesis of psoriasis. Cell Mol Immunol.

Calton, E.K., Keane, K.N., Newsholme, P., Zhao, Y., and Soares, M.J. (2017). The impact of cholecalciferol supplementation on the systemic inflammatory profile: a systematic review and meta-analysis of high-quality randomized controlled trials. Eur J Clin Nutr *104*, 295.

Campos, E.I., and Reinberg, D. (2009). Histones: annotating chromatin. Annu. Rev. Genet. *43*, 559–599.

Cantorna, M.T., Snyder, L., Lin, Y.-D., and Yang, L. (2015). Vitamin D and 1,25(OH)2D regulation of T cells. Nutrients *7*, 3011–3021.

Carlberg, C. (2014). Genome-wide (over) view on the actions of vitamin D. Front Physiol.

Carlberg, C., and Campbell, M.J. (2013). Vitamin D receptor signaling mechanisms: integrated actions of a well-defined transcription factor. Steroids.

Carlberg, C., and Polly, P. (1998). Gene regulation by vitamin D3. Crit. Rev. Eukaryot. Gene Expr. *8*, 19–42.

Chambers, E.S., and Hawrylowicz, C.M. (2011). The impact of vitamin D on regulatory T cells. Curr Allergy Asthma Rep *11*, 29–36.

Chandra, P., Binongo, J., Ziegler, T., and Schlanger, L. (2008). Cholecalciferol (vitamin D3) therapy and vitamin D insufficiency in patients with chronic kidney disease: a randomized controlled pilot study. Endocr Pract *14*, 10–17.

Chen, S., Sims, G.P., Chen, X.X., Gu, Y.Y., Chen, S., and Lipsky, P.E. (2007). Modulatory Effects of 1,25-Dihydroxyvitamin D3 on Human B Cell Differentiation. J. Immunol. *179*, 1634–1647.

Cooper, G.M., Stone, E.A., Asimenos, G., NISC Comparative Sequencing Program, Green, E.D., Batzoglou, S., and Sidow, A. (2005). Distribution and intensity of constraint in mammalian genomic sequence. Genome Res. *15*, 901–913.

Cope, A., Le Friec, G., Cardone, J., and Kemper, C. (2011). The Th1 life cycle: molecular control of IFN-γ to IL-10 switching. Trends Immunol. *32*, 278–286.

Correale, J., Ysrraelit, M.C., and Gaitán, M.I. (2009). Immunomodulatory effects of Vitamin D in multiple sclerosis. Brain.

Creyghton, M.P., Cheng, A.W., Welstead, G.G., Kooistra, T., Carey, B.W., Steine, E.J., Hanna, J., Lodato, M.A., Frampton, G.M., Sharp, P.A., et al. (2010). Histone H3K27ac separates active from poised enhancers and predicts developmental state. Proc. Natl. Acad. Sci. U.S.a. *107*, 21931–21936.

D'Ambrosio, D., Cippitelli, M., Cocciolo, M.G., Mazzeo, D., Di Lucia, P., Lang, R., Sinigaglia, F., and Panina-Bordignon, P. (1998). Inhibition of IL-12 production by 1,25-dihydroxyvitamin D3. Involvement of NF-kappaB downregulation in transcriptional repression of the p40 gene. J. Clin. Invest. *101*, 252–262.

Dadaei, T., Safapoor, M.H., Asadzadeh Aghdaei, H., Balaii, H., Pourhoseingholi, M.A., Naderi, N., Zojaji, H., Azimzadeh, P., Mohammadi, P., and Zali, M.R. (2015). Effect of vitamin D3 supplementation on TNF-α serum level and disease activity index in Iranian IBD patients. Gastroenterol Hepatol Bed Bench *8*, 49–55.

Dankers, W., Colin, E.M., van Hamburg, J.P., and Lubberts, E. (2016). Vitamin D in Autoimmunity: Molecular Mechanisms and Therapeutic Potential. Front Immunol *7*, 697.

Deeb, K.K., Trump, D.L., and Johnson, C.S. (2007). Vitamin D signalling pathways in cancer: potential for anticancer therapeutics. Nat. Rev. Cancer *7*, 684–700.

DeLuca, H.F. (2008). Evolution of our understanding of vitamin D. Nutr Rev *66*, S73–S87.

DeLuca, H.F. (2014). History of the discovery of vitamin D and its active metabolites. Bonekey Reports *3*, 479.

Descamps-Latscha, B., and Chatenoud, L. (1996). T cells and B cells in chronic renal failure. Semin. Nephrol. *16*, 183–191.

Diaz, L., Martinez-Reza, I., García-Becerra, R., González, L., Larrea, F., and Méndez, I. (2011). Calcitriol stimulates prolactin expression in non-activated human peripheral blood mononuclear cells: breaking paradigms. Cytokine *55*, 188–194.

Dobnig, H., Pilz, S., Scharnagl, H., Renner, W., Seelhorst, U., Wellnitz, B., Kinkeldei, J., Boehm, B.O., Weihrauch, G., and Maerz, W. (2008). Independent association of low serum 25-hydroxyvitamin d and 1,25-dihydroxyvitamin d levels with all-cause and cardiovascular mortality. Arch. Intern. Med. *168*, 1340–1349.

Doig, C.L., Singh, P.K., Dhiman, V.K., Thorne, J.L., Battaglia, S., Sobolewski, M., Maguire, O., O'Neill, L.P., Turner, B.M., McCabe, C.J., et al. (2013). Recruitment of NCOR1 to VDR target genes is enhanced in prostate cancer cells and associates with altered DNA methylation patterns. Carcinogenesis *34*, 248–256.

Dumitriu, I.E. (2015). The life (and death) of CD4+ CD28(null) T cells in inflammatory diseases. Immunology *146*, 185–193.

Elbrecht, A., Chen, Y., Cullinan, C.A., Hayes, N., Leibowitz, M., Moller, D.E., and Berger, J. (1996). Molecular cloning, expression and characterization of human peroxisome proliferator activated receptors gamma 1 and gamma 2. Biochem. Biophys. Res. Commun. *224*, 431–437.

Elder, G.J. (2007). Vitamin D levels, bone turnover and bone mineral density show seasonal variation in patients with chronic kidney disease stage 5. Nephrology (Carlton) *12*, 90–94.

Essen, Von, M.R., Kongsbak, M., and Schjerling, P. (2010). Vitamin D controls T cell antigen receptor signaling and activation of human T cells. Nat Immunol.

Fabri, M., Stenger, S., Shin, D.-M.M., Yuk, J.-M.M., Liu, P.T., Realegeno, S., Lee, H.-M.M., Krutzik, S.R., Schenk, M., Sieling, P.A., et al. (2011). Vitamin D is required for IFN-gamma-mediated antimicrobial activity of human macrophages. Sci Transl Med *3*, 104ra102.

Farias, A.S., Spagnol, G.S., Bordeaux-Rego, P., Oliveira, C.O., Fontana, A.G., de Paula, R.F., Santos, M.P., Pradella, F., Moraes, A.S., Oliveira, E.C., et al. (2013). Vitamin D3 induces IDO+ tolerogenic DCs and enhances Treg, reducing the severity of EAE. CNS Neurosci Ther *19*, 269–277.

Fetahu, I.S., Höbaus, J., and Kállay, E. (2014). Vitamin D and the epigenome. Front Physiol.

Fraser, W.D., and Milan, A.M. (2013). Vitamin D assays: past and present debates, difficulties, and developments. Calcif. Tissue Int. *92*, 118–127.

Gagliani, N., Magnani, C.F., Huber, S., Gianolini, M.E., Pala, M., Licona-Limón, P., Guo, B., Herbert, D.R., Bulfone, A., Trentini, F., et al. (2013). Coexpression of CD49b and LAG-3 identifies human and mouse T regulatory type 1 cells. Nat. Med. *19*, 739–746.

Gallucci, R.M., Simeonova, P.P., and Matheson, J.M. (2000). Impaired cutaneous wound healing in interleukin-6–deficient and immunosuppressed mice. Faseb J.

Ginde, A.A., Mansbach, J.M., and Camargo, C.A. (2009). Vitamin D, respiratory infections, and asthma. Curr Allergy Asthma Rep *9*, 81–87.

Giresi, P.G., Kim, J., McDaniell, R.M., Iyer, V.R., and Lieb, J.D. (2007). FAIRE (Formaldehyde-Assisted Isolation of Regulatory Elements) isolates active regulatory elements from human chromatin. Genome Res. *17*, 877–885.

Girndt, M., Sester, M., Sester, U., Kaul, H., and Köhler, H. (2001). Defective expression of B7-2 (CD86) on monocytes of dialysis patients correlates to the uremia-associated immune defect. Kidney Int. *59*, 1382–1389.

Giulietti, A., van Etten, E., Overbergh, L., Stoffels, K., Bouillon, R., and Mathieu, C. (2007). Monocytes from type 2 diabetic patients have a pro-inflammatory profile. 1,25-Dihydroxyvitamin D(3) works as anti-inflammatory. Diabetes Res. Clin. Pract. *77*, 47–57.

Go, A.S., Chertow, G.M., and Fan, D. (2004). Chronic kidney disease and the risks of death, cardiovascular events, and hospitalization. N Engl J Med.

Griffin, M.D., Lutz, W., Phan, V.A., Bachman, L.A., McKean, D.J., and Kumar, R. (2001). Dendritic cell modulation by 1alpha,25 dihydroxyvitamin D3 and its analogs: a vitamin D receptor-dependent pathway that promotes a persistent state of immaturity in vitro and in vivo. Proc. Natl. Acad. Sci. U.S.a. *98*, 6800–6805.

Gunta, S.S., Thadhani, R.I., and Mak, R.H. (2013). The effect of vitamin D status on risk factors for cardiovascular disease. Nat Rev Nephrol.

Handel, A.E., Sandve, G.K., Disanto, G., Berlanga-Taylor, A.J., Gallone, G., Hanwell, H., Drabløs, F., Giovannoni, G., Ebers, G.C., and Ramagopalan, S.V. (2013). Vitamin D receptor ChIP-seq in primary CD4+ cells: relationship to serum 25-hydroxyvitamin D levels and autoimmune disease. BMC Med *11*, 163.

Haussler, M.R., Whitfield, G.K., Haussler, C.A., Hsieh, J.C., Thompson, P.D., Selznick, S.H., Dominguez, C.E., and Jurutka, P.W. (1998). The nuclear vitamin D receptor: biological and molecular regulatory properties revealed. J. Bone Miner. Res. *13*, 325–349.

Haussler, M.R., Jurutka, P.W., Mizwicki, M., and Norman, A.W. (2011). Vitamin D receptor (VDR)-mediated actions of $1\alpha,25(OH)_2$vitamin $D_3$: genomic and non-genomic

mechanisms. *25*, 543–559.

Haussler, M.R., Whitfield, G.K., Kaneko, I., Haussler, C.A., Hsieh, D., Hsieh, J.-C., and Jurutka, P.W. (2013). Molecular Mechanisms of Vitamin D Action. Calcif. Tissue Int. *92*, 77–98.

Hawrylowicz, C.M., and O'Garra, A. (2005). Potential role of interleukin-10-secreting regulatory T cells in allergy and asthma. Nat. Rev. Immunol. *5*, 271–283.

Hayes, C., Hubler, S.L., Moore, J.R., Barta, L.E., Praska, C.E., and Nashold, F.E. (2015). Vitamin D Actions on CD4+ T Cells in Autoimmune Disease. Frontiers Immunol *6*, 100.

Heikkinen, S., Väisänen, S., Pehkonen, P., Seuter, S., Benes, V., and Carlberg, C. (2011). Nuclear hormone 1α,25-dihydroxyvitamin D3 elicits a genome-wide shift in the locations of VDR chromatin occupancy. Nucleic Acids Res. *39*, 9181–9193.

Heine, G., Niesner, U., Chang, H.-D., Steinmeyer, A., Zügel, U., Zuberbier, T., Radbruch, A., and Worm, M. (2008). 1,25-dihydroxyvitamin D(3) promotes IL-10 production in human B cells. Eur. J. Immunol. *38*, 2210–2218.

Heinz, S., Benner, C., Spann, N., Bertolino, E., Lin, Y.C., Laslo, P., Cheng, J.X., Murre, C., Singh, H., and Glass, C.K. (2010). Simple combinations of lineage-determining transcription factors prime cis-regulatory elements required for macrophage and B cell identities. Mol. Cell *38*, 576–589.

Hendrikx, T.K., van Gurp, E.A.F.J., Mol, W.M., Schoordijk, W., Sewgobind, V.D.K.D., Ijzermans, J.N.M., Weimar, W., and Baan, C.C. (2009). End-stage renal failure and regulatory activities of CD4+CD25bright+FoxP3+ T-cells. Nephrol. Dial. Transplant. *24*, 1969–1978.

Herman, J.G., and Baylin, S.B. (2003). Gene silencing in cancer in association with promoter hypermethylation. N. Engl. J. Med. *349*, 2042–2054.

Hesselink, D.A., Betjes, M.G.H., Verkade, M.A., Athanassopoulos, P., Baan, C.C., and Weimar, W. (2005). The effects of chronic kidney disease and renal replacement therapy on circulating dendritic cells. Nephrol. Dial. Transplant. *20*, 1868–1873.

Hewison, M. (2012). An update on vitamin D and human immunity. Clin Endocrinol.

Hewison, M., Zehnder, D., Bland, R., and Stewart, P.M. (2000). 1alpha-Hydroxylase and the action of vitamin D. J. Mol. Endocrinol. *25*, 141–148.

Holick, M.F. (2009). Vitamin D status: measurement, interpretation, and clinical application. Ann Epudemiol.

Hong, Q., Xu, J., Xu, S., Lian, L., Zhang, M., and Ding, C. (2014). Associations between serum 25-hydroxyvitamin D and disease activity, inflammatory cytokines and bone loss in patients with rheumatoid arthritis. Rheumatology (Oxford) *53*, 1994–2001.

Hunter, C.A., and Jones, S.A. (2015). IL-6 as a keystone cytokine in health and disease. Nat Immunol.

Hunter, C.A., Ellis-Neyes, L.A., Slifer, T., Kanaly, S., Grünig, G., Fort, M., Rennick, D., and Araujo, F.G. (1997). IL-10 is required to prevent immune hyperactivity during infection with Trypanosoma cruzi. J. Immunol. *158*, 3311–3316.

Inaguma, D., Nagaya, H., Hara, K., and Tatematsu, M. (2008). Relationship between serum 1, 25-dihydroxyvitamin D and mortality in patients with pre-dialysis chronic kidney disease. Clinical and ….

Ivanov, I.I., McKenzie, B.S., Zhou, L., Tadokoro, C.E., Lepelley, A., Lafaille, J.J., Cua, D.J., and Littman, D.R. (2006). The orphan nuclear receptor RORgammat directs the differentiation program of proinflammatory IL-17+ T helper cells. Cell *126*, 1121–1133.

Jaber, B.L. (2005). Bacterial infections in hemodialysis patients: pathogenesis and prevention. Kidney Int.

Janssen, M.J.W., Wielders, J.P.M., Bekker, C.C., Boesten, L.S.M., Buijs, M.M., Heijboer, A.C., van der Horst, F.A.L., Loupatty, F.J., and van den Ouweland, J.M.W. (2012). Multicenter comparison study of current methods to measure 25-hydroxyvitamin D in serum. Steroids *77*, 1366–1372.

Jayedi, A., Soltani, S., and Shab-Bidar, S. (2017). Vitamin D status and all-cause mortality in patients with chronic kidney disease: A systematic review and dose-response meta-analysis. J. Clin. Endocrinol. Metab.

Jean, G., Souberbielle, J.-C., and Chazot, C. (2009). Monthly cholecalciferol administration in haemodialysis patients: a simple and efficient strategy for vitamin D supplementation. Nephrol. Dial. Transplant. *24*, 3799–3805.

Jeffery, L.E., Qureshi, O.S., Gardner, D., Hou, T.Z., and Briggs, Z. (2015). Vitamin D antagonises the suppressive effect of inflammatory cytokines on CTLA-4 expression and regulatory function. PLoS ONE.

Jeffery, L.E., Burke, F., Mura, M., Zheng, Y., Qureshi, O.S., Hewison, M., Walker, L.S., Lammas, D.A., Raza, K., and Sansom, D.M. (2009). 1,25-Dihydroxyvitamin D3 and IL-2 combine to inhibit T cell production of inflammatory cytokines and promote development of regulatory T cells expressing CTLA-4 and FoxP3. J. Immunol. *183*, 5458–5467.

Jenuwein, T., and Allis, C.D. (2001). Translating the histone code. Science *293*, 1074–1080.

Jones, G.W., Greenhill, C.J., Williams, J.O., Nowell, M.A., Williams, A.S., Jenkins, B.J., and Jones, S.A. (2013). Exacerbated inflammatory arthritis in response to hyperactive gp130 signalling is independent of IL-17A. Ann. Rheum. Dis. *72*, 1738–1742.

Jones, L.L., Alli, R., Li, B., and Geiger, T.L. (2016). Differential T Cell Cytokine Receptivity and Not Signal Quality Distinguishes IL-6 and IL-10 Signaling during Th17 Differentiation. J. Immunol.

Jones, S.A., Scheller, J., and Rose-John, S. (2011). Therapeutic strategies for the clinical blockade of IL-6/gp130 signaling. J. Clin. Invest. *121*, 3375–3383.

Joshi, S., Pantalena, L.-C., Liu, X.K., Gaffen, S.L., Liu, H., Rohowsky-Kochan, C., Ichiyama, K., Yoshimura, A., Steinman, L., Christakos, S., et al. (2011). 1,25-dihydroxyvitamin D(3) ameliorates Th17 autoimmunity via transcriptional modulation of interleukin-17A. Mol. Cell. Biol. *31*, 3653–3669.

Kalantar-Zadeh, K., Kuwae, N., Regidor, D.L., Kovesdy, C.P., Kilpatrick, R.D., Shinaberger, C.S., McAllister, C.J., Budoff, M.J., Salusky, I.B., and Kopple, J.D. (2006). Survival predictability of time-varying indicators of bone disease in maintenance hemodialysis patients. Kidney Int. *70*, 771–780.

Kalantar-Zadeh, K., and Kovesdy, C.P. (2009). Clinical outcomes with active versus nutritional vitamin D compounds in chronic kidney disease. Clin J Am Soc Nephrol *4*, 1529–1539.

Kallas, M., Green, F., Hewison, M., White, C., and Kline, G. (2010). Rare causes of calcitriol-mediated hypercalcemia: a case report and literature review. *95*, 3111–3117.

Kastner, P., Krust, A., Turcotte, B., Stropp, U., Tora, L., Gronemeyer, H., and Chambon, P. (1990). Two distinct estrogen-regulated promoters generate transcripts encoding the two functionally different human progesterone receptor forms A and B. Embo J. *9*, 1603–1614.

Kato, S., Chmielewski, M., Honda, H., Pecoits-Filho, R., Matsuo, S., Yuzawa, Y., Tranaeus, A., Stenvinkel, P., and Lindholm, B. (2008). Aspects of immune dysfunction in end-stage renal disease. Clin J Am Soc Nephrol *3*, 1526–1533.

Kerner, S.A., Scott, R.A., and Pike, J.W. (1989). Sequence elements in the human osteocalcin gene confer basal activation and inducible response to hormonal vitamin D3. Proc. Natl. Acad. Sci. U.S.a. *86*, 4455–4459.

Khoo, A.L., Koenen, H., Chai, L., and Sweep, F. (2012). Seasonal variation in vitamin D3 levels is paralleled by changes in the peripheral blood human T cell compartment. PLoS ONE *7*, e29250.

Kidir, V., Ersoy, I., Altuntas, A., Gultekin, F., and Inal, S. (2015). Effect of cholecalciferol replacement on vascular calcification and left ventricular mass index in dialysis patients. Ren Fail.

Kimmel, P.L., Phillips, T.M., Simmens, S.J., Peterson, R.A., Weihs, K.L., Alleyne, S., Cruz, I., Yanovski, J.A., and Veis, J.H. (1998). Immunologic function and survival in hemodialysis patients. Kidney Int. *54*, 236–244.

Kmieciak, M., Gowda, M., Graham, L., Godder, K., Bear, H.D., Marincola, F.M., and Manjili, M.H. (2009). Human T cells express CD25 and Foxp3 upon activation and exhibit effector/memory phenotypes without any regulatory/suppressor function. J Transl Med *7*, 89.

Kong, X.F., Zhu, X.H., Pei, Y.L., Jackson, D.M., and Holick, M.F. (1999). Molecular cloning, characterization, and promoter analysis of the human 25-hydroxyvitamin D3-1alpha-hydroxylase gene. Proc. Natl. Acad. Sci. U.S.a. *96*, 6988–6993.

Kongsbak, M., and Essen, Von, M.R. (2014). Vitamin D-binding protein controls T cell responses to vitamin D. Bmc I.

Kongsbak, M., Marina, R., Boding, L., and Levring, T.B. (2014). Vitamin D up-regulates the vitamin D receptor by protecting it from proteasomal degradation in human CD4+ T cells. PLoS ONE *9*, e96695.

Krutzik, P.O., and Nolan, G.P. (2006). Fluorescent cell barcoding in flow cytometry allows high-throughput drug screening and signaling profiling. Nat Meth.

Laaksi, I., Ruohola, J.-P., Tuohimaa, P., Auvinen, A., Haataja, R., Pihlajamäki, H., and Ylikomi, T. (2007). An association of serum vitamin D concentrations < 40 nmol/L with acute respiratory tract infection in young Finnish men. Am. J. Clin. Nutr. *86*, 714–717.

Lacey, D.L., Axelrod, J., Chappel, J.C., Kahn, A.J., and Teitelbaum, S.L. (1987). Vitamin D affects proliferation of a murine T helper cell clone. J. Immunol. *138*, 1680–1686.

Lam, C.W.K. (2009). 2. Inflammation, Cytokines and Chemokines in Chronic Kidney Disease. Ejifcc *20*, 12–20.

Langmead, B., Trapnell, C., Pop, M., and Salzberg, S.L. (2009). Ultrafast and memory-efficient alignment of short DNA sequences to the human genome. Genome Biol. *10*, R25.

Lanske, B., Densmore, M.J., and Erben, R.G. (2014). Vitamin D endocrine system and osteocytes. Bonekey Reports *3*, 494.

Laurent, S., Le Parc, J.-M., Clérici, T., Bréban, M., and Mahé, E. (2010). Onset of psoriasis following treatment with tocilizumab. Br. J. Dermatol. *163*, 1364–1365.

Lee, Y.H., Choi, S.J., Ji, J.D., and Song, G.G. (2012). Vitamin D receptor ApaI, TaqI, BsmI, and FokI polymorphisms and psoriasis susceptibility: a meta-analysis. Mol. Biol. Rep. *39*, 6471–6478.

Lefebvre, P., Benomar, Y., and Staels, B. (2010). Retinoid X receptors: common heterodimerization partners with distinct functions. Trends Endocrinol. Metab. *21*, 676–683.

Lehmann, B., Genehr, T., Knuschke, P., Pietzsch, J., and Meurer, M. (2001). UVB-

induced conversion of 7-dehydrocholesterol to 1alpha,25-dihydroxyvitamin D3 in an in vitro human skin equivalent model. J. Invest. Dermatol. *117*, 1179–1185.

Lemire, J.M., Adams, J.S., Kermani-Arab, V., Bakke, A.C., Sakai, R., and Jordan, S.C. (1985). 1,25-Dihydroxyvitamin D3 suppresses human T helper/inducer lymphocyte activity in vitro. J. Immunol. *134*, 3032–3035.

Lerdrup, M., Johansen, J.V., Agrawal-Singh, S., and Hansen, K. (2016). An interactive environment for agile analysis and visualization of ChIP-sequencing data. Nat. Struct. Mol. Biol. *23*, 349–357.

Lin, Z.-Q., Kondo, T., Ishida, Y., Takayasu, T., and Mukaida, N. (2003). Essential involvement of IL-6 in the skin wound-healing process as evidenced by delayed wound healing in IL-6-deficient mice. J Leukoc Biol *73*, 713–721.

Litjens, N.H.R., van Druningen, C.J., and Betjes, M.G.H. (2006). Progressive loss of renal function is associated with activation and depletion of naive T lymphocytes. Clin. Immunol. *118*, 83–91.

Liu, P.T., Stenger, S., Li, H., Wenzel, L., Tan, B.H., Krutzik, S.R., Ochoa, M.T., Schauber, J., Wu, K., Meinken, C., et al. (2006). Toll-like receptor triggering of a vitamin D-mediated human antimicrobial response. Science *311*, 1770–1773.

Lopes, N., Carvalho, J., Durães, C.'.L., Sousa, B., Gomes, M., Costa, J.L.L., Oliveira, C., Paredes, J., and Schmitt, F. (2012). 1Alpha,25-dihydroxyvitamin D3 induces de novo E-cadherin expression in triple-negative breast cancer cells by CDH1-promoter demethylation. Anticancer Res. *32*, 249–257.

Lu, R.J., Zhu, S.M., Tang, F.L., Zhu, X.S., Fan, Z.D., Wang, G.L., Jiang, Y.F., and Zhang, Y. (2017). Effects of vitamin D or its analogues on the mortality of patients with chronic kidney disease: an updated systematic review and meta-analysis. Eur J Clin Nutr *71*, 683–693.

Lyons, P.A., McKinney, E.F., Rayner, T.F., and Hatton, A. (2010). Novel expression signatures identified by transcriptional analysis of separated leucocyte subsets in systemic lupus erythematosus and vasculitis. Anns Rheum Dis *69*, 1208–1213.

MacDonald, P.N., Sherman, D.R., Dowd, D.R., Jefcoat, S.C., and DeLisle, R.K. (1995). The vitamin D receptor interacts with general transcription factor IIB. J. Biol. Chem. *270*, 4748–4752.

Mahon, B.D., Wittke, A., and Weaver, V. (2003). The targets of vitamin D depend on the differentiation and activation status of CD4 positive T cells. J Cell Biochem.

Malinen, M., Saramäki, A., Ropponen, A., Degenhardt, T., Väisänen, S., and Carlberg, C. (2008). Distinct HDACs regulate the transcriptional response of human cyclin-dependent kinase inhibitor genes to Trichostatin A and 1alpha,25-dihydroxyvitamin D3. Nucleic Acids Res. *36*, 121–132.

Marchal, K., Verlinden, L., Verstuyf, A., and Nogueira, T. Vitamin D3 Induces Tolerance in Human Dendritic Cells by Activation of Intracellular Metabolic Pathways. Cell Rep.

Marcinkowska, E. (2001). A run for a membrane vitamin D receptor. Biol Signals Recept *10*, 341–349.

Martins, D., Wolf, M., Pan, D., Zadshir, A., Tareen, N., Thadhani, R., Felsenfeld, A., Levine, B., Mehrotra, R., and Norris, K. (2007). Prevalence of cardiovascular risk factors and the serum levels of 25-hydroxyvitamin D in the United States: data from the Third National Health and Nutrition Examination Survey. Arch. Intern. Med. *167*, 1159–1165.

Masuyama, H., Brownfield, C.M., St-Arnaud, R., and MacDonald, P.N. (1997). Evidence for ligand-dependent intramolecular folding of the AF-2 domain in vitamin D receptor-activated transcription and coactivator interaction. Mol. Endocrinol. *11*, 1507–1517.

Mathelier, A., Zhao, X., Zhang, A.W., Parcy, F., Worsley-Hunt, R., Arenillas, D.J., Buchman, S., Chen, C.-Y., Chou, A., Ienasescu, H., et al. (2014). JASPAR 2014: an extensively expanded and updated open-access database of transcription factor binding profiles. Nucleic Acids Res. *42*, D142–D147.

Matilainen, J.M., Husso, T., Toropainen, S., Seuter, S., Turunen, M.P., Gynther, P., Ylä-Herttuala, S., Carlberg, C., and Väisänen, S. (2010). Primary effect of $1\alpha,25(OH)_2D_3$ on IL-10 expression in monocytes is short-term down-regulation. Biochim. Biophys. Acta *1803*, 1276–1286.

McGeachy, M.J., Bak-Jensen, K.S., and Chen, Y.I. (2007). TGF-[beta] and IL-6 drive the production of IL-17 and IL-10 by T cells and restrain TH-17 cell-mediated pathology. Nat Immunol.

McGregor, R., Li, G., Penny, H., and Lombardi, G. (2014). Vitamin D in renal transplantation–from biological mechanisms to clinical benefits. Am J Transplant.

McKenna, N.J., and O'Malley, B.W. (2002). Combinatorial control of gene expression by nuclear receptors and coregulators. Cell *108*, 465–474.

Meehan, M.A., Kerman, R.H., and Lemire, J.M. (1992). 1,25-Dihydroxyvitamin D3 enhances the generation of nonspecific suppressor cells while inhibiting the induction of cytotoxic cells in a human MLR. Cell. Immunol. *140*, 400–409.

Mehrotra, R., Kermah, D.A., Salusky, I.B., Wolf, M.S., Thadhani, R.I., Chiu, Y.-W.W., Martins, D., Adler, S.G., and Norris, K.C. (2009). Chronic kidney disease, hypovitaminosis D, and mortality in the United States. *76*, 977–983.

Meier, P., Golshayan, D., Blanc, E., Pascual, M., and Burnier, M. (2009). Oxidized LDL modulates apoptosis of regulatory T cells in patients with ESRD. J. Am. Soc. Nephrol. *20*, 1368–1384.

Melamed, M.L., Eustace, J.A., Plantinga, L., Jaar, B.G., Fink, N.E., Coresh, J., Klag, M.J.,

and Powe, N.R. (2006). Changes in serum calcium, phosphate, and PTH and the risk of death in incident dialysis patients: a longitudinal study. Kidney Int. *70*, 351–357.

Meyer, M.B., Goetsch, P.D., and Pike, J.W. (2010). Genome-wide analysis of the VDR/RXR cistrome in osteoblast cells provides new mechanistic insight into the actions of the vitamin D hormone. J. Steroid Biochem. Mol. Biol. *121*, 136–141.

Mihara, M., Ohsugi, Y., and Kishimoto, T. (2011). Tocilizumab, a humanized anti-interleukin-6 receptor antibody, for treatment of rheumatoid arthritis. Open Access Rheumatology: ….

Miller, W.L. (1988). Molecular biology of steroid hormone synthesis. Endocr. Rev. *9*, 295–318.

Mohn, F., and Schübeler, D. (2009). Genetics and epigenetics: stability and plasticity during cellular differentiation. Trends Genet. *25*, 129–136.

Mora, J.R., Iwata, M., and Andrian, Von, U.H. (2008). Vitamin effects on the immune system: vitamins A and D take centre stage. Nat. Rev. Immunol.

Moss, R.B., Moll, T., El-Kalay, M., Kohne, C., Soo Hoo, W., Encinas, J., and Carlo, D.J. (2004). Th1/Th2 cells in inflammatory disease states: therapeutic implications. Expert Opin Biol Ther *4*, 1887–1896.

Müller, K., and Bendtzen, K. (1993). Inhibition of human T lymphocyte proliferation and cytokine production by 1, 25-dihydroxyvitamin D3. Differential effects on CD45RA+ and CD45R0+ cells. Autoimmunity *14*, 37–43.

Møller, K.I., Kongshoj, B., and Philipsen, P.A. (2005). How Finsen's light cured lupus vulgaris. Photodermatology.

Nanzer, A.M., Chambers, E.S., and Ryanna, K. (2013). Enhanced production of IL-17A in patients with severe asthma is inhibited by 1α, 25-dihydroxyvitamin D3 in a glucocorticoid-independent fashion. J Allergy Clin Immunol.

Nemere, I., Schwartz, Z., Pedrozo, H., Sylvia, V.L., Dean, D.D., and Boyan, B.D. (1998). Identification of a membrane receptor for 1,25-dihydroxyvitamin D3 which mediates rapid activation of protein kinase C. J. Bone Miner. Res. *13*, 1353–1359.

Nishikawa, Y., Tragoolpua, K., Inoue, N., Makala, L., Nagasawa, H., Otsuka, H., and Mikami, T. (2001). In the absence of endogenous gamma interferon, mice acutely infected with Neospora caninum succumb to a lethal immune response characterized by inactivation of peritoneal macrophages. Clin. Diagn. Lab. Immunol. *8*, 811–816.

O'Garra, A., and Vieira, P. (2007). T(H)1 cells control themselves by producing interleukin-10. Nat. Rev. Immunol. *7*, 425–428.

Omdahl, J.L., Morris, H.A., and May, B.K. (2002). Hydroxylase enzymes of the vitamin D

pathway: expression, function, and regulation. Annu. Rev. Nutr. *22*, 139–166.

Osugi, Y., Vuckovic, S., and Hart, D.N.J. (2002). Myeloid blood CD11c+ dendritic cells and monocyte-derived dendritic cells differ in their ability to stimulate T lymphocytes. Blood *100*, 2858–2866.

Özdemir, B.H., Özdemir, A.A., Sezer, S., and Çolak, T. (2011). Influence of 1, 25-dihydroxyvitamin D3 on human leukocyte antigen-DR expression, macrophage infiltration, and graft survival in renal allografts. Transplant Proc.

Pálmer, H.G.G., Sánchez-Carbayo, M., Ordóñez-Morán, P., Larriba, M.'.A.J.J., Cordón-Cardó, C., and Muñoz, A. (2003). Genetic signatures of differentiation induced by 1alpha,25-dihydroxyvitamin D3 in human colon cancer cells. Cancer Res. *63*, 7799–7806.

Pengelly, A.R., Copur, Ö., Jäckle, H., Herzig, A., and Müller, J. (2013). A histone mutant reproduces the phenotype caused by loss of histone-modifying factor Polycomb. Science *339*, 698–699.

Penna, G., and Adorini, L. (2000). 1 Alpha,25-dihydroxyvitamin D3 inhibits differentiation, maturation, activation, and survival of dendritic cells leading to impaired alloreactive T cell activation. J. Immunol. *164*, 2405–2411.

Pereira, R., Costa, E., Gonçalves, M., Miranda, V., do Sameiro Faria, M., Quintanilha, A., Belo, L., Lima, M., and Santos-Silva, A. (2010). Neutrophil and monocyte activation in chronic kidney disease patients under hemodialysis and its relationship with resistance to recombinant human erythropoietin and to the hemodialysis procedure. Hemodial Int *14*, 295–301.

Peterlik, M. (2012). Vitamin D insufficiency and chronic diseases: hype and reality. Food Funct *3*, 784–794.

Pike, J.W., and Meyer, M.B. (2012). Regulation of mouse Cyp24a1 expression via promoter-proximal and downstream-distal enhancers highlights new concepts of 1,25-dihydroxyvitamin D(3) action. Arch. Biochem. Biophys. *523*, 2–8.

Pike, J.W., Meyer, M.B., and Bishop, K.A. (2012). Regulation of target gene expression by the vitamin D receptor - an update on mechanisms. Rev Endocr Metab Disord *13*, 45–55.

Povoleri, G.A.M., Scotta, C., Nova-Lamperti, E.A., John, S., Lombardi, G., and Afzali, B. (2013). Thymic versus induced regulatory T cells - who regulates the regulators? Front Immunol *4*, 169.

Provvedini, D.M., Tsoukas, C.D., Deftos, L.J., and Manolagas, S.C. (1983). 1,25-dihydroxyvitamin D3 receptors in human leukocytes. Science *221*, 1181–1183.

Quarona, V., Zaccarello, G., Chillemi, A., Brunetti, E., Singh, V.K., Ferrero, E., Funaro, A.,

Horenstein, A.L., and Malavasi, F. (2013). CD38 and CD157: a long journey from activation markers to multifunctional molecules. Cytometry B Clin Cytom *84*, 207–217.

Querfeld, U. (2013). Vitamin D and inflammation. Pediatr. Nephrol. *28*, 605–610.

Ramagopalan, S.V., Heger, A., and Berlanga, A.J. (2010). A ChIP-seq defined genome-wide map of vitamin D receptor binding: associations with disease and evolution. Gen Res *20*, 1352–1360.

Ramírez, F., Dündar, F., Diehl, S., Grüning, B.A., and Manke, T. (2014). deepTools: a flexible platform for exploring deep-sequencing data. Nucleic Acids Res. *42*, W187–W191.

Ramírez, F., Ryan, D.P., Grüning, B., Bhardwaj, V., Kilpert, F., Richter, A.S., Heyne, S., Dündar, F., and Manke, T. (2016). deepTools2: a next generation web server for deep-sequencing data analysis. Nucleic Acids Res. *44*, W160–W165.

Razin, A. (1998). CpG methylation, chromatin structure and gene silencing-a three-way connection. Embo J. *17*, 4905–4908.

Rigby, W.F., Stacy, T., and Fanger, M.W. (1984). Inhibition of T lymphocyte mitogenesis by 1,25-dihydroxyvitamin D3 (calcitriol). J. Clin. Invest. *74*, 1451–1455.

Rigby, W.F., Yirinec, B., Oldershaw, R.L., and Fanger, M.W. (1987). Comparison of the effects of 1,25-dihydroxyvitamin D3 on T lymphocyte subpopulations. Eur. J. Immunol. *17*, 563–566.

Rincón, M., Anguita, J., Nakamura, T., Fikrig, E., and Flavell, R.A. (1997). Interleukin (IL)-6 directs the differentiation of IL-4-producing CD4+ T cells. J Exp Med *185*, 461–469.

Ritter, C.S., Armbrecht, H.J., Slatopolsky, E., and Brown, A.J. (2006). 25-Hydroxyvitamin D(3) suppresses PTH synthesis and secretion by bovine parathyroid cells. Kidney Int. *70*, 654–659.

Robinson, J.T., Thorvaldsdóttir, H., Winckler, W., Guttman, M., Lander, E.S., Getz, G., and Mesirov, J.P. (2011). Integrative genomics viewer. Nat Biotechnol *29*, 24–26.

Rodríguez-Paredes, M., and Esteller, M. (2011). Cancer epigenetics reaches mainstream oncology. Nat. Med. *17*, 330–339.

Rook, G.A., Steele, J., Fraher, L., Barker, S., Karmali, R., O'Riordan, J., and Stanford, J. (1986). Vitamin D3, gamma interferon, and control of proliferation of Mycobacterium tuberculosis by human monocytes. Immunology *57*, 159–163.

Rudensky, A.Y. (2011). Regulatory T cells and Foxp3. Immunol. Rev. *241*, 260–268.

Saraiva, M., and O'Garra, A. (2010). The regulation of IL-10 production by immune cells. Nat Rev Immunol *10*, 170–181.

Saramäki, A., Diermeier, S., Kellner, R., Laitinen, H., Va i sänen, S., and Carlberg, C. (2009). Cyclical chromatin looping and transcription factor association on the regulatory regions of the p21 (CDKN1A) gene in response to 1alpha,25-dihydroxyvitamin D3. J. Biol. Chem. *284*, 8073–8082.

Satirapoj, B., Limwannata, P., Chaiprasert, A., Supasyndh, O., and Choovichian, P. (2013). Vitamin D insufficiency and deficiency with stages of chronic kidney disease in an Asian population. BMC Nephrol *14*, 206.

Scherberich, J.E., Estner, H., and Segerer, W. (2004). Impact of different immunosuppressive regimens on antigen-presenting blood cells in kidney transplant patients. Kidney Blood Press. Res. *27*, 177–180.

Schiffrin, E.L., Lipman, M.L., and Mann, J.F.E. (2007). Chronic kidney disease: effects on the cardiovascular system. Circulation *116*, 85–97.

Seuter, S., Pehkonen, P., Heikkinen, S., and Carlberg, C. (2013). Dynamics of 1α,25-dihydroxyvitamin D3-dependent chromatin accessibility of early vitamin D receptor target genes. Biochim. Biophys. Acta *1829*, 1266–1275.

Shlyueva, D., Stampfel, G., and Stark, A. (2014). Transcriptional enhancers: from properties to genome-wide predictions. Nature Reviews Genetics *15*, 272–286.

Sigmundsdottir, H., Pan, J., Debes, G.F., Alt, C., Habtezion, A., Soler, D., and Butcher, E.C. (2007). DCs metabolize sunlight-induced vitamin D3 to “program” T cell attraction to the epidermal chemokine CCL27. Nat Immunol *8*, 285–293.

Skene, P.J., and Henikoff, S. (2017). An efficient targeted nuclease strategy for high-resolution mapping of DNA binding sites. Elife *6*, 576.

Sotirchos, E.S., Bhargava, P., Eckstein, C., Van Haren, K., Baynes, M., Ntranos, A., Gocke, A., Steinman, L., Mowry, E.M., and Calabresi, P.A. (2016). Safety and immunologic effects of high- vs low-dose cholecalciferol in multiple sclerosis. Neurology *86*, 382–390.

Staeva-Vieira, T.P., and Freedman, L.P. (2002). 1,25-Dihydroxyvitamin D3 Inhibits IFN-γ and IL-4 Levels During In Vitro Polarization of Primary Murine CD4+ T Cells. J. Immunol. *168*, 1181–1189.

Steenbock, H. (1924). The induction of growth promoting and calcifying properties in a ration by exposure to light. Science *60*, 224–225.

Steensberg, A., Fischer, C.P., Keller, C., Møller, K., and Pedersen, B.K. (2003). IL-6 enhances plasma IL-1ra, IL-10, and cortisol in humans. American Journal of Physiology - Endocrinology and Metabolism *285*, E433–E437.

Stein, E.M., and Shane, E. (2011). Vitamin D in organ transplantation. Osteoporos Int *22*, 2107–2118.

Sterling, K.A., Eftekhari, P., Girndt, M., and Kimmel, P.L. (2012). The immunoregulatory function of vitamin D: implications in chronic kidney disease. Nat Rev Nephrol.

Stinghen, A.E.M., Bucharles, S., Riella, M.C., and Pecoits-Filho, R. (2010). Immune mechanisms involved in cardiovascular complications of chronic kidney disease. Blood Purif. *29*, 114–120.

Stumhofer, J.S., Silver, J.S., and Laurence, A. (2007). Interleukins 27 and 6 induce STAT3-mediated T cell production of interleukin 10. Nat Immunol.

Sui, W., Tan, J., Guo, J., Du, G., and Dai, Y. (2009). An altered TH1/TH2 and pro-inflammatory cytokine profile in patients with end-stage renal disease detected by suspension array technology. Ren Fail *31*, 1–5.

Sunn, K.L., Cock, T.A., Crofts, L.A., Eisman, J.A., and Gardiner, E.M. (2001). Novel N-terminal variant of human VDR. Mol. Endocrinol. *15*, 1599–1609.

Suzuki, T., Tazoe, H., Taguchi, K., Koyama, Y., Ichikawa, H., Hayakawa, S., Munakata, H., and Isemura, M. (2006). DNA microarray analysis of changes in gene expression induced by 1,25-dihydroxyvitamin D3 in human promyelocytic leukemia HL-60 cells. Biomed. Res. *27*, 99–109.

Talmor, Y., Golan, E., Benchetrit, S., Bernheim, J., Klein, O., Green, J., and Rashid, G. (2008). Calcitriol blunts the deleterious impact of advanced glycation end products on endothelial cells. Am. J. Physiol. Renal Physiol. *294*, F1059–F1064.

Tan, X., Wen, X., and Liu, Y. (2008). Paricalcitol inhibits renal inflammation by promoting vitamin D receptor-mediated sequestration of NF-kappaB signaling. J. Am. Soc. Nephrol. *19*, 1741–1752.

Tanaci, N., Karakose, H., Guvener, N., Tutuncu, N.B., Çolak, T., and Haberal, M. (2003). Influence of 1,25-dihydroxyvitamin D3 as an immunomodulator in renal transplant recipients: a retrospective cohort study. Transplant. Proc. *35*, 2885–2887.

Tanaka, T., Narazaki, M., and Kishimoto, T. (2014). IL-6 in inflammation, immunity, and disease. Cold Spring Harb Perspect Biol *6*, a016295–a016295.

Teng, M., Wolf, M., Ofsthun, M.N., Lazarus, J.M., Hernán, M.A., Camargo, C.A., and Thadhani, R. (2005). Activated injectable vitamin D and hemodialysis survival: a historical cohort study. J. Am. Soc. Nephrol. *16*, 1115–1125.

Theodoratou, E., Tzoulaki, I., Zgaga, L., and Ioannidis, J. (2014). Vitamin D and multiple health outcomes: umbrella review of systematic reviews and meta-analyses of observational studies and randomised trials. Bmj *348*, g2035.

Tomkins, G.M., and Martin, D.W. (1970). Hormones and gene expression. Annu. Rev. Genet. *4*, 91–106.

Torgerson, T.R., and Ochs, H.D. (2007). Immune dysregulation, polyendocrinopathy, enteropathy, X-linked: forkhead box protein 3 mutations and lack of regulatory T cells. J. Allergy Clin. Immunol. *120*, 744–50–quiz751–2.

Tripathi, S., Pohl, M.O., Zhou, Y., Rodriguez-Frandsen, A., Wang, G., Stein, D.A., Moulton, H.M., DeJesus, P., Che, J., Mulder, L.C.F., et al. (2015). Meta- and Orthogonal Integration of Influenza "OMICs" Data Defines a Role for UBR4 in Virus Budding. Cell Host Microbe *18*, 723–735.

Tsoi, L.C., Spain, S.L., Knight, J., Ellinghaus, E., Stuart, P.E., Capon, F., Ding, J., Li, Y., Tejasvi, T., Gudjonsson, J.E., et al. (2012). Identification of 15 new psoriasis susceptibility loci highlights the role of innate immunity. Nat. Genet. *44*, 1341–1348.

Tung, J.W., Parks, D.R., Moore, W.A., Herzenberg, L.A., and Herzenberg, L.A. (2004). New approaches to fluorescence compensation and visualization of FACS data. Clin. Immunol. *110*, 277–283.

Tuoresmäki, P., Väisänen, S., Neme, A., Heikkinen, S., and Carlberg, C. (2014). Patterns of genome-wide VDR locations. PLoS ONE *9*, e96105.

Turunen, M.M., Dunlop, T.W., Carlberg, C., and Väisänen, S. (2007). Selective use of multiple vitamin D response elements underlies the 1 alpha,25-dihydroxyvitamin D3-mediated negative regulation of the human CYP27B1 gene. Nucleic Acids Res. *35*, 2734–2747.

Umesono, K., Murakami, K.K., Thompson, C.C., and Evans, R.M. (1991). Direct repeats as selective response elements for the thyroid hormone, retinoic acid, and vitamin D3 receptors. Cell *65*, 1255–1266.

Urry, Z., Chambers, E.S., Xystrakis, E., Dimeloe, S., Richards, D.F., Gabryšová, L., Christensen, J., Gupta, A., Saglani, S., Bush, A., et al. (2012). The role of 1α,25-dihydroxyvitamin D3 and cytokines in the promotion of distinct Foxp3+ and IL-10+ CD4+ T cells. Eur J Immunol *42*, 2697–2708.

Uyar, M., Sezer, S., Arat, Z., Elsurer, R., Ozdemir, F.N., and Haberal, M. (2006). 1,25-dihydroxyvitamin D(3) therapy is protective for renal function and prevents hyperparathyroidism in renal allograft recipients. Transplant. Proc. *38*, 2069–2073.

Vacher-Coponat, H., Brunet, C., Lyonnet, L., Bonnet, E., Loundou, A., Sampol, J., Moal, V., Dussol, B., Brunet, P., Berland, Y., et al. (2008). Natural killer cell alterations correlate with loss of renal function and dialysis duration in uraemic patients. Nephrol. Dial. Transplant. *23*, 1406–1414.

van Etten, E., and Mathieu, C. (2005). Immunoregulation by 1, 25-dihydroxyvitamin D 3: basic concepts. J Steroid Biochem Mol Biol.

Vanholder, R., and Ringoir, S. (1993). Infectious morbidity and defects of phagocytic function in end-stage renal disease: a review. J. Am. Soc. Nephrol. *3*, 1541–1554.

Vanhooke, J.L., Prahl, J.M., Kimmel-Jehan, C., Mendelsohn, M., Danielson, E.W., Healy, K.D., and DeLuca, H.F. (2006). CYP27B1 null mice with LacZreporter gene display no 25-hydroxyvitamin D3-1alpha-hydroxylase promoter activity in the skin. Proc. Natl. Acad. Sci. U.S.a. *103*, 75–80.

Vanoirbeek, E., Eelen, G., Verlinden, L., Carmeliet, G., Mathieu, C., Bouillon, R., O'Connor, R., Xiao, G., and Verstuyf, A. (2014). PDLIM2 expression is driven by vitamin D and is involved in the pro-adhesion, and anti-migration and -invasion activity of vitamin D. Oncogene *33*, 1904–1911.

Vantieghem, K., Kissmeyer, A.M., and Haes, P.D. (2006). UVB-induced production of 1, 25-dihydroxyvitamin D3 and vitamin D activity in human keratinocytes pretreated with a sterol Δ7-reductase inhibitor. J Cell Biochem *98*, 81–92.

Wang, T.-T.T., Nestel, F.P., Bourdeau, V., Nagai, Y., Wang, Q., Liao, J., Tavera-Mendoza, L., Lin, R., Hanrahan, J.W., Mader, S., et al. (2004). Cutting edge: 1,25-dihydroxyvitamin D3 is a direct inducer of antimicrobial peptide gene expression. J. Immunol. *173*, 2909–2912.

Wang, T.-T.T., Tavera-Mendoza, L.E., Laperriere, D., Libby, E., MacLeod, N.B., Nagai, Y., Bourdeau, V., Konstorum, A., Lallemant, B., Zhang, R., et al. (2005). Large-scale in silico and microarray-based identification of direct 1,25-dihydroxyvitamin D3 target genes. Mol. Endocrinol. *19*, 2685–2695.

Wendling, D., Letho-Gyselinck, H., Guillot, X., and Prati, C. (2012). Psoriasis onset with tocilizumab treatment for rheumatoid arthritis. The Journal of Rheumatology *39*, 657–657.

White, M.J., Nielsen, C.M., McGregor, R.H.C., Riley, E.H.C., and Goodier, M.R. (2014). Differential activation of CD57-defined natural killer cell subsets during recall responses to vaccine antigens. Immunology *142*, 140–150.

White, S.L., Belov, L., Barber, N., Hodgkin, P.D., and Christopherson, R.I. (2005). Immunophenotypic changes induced on human HL60 leukaemia cells by 1alpha,25-dihydroxyvitamin D3 and 12-O-tetradecanoyl phorbol-13-acetate. Leuk. Res. *29*, 1141–1151.

Wolf, M., Shah, A., Gutierrez, O., Ankers, E., Monroy, M., Tamez, H., Steele, D., Chang, Y., Camargo, C.A., Tonelli, M., et al. (2007). Vitamin D levels and early mortality among incident hemodialysis patients. Kidney Int. *72*, 1004–1013.

Yadav, A.K., Banerjee, D., Lal, A., and Jha, V. (2012). Vitamin D deficiency, CD4+CD28null cells and accelerated atherosclerosis in chronic kidney disease. Nephrology (Carlton) *17*, 575–581.

Yates, A., Akanni, W., Amode, M.R., Barrell, D., Billis, K., Carvalho-Silva, D., Cummins, C., Clapham, P., Fitzgerald, S., Gil, L., et al. (2016). Ensembl 2016. Nucleic Acids Res. *44*, D710–D716.

Ziegler-Heitbrock, L. (2007). The CD14+ CD16+ blood monocytes: their role in infection and inflammation. J Leukoc Biol *81*, 584–592.

Zittermann, A., Ernst, J.B., Prokop, S., Fuchs, U., Dreier, J., Kuhn, J., Knabbe, C., Birschmann, I., Schulz, U., Berthold, H.K., et al. (2017). Effect of vitamin D on all-cause mortality in heart failure (EVITA): a 3-year randomized clinical trial with 4000 IU vitamin D daily. Eur. Heart J.

Zubiaga, A.M., Munoz, E., Merrow, M., and Huber, B.T. (1990). Regulation of interleukin 6 production in T helper cells. Int. Immunol. *2*, 1047–1054.

(2012). An integrated encyclopedia of DNA elements in the human genome. Nature *489*, 57–74.

# Appendix

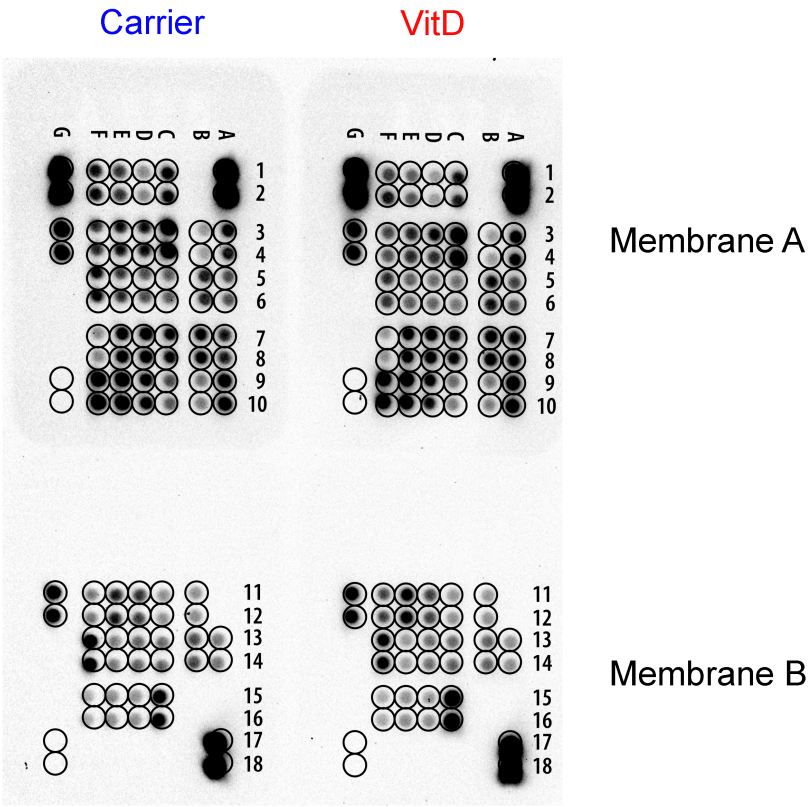


**Appendix 1|Full phospho-kinase antibody array|**
Both membrane A and membrane B of phospho array, in Carrier and VitD treated conditions. Location of all proteins are circled and numbered. Numbers can be cross referenced with Appendix 2.

| Membrane/ Coordinate | Target/Control | Phosphorylation Site |
|---|---|---|
| A-A1, A2 | Reference Spot | —— |
| A-A3, A4 | p38α | T180/Y182 |
| A-A5, A6 | ERK1/2 | T202/Y204, T185/ Y187 |
| A-A7, A8 | JNK 1/2/3 | T183/Y185, T221/ Y223 |
| A-A9, A10 | GSK-3α/β | S21/S9 |
| B-A13, A14 | p53 | S392 |
| B-A17, A18 | Reference Spot | —— |
| A-B3, B4 | EGF R | Y1086 |
| A-B5, B6 | MSK1/2 | S376/S360 |
| A-B7, B8 | AMPKα1 | T183 |
| A-B9, B10 | Akt 1/2/3 | S473 |
| B-B11, B12 | Akt 1/2/3 | T308 |
| B-B13, B14 | p53 | S46 |
| A-C1, C2 | TOR | S2448 |
| A-C3, C4 | CREB | S133 |
| A-C5, C6 | HSP27 | S78/S82 |
| A-C7, C8 | AMPKα2 | T172 |
| A-C9, C10 | β-Catenin | —— |
| B-C11, C12 | p70 S6 Kinase | T389 |
| B-C13, C14 | p53 | S15 |
| B-C15, C16 | c-Jun | S63 |
| A-D1, D2 | Src | Y419 |
| A-D3, D4 | Lyn | Y397 |
| A-D5, D6 | Lck | Y394 |
| A-D7, D8 | STAT2 | Y689 |
| A-D9, D10 | STAT5a | Y694 |
| B-D11, D12 | p70 S6 Kinase | T421/S424 |
| B-D13, D14 | RSK1/2/3 | S380/S386/S377 |
| B-D15, D16 | eNOS | S1177 |

| Membrane/ Coordinate | Target/Control | Phosphorylation Site |
|---|---|---|
| A-E1, E2 | Fyn | Y420 |
| A-E3, E4 | Yes | Y426 |
| A-E5, E6 | Fgr | Y412 |
| A-E7, E8 | STAT6 | Y641 |
| A-E9, E10 | STAT5b | Y699 |
| B-E11, E12 | STAT3 | Y705 |
| B-E13, E14 | p27 | T198 |
| B-E15, E16 | PLC-γ1 | Y783 |
| A-F1, F2 | Hck | Y411 |
| A-F3, F4 | Chk-2 | T68 |
| A-F5, F6 | FAK | Y397 |
| A-F7, F8 | PDGF Rβ | Y751 |
| A-F9, F10 | STAT5a/b | Y694/Y699 |
| B-F11, F12 | STAT3 | S727 |
| B-F13, F14 | WNK1 | T60 |
| B-F15, F16 | PYK2 | Y402 |
| A-G1, G2 | Reference Spot | —— |
| A-G3, G4 | PRAS40 | T246 |
| A-G9, G10 | PBS (Negative Control) | —— |
| B-G11, G12 | HSP60 | —— |
| B-G17, G18 | PBS (Negative Control) | —— |

**Appendix 2|Reference tables for full phospho-kinase antibody array|**

Tables indicating membrane co-ordinates for all proteins in Appendix 1 with phosphorylation site present in membrane also indicated.